

**London South Bank**  
University

**STRUCTURAL INTEGRITY  
MANAGEMENT AND IMPROVED JOINT  
FLEXIBILITY EQUATIONS FOR  
UNI-PLANAR K-TYPE TUBULAR JOINTS  
OF FIXED OFFSHORE STRUCTURES**

**RIAZ KHAN**

<http://orcid.org/0000-0001-6879-5290>

**A thesis submitted in partial fulfillment of the  
requirements of London South Bank University for the  
degree of Doctor of Philosophy**

**October 2016**

## **Acknowledgements**

I would like to take the opportunity to thank my supervisors Mr. Kenneth Smith, Dr Ivana Kraincanic and Professor Mike Gunn for their constant support, technical guidance and encouragement throughout this research. I am particularly indebted to Dr Kaisheng Chen for his technical insight on the finite element modeling of fatigue and ultimate strength criteria for fixed offshore structures.

I am grateful to Patrick O'Connor for his passion, understanding and knowledge in key areas on the subject matter over the past thirty years. I am eternally grateful to my colleagues Professor Mike Willmore, Nigel Wayne Nichols, Dr Adrian Dier, Justin Bucknell, Dr Paul Freize and Professor Choo Yoo Sang for having lengthy discussions with me over the course of this research, which have proven fruitful in generating ideas.

This journey would not have been possible without the patience and support from my wife, Michelle, and son, Emre. Special thanks to my parents for their kind support and encouragement over the years.

## **Abstract**

The distribution of fixed steel offshore platforms around the world reveal a global fleet that has exceeded or is approaching the end of the design life. In many operating areas, there is an attraction to continue using these aging facilities due to continued production or as an adjoining structure to facilitate a new field development or expansion. To justify continued life extension of the fixed platform, various integrity assessment techniques are often used. One of the major techniques incorporated is the phenomena of Local Joint Flexibility (LJF). The derivations of existing LJF equations have evolved in many ways, including use of finite element methods to predict the joint behaviour. There has been insufficient credible benchmarking to large scale experimental test data.

In the early 1980s, AMOCO performed the only large scale test results of LJF which, prior to this research, has not been in the public domain. A major objective of this research is to develop a suite of improved LJF equations that have been appropriately benchmarked to large scale tests. In addition, with the issue of the API RP 2SIM (2014) 1st Edition and the development of the ISO 19901-09 SIM (DIS), this research also provides a basis for further Asset Life Extension (ALE) of an aging fixed offshore platform in terms of ultimate strength by using an improved suite of LJF equations. Furthermore, the research puts the structural assessments such as LJF in the context of a structural integrity management framework, which enables operators to manage their facilities holistically rather than isolated processes.

The research within this thesis critically examined the suitability of the existing LJF equations, reviewed the guidance provided in the existing studies and described their limitations for gapped K-type tubular joints. A comparison study and benchmarking study demonstrated that a proposed finite element model provides a good fit with large scale experimental data (AMOCO) and was used to develop a suite of improved LJF equations for

gapped K-type tubular joints. The LJF equations derived from this research were validated against the BOMEL large scale structural frame tests in terms of ultimate strength and demonstrated an improvement on the current MSL-ISO equations for uni-planar K-type tubular joints in the ISO 19902.2007 Fixed Offshore Structures code of practice. This research also provides a basis to update current offshore structures codes and standards for uni-planar gapped K-joints and also provide a standardized methodology for the derivation of LJFs from credible large scale test data for other tubular joint configurations including multi-planar K-joints, T-joints, Y-joints and X-joints.

The LJF equations developed in this research will have high impact in terms of the structural integrity management of fixed offshore structures for OGP's globally, as they provide an improvement to the current MSL-ISO joint equations, for gapped uni-planar joints. Offshore structures are now able to operate more safely without compromising structural integrity and incurring costly underwater repairs and inspections as before. OGP's are now able to prioritize limited resources to other areas of concerns based on ALARP principles.

## Abbreviations

ABAQUS	ABAQUS Suite of Finite Element Analysis Software
ALE	Asset Life Extension
AMOCO	American Oil Corporation
ANSYS	ANSYS Suite of Software
API	American Petroleum Institute
ASAS	Atkins Structural Analysis System
Atkins	WS Atkins Inc
BOMEL	Billington Osbourne Moss Engineering Limited
BP	British Petroleum
BS	British Standard
DIS	Draft Industry Standard
DNV	Det Norske Veritas
FEM	Finite Element Methods
FEA	Finite Element Analysis
FFP	Fitness for Purpose
GoM	Gulf of Mexico
HSE	Health, Safety and Environment
ICE	Institution of Civil Engineers
IPB	In-Plane Bending
ISO	International Standards Organization

JIP	Joint Industry Project
LJF	Local Joint Flexibility
LSBU	London South Bank University
LR	Lloyds Register of Shipping
MSL	MSL Engineering Corporation
NUS	National University Singapore
OGP	Oil and Gas Producer
OPB	Out-of-Plane Bending
OTC	Offshore Technological Conference (Houston)
RBI	Risk Based Inspection
RBUI	Risk Based Underwater Inspection
RLA	Remaining Life Assessment
RP	Recommended Practice
RSR	Reserve Strength Ratio
SACS	Structural Analysis Computer System
SCF	Stress Concentration Factor
S-N Curve	Cyclic stress (S) vs logarithmic scale of cycles to failure (N) graph
SINTEF	SINTEF Civil and Environmental Engineering
SICS	Structural Integrity Compliance System
SIM	Structural Integrity Management
STRAND 7	STRAND 7 Finite Element Software

UEG	Underwater Engineering Group (UK)
ULS	Ultimate Limit State
USFOS	Ultimate Strength Finite Element Software
WiD	Wave in Deck
Wimpey	Wimpey Laboratories Limited

## Symbols

D	Chord diameter
d	Brace diameter
$\delta$	Axial displacement of the brace
$\delta F$	Displacement attributable to joint flexibility
E	Young's Modulus of Elasticity
F	Axial force
fkj	Flexibility matrix terms
T	Chord Thickness
t	Brace thickness
$\phi$	Angle between brace and x-z plane (degrees)
$\theta$	Angle between the brace and the x-axis
K	Joint stiffness coefficient
L	Chord length
M	Bending moment
gl	Longitudinal gap length
gt	Transverse gap length
$\lambda$	Cross sectional area of the brace
$\tau$	Brace to chord wall thickness ratio
$\beta$	Brace to chord diameter ratio
$\alpha$	Chord length to chord radius ratio
$\gamma$	Radius to wall thickness ratio of the chord
$\zeta$	Gap parameter for K-joints

# Table of Contents

<b>Acknowledgements.....</b>	<b>ii</b>
<b>Abstract.....</b>	<b>iii</b>
<b>Abbreviations .....</b>	<b>v</b>
<b>Symbols .....</b>	<b>viii</b>
<b>Table of Contents .....</b>	<b>ix</b>
<b>List of Figures.....</b>	<b>xv</b>
<b>List of Tables .....</b>	<b>xxiii</b>
<b>CHAPTER 1 Introduction .....</b>	<b>1</b>
1.1 Background .....	1
1.2 Fixed Offshore Structures .....	2
1.3 Tubular Joints.....	3
1.4 Remaining Life of Fixed Offshore Structures .....	5
1.5 Problem Description.....	7
1.6 Scope of Present Research .....	8
1.7 Organization of the Thesis .....	9
<b>CHAPTER 2 The Role of Local Joint Flexibility in the Structural Integrity Management (SIM) of Fixed Offshore Structures.....</b>	<b>11</b>
2.1 Introduction .....	11
2.2 Structural Integrity Management (SIM).....	11

2.3 Assessment versus Design Approach.....	18
2.4 Codes and Standards .....	21
2.5 Summary and Conclusions.....	26

## **CHAPTER 3 Literature Review: Parametric Equations and Empirical**

### **Formulae for Local Joint Flexibility .....28**

3.1 Introduction .....	28
3.2 Det Norske Veritas (1977) .....	30
3.3 Fessler et al (1983) .....	31
3.4 Efthymiou (1985) .....	32
3.5 Fessler et al (1986) .....	34
3.6 Ueda, Rashed and Nakacho (1987).....	41
3.7 Hoshyari and Kohoutek (1993).....	42
3.8 Chen, Hu and Ma (1993).....	44
3.9 Buitrago, Healy and Chang (1993).....	48
3.10 MSL - JOINT Module (2002) .....	52
3.11 Qian, Zhang and Yoo Sang (2013).....	59
3.12 Asgarian, Mokarram and Alanjari (2014) .....	63
3.13 Summary and Conclusions.....	64

## **CHAPTER 4 Literature Review: Local Joint Flexibility Studies .....67**

4.1 Introduction .....	67
4.2 Laboratory Testing .....	67
4.3 Analytical Methods .....	69

4.4 Fatigue Studies .....	80
4.5 Global Effects of LJF on Frame Structures .....	86
4.6 Summary and Conclusions .....	96
<b>CHAPTER 5 Gapped K-Joint Testing and Local Joint Flexibility .....</b>	<b>99</b>
5.1 Introduction .....	99
5.2 AMOCO K-Joint Tests.....	100
5.3 Rationale for the AMOCO K-Joint Study .....	100
5.4 AMOCO K-Joint Geometry .....	101
5.5 Local Joint Flexibility Definition .....	102
5.5.1 LJF for Axial Brace Loads .....	103
5.5.2 LJF for In-Plane Bending .....	104
5.5.3 LJF for Out-of-Plane Bending.....	105
5.6 Test Specimens.....	106
5.7 Test Procedures .....	109
5.8 Loading.....	112
5.8.1 Axial Load.....	113
5.8.2 Compression Loading.....	113
5.8.3 Tension Loading.....	113
5.8.4. Bending Load .....	114
5.9 Da Silva LJF Small Scale Tests .....	117
5.10 Summary and Conclusions .....	119

## **CHAPTER 6 Finite Element Modeling of Uni-Planar Tubular K-Type**

### **Tubular Joints, Results and Comparison with Experimental Data.....121**

6.1 Background .....	121
6.2 Shell Finite Elements.....	126
6.3 Finite Element Mesh Analysis .....	128
6.4 Benchmarking Study of FE Model and the AMOCO K-Joint Tests.....	132
6.5 Benchmarking Study Results .....	135
6.6 LJF Comparison Study with AMOCO K-Joint Tests.....	137
6.7 Summary and Conclusions.....	140

## **CHAPTER 7 Developing an Improved Suite of LJF Parametric Equations**

### **.....142**

7.1 Introduction .....	142
7.2 Database of In-Service Fixed Offshore Structures .....	143
7.3 Finite Element Modeling of Database of K-Type Joints.....	146
7.3.1 Developing the Structural Models.....	146
7.3.2 Finite Element Analysis Results.....	148
7.4 Developing LJF Parametric Equations .....	161
7.4.1 Axial Balanced Condition .....	162
7.4.2 In-Plane Bending Condition .....	162
7.4.3 Out-of-Plane Bending Condition.....	163
7.5 RK Suite of LJF Equations for Gapped Uni-planar K-type Tubular Joints .....	169
7.6 Gap Sensitivity Study.....	170

7.6.1 Gap Size and the Axial Condition .....	170
7.6.2 Gap Size and the In-Plane Condition .....	171
7.6.3 Gap Size and the Out-of-Plane Condition .....	172
7.7 LJF Comparison Study for varying $\beta$ .....	172
7.8 Summary and Conclusions .....	175
<b>CHAPTER 8 Validation of the RK-LJF Formulations in Global Structural Assessments.....</b>	<b>177</b>
8.1 Introduction .....	177
8.2 Ultimate Strength of Fixed Offshore Structures.....	178
8.3 Ultimate Strength Finite Element Software for Offshore Structures (USFOS) .....	184
8.4 Validation RK-LJF Equations in 2D Frame Tests .....	184
8.5 Recent understanding on the fatigue phenomena on fixed offshore structures .....	188
8.6 Summary and Conclusions .....	192
<b>CHAPTER 9 Concluding Remarks and Recommendations for Further Work.....</b>	<b>193</b>
9.1 Concluding Remarks .....	193
9.2 Recommendations for Further Work.....	196
<b>REFERENCES.....</b>	<b>198</b>
<b>APPENDICES .....</b>	<b>205</b>
APPENDIX 1 - Glossary of Terms .....	206
APPENDIX 2 - Shear Flexible Small-Strain Shell Elements .....	210

APPENDIX 3 - LJF Calculations from the AMOCO K-Joint Test Results.....	214
APPENDIX 4 - LJF Calculations for Benchmarking Model .....	248
APPENDIX 5 - Sample Calculations for LJF for AXIAL, IPB, OPB .....	260
APPENDIX 6 - USFOS Files for the Development of the K-Frame Analysis .....	271

## List of Figures

Figure 1.1 Platform lives in the Gulf of Mexico.....	1
Figure 1.2 Conventional fixed steel jacket structure .....	3
Figure 1.3 Classification of tubular joints.....	4
Figure 1.4 Gapped K-Type tubular joint.....	4
Figure 1.5 Basic structure of the decision making process.....	6
Figure 1.6 Continuous risk reduction to manage structural risk .....	7
Figure 2.1 The role of LJF in the Structural Integrity Management of Offshore Structures ...	11
Figure 2.2 Evolution of the API RP structures codes .....	12
Figure 2.3 Bracing configurations for fixed offshore jacket structures .....	13
Figure 2.4 Platform robustness based on bracing configuration.....	14
Figure 2.5 The SIM process.....	15
Figure 2.6 Assessment methods in the Structural Integrity Management framework.....	15
Figure 2.7 Flowchart of the assessment process.....	17
Figure 2.8 Defect/damage trends in UK and US Gulf of Mexico Waters .....	19
Figure 2.9 Assessment techniques vs design techniques .....	20
Figure 2.10 Assessment refinement, including LJF.....	21
Figure 3.1 Overview of Local Joint Flexibility Literature Review .....	29
Figure 3.2 Test Rig used by Fessler (1981) .....	32
Figure 3.3 Efthymiou's measured rotations for LJF calculation .....	33
Figure 3.4 Joint with loaded and unloaded braces in the same plane .....	36

Figure 3.5 Joint with unloaded brace in the 90° plane .....	37
Figure 3.6 Joint with unloaded brace in the 180° plane .....	38
Figure 3.7 Joint with unloaded brace in the 270° plane .....	38
Figure 3.8 Joint Model, T and Y Joint .....	41
Figure 3.9 Load displacement relationship for one load case.....	41
Figure 3.10 Diagrammatic test set-up for frequency measurements of T-joints .....	42
Figure 3.11 The equivalent element method by Chen (1993) .....	44
Figure 3.12 General Joint Geometry, Loads and Degrees of Freedom .....	49
Figure 3.13 FE Mesh for K-Joint $\beta = 0.4$ .....	55
Figure 3.14 $P\delta$ curves for K-Joint $\beta = 0.4, \gamma = 15, \tau = 0.81$ .....	55
Figure 3.15 BOMEL Frame Tests VII behaviour compared to test measurements.....	56
Figure 3.16 (a) Joint Spring representation in the global frame analysis .....	59
Figure 3.17 CHS K-Joint Test .....	60
Figure 3.18 Configuration of BOMEL 2D Frames.....	60
Figure 3.19 Comparison of the Global load deformation response between numerical analysis and experimental records .....	61
Figure 3.20 Comparison of the Global load deformation response between numerical analysis and experimental records for BOMEL 3D Tests .....	62
Figure 3.21 Mesh generation for the intersection areas between chord and braces .....	64
Figure 3.22 Deformed and unformed shape of a model under loading .....	64
Figure 4.1 Tubular joint model .....	70

Figure 4.2 Cylindrical vessel model ..... 70

Figure 4.3 Alternative Methods for modeling joints ..... 71

Figure 4.4 LJF as a spring element in K-Joints ..... 73

Figure 4.5 Shell Element..... 74

Figure 4.6 Joint Flexibility Model ..... 74

Figure 4.7 Joint super element used by Souissi (1989) ..... 75

Figure 4.8 Joint Definitions ..... 76

Figure 4.9 Finite Element Models 1-5 ..... 78

Figure 4.10 3D Isometric Structure ..... 81

Figure 4.11 Joint Fatigue Life Comparison ..... 82

Figure 4.12 bpTT Cassia A platform ..... 84

Figure 4.13 Calculated Fatigue Lives of Joints ..... 85

Figure 4.14 Model of Joint Substructures..... 86

Figure 4.15 Tower Frame ..... 87

Figure 4.16 Nodal points considered for UEG Study ..... 88

Figure 4.17 Structure 1 ..... 89

Figure 4.18 Structure 2 ..... 90

Figure 4.19 Structure 3 ..... 91

Figure 4.20 bpTT Cassia A Platform..... 92

Figure 4.21 bpTT Cassia A Platform, Load Deformation curves..... 93

Figure 4.22 Y-type Tubular Joint Model ..... 93

Figure 4.23 Finite Element model and mesh discretization for Y and T type connections .....	94
Figure 4.24 General configuration and member sizes for 2D frame .....	95
Figure 4.25 Results of Ultimate Strength Analysis .....	95
Figure 5.1 Geometry of the Specimens.....	101
Figure 5.2 Definition of Local Joint Flexibility for Brace Axial Loads .....	103
Figure 5.3 Definition of Local Joint Flexibility for In-Plane Bending .....	104
Figure 5.4 Definition of Local Joint Flexibility for Out-of-Plane Bending.....	105
Figure 5.5 K-Joint Loading Configuration .....	106
Figure 5.6 Position of the Transducers and Gauges on Specimen 1, during Axial Loading .	107
Figure 5.7 Displacement transducer numbers.....	108
Figure 5.8 Strain Gauge by number reference .....	108
Figure 5.9 Specimen 1 under Ultimate Strength.....	109
Figure 5.10 Loadings on Specimens 1 & 2.....	112
Figure 5.11 Brace Compression only.....	113
Figure 5.12 Brace Tension only or Tension and Compression.....	114
Figure 5.13 Bending.....	115
Figure 5.14 Schematic Drawing of Test Rig .....	115
Figure 5.15 General Arrangement of Test Rig and Specimen.....	116
Figure 5.16 Compression and Tension Loading Arrangement .....	116
Figure 5.17 Details of Strain Gauges .....	117
Figure 5.18 Transducer position .....	118

Figure 6.1 Beam Bending Moments for the fixed, pinned and intermediate end conditions	121
Figure 6.2 The degrees of freedom provided by Fessler’s experimental work .....	122
Figure 6.3 The degrees of freedom required in the Joint Stiffness Matrix .....	123
Figure 6.4 Loads and relative displacements of a two braced joint.....	123
Figure 6.5 Flexibility Matrix for Uni-Planar Two Braced Joint (global representation).....	124
Figure 6.6 Flexibility Matrix in Cartesian Co-ordinate Form.....	125
Figure 6.7 Naming Convention for three-dimensional shell elements .....	126
Figure 6.8 4-Noded Reduced Integration Element, Numbering of Integration points for output, Stress/Displacement Analysis.....	127
Figure 6.9 Setting Element Type, 4-Noded Quadrilateral Thin Shell Elements .....	129
Figure 6.10 Refined Mesh in Mesh Generator.....	130
Figure 6.11 Refined Mesh with Elements.....	130
Figure 6.12 AMOCO K-Joint Finite Element Benchmark Model, Y-Z plane view.....	132
Figure 6.13 AMOCO K-Joint Finite Element Benchmark Model, X-Y plane view .....	133
Figure 6.14 AMOCO K-Joint Finite Element Benchmark Model, X-Y-Z plane view .....	133
Figure 6.15 AMOCO K-Joint Finite Element Benchmark Model, Applying Boundary Conditions (generated in ABAQUS 6.11) .....	133
Figure 6.16 AMOCO K-Joint Finite Element Benchmark Model, Creating Load Step.....	134
Figure 6.17 AMOCO K-Joint Finite Element Benchmark Model, Deformed Mesh & Stress Contours (generated in ABAQUS for Load Case 10) .....	134
Figure 6.18 Procedure for the calculation of LJF for Axial, OPB and IPB .....	135

Figure 6.19 Flexibility Coefficients in the Matrix Form .....	136
Figure 6.20 LJF Comparison for Axial Loading (Direct Terms).....	138
Figure 6.21 LJF Comparison for Out-of-Plane Bending .....	139
Figure 6.22 LJF Comparison for In-Plane Bending.....	139
Figure 7.1 Six Step Work Flow Process to develop the RK-LJF Parametric Equations .....	142
Figure 7.2 Structural Integrity Compliance System (SICS) Document Register .....	143
Figure 7.3 Typical Fixed Jacket Structure (from SICS database) .....	144
Figure 7.4 Geometric Ranges of Tubular K-Joints (input for ABAQUS).....	146
Figure 7.5 K-Type Tubular Joint model: $\beta = 0.3, \gamma = 10, \theta = 30^\circ$ .....	147
Figure 7.6 K-Type Tubular Joint model: $\beta = 0.3, \gamma = 10, \theta = 45^\circ$ .....	147
Figure 7.7 K-Type Tubular Joint Model: $\beta = 0.5, \gamma = 15, \theta = 60^\circ$ .....	148
Figure 7.8 LJF Results for Axial: $\beta = 0.3, \gamma = 8-30, \theta = 30^\circ, 45^\circ, 60^\circ$ .....	153
Figure 7.9 LJF Results for IPB <sub>22</sub> : $\beta = 0.3, \gamma = 8-30, \theta = 30^\circ, 45^\circ, 60^\circ$ .....	154
Figure 7.10 LJF Results for OPB <sub>22</sub> : $\beta = 0.3, \gamma = 8-30, \theta = 30^\circ, 45^\circ, 60^\circ$ .....	154
Figure 7.11 LJF Results for OPB <sub>21</sub> : $\beta = 0.3, \gamma = 8-30, \theta = 30^\circ, 45^\circ, 60^\circ$ .....	155
Figure 7.12 LJF Results for IPB <sub>22</sub> : $\beta = 0.5, \gamma = 8-30, \theta = 30^\circ, 45^\circ, 60^\circ$ .....	155
Figure 7.13 LJF Results for OPB <sub>22</sub> : $\beta = 0.5, \gamma = 8-30, \theta = 30^\circ, 45^\circ, 60^\circ$ .....	156
Figure 7.14 LJF Results for OPB <sub>22</sub> : $\beta = 0.5, \gamma = 8-30, \theta = 30^\circ, 45^\circ, 60^\circ$ .....	156
Figure 7.15 LJF Results for IPB <sub>21</sub> : $\beta = 0.5, \gamma = 8-30, \theta = 30^\circ, 45^\circ, 60^\circ$ .....	157
Figure 7.16 LJF Results for OPB <sub>21</sub> : $\beta = 0.5, \gamma = 8-30, \theta = 30^\circ, 45^\circ, 60^\circ$ .....	158
Figure 7.17 LJF Results for Axial: $\beta = 0.3-0.89, \gamma = 8-30, \theta = 30^\circ$ .....	158

Figure 7.18 LJF Results for IPB <sub>22</sub> : $\beta = 0.3-0.89$ , $\gamma = 8-30$ , $\theta = 30^\circ$ .....	159
Figure 7.19 LJF Results for OPB <sub>22</sub> : $\beta = 0.3-0.89$ , $\gamma = 8-30$ , $\theta = 30^\circ$ .....	159
Figure 7.20 LJF Results for IPB <sub>21</sub> : $\beta = 0.5$ , $\gamma = 8-30$ , $\theta = 30^\circ$ .....	160
Figure 7.21 LJF Results for OPB <sub>21</sub> : $\beta = 0.5$ , $\gamma = 8-30$ , $\theta = 30^\circ$ .....	160
Figure 7.22 LJF Expression for the Axially Balanced Condition.....	164
Figure 7.23 LJF Expression for the IPB for the loaded Brace (IPB <sub>22</sub> ) .....	165
Figure 7.24 LJF Expression for the OPB for the loaded Brace (OPB <sub>22</sub> ).....	166
Figure 7.25 LJF Expression for the IPB for the unloaded Brace (IPB <sub>21</sub> ) .....	167
Figure 7.26 LJF Expression for the OPB for the unloaded Brace (OPB <sub>21</sub> ).....	168
Figure 7.27 Gap Sensitivity Analysis – Gap vs Axial LJF .....	171
Figure 7.28 Gap Sensitivity Analysis – Gap vs IPB LJF.....	171
Figure 7.29 Gap Sensitivity Analysis – Gap vs OPB LJF .....	172
Figure 7.30 LJF Comparison for Axial loading vs varying $\beta$ .....	173
Figure 7.31 LJF Comparison for OPB vs varying $\beta$ .....	174
Figure 7.32 LJF Comparison for IPB vs varying $\beta$ .....	175
Figure 8.1 Global Structural Failure from Hurricane Lilli .....	178
Figure 8.2 Ultimate strength load displacement curve .....	179
Figure 8.3 Assessment approaches for ultimate strength.....	179
Figure 8.4 Wave Loading on Fixed Offshore Structures .....	180
Figure 8.5 Frame VII - Model Configuration .....	181
Figure 8.6 Frame VII – Behaviour compared to Test Specimens.....	182

Figure 8.7 Comparison of fitted curve to experimental data for force deformation behaviour of a simple tubular joint .....	183
Figure 8.8 BOMEL Frame VII modeled in USFOS (No LJF) .....	186
Figure 8.9 BOMEL Frame VII modeled in USFOS (LJF included) .....	187
Figure 8.10 Load vs Displacement Curve.....	188
Figure 8.11 Pre-API RP 2A Vintage Platforms with multiple fatigue cracks .....	189
Figure 8.12 Inspected Platforms, Water Depth increase with time .....	190

## List of Tables

Table 1.1 Petronas Carigali Snd Bhd Platform Profile, 2006 – Age Distribution .....	2
Table 2.1 Classification of fixed offshore structures, based on their design .....	13
Table 2.2 Comparison of design and assessment approaches.....	18
Table 2.3 Code of Practice guidance on joint flexibility .....	25
Table 3.1 Parametric Equations developed to calculate the effects of local joint flexibilities	30
Table 3.2 Mean joint capacities for use in $P\delta$ and $M\theta$ Equations.....	58
Table 3.3 Coefficient in the proposed formulation for K-joints .....	61
Table 3.4 Summary of the applicability of Local Joint Flexibility Equations.....	66
Table 4.1 Measured LJF coefficients for as-welded and grouted tubular joints by Wimpey (1982).....	68
Table 4.2 Fessler’s Tests on Multi-brace Joints.....	69
Table 4.3 Joint model criteria .....	77
Table 4.4 Average Factor on Fatigue Life (MSL 2001) .....	81
Table 4.5 bpTT Cassia A Comparison of Fatigue Life Assessments .....	84
Table 4.6 Maximum Responses when including LJFs compared to conventional design .....	97
Table 5.1 Local Joint Flexibility for Specimen 1 .....	111
Table 6.1 Mesh Sensitivity Results.....	132
Table 6.2 Comparison of AMOCO K-Joint Tests and FE Modeling Results .....	136
Table 6.3 Flexibility Matrix Coefficients from AMOCO K-Joint Tests and FE Modeling ..	137
Table 6.4 LJF Comparison Study Results Summary .....	141

Table 7.1 K-Joint Geometric Ranges (input for ABAQUS Analysis).....	145
Table 7.2 Basic Input parameters.....	146
Table 7.3 Loading System for all geometric models .....	147
Table 7.4 Uni-planar K-Joint LJFs for IPB, OPB and Axial Balanced for $\beta = 0.3$ .....	149
Table 7.5 Uni-planar K-Joint LJFs for IPB, OPB and Axial Balanced for $\beta = 0.5$ .....	150
Table 7.6 Uni-planar K-Joint LJFs for IPB, OPB and Axial Balanced for $\beta = 0.7$ .....	151
Table 7.7 Uni-planar K-Joint LJFs for IPB, OPB and Axial Balanced for $\beta = 0.89$ .....	152
Table 7.8 RK-LJF Parametric Equations for Axial, IPB and OPB.....	169
Table 7.9 Gap Sensitivity Study for IPB, OPB and Axial Balanced for $\beta = 0.89$ .....	170
Table 8.1 Joint Flexibility Options for RK 2D Frame validation study .....	185

# CHAPTER 1

## Introduction

### 1.1 Background

The vintage of fixed offshore steel structures globally range from those installed in the 1950s to those designed to the latest code of practice. A great variety of the grandfather type structures are still operating well beyond their design life and leading the industry to believe they are still fit for purpose with regards to fatigue lives and ultimate strength. However, this needs further qualification for structural integrity, which is the research question addressed within this thesis. Figure 1.1 shows that as of 2005, 48% (1947 of 4024) of the fixed offshore structures currently operating in the Gulf of Mexico have exceeded their design life (of 25 years). Interestingly, another 40% will be at the end of their design life by 2015.

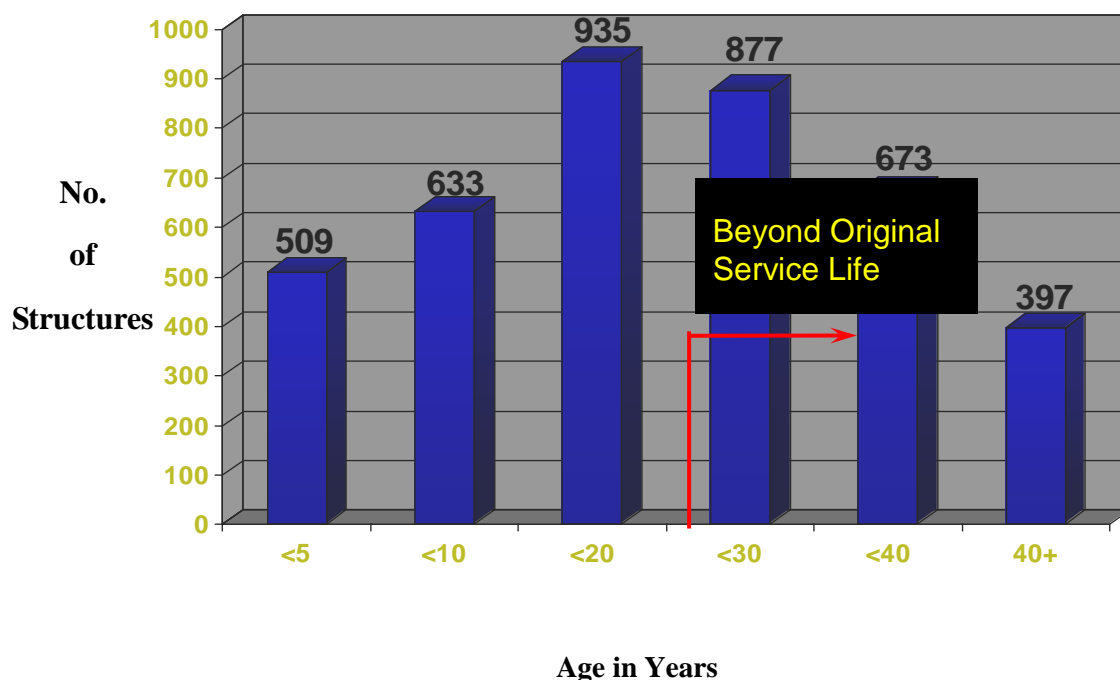


**Figure 1.1 Platform lives in the Gulf of Mexico**  
(Adapted from O'Connor et al, 2005)

Nichols et al (2006) also identified a similar trend in the aging of offshore facilities in Malaysian waters. They provided the following table as evidence of an aging fleet for 3 operating regions in Malaysia.

	Age Distribution, $x$ (Years)				
	$x < 10$	$10 < x < 20$	$20 < x < 25$	$25 < x < 30$	$x > 30$
Region A	13	5	13	4	
Region B	1	3	7	10	6
Region C	1	33	17	19	33

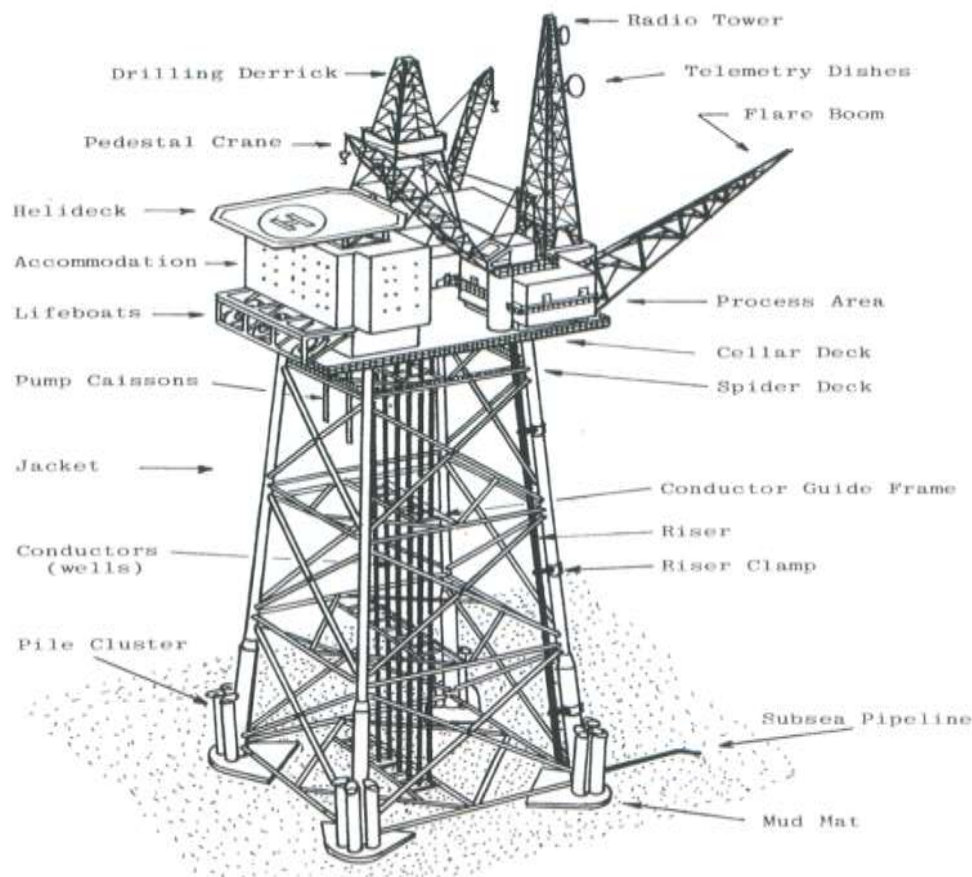
**Table 1.1 Petronas Carigali Snd Bhd Platform Profile, 2006 – Age Distribution  
(Nichols et al, 2006)**

Table 1.1 indicate that of the 165 offshore structures operating by Petronas Carigali Snd Bhd (as of 2006), approximately 44% are operating beyond 25 years and approximately 24% were operating beyond 30 years. While the offshore oil and gas industry has been in existence for the past 75 years, there has been a lack of understanding of assessment engineering techniques with regards to fitness for purpose and acceptance criteria around offshore structures.

## 1.2 Fixed Offshore Structures

The most common type of offshore structure in service today is the jacket (or template) structure, illustrated in Figure 1.2. The template was derived from the function of the first offshore structures to serve as a guide for the piles and has now become commonplace in the industry. The template or jacket structure is a steel space frame composed of tubular members welded at joints that supports, above water, a superstructure comprising one or more decks for production equipment and facilities needed to support and maintain production. The production tasks may include separation of oil, gas, water and sand,

treatment and measurement of oil and/or gas for sales and treatment of water and/or solids for disposal.



**Figure 1.2 Conventional fixed steel jacket structure**  
(Adapted from Lalani et al, 2001)

### **1.3 Tubular Joints**

The design of fixed offshore platforms depends upon the service and environmental loads including wave, current, wind and seismic, in the region of which the structure is operating. Tubular members (within the substructure or platform jacket structure) are mainly used to withstand these loads since they are hollow and can effectively produce buoyancy upon installation, compared to other steel members.

Tubular members are applicable not only in the offshore industry, but also in the manufacturing of space truss structures, telecommunication towers and crane structures.

Moreover, tubular members are superior in comparison with other cross sections in several aspects such as high torsional strength, symmetry in cross section, almost perfect in welding of connections and being economical when used in design. Considering these parameters, the study of tubular connections has become increasingly important over the past three decades, as they are the major sectional type for jacket template structures (substructure) for fixed offshore structures. The general classification of tubular joints is shown on Figure 1.3 and the geometric parameters in Figure 1.4.

T-Joints	X-Joints	K-Joints	TT-Joints
XX-Joints	TX-Joints	KK-Joints	definition of axes

**Figure 1.3 Classification of tubular joints**

(Adapted from Makino et al, 1986)

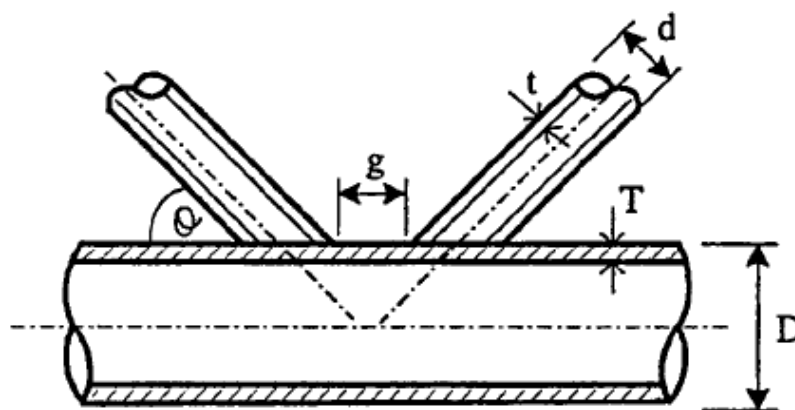


**Figure 1.4 Gapped K-Type tubular joint**

(Adapted from Ultigude, 1999)

*Note 1: The definitions for each of the geometric properties are provided under Symbols*

## 1.4 Remaining Life of Fixed Offshore Structures

In 1993, Buitrago concluded that the inclusion of local joint flexibility in the global structural analysis of offshore structures leads to significant redistribution of calculated member-end forces and moments, which in turn, may result in lesser structural demands on the tubular joints. It is through this phenomenon of localized joint flexibility, that operators are able to justify the remaining life of structural critical joints, because the original design analysis omitted this secondary effect. In providing a Remaining Life Assessment (RLA) for an aging structure, operators are required to provide a long-term inspection plan, mitigation plan to manage the residual structural risk of the structure, which is based on the findings of the assessment engineering incorporating localized joint flexibility in the global analysis.

The majority of aging jacket type structures around the world are primarily of the tubular K-joint type (Figure 1.4), as this was the joint configuration that was used over the first 40 years of the offshore structural industry. Some of these structures are in existence today and are still producing assets for many Oil and Gas Producers (OGPs). It is from this perspective that this study concentrates on the K-type joint, as local joint flexibility can provide ample justification for continued operations of these predominately K-type jacket type structures.

MSL Engineering in 2001, on behalf of the UK Health and Safety Executive, undertook the study *“The effects of local joint flexibility on the reliability of fatigue life estimates and inspection planning.”* The findings of this study supported the industry view that conventional rigid joint analysis under-predicts fatigue life, while implementing local joint flexibility allows for a more accurate fatigue life prediction and closer agreement with results from underwater inspection and reducing the requirement for costly underwater inspections by approximately 75%. It is through studies such as these that the benefits of local joint flexibility can be realized and provide a basis for further research on local joint flexibility, as operators are faced with fitness for purpose engineering evaluations for an aging global fleet.

The decision to continue operating by OGP's will generally adopt a model similar to that proposed by Aven (2003), Figure 1.5.

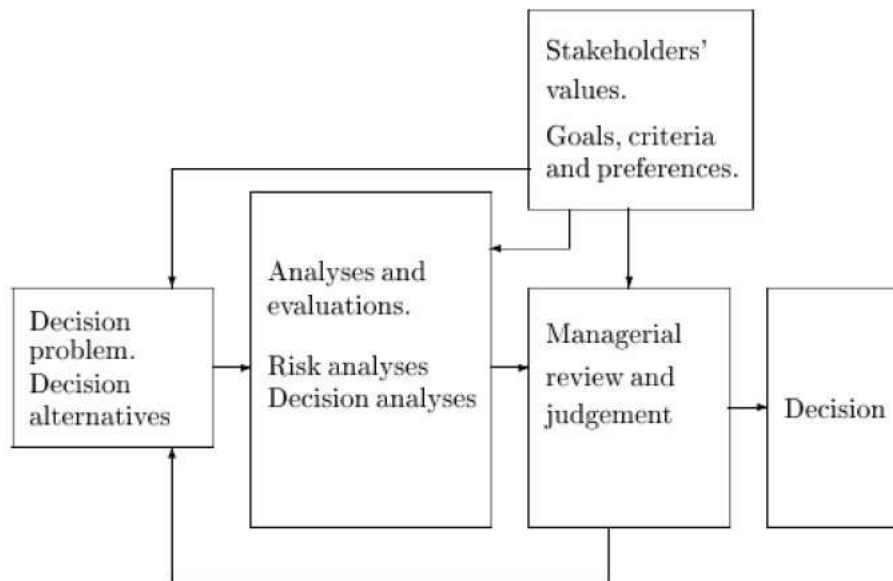


**Figure 1.5 Basic structure of the decision making process  
(Aven, 2003)**

For most OGP's, they normally practice the As Low As Reasonably Practicable (ALARP) principles when making decisions on the risk analysis as proposed by Aven (2003). For aging structures, tools such as LJI, allow operators to make better informed decisions with their aging assets by better understanding their operating risk. O'Connor et al (2005) has argued that the structural integrity management (SIM) of fixed offshore structures is about understanding structural risk and seeking for continuous risk reduction of the structure while it operates (Figure 1.6). If technological achievements such as LJI are used when assessing structures, then operators may be able to avoid costly frequent inspections (by adopting a Risk Based Inspection (RBI) approach) and hazardous and costly strengthening, modification and underwater repair schemes.

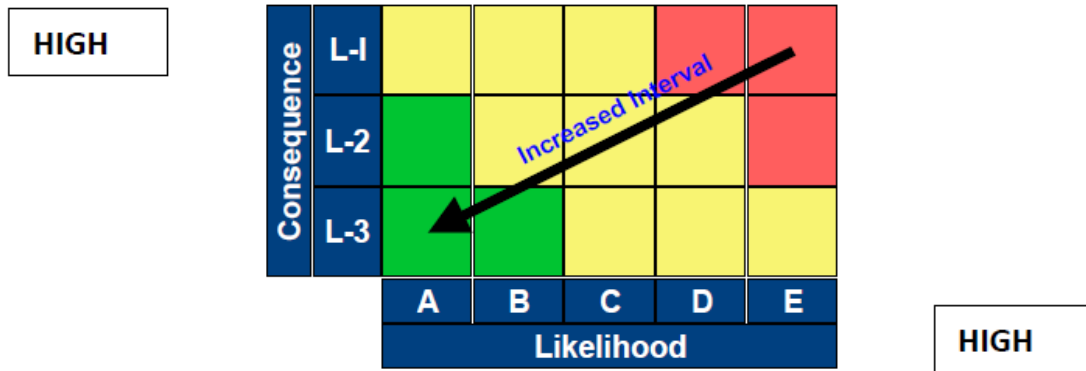


**Figure 1.6 Continuous risk reduction to manage structural risk**  
(O'Connor et al, 2005)

### 1.5 Problem Description

In many cases, integrity management is viewed as restoring to the as-built condition and considerable sums are invested in inspections, or platforms are shut down due to Health, Safety and Environmental (HSE) requirements, when they need not be. Additionally, drilling operations over the past decade has indicated that offshore oil and gas exploration is proceeding to the deeper waters using floating structures rather than the fixed types, predominantly used in the shallower waters. Therefore, more and more the emphasis from operators is to provide justification to continue operating their aging fixed assets while they move strategically to floating assets in deeper waters. An offshore facility which is well managed under an operator structural integrity management system and the use of assessment techniques ensures that the operator has an in-depth knowledge of the structure from installation/acquisition to decommissioning and can make informed decisions on platform life extension especially for aging structures.

A major objective of this thesis is to demonstrate that operating lives of offshore structures can be extended appropriately in the context of structural integrity management of fixed offshore structures, with an improved suite of LKF equations. The suite of LKF equations is applicable to uni-planar K-type joints which will have a significant impact to the industry by

demonstrating greater ultimate strength capacity of fixed offshore jacket template structures. Greater ultimate strength would mean extension of the intervals between the platform underwater inspections and avoidance of costly underwater repairs.

## **1.6 Scope of Present Research**

In 1983, AMOCO conducted an experimental study primarily to determine stress concentration factors associated with gapped K-type steel tubular joints. The LJFs were also calculated as part of the study by using the chord and brace displacements observed of two specimens under eleven load cases. The LJFs calculated were based on the effects of in-plane bending, out-of-plane bending and axial compression and tension. Torsional effects are considered as chord and brace rotations for the out-of-plane condition and defined on Figure 5.4. These test results represent the only published large scale test data on LJF.

Presently there are ten sets of LJF equations that have been used since the 1980s to predict fatigue life and ultimate strength. The derivations of these equations have evolved in many ways to predict the joint behaviour. There is a clear gap in the derivation of all LJF equations currently used in the offshore industry as they are not benchmarked to credible LJF test data but rather to finite element analysis, engineering judgment and ultimate strength test data. Furthermore, the LJF application studies, including codes of practices published, provide limited guidance on the finite element modeling, the incorporation of LJF in the framework to demonstrate its effect on the overall frame mechanism and the applicability of LJF for ultimate strength and fatigue life predictions.

This thesis critically examines the suitability of the existing LJF equations, reviews the guidance provided in the existing studies and describes their limitations for gapped K-type tubular joints. A comparison study and benchmarking study demonstrate that a proposed finite element model provides a good fit with large scale experimental data and is used to develop a suite of improved LJF equations for gapped uni-planar K-type tubular joints. Apart

from producing an improved suite of LJF formulations, the thesis provides a basis to update current offshore structures codes and standards for uni-planar gapped K-joints but also provides a methodology for the derivation of LJFs from credible large scale test data for other tubular joint configurations including multi-planar K-joints, T-joints, Y-joints and X-joints.

## **1.7 Organization of the Thesis**

This thesis presents the research carried out to achieve the above goals in nine chapters. This chapter introduces the subject of study. Brief outlines of the other chapters are presented below.

- Chapter 2 describes the role of LJF within the Structural Integrity Management (SIM) framework for fixed offshore structures.
- Chapter 3 provides a critical literature review of the currently existing LJF formulations showing the merits and limitations of each.
- Chapter 4 provides a critical review of the various LJF studies that have been used in the structural assessments for fixed offshore structures
- Chapter 5 provides a critical review of the AMOCO K-Joint tests and discusses the limitations of the test results and recent studies that have been used to validate the use of the test results within this study.
- Chapter 6 provides details to the development of a finite element model that has been benchmarked to the AMOCO K-Joints and provides a comparison of existing LJF formulations with regards to the AMOCO K-Joint test geometric parameters.
- Chapter 7 provides details on the methodology for the development, by the author, Riaz Khan (RK) LJF equations for uni-planar K-joints which is representative of the geometric ranges of in-service uni-planar gapped K-type joints.

- Chapter 8 provides a validation study of the new RK-LJF equations to demonstrate their appropriateness to ultimate strength against large scale frame test results and fatigue considerations against current industry practices.
- Chapter 9 provides a summary of conclusions and the major findings of the thesis are highlighted. It also provides some suggestions for future work based on the findings of the thesis.

A Glossary of offshore engineering terminologies, relevant to this thesis, is provided in Appendix 1. Appendix 2 provides the details on the thin shell finite elements that have been used extensively in this research. Appendix 3 provides calculations used in developing an initial finite element tubular joint model (RK-FEA) as outlined in Chapter 6. Appendix 4 provides detailed calculations to support the development of the RK-LJF equations. Appendix 5 provides the USFOS input model files for the validation of the RK-LJF equations.

## CHAPTER 2

# The Role of Local Joint Flexibility in the Structural Integrity Management (SIM) of Fixed Offshore Structures

## 2.1 Introduction

This Chapter provides the a basis for the inclusion of LJF in the assessment of fixed offshore structures and demonstrates the role of assessment in the structural integrity management (SIM) framework of fixed offshore structures.

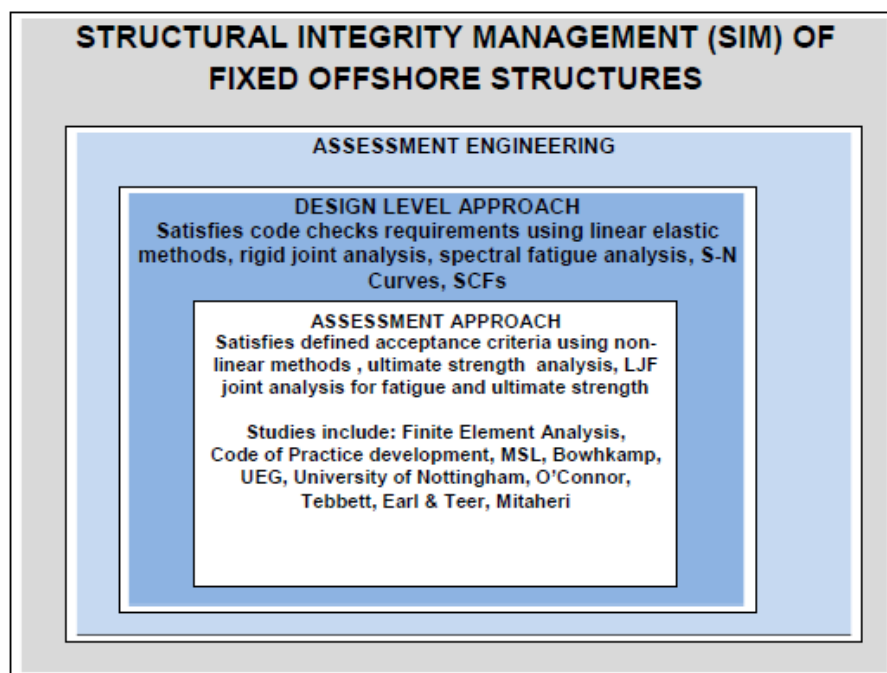


**Figure 2.1 The role of LJF in the Structural Integrity Management of Offshore Structures**

*Note 2: The definitions for offshore engineering terminologies are provided in the Glossary, Appendix 1*

## 2.2 Structural Integrity Management (SIM)

The design process has evolved since offshore platforms were first installed in the Gulf of Mexico in the late 1940s. The first edition of the American Petroleum Institute, API RP 2A used for designing fixed offshore platforms in 1971 to the most recently published API RP 2A 22nd Edition (2014), shows an evolution of the code borne out of significant catastrophic

events, such as the destruction left by Hurricane Camille in 1969 to Hurricanes Ivan, Katrina and Rita in 2004 and 2005. In the case of the latter, over 120 offshore structures were destroyed and an equal number was damaged, with most of these platforms being fixed based structures installed prior to 1980. Figure 2.2 shows the evolution of the API RP Structures Codes up to 2006.

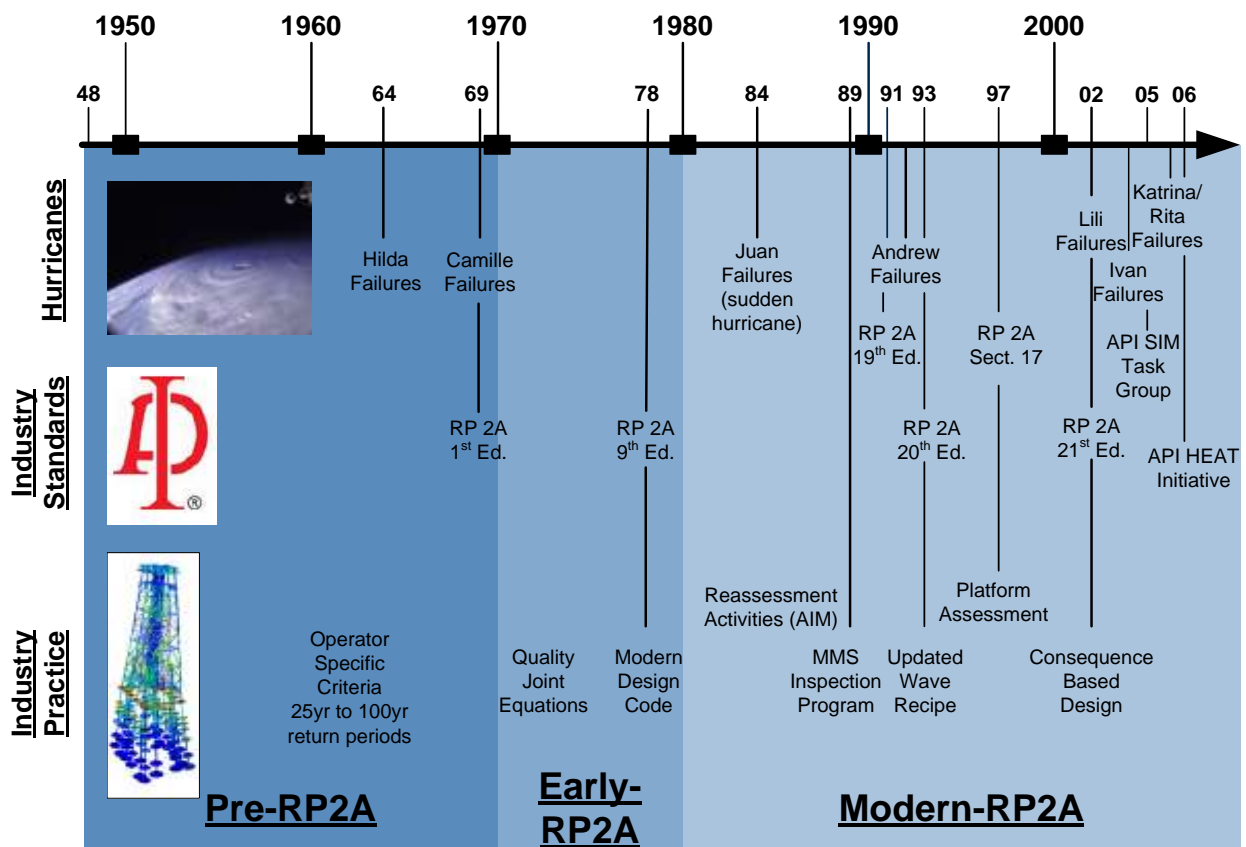


**Figure 2.2 Evolution of the API RP structures codes**  
(O'Connor et al, 2006)

Fixed offshore structures are often classified as pre-API, early API designed up to 1979, modern design API designed from 1980 to 2013 and then 2014 onwards, which will conform to the new API RP 2A 22nd Edition. The majority of structures in existence today will not be able to comply with the most recent design codes of practices as some of them do not have the capacity to pass a code check, especially those designed with K-type, diagonal (D) bracing configurations (Table 2.1). It does not mean that structures with these configurations are not fit for purpose, but there needs to be a further level of assessment to justify continued

operations. Generally, structures designed to current codes exhibit higher levels of structural performance due to better framing systems which introduce higher levels of redundancy into the jacket truss framework. Current design codes tend to be more conservative than assessment codes, as the design process is confined to linear elastic code checks of components such as structural beams, columns and tubular joints. The design of each of these components will have high levels of safety characterized by design factors of safety.

Pre API (before 1971)	Early API (designed from 1971 to 1979)	Modern API (designed 1979 to 2013)	API RP 2A 22 <sup>nd</sup> Edition (2014)
No code of practice exists. Platforms designed based on classic elastic analysis. A variety of bracing configurations.	After Hurricane Camille (1969), the offshore industry presented a set of guidelines for the design fixed offshore structures in the GOM. This formed the basis for the first version of API RP 2A. A variety of bracing configurations including K-type, diagonal (D).	In 1979, API RP 2A 9th Edition provided up-to-date joint configurations based on research on fatigue sensitive joints and industry experience. The industry moved away from K-type bracing to the X-type arrangement.	API RP 2A 22 <sup>nd</sup> Edition implicitly prescribes the use of XH type bracing with perimeter horizontal members when designing steel jacket substructures. API RP 2A 22 <sup>nd</sup> Edition promotes using a baseline ultimate strength analysis at the design stage.

**Table 2.1 Classification of fixed offshore structures, based on their design**

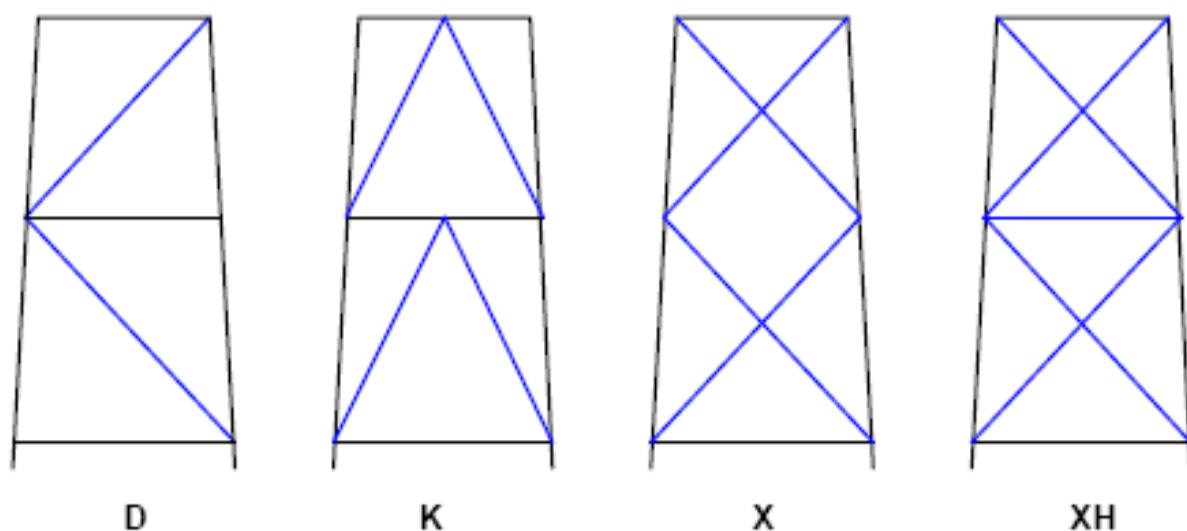


**Figure 2.3 Bracing configurations for fixed offshore jacket structures**

When performing structural fitness for purpose assessments using such technologies as LJF, the focus is on reducing the high levels of design factors of safety to within a tolerable level. These fitness for purpose assessments are usually performed in the form of non-linear analysis and results are required to comfortably exceed the regional acceptance criteria for collapse of the structure. In such cases, the safety of the personnel and offshore structures are never compromised.

		Number of Legs				
		3	4	6	8	M
Brace Configuration	K	NR	NR	NR	MR	R
	D	NR	NR	MR	R	R
	X	NR	MR	R	R	R
	XH	MR	R	R	R	R

NR	MR	R
non-robust	moderate robust	robust

**Figure 2.4 Platform robustness based on bracing configuration (O'Connor, 2005)**

O'Connor (2005) defines the platform robustness is the term used to determine an offshore structure's tolerance to damage and loading beyond its design criteria. Figure 2.4 shows that K-braced structures are considered less tolerant to damage and less robust compared to other configurations. As the K-braced structure becomes older and it becomes susceptible to loss of strength due to corrosion and fatigue, it becomes more important to understand its robustness against its fitness for purpose.

Since the late 1980s and early 1990s, there has been a great debate in the offshore structures community on the format for assessing the integrity of an existing structure. Kreiger et al (1994), Kallaby and O'Connor (1994) and Turner et al (1994) have all put forth methods of assessing and mitigating the effects of an aging structure. O'Connor et al (2005) proposed a framework for the Structural Integrity Management (SIM) framework for fixed offshore

structures, which was the genesis of the current API RP 2SIM. O'Connor et al (2005) discussed the need for having a clear management system for the **Data, Evaluation, Strategy, Program** processes within the lifecycle of an offshore structure. As such, all tools including assessment methods and the LJF approach, found their way under the Evaluation and Strategy processes of the SIM framework (Figures 2.5 and 2.6). O'Connor has specifically acknowledged Local Joint Flexibility (LJF) as a primary tool in both fatigue life estimation and ultimate strength capacity for continuous operations.

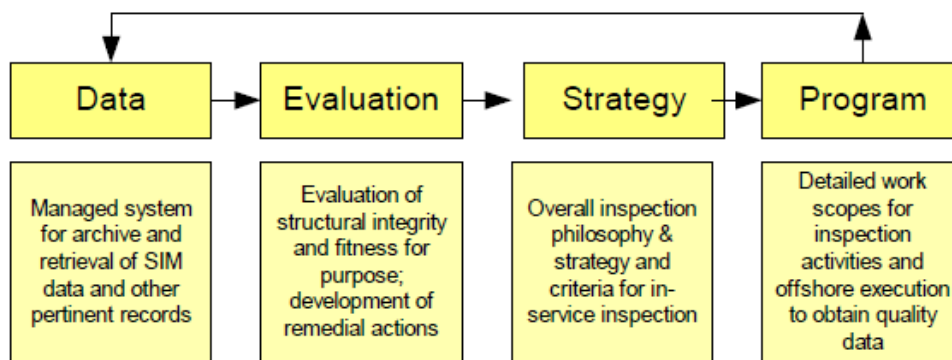


**Figure 2.5 The SIM process**  
(O'Connor, 2005)

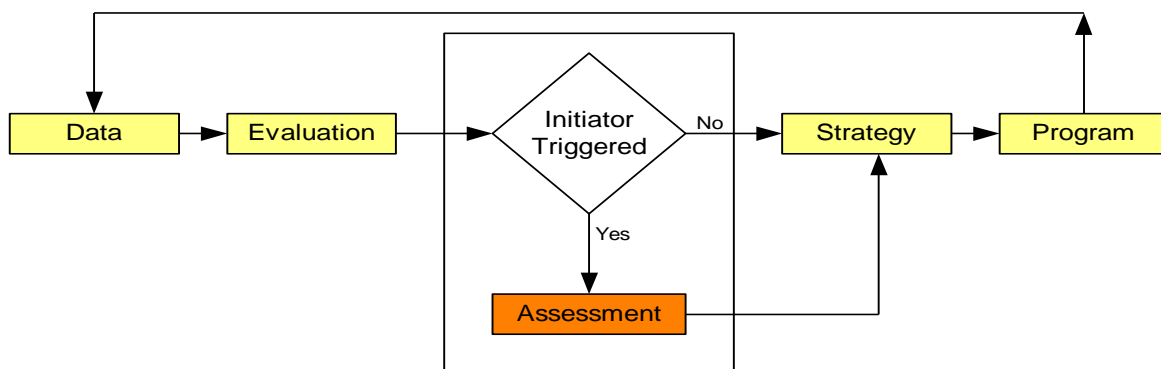


**Figure 2.6 Assessment methods in the Structural Integrity Management framework**  
(O'Connor et al, 2005)

In 2007, ISO 19902 proposed a flowchart for the assessment process for aging structures, (Figure 2.7). If design level checks are not met, then further assessments have to be performed to determine fitness for purpose. There are many assessment initiators that may

trigger a structural assessment. For fixed offshore structures, fundamentally a change in met-ocean loading (i.e. wind, wave or current) acting on the structure will be such a trigger. Structural assessments range from the linear elastic in-place analysis (design level checks) to the non-linear ultimate strength or pushover analysis. The inclusion of LJF in the assessment process is within the *Perform ultimate strength analysis* in the process flow of Figure 2.7. More detail explanation on the relationship between LJF and ultimate strength is provided within Chapters 7 and 8.

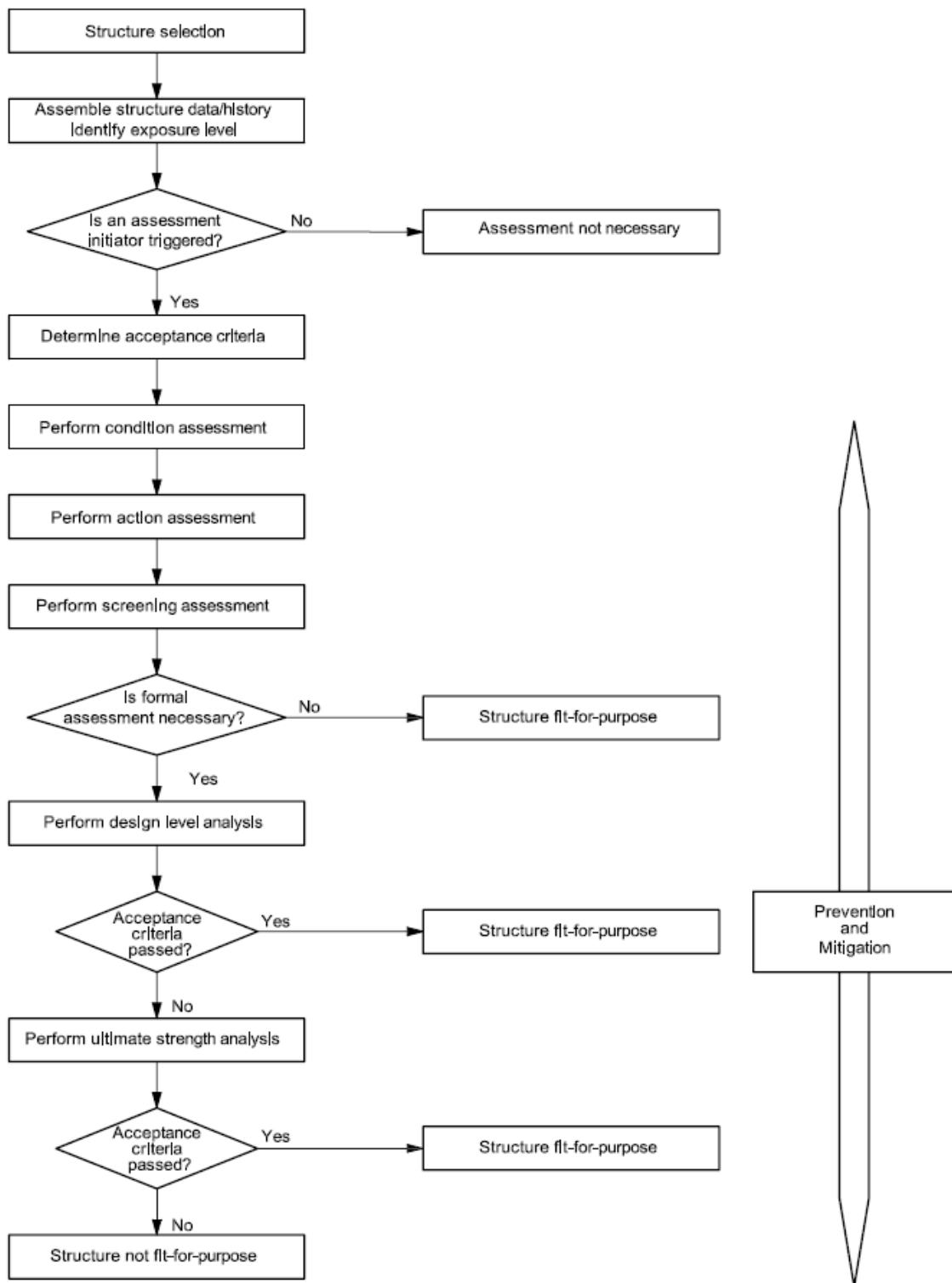


**Figure 2.7 Flowchart of the assessment process  
(Adapted from ISO 19902, 2007)**

### 2.3 Assessment versus Design Approach

This design approach to fatigue life determination is a conservative approach based on the original design some 30 years ago. It considers the stress concentration factor (SCF), the S-N curve, the modeling of the loading and response of the structure and, most significantly, ignores the flexibility of the joints. In the design approach, the joints are modeled as rigid joints with little or no movement. A modified approach uses a more accurate and less conservative combination of S-N curve (i.e. the 1995 T' curve) and SCF formulation than that provided in the API code. The full assessment approach uses the improved SCF and S-N curve but also accounts explicitly for joint flexibility in the analysis. Table 2.2 shows a comparison of the design approach with a modified design approach and a full-blown assessment approach.

	<b>Design Approach</b>	<b>Modified Design Approach</b>	<b>Assessment Approach</b>
S-N Curves	API X'	HSE 1995 T'	HSE 1995 T'
SCF	API	Efthymiou	Efthymiou
Joint Flexibility	Rigid	Rigid	Flexible

**Table 2.2 Comparison of design and assessment approaches  
(O'Connor, 2005)**

This conservatism of original design has been responsible for the extended service of many thousands of platforms operating beyond their design lives without suffering fatigue damage. Since the fatigue design practice is generally adequate for design of new structures, the true fatigue performance of tubular joints is not always widely understood in the design community. When the design approach is used for assessing existing older structures, the implications for project teams can be costly, including unnecessary underwater repairs or strengthening, to return it to as-built condition or perhaps prevention of the project altogether. In assessing an existing older platform the conservatism will inevitably identify many joints well below the desired remaining life of the facility due to micro-cracks and corroded

sections. This is true in all regions of the world, which show consistent distribution in damage and defect trends and damage tolerance. A comparison of damage types in the UK Southern and Central North Sea with damage on Gulf of Mexico (GoM) platforms is shown in Figure 2.8. It is from this perspective that it can be deduced that offshore platforms operating in all regions globally show similar trends in structural performance and studies generated in one operating region can be applicable to other regions.

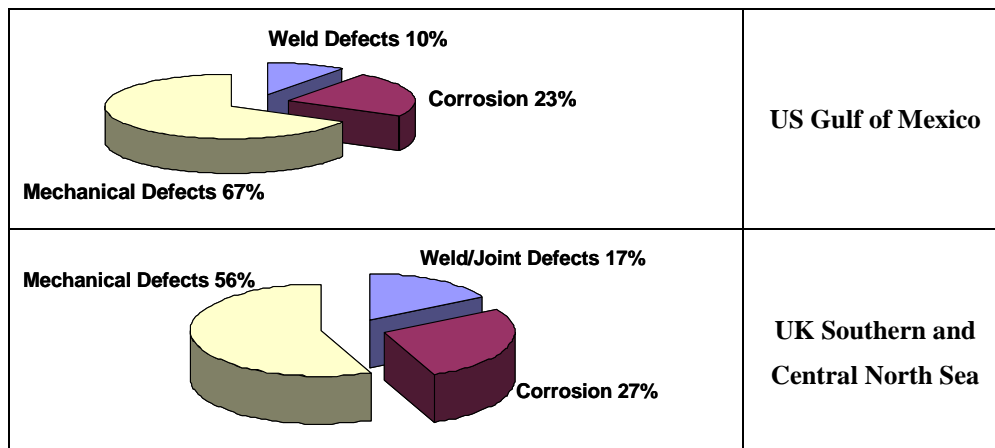


**Figure 2.8 Defect/damage trends in UK and US Gulf of Mexico Waters**  
(O'Connor et al, 2005)

Kallaby and O'Connor (1994) made clear distinction in the analytical techniques for design level and assessment (integrity) level checks on an offshore facility and proposes the use of joint flexibility during the assessment approach as demonstrated by their simplified chart (Figure 2.9), under *Stress Analysis*. With the advent of climate change creating higher waves and wind loads, the use of LJF in any new designs will retain safety factors without excessively increasing costs.

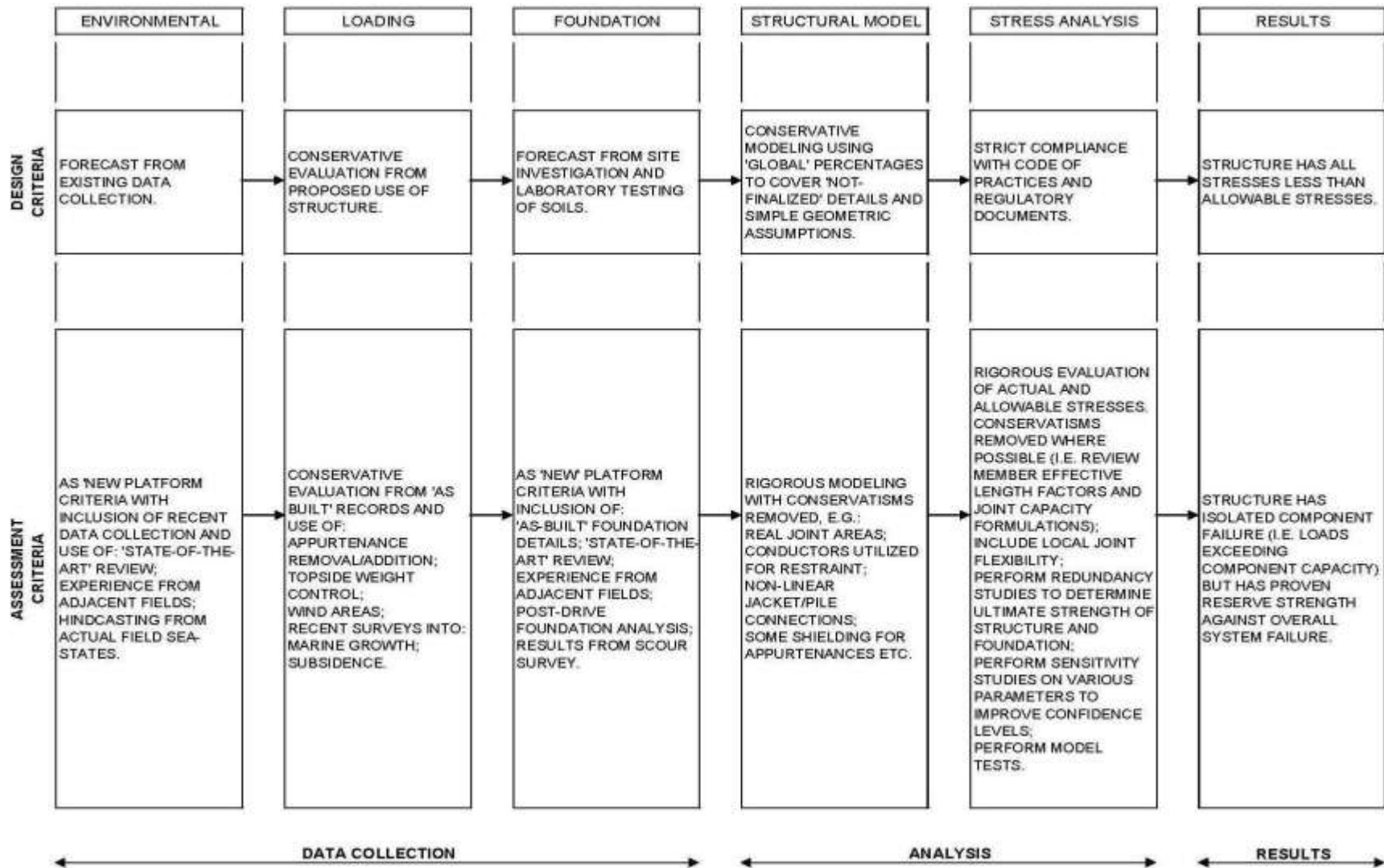


Figure 2.9 Assessment techniques vs design techniques  
(Adapted from Kallaby and O'Connor, 1994)

<b>ASSESSMENT REFINEMENTS</b>	
<b>ANALYSIS</b>	<b>POST PROCESSING / CODE-CHECKING</b>
<b>BASIC ANALYSIS</b> • As-built + modifications • Node-to-node stick model • Remove damaged member?	<b>STANDARD CODE CHECK (API RP2A)</b> • Yield based on SMYS
<b>SIMPLE REFINED ANALYSIS</b> • Member eccentricities/offsets • Remove double counting of wave load • Residual stiffness of damaged member	<b>REFINED P-P / C-C</b> • Yield based on Mill Certificates • Review member effective lengths • Review SCFs
<b>COMPLEX REFINED ANALYSIS</b> • Local Joint Flexibilities (LJFs) • Hindcast site data • Probabilistic loading combinations	• Appraise capacity of damaged elements - Assessment of existing test data - Conduct Fracture Mechanics study • Reliability analysis
<b>ADVANCED ANALYSIS (PUSHOVER)</b> • Non-linear member behaviour • Non-linear joint behaviour	<b>ADVANCED P-P / C-C</b> • Conduct FEA component study • Commission tests

**Figure 2.10 Assessment refinement, including LJF**  
(Adapted from Dier, 2003)

*Note 3: The definitions for offshore engineering terminologies are provided in the Glossary, Appendix 1*

Dier (2003) refers to LJF as an assessment refinement and is generally classified as a complex analysis for joint analysis. Figure 2.10 illustrates the role to LJF by Dier within the assessment process.

## 2.4 Codes and Standards

The main codes and standards used in the offshore structural engineering industry have been the American Petroleum Institute (API), Det Norske Veritas, DNV, NORSOK and International Standards, ISO. The API has been an industry leader in codifying the offshore structural design since the advent of Hurricane Camille in 1969. Since then, API have consistently developed the API RP 2A Working Stress Design (WSD) borne out of the demands of the severe metocean (wind, wave and currents) in the Gulf of Mexico (GoM). Figure 2.10, shows the evolution of the API RP Structures codes up to 2006. Since many of the world’s operating regions do not have their own codes and standards, they have used the API RP 2A to design their structures to the GoM standard. In recent years, OGP’s have acknowledged this is not a good practice and in the early 2000s attempted to improve this by coming together under various task groups to develop a global standard. The ISO 19902, issued in 2007, became the first global code of practice for design of fixed offshore structures.

The main advantage of the ISO 19902 is that it included regional annexes of site specific data (metocean, seismic, vessel collision, etc.) to be used for each of the world's operating regions for design. Furthermore, ISO 19902 provided the then new MSL-ISO joint capacity equations which have been benchmarked to the BOMEL frames tests (1993, 1995). This allowed practicing engineers to consider the effects and benefits of global pushover analyses to determine safety levels rather than relying solely on the classical component design of individual structural components (e.g. beams, bracing, joints, etc.) of the structure.

With a growing aging global fleet, the OGP's realized that guidance must also be provided to consider the structural integrity of existing structures and not only new designs. In recent years, API Recommended Practice, Structural Integrity Management, API RP 2SIM, has been developed to provide guidance to operators for an aging fleet, with some elements of ISO 19902, API RP 21st Ed (Sections 14 and 17) incorporated within it. The publishing of API RP 2SIM took considerable time from its inception in 2006 to final issue in 2014. Due to the many perspectives of each OGP involved in the code development with regards to their then current practices, it was very difficult to gain consensus on a prescribed format for managing the integrity of the fixed structures. As such, there were still areas of ambiguity in API RP 2SIM at the time of issue. In 2014, a new OGP/ISO 19901-09 Task Force was launched to present the format for a new ISO SIM code of practice and to build on the work done by API RP 2SIM to have a more global reach as with ISO 19902. The author of this thesis (Riaz Khan) is a Committee Chair of the ISO 19901-09 SIM Code of Practice. As of mid-2016, the ISO 19901-09 SIM has proceeded for ballot and is currently a DIS (Draft Industry Standard) with an intended issue in late 2016. The codes of practice for offshore structures have specifically mentioned the use of local joint flexibility of tubular joints, but in each case the guidance is fairly limited in scope and not well defined. The only standard that explicitly quotes equations for use is the DNV Offshore Standard (2010), which only makes reference to the Buitrago's suite of equations.

DNV-SINTEF-BOMEL (1999) published the findings of their ultimate strength study entitled "*Best Practices for use of Non-Linear Analysis Methods in Documentation of Ultimate Limit States for*

*Jacket Type Offshore Structures.*” or *Ultiguide*. BOMEL et al encouraged the use of Local Joint Flexibility (LJF) and they acknowledged “*For typical structures the joints may be modeled as rigid connections at the brace to chord intersections. For conventional structures this introduces some conservatism in the analysis results. Joint Flexibility may be modeled by separate finite elements introduced between a node at the chord to brace intersection and the chord center node. The flexibility properties may be assigned to formulae developed by various researchers*”. Table 2.3 provides some of the limited guidance that is provided within the current codes with regards to joint flexibility.

Code of Practice	Clause relevant to local joint flexibility	Interpretation
<p>API Recommended Practice for the “Planning, Designing and Constructing Fixed Offshore Platforms - WSD”. RP 2A</p>	<p>Under the general heading of tubular joints, a self-explanatory section reads:</p> <p><i>“Brace axial loads and bending moments essential to the integrity of the structure * should be included in the calculation of acting punching shear”.</i></p>	<p>The asterisk refers to “<i>Reductions in secondary (deflection-induced) bending moments due to joint flexibility or inelastic relaxation may be considered</i>”</p> <p>Thus the design engineer may carry out a global analysis which incorporates the inherent flexibility of tubular joints. However, no guidance is given on how to obtain the flexibility coefficients. The inelastic relaxation permits the design engineer to redistribute moment loads prior to checking joint strengths.</p> <p>API RP 2A permits an eccentricity of +/- D/4 for normally concentric tubular joints (e = 0 in global analysis) for the purposes of joint detailing. However, API RP 2A requires that for tubular joints where the eccentricity exceeds +/- D/4, the secondary moments caused by this eccentricity should be considered in the global analysis. This is particularly relevant to tubular joints with members of similar diameter.</p>

<p>Det Norske Veritas, DNV  <i>“Rules for the Design, Construction and Inspection of Offshore Structures”</i></p>	<p>Under the section entitled “Buckling of Frames”, DNV require that <i>“Any joint flexibility in the connection of a member to a joint which is of importance for the force distribution in the structure, should be accounted for in the stiffness of the flexibility matrix of the total structure”</i>.</p> <p>DNV further states that, <i>“The rotational flexibility in the connection of the brace to a leg should be taken into account in the global analysis to secure a better estimate of frame bending stresses and bending stresses due to lateral wave and current loading”</i>.</p>	<p>To enable the design engineer to obtain flexibility coefficients, DNV gave two formulae for the rotational spring stiffness for T-joints for in-plane and out-of-plane bending. These formulae are presented as equations (1) and (2) in Section 2.5.1.</p>
<p>British Standards International Standards Organization, ISO 19902 (2007): <i>Fixed Steel Offshore Structures</i></p>	<p>In Section A.12.3.3.3, ISO 19902 states that <i>“Joint flexibility does not significantly affect the primary axial loading in the framework. However, joint flexibility does tend to reduce member end bending moments and increase mid-span moments. The exclusion of joint flexibility will therefore cause an overestimation of end moments and have a conservative effect when checking the framework against joint and member strength requirements”</i>.</p> <p>ISO 19902 further states that <i>“The inclusion of joint flexibility and member end offsets may reduce the global stiffness of the framework and thus increase the fundamental periods of vibration (lateral sway modes) by 3%-6%. Where measured periods are available (e.g. for assessment of existing structures) the structural model may be modified to reflect the measured values”</i>.</p>	

<p>API RP 2SIM <i>“Recommended Practice for the Structural Integrity Management of Fixed Offshore Structures”</i>, 2014</p>	<p>Section C7.6.2 “Analysis Procedures”. The section explicitly states that <i>“Significant redistribution of member forces can result if joint flexibility is accounted for, especially for short bracing with small length-to-depth ratios, and for large leg joint can diameters where skirt piles are used. Joint flexibility analysis may use finite element methods as appropriate”</i>.</p>	
<p>ISO 19901-09 <i>Specific Requirements for Offshore Structures. Structural Integrity Management (DIS)</i></p>	<p>Section A13-1 <i>“Use of theoretical fatigue life in establishing the extent and frequency of joint inspection should account for the actual in-service performance of the surveyed member / joint connections, the effects of joint flexibility on fatigue life, and the influence of each connection on the overall platform safety. Historical inspection data indicates that joint fatigue is not a common occurrence in complex multi-planar connections of older platforms. However, fatigue could be more common in fixed platforms having stiffer joint connections”</i></p>	

**Table 2.3 Code of Practice guidance on joint flexibility  
(ISO 19902, API RP 2SIM, API RP 2A, ISO 19901-09 (DIS))**

The existing codes and standards often consider the use of LJF only in the assessment approach and ignore the benefits that can be derived by using LJF at the design stage, especially in operating regions where the metocean and environmental requirements are severe and thicker and larger sections can be avoided if LJF is implemented. Optimized sections using LJF can provide tremendous cost benefits for large projects, without compromising the inherent safety in design.

Nichols and Khan (2015), while managing the integrity of a fleet of over 200 fixed offshore platforms in South East Asia, have used the API RP 2SIM (2014) as the basis for developing their company’s SIM program. Their structures range from pre-API to those designed to modern API and ISO. They

have also adopted an approach of combining the use of ultimate strength pushover analyses together with LJF to continuously demonstrate fitness for purpose (FFP) as prescribed by ISO 19902. This approach has proved quite beneficial as limited resources can be reallocated, without compromising the integrity and safety of their existing structures, due to LJF implementation. A paper entitled “*Structural Integrity Management System (SIMS) Implementation within PETRONAS’ Operations*” was published by Nichols and Khan (2015) through the Journal of Marine Engineering and Technology (JMET) to demonstrate the holistic implementation of structural integrity management within a global operating company.

In the context of the structural integrity management of fixed offshore structures, there is little published literature on the concept of LJF as a subset to structural assessment process and the limitation of current LJF equations. A paper entitled “*The Role of Local Joint Flexibility (LJF) in the Structural Assessments of Aging Offshore Structures*” by Khan et al (2016) has been accepted for presentation and inclusion of the proceedings at the 12th International Standards of Petroleum Engineers (ISOPE) Conference in Brisbane and provides a summarization of the key concepts on LJF based on the Literature Review (Chapters, 2, 3, 4 and 5) in this thesis.

## **2.5 Summary and Conclusions**

Local Joint Flexibility analysis is an assessment method which is an integral part of the evaluation and strategy processes, within a wider SIM framework, for the continuous operation of an aging structure. It is required to assess the structure for its structural risk at the operating stage of its lifecycle, taking into consideration the structure’s tolerance to damage and corrosion. Early structures were designed to a K-brace type configuration with the K-type tubular joints being a key feature of this configuration. To continue operations for these K-braced structures that have exceeded or are approaching their design life, LJF provides an assessment tool that can refine the structural analysis of the K-joint and provide justification for OGP’s to continue operating. The existing codes of practice provide limited guidance on the applicability of LJF and formulations.

The development of codes and standards may have not been comprehensive enough to provide sufficient guidance to design and integrity engineers to manage fixed offshore structures. It is only with the advent of work done by MSL (1994, 1998) that the industry has been moving to a deeper understanding of the overall system strength for the jacket structures, rather than individual structural components. API RP 2A 22nd Edition Working Stress Design (2014) now advocates the use of ultimate strength analysis at the design stage to consider a baseline risk level for all new installations. There is also an opportunity for OGP's to further combine the ultimate strength analysis with the LJF to get a more effective solution to managing their aging assets especially if the fleet is large in number and resources are limited.

In principle, the current codes and standards do not provide sufficient guidance on the use of LJF but merely makes reference to the possibility of using LJF as an assessment tool. Furthermore, due to this lack of guidance in the codes and standards, many practicing offshore engineers are reluctant to use LJF as they are unsure of its applicability for both the fatigue and ultimate strength considerations. This thesis will address both concepts of structural assessments and demonstrate the applicability of the proposed RK-LJF equations.

The new ISO 19901-09 SIM (DIS) also provides limited guidance on the use of LJF (Table 2.3), but a recently formed ISO task group on tubular joints for ISO 19902 (second edition), has considered a more detailed explanation to be included on LJF in the second edition. This thesis is the most current research with regards to LJF for uni-planar K-type joints and will provide appropriate guidance on the use of the RK-LJF equations and a methodology for developing further LJF formulations for other joint configurations, which can be included in a future ISO 19901-02 second edition, scheduled for issue in early 2017.

## CHAPTER 3

# Literature Review: Parametric Equations and Empirical Formulae for Local Joint Flexibility

### 3.1 Introduction

The body of existing literature on local joint flexibility (LJF) is varied. However, it can be categorized under five major areas, with some overlap from one area to the other. These areas of interest include:

- guidance from offshore structures codes of practices
- finite element modeling
- a series of studies where local joint flexibilities have been applied
- derivation of empirical formulae for local joint flexibility calculations
- tests and experimental data

Figure 3.1 provides an overview of the various studies and guidance that has been reviewed and included as part of this Literature Review. Presently, there are ten published sets of LJF equations that have been used since the 1980s to predict fatigue life and ultimate strength of the jacket structures. The LJF derivations have evolved in many ways, including use of finite element methods to predict the joint behaviour. There has been insufficient benchmarking exercise to large scale experiment. The details of the existing LJF formulations are provided in Table 3.1. This Chapter provides a summarization of each of the ten parametric equations and discusses the merits and limitations of each. From the basic geometry of tubular joints shown in Figure 1.4, the following are definitions to the key parameters that are established within LJF parametric equations. They include  $\beta = d/D$  where  $d$  is the diameter of the brace,  $D$  the diameter of the chord.  $\gamma = D/T$ , where  $T$  is the chord thickness. The gap parameter  $\zeta = g/D$ , where  $g$  is the gap size and  $\theta$  represents angle between brace and chord.

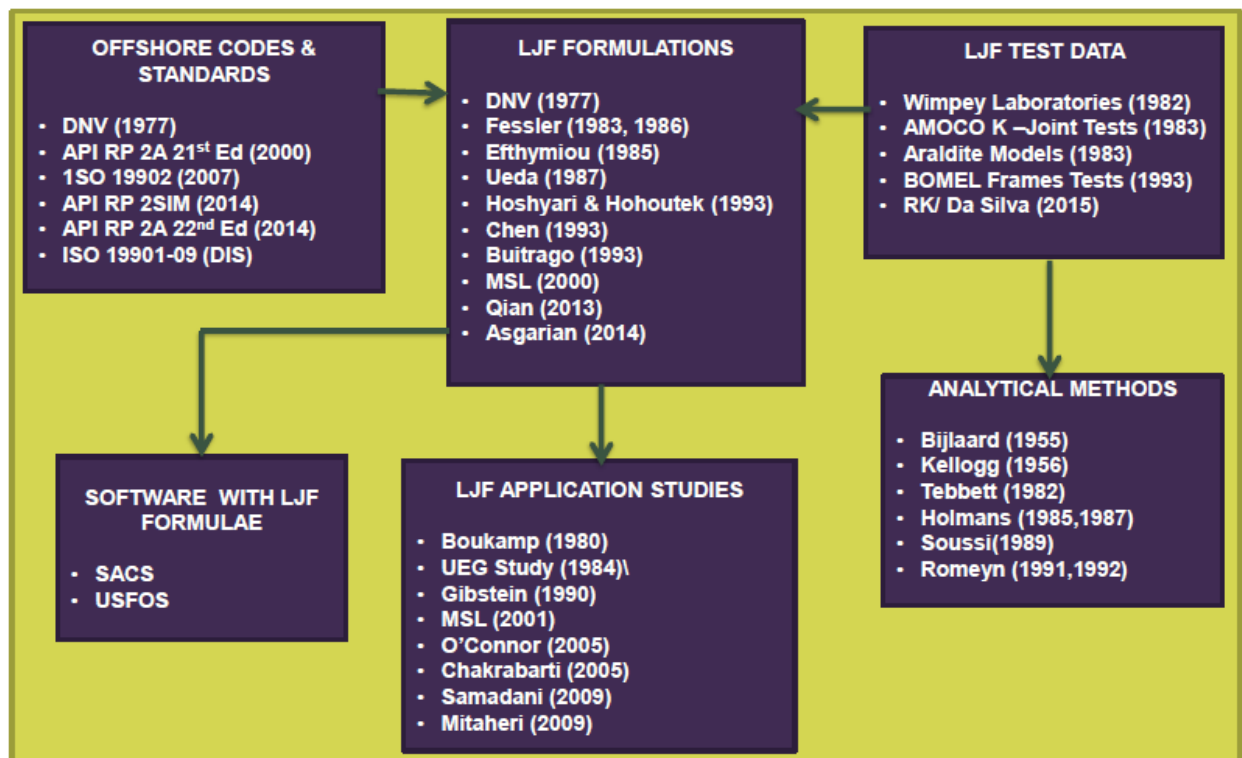


Figure 3.1 Overview of Local Joint Flexibility Literature Review

No.	Year of Study	Researcher	Research/Study
1	1977	Det Norske Veritas (DNV)	Proposed formulae for the translational and rotational spring stiffness for T-joints within the DNV (1977) “ <i>Design, Construction and Inspection of Offshore Structures</i> ”
2	1983 & 1986	Fessler et al. at Nottingham University	Published a set of LJF formulae for T/Y joints based on tests on precision-cast epoxy specimens. The formulae have been updated in 1986 and are generally referred to as the Fessler improved equations. Formulations have now been adopted within the SACS software.
3	1985	Efthymiou	Produced a series of LJF expressions for the bending load cases.
4	1987	Ueda et al	Published LJF equations for 90 degree T-joints under axial load and in-plane bending.
5	1993	Hoshyari and Kohoutek	Published expressions for the flexibility of tubular T-joints studied using a dynamic method of analysis.
6	1993	Chen et al	Modified the earlier work on the semi-analytical method to account for T/Y, K symmetric and K non-symmetric joints and extended the work to cater for multi planar braces.
7	1993	Buitrago et al.	Developed LJF parametric equations which showed a strong dependency on the $\beta$ and $\gamma$ with a lesser influence on the $\tau$ and $\theta$ parameters. Formulations have now been adopted within the SACS software.

8	2002	MSL-Joint	Developed as a part of JIP for ultimate strength, the formulations are now adopted within the SACS and USFOS Software.
9	2013	Qian et al	Attempted to benchmark current research at National University Singapore to MSL equations and BOMEL Frame Tests.
10	2014	Asgarian et al	An FE based study of uni-planar multi-brace tubular Y-T and K-Joints

**Table 3.1 Parametric Equations developed to calculate the effects of local joint flexibilities**

### 3.2 Det Norske Veritas (1977)

The earliest documented work on LJF equations came from a DNV publication in 1977. In Appendix C, Section C1.5.1 entitled “*Buckling of braced frames*” within the 1977 DNV *Rules for the Design, Construction and Inspection of Offshore Structures*, formulae for the rotational spring stiffness for T-joint are presented. In terms of Local Joint Flexibilities (LJF), these equations are expressed as:

$$LJF_{OPB} = 5000 (215-135\beta)^{-1}(\gamma^{-1} - 0.02)^{(1.6\beta-2.45)}/ED^3 \quad (3.1)$$

$$LJF_{IPB} = 18.6 (\gamma^{-1} - 0.01)^{(1.5\beta-2.96)}/ED^3 \quad (3.2)$$

The applicability of the above formulae is for the range

$$10 \leq \gamma \leq 30, \quad 0.33 \leq \beta \leq 0.80, \quad \theta = 90^\circ$$

DNV explains that there are benefits to frame structures by including LJF as part of global performance by considering the performance of joints in relation to the in-plane bending and out-of-plane bending conditions. DNV states that “*Any local flexibility in the connection of a member to a joint which is of importance for the force distribution in the structure should be accounted for in the stiffness or flexibility matrix of the total structure.*” DNV also stated that “*The rotational flexibility in the connection of the brace to a leg should be taken into account in the global analysis to secure a better estimate of frame bending stresses and bending stresses due to lateral wave and current loading.*” DNV considered the effects of LJF on the ultimate strength of the jacket template and ignores any possible effects of LJF on the fatigue prediction of tubular joints. There is also no

background to these formulae that were presented within the DNV document, although Buitrago (1993) did state that these formulae were based on a limited number of finite element analyses. The formulae are limited to the IPB and OPB conditions of T-type joints and no guidance is provided to the axial loaded braces.

As an initial starting point, DNV's work is critical as it links the performance of tubular joints to the IPB and OPB conditions and proposes equations that can be used to consider the effects of LJF on the global performance of a frame structure.

### 3.3 Fessler et al (1983)

By the early 1980s, the DNV equations had been widely used by the OGP's to explain the phenomenon of LJF. However, there was a need to expand the work to develop a full suite of equations for axial, OPB and IPB loading effects for other joint configurations. While the 1983 equations were published by Fessler et al, the work was initiated by OGP's from the North Sea operating region in the form of a major Joint Industry Project (JIP). As funding levels decreased from the OGP's, due to decreased revenues from oil production in the North Sea at the time, Fessler migrated the research fully to the University of Nottingham for completion. In 1983, Fessler of Nottingham University completed a set of joint flexibility formulae for T/Y joints based on precision-cast epoxy resin specimens. The equations were later published in a UEG publication (1985) UR33, "*Design of Offshore Tubular Joints of Offshore Structures.*"

Fessler's formulae for T/Y joints are:

$$LJF_{Axial} = 2.3 \gamma^{2.3} \exp(-3.3\beta) \sin^2 \theta / ED \quad (3.3)$$

$$LJF_{OPB} = 48.1 \gamma^{2.5} \exp(-3.7\beta) \sin^2 \theta / ED^3 \quad (3.4)$$

$$LJF_{IPB} = 171 \gamma^{1.65} \exp(-4.6\beta) \sin^{1.7} \theta / ED^3 \quad (3.5)$$

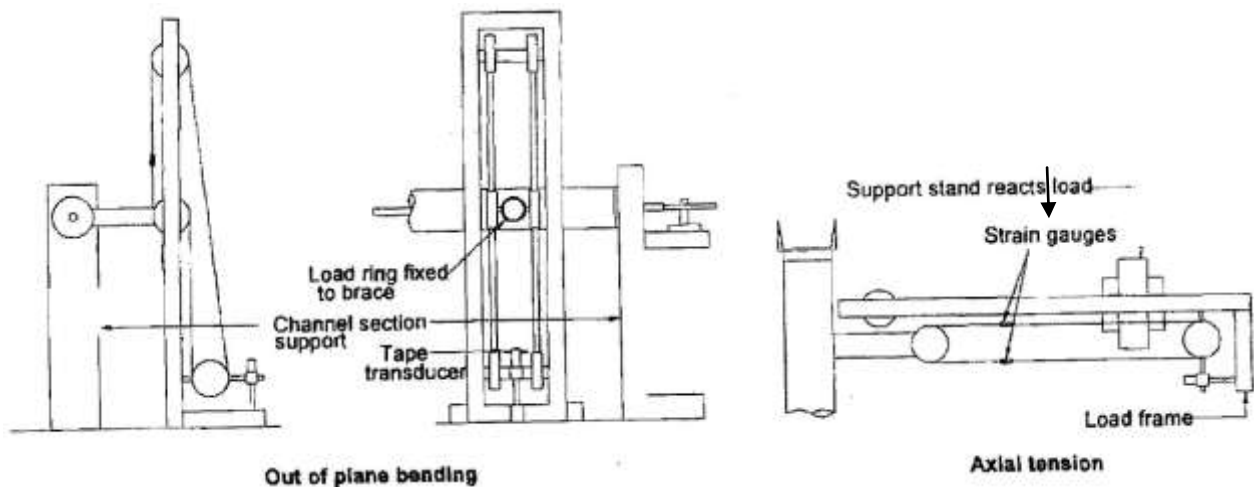


**Figure 3.2 Test Rig used by Fessler (1981)**

There was no range of applicability for these formulae given in the report. Fessler's early work considered the effects of axial loading to improve on the DNV suite of equations and the effects of LJF on the global structure, a fundamental benefit stated in the previous work by DNV. However, the time consuming nature for the experimental work and the high cost of equipment (Figure 3.2), he concluded that there was a need for simpler apparatus to measure the effects of LJF for bending and axial conditions in the future. It is from this perspective that future researchers on LJF performed experimental work on tubular joints rather than the entire frame structure, unless funded by OGP.

### **3.4 Efthymiou (1985)**

In 1985, Efthymiou of Shell/KSEPL attempted to build on the work done by DNV and early Fessler. A fundamental inclusion on this work is that he considered a variety of joint configurations including T, Y and K-type joints. Furthermore, he measured rotations at the end of the brace as shown in Figure 3.3. This is different from all the previous methods where the measurements were made on the chord wall. Fundamentally, Efthymiou did not limit the effects of LJF to the chord only, but demonstrated that the brace deflections also contribute to the overall LJF of the entire joint. He produced a series of joint flexibility expressions for the bending and moment load cases. The report was originally confidential within Shell/KSEPL but is now available to use without confidential restrictions. Twenty four joints were investigated using the finite element method. Thin-shell elements for the members

were combined with brick elements at the weld region. Efthymiou analyzed the linear behaviour of the twenty four tubular joints under out-of-plane bending and in-plane bending. For comparison, one type of geometry was also analyzed using the SATE finite element program which describes the mid-surface of an element. Twelve T-joints, three Y-joints and nine 90°/45° gap/overlap K-joints (with only the 90° brace loaded) were investigated covering a parametric range of:

$$0.31 \leq \tau \leq 0.75, \quad 0.35 \leq \beta \leq 0.75, \quad 12.5 \leq \gamma \leq 30$$

$$45^\circ \leq \theta \leq 90^\circ, \quad -0.50 \leq \zeta \leq 0.75, \quad 6 \leq \alpha \leq 16$$

Efthymiou's formulae for LJF are:

$$LJF_{OPB} = 3.478 \beta^{2.12\gamma(2.2 - 0.7(0.55\beta))} \sin^{(\beta + 1.31)} \theta / ED^3 \quad (3.6)$$

For T/Y and K-Joints, and

$$LJF_{IPB(T/Y)} = 6.154 \beta^{-(2.25 + \gamma/125)} \gamma^{1.44} \sin^{(\beta + 0.4)} \theta / ED^3 \quad (3.7a)$$

$$LJF_{IPB(K\text{ Gap})} = LJF_{INP(T/Y)} / [1 + 0.4\tau \beta^{-1.1} \exp(-1.2\zeta)] \quad (3.7b)$$

$$LJF_{IPB(K\text{ Overlap})} = LJF_{INP(T/Y)} / [1 + 1.9 \tau \beta^{-1.1} \exp(-0.8 \{\zeta \sin \theta_A / \beta_A\})] \quad (3.7c)$$

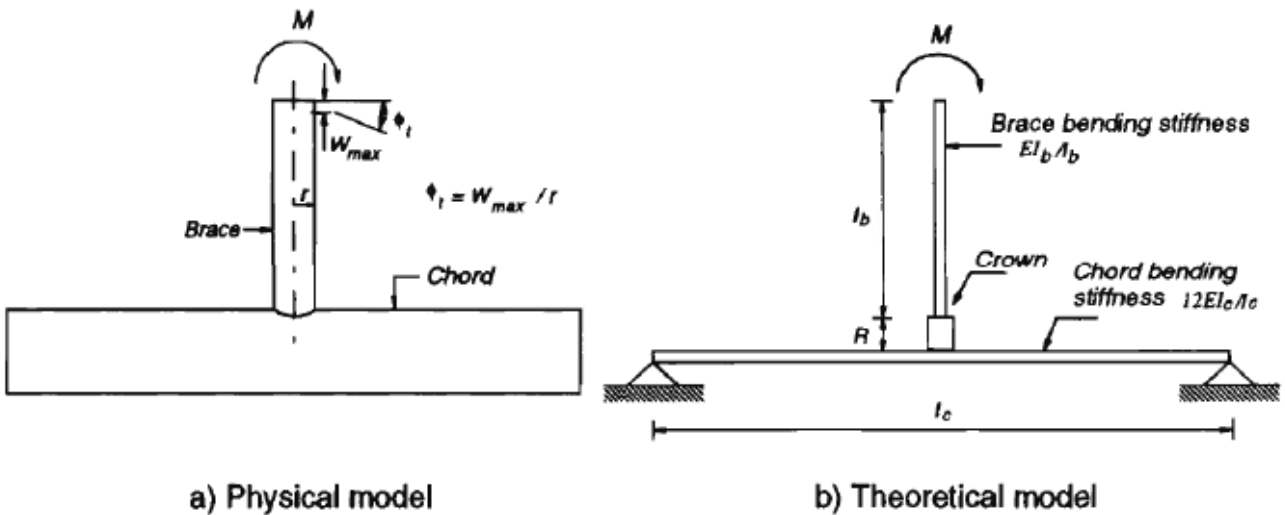


Figure 3.3 Efthymiou's measured rotations for LJF calculation

Efthymiou presents his LJF formulae in a paper as joint stiffness K, where  $K = M/\phi = 1/LJF$ ; however they do not address axial compression and tension loading, which is also a primary load effect for

tubular joints in the offshore industry. When comparing the predicted stiffness values to those in a curve fitting exercise, the values are within 15% for T and Y-joints. For K-type joints, the values are within 30% of the measured stiffness values. His work was inclusive of the common types of joints in the industry but the database of joint geometric parameters is limited. He confined his research to  $\beta$  and  $\gamma$  parameters from the database. A key element to developing a suite of LJF equations is to use an extensive database with a wide range of geometric parameters for the finite element modeling and curve fitting exercise, which will be addressed within this thesis. Furthermore, Efthymiou's work was based on finite element analysis and does not have any comparison with experimental findings, which has proved a limitation on the credible use of his LJF equations.

### 3.5 Fessler et al (1986)

Based on the previous work by Efthymiou and feedback on the applicability of early Fessler's equations, Fessler (1986) re-published his work based on an extensive curve fitting exercise. His database considered more permutations of geometric ranges than did either Efthymiou or early Fessler. Furthermore, Fessler attempted to include the effects of braces and chords on the overall LJF of the joint and presented them as coefficients in a flexibility matrix. Additionally, Fessler extended the knowledge of LJF by not limiting to the effects of uni-planar joints, but proposed additional equations to consider the effects of multi-planar joints. Fessler's formulae were updated in 1986 and the new equations were generally referred to as the Fessler improved formulae:

$$\text{LJF}_{\text{Axial}} = 1.95 \gamma^{2.15} (1-\beta)^{1.3} \sin^{2.19} \theta / ED \quad (3.8)$$

$$\text{LJF}_{\text{OPB}} = 85.5 \gamma^{2.2} \exp(-3.85\beta) \sin^{2.16} \theta / ED^3 \quad (3.9)$$

$$\text{LJF}_{\text{IPB}} = 134 \gamma^{1.73} \exp(-4.52\beta) \sin^{1.22} \theta / ED^3 \quad (3.10)$$

The proposed range of applicability for these improved expressions is:

$$10 \leq \gamma \leq 20, \quad 0.30 \leq \beta \leq 0.80, \quad 30^\circ \leq \theta \leq 90^\circ$$

By locating displacement gauges along the chord and not just near the brace/chord footprint, Fessler determined the displacement at brace locations caused by loading the single brace. Fessler et al

defined the joint flexibilities as the displacements of the braces per unit load attributable to local distortion of the chord cross-section only. The displacements of the brace are determined from the displacements of the four points under the brace on the chord surface. Although a joint may have up to twelve braces (three in each orthogonal plane), only two braces are ever considered at one time, when deriving the flexibility matrix. The displacements, under the unloaded brace, are used to obtain a flexibility sub-matrix (of the complete 6x6 matrix of a two-brace joint) defined by the following equation:

$$\begin{pmatrix} \frac{\delta}{P} \\ \Phi_o \\ \Phi_i \end{pmatrix} = \begin{pmatrix} f_{41} & f_{42} & f_{43} \\ f_{51} & f_{52} & f_{53} \\ f_{61} & f_{62} & f_{63} \end{pmatrix} \begin{pmatrix} \frac{P}{ED} \\ \frac{M_o}{ED^3} \\ \frac{M_i}{ED^3} \end{pmatrix} \quad (3.11)$$

Where:

P is the tension applied to the brace

M<sub>i</sub> is the in-plane bending moment applied to the brace

M<sub>o</sub> is the out-of-plane bending moment applied to the brace

Φ<sub>i</sub> is the in-plane tilt of the brace

Φ<sub>o</sub> is the out-of-plane tilt of the brace

It should be noted that while these formulae cover e/D in the range -0.25 ≤ e/D ≤ 0.25, overlapping braces were specifically excluded. The factors f<sub>11</sub>, f<sub>22</sub> and f<sub>33</sub> are the single brace T/Y joint equations.

Fessler also concluded that any flexibility matrix, which has a displacement ratio less than 0.1 were assumed to be insignificant. For braces in all three planes, no significant values were obtained for the f<sub>63</sub> flexibilities, and for braces in the 180° plane, no significant values were obtained for the f<sub>43</sub>

flexibilities either. It was found that above displacement ratio criterion excluded all data for the  $f_{62}$  term for braces in the  $90^\circ$  plane except that for  $\gamma = 20$ . Hence it was not possible to establish a relationship between the remaining data and  $\gamma$ . However, as the largest value of the displacement ratio for this term for any of the data was still only 0.14, it was assumed that this flexibility could also be neglected. Parametric equations were derived for all of the non-zero terms. Figures 3.4 through 3.7 show the direction of positive loads and displacements to typical joints and the relevant joint parameters.

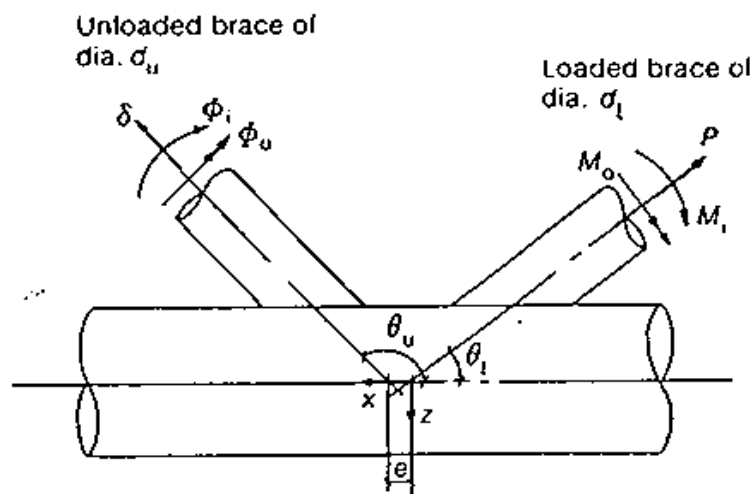


**Figure 3.4 Joint with loaded and unloaded braces in the same plane  
(Fessler)**

Fessler compared the results of his uni-planar equations (Equations 3.8–3.10) with the existing formulations at that time, notably DNV and Efthymiou. He also compared with the values obtained from Tebbett's (1982) experimental work. He reported that Fessler's, Efthymiou's and DNV's LJFs under-predict the axial flexibility term  $f_{11}$  by 15% - 30%. For the OPB condition, both DNV and Efthymiou overestimate by approximately 30% compared to experimental results. For the IPB condition, both DNV and Efthymiou overestimate by approximately 25%. He further concluded that the Fessler's equations give a better agreement (within 20%) with the experimental work compared to the existing LJF equations at the time. Fessler does not consider the brace thickness as having any major contribution to the LJF. The results is not altogether unexpected, as his research is confined to

addressing the chord thickness in the LJF formulation, but brace thickness also has contributing factor to the overall LJF of the system and cannot simply be ignored.

To simplify his LJF formulations, Fessler ignored flexibility matrix terms that he considered insignificant. Since the early 2000s, the advances in computing power have improved considerably to perform structural analysis of tubular joints via finite element modeling. The flexibility matrix terms that Fessler ignored are  $f_{11}$ ,  $f_{43}$  and  $f_{63}$  during his LJF formulation development can now be considered when a modern FE analysis is performed on the tubular joint, to represent the overall LJF flexibility.

In 1986, in a companion paper, Fessler published a set of equations (Equations 3.12-3.14) which relates to the contribution of multi-planar joints or to determine cross-flexibility between any two braces, which may be at orthogonal planes at a joint (Figures 3.6-3.7). As with the work on uni-planar joints, Fessler ignores the thickness of the brace when developing his equations.

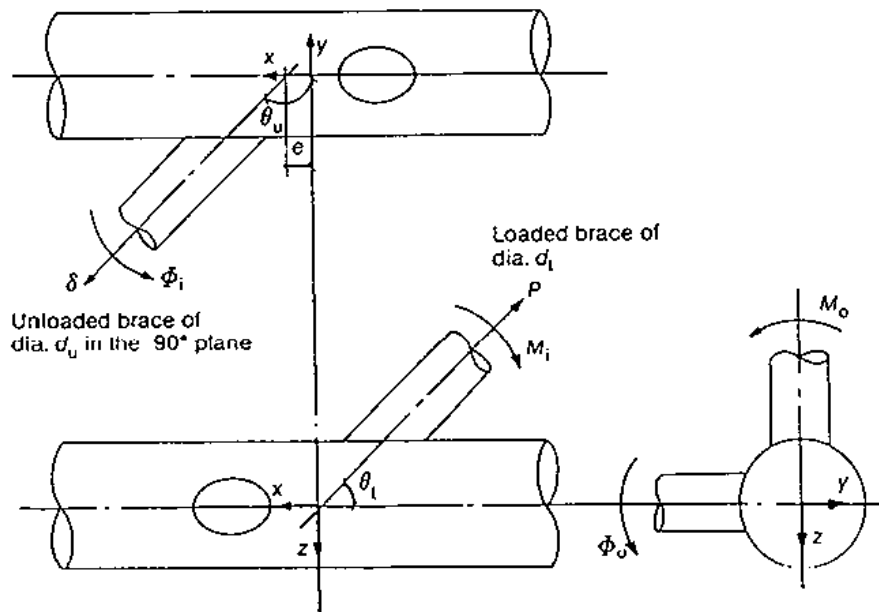


**Figure 3.5 Joint with unloaded brace in the  $90^\circ$  plane  
(Fessler)**

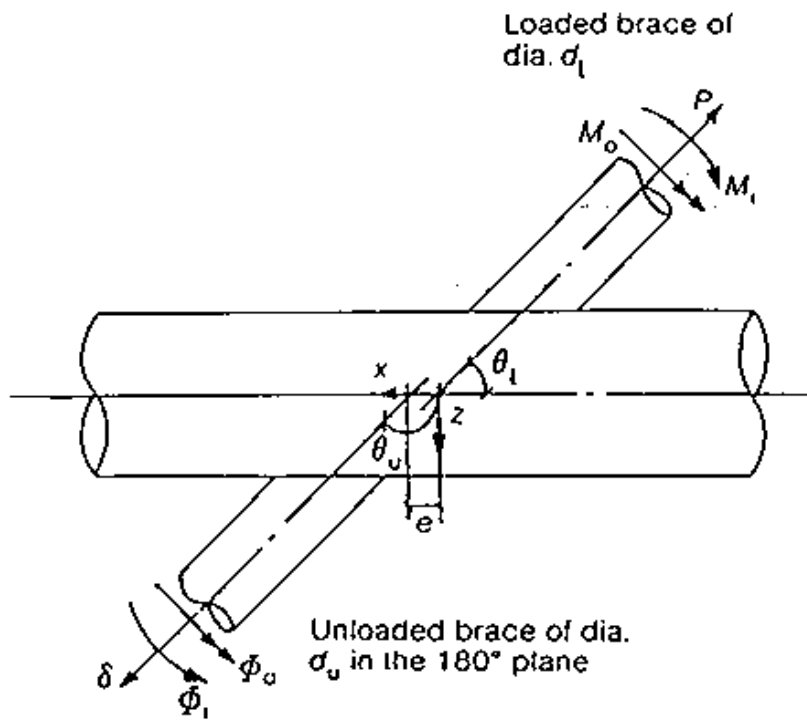


Figure 3.6 Joint with unloaded brace in the  $180^\circ$  plane

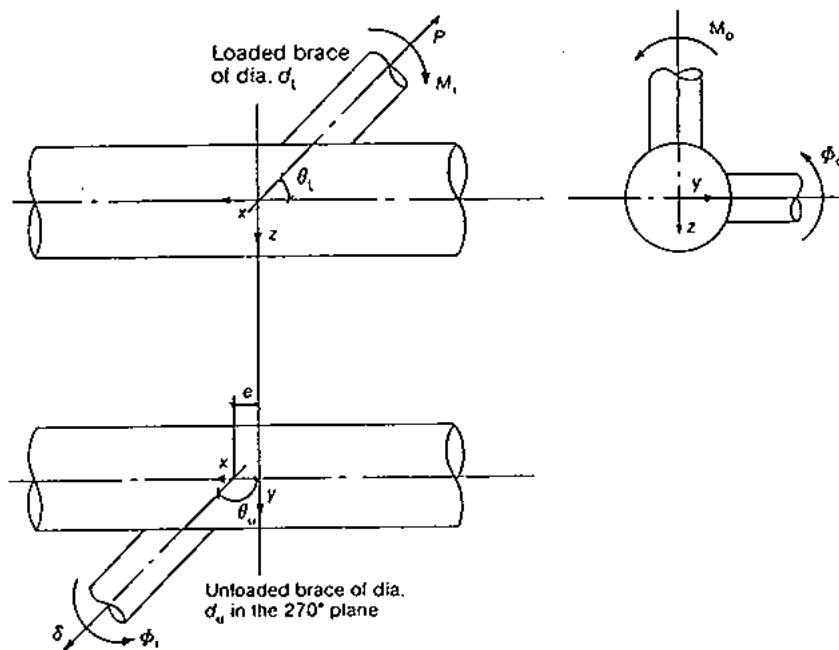


Figure 3.7 Joint with unloaded brace in the  $270^\circ$  plane

In these expressions, subscripts L and U apply to loaded and unloaded braces respectively. It should be noted that  $e$  refers to the exponential function in these equations while the joint eccentricity ( $e$ ) is always referred to in the ratio  $e/D$ .

**a) Braces in 0° plane ( $\theta_L \leq 90^\circ$ ,  $\theta_U \geq 90^\circ$ ) (See Figure 3.4)**

$$f_{41} = 1.26 \gamma^{2.3} (1-\beta_L)^{0.71} \sin^{1.58} \theta_L (1-\beta_U)^{0.48} \sin^{1.76} \theta_U e^{-0.58 e/D} \quad (3.12a)$$

$$f_{43} = 9.42 \gamma^{1.84} \sin^{0.79} \theta_L e^{-1.67 \beta_L} e^{-0.81 \beta_U} \cos(0.52 \theta_U) e^{-0.52 e/D} \quad (3.12b)$$

$$f_{52} = 67.9 \gamma^{2.04} \sin^{1.61} \theta_L e^{-1.22 \beta_L} e^{-1.55 \beta_U} \sin^{2.34} \theta_U e^{-0.94 e/D} \quad (3.12c)$$

$$f_{61} = -16.5 \gamma^{1.2} (1-\beta_L)^{1.62} \sin^{0.71} \theta_L (1-\beta_U)^{0.08} \sin^{-0.36} \theta_U e^{-0.42 e/D} \quad (3.12d)$$

**b) Braces in 90° plane ( $\theta_L \leq 90^\circ$ ) (See Figure 3.5)**

$$f_{41} = -0.77 \gamma^{2.3} \sin^{1.11} \theta_L (1-\beta_L)^{0.58} \sin^{1.35} \theta_U (1-\beta_U)^{0.41} e^{-0.22 e/D} \quad (3.13a)$$

$$f_{42} = 8.67 \gamma^{2.06} \sin \theta_L e^{-2.97 \beta_L} \sin^{1.36} \theta_U e^{-1.76 \beta_U} e^{-0.24 e/D} \quad (3.13b)$$

$$f_{43} = 1.39 \gamma^{1.49} \sin^{0.15} \theta_L \cos(1.56 \theta_U) e^{0.14 e/D} \quad (3.13c)$$

$$f_{51} = -58.4 \gamma^{1.23} \sin^{1.18} \theta_L (1-\beta_L)^{1.60} \sin^{1.20} \theta_U (1-\beta_U)^{1.22} \quad (3.13d)$$

$$f_{52} = -5.48 \gamma^{2.29} \sin^{1.13} \theta_L e^{-0.14 \beta_L} \sin^{1.28} \theta_U e^{-0.79 \beta_U} e^{-0.22 e/D} \quad (3.13e)$$

$$f_{53} = 34.2 \gamma \sin \theta_L \cos \theta_U e^{0.66 e/D} \quad (3.13f)$$

$$f_{61} = -5.83 \gamma^{1.36} \sin^{1.19} \theta_L (1-\beta_L)^{0.29} \cos(1.02 \theta_U) (1-\beta_U)^{0.10} e^{0.60 e/D} \quad (3.13g)$$

**c) Braces in 180° plane ( $\theta_L \leq 90^\circ$ ) (See Figure 3.6)**

$$f_{41} = -0.85 \gamma^{2.24} \sin^{1.14} \theta_L (1-\beta_L)^{0.49} \sin^{1.41} \theta_U (1-\beta_U)^{0.31} e^{-0.28 e/D} \quad (3.14a)$$

$$f_{52} = 3.06 \gamma^{2.32} \sin^{1.21} \theta_L e^{-0.73 \beta_L} \sin^{1.15} \theta_U e^{-0.14 e/D} \quad (3.14b)$$

$$f_{61} = 2.42 \gamma^{1.61} \sin^{1.07} \theta_L (1-\beta_L)^{0.27} \cos(1.03 \theta_U) (1-\beta_U)^{0.11} e^{0.69 e/D} \quad (3.14c)$$

**d) Braces in the 270° plane (See Figure 3.7)**

Equations for braces in the 90° plane, (Figure 3.4) above, can be applied when the unloaded brace is in the 270° plane. However, the signs of the  $f_{42}$ ,  $f_{51}$  and  $f_{53}$  terms have been reversed when the unloaded brace is in the 270°. The results from the sign conventions which define the directions of the loads and displacements are shown in Figures 3.6 and 3.7 for the two load cases respectively.

For the multi-planar joints, Fessler reported that the LJF equations gave an overestimation of up to 70% for joints of high flexibility where a small diameter brace is surrounded by larger diameter braces. While Fessler considered multi-planar configurations when developing his LJF equations, the overall effects of distortion of the chord and the contribution of all braces to this distortion needed further investigation. This work will be addressed further by Chen (1993) and Buitrago (1993) when developing their suite of LJF equations.

Fessler's equations are primarily based on epoxy resins but have not been derived or benchmarked against the performance of tubular steel joints. The performance of steel tubular joints has always been the primary concern of the offshore industry and this thesis will address LJF with regards to steel uni-planar gapped K-joints and validate its derived LJF equations against large scale testing. For the multi-planar work, Fessler uses the same limited database as that used in his uni-planar derivation of LJF equations and also ignores the effects of brace thickness in both formulations. While the experimental methods may have been applicable for the time of testing, the main criticism of the derivation of Fessler's LJF equations comes from him ignoring terms in the flexibility matrix that he considered insignificant, but may not be so. His assumptions were partly due to the lack of advanced computing and engineering software available to researchers at that time. Therefore, Fessler opted for a conservative approach to derive his LJF formulations, which lead to discrepancies between other formulations and experimental results at the time for both uni-planar and multi-planar joints.

This thesis will address the shortcomings of the Fessler work for uni-planar K-type joints, by using appropriate finite element software, like the ABAQUS suite which is a well-established suite for structural engineering applications, a selection of tubular joints that represents a global in service fleet and comparison to tubular joint test results and validation against a 2D frame test results.

### 3.6 Ueda, Rashed and Nakacho (1987)

In 1987, Ueda et al published LJF equations for 90° T-joints under 7 axial load tests at the braces and eleven tests on in-plane bending based conditions. The joint flexibility formulae published by Ueda for T-joints are:

$$LJF_{Axial} = 0.312 \gamma^{2.3} \beta^{1.2} \sin^2 \theta / ED \quad (3.15a)$$

$$LJF_{IPB} = 4.22 \gamma^{1.7} \beta^{-2.2} \sin \theta / ED^3 \quad (3.15b)$$

Their main improvement to the previous work is to provide a suite of LJF equations that are applicable in both the elastic as well as the elastic-plastic ranges and present them on a series of load displacement curves (Figure 3.9) for T and Y-type tubular joints.

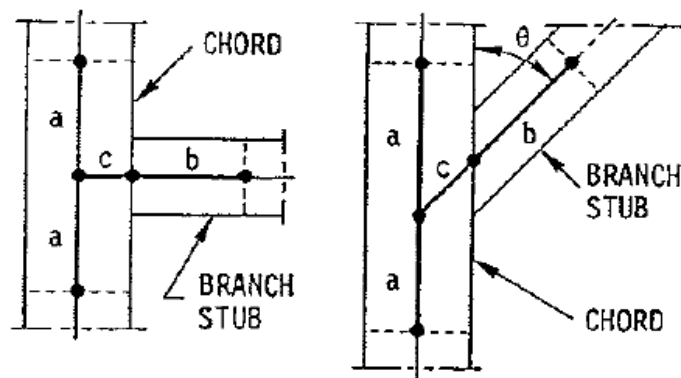


Figure 3.8 Joint Model, T and Y Joint  
(Ueda, 1987)

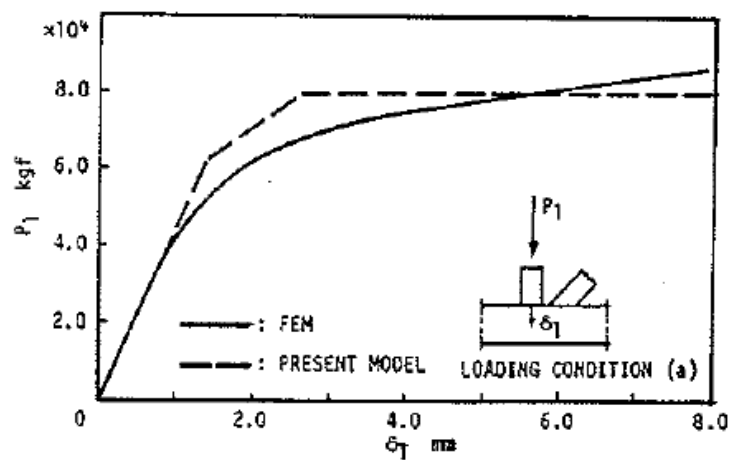


Figure 3.9 Load displacement relationship for one load case  
(Ueda, 1987)

The finite element model was developed similar to Efthymiou model using thin shell elements and compared to the experimental test results. The experimental database is limited to IPB and axial loading but does not consider the OPB condition. No comparison of results is made to the other researchers at the time, such as DNV, Efthymiou or Fessler. These equations are very restrictive as far as the relative size of the members is concerned with the  $\beta$  varying from  $\beta = 0.35-0.55$ . These expressions are valid within the following range:

$$0.35 \leq \beta \leq 0.55, \quad 8 \leq \gamma \leq 30, \quad \theta = 90^\circ$$

and are only applicable for in-plane bending and axial loading effects. Further work was required to the applicability of the LJF equations to other joint configurations and validation in a large scale tubular testing or ultimate strength of large scale frames.

### 3.7 Hoshyari and Kohoutek (1993)

In 1993, Hoshyari and Kohoutek of the University of Wollongong, Australia, published the expressions for the flexibility of tubular T-joints studies. They built their research on the work done by Fessler, Efthymiou and Ueda. Their fundamental contribution to the knowledge on the subject of LJF was to study the effects of LJF on dynamic sensitive structures. Joint flexibility was calculated using a dynamic method using measured natural frequencies. In this study, the in-plane and out-of-plane rigidity of T-joints are investigated experimentally. The test set up to determine the joint rigidity is shown in Figure 3.10.

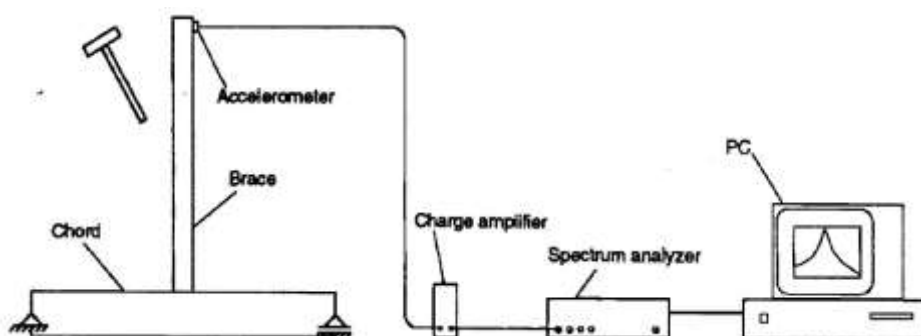


**Figure 3.10 Diagrammatic test set-up for frequency measurements of T-joints (Hoshyari and Kohoutek, 1993)**

From Figure 3.10, the vibration induced by impacting the cantilever, was picked up by an accelerometer mounted on the tip of the cantilever at the joint. The output signal from the accelerometer was amplified and then processed by the Fourier analyzer. The natural frequencies can now be determined from the experimental data. The method used to determine the stiffness or rigidity of the joints via dynamic measurements is the free vibration method. Free vibration method considers the natural frequencies of the structure. Natural frequencies are the eigenvalues of the stiffness matrix of a structure and include the interaction of the members meeting at a joint. Therefore, by knowing the natural frequencies, the rigidity of a joint can be determined by

$$Kx = 0 \text{ or } \text{Det } [K] = 0 \quad (3.16)$$

Using the ALGOR finite element package, 90 degree T-joint configurations with  $D = 219$  mm and  $\alpha = 13.7$  were modeled under three load cases. Stiffness formulae for T-joints are presented based on the finite element results obtained and the effect upon stiffness of the  $\tau$  parameter has been incorporated (the first set of empirical stiffness formulae to do so). Good correlation between the finite element analysis and these formulae were reported, although the finite element data has yet to be published.

The stiffness formulae derived are presented in terms of LJF:

$$\text{LJF}_{\text{Axial}} = 0.436 \tau^{-0.74} \gamma^{(3.1.1.38\beta)} \beta^{(0.31+\gamma/27.7)}/ED \quad (3.17a)$$

$$\text{LJF}_{\text{OPB}} = 11.36 \tau^{-0.312} \gamma^{(3.27-1.87\beta)} \gamma^{(0.31+\gamma/86.4)}/ED^3 \quad (3.17b)$$

$$\text{LJF}_{\text{IPB}} = 6.99 \tau^{-0.205} \gamma^{(1.75-\beta/2.31)} \gamma^{(1.51+\gamma/109.8)}/ED^3 \quad (3.17c)$$

For the following range of validity

$$13 < \tau < 30, \quad 0.3 < \beta < 0.9$$

$$0.2 \leq \tau \leq 1.0, \quad \theta = 90^\circ$$

The experimental measurements and the finite element modeling of the T-joint were compared. With no published finite element data published, the credibility of the derived equations can easily be

questioned. The equations are limited to T-joints and are not applicable to K-joints, which is a major bracing mechanism for aging structures. At this time, there has been little research performed on the effects of dynamics and LJF on the overall performance on fixed offshore structures. The majority of LJF researchers have confined their efforts to the effects of LJF in the static realm. There is an opportunity for more research in this area as some structures are now being installed in deeper waters and some display natural frequencies greater than 3.0 seconds. API RP 2A 22<sup>nd</sup> Edition (2014) classifies dynamically sensitive structures as those having a natural frequency greater than 3.0 seconds.

### 3.8 Chen, Hu and Ma (1993)

In 1990, Chen et al at Shanghai Jiao Tong University, China, used closed form equations together with finite element methods to evaluate components of the joint flexibility matrix. The basis of the work builds on the flexibility equations published by Ueda previously. In 1993, Hu et al modified the earlier work by Chen to account for T/Y, K symmetric and K non-symmetric joints and extended his approach to cater for multi-planar braces, which was introduced previously by Fessler. For T/Y joints, local joint flexibilities were derived based on the local transitional displacement/rotation in the direction of the brace axis.

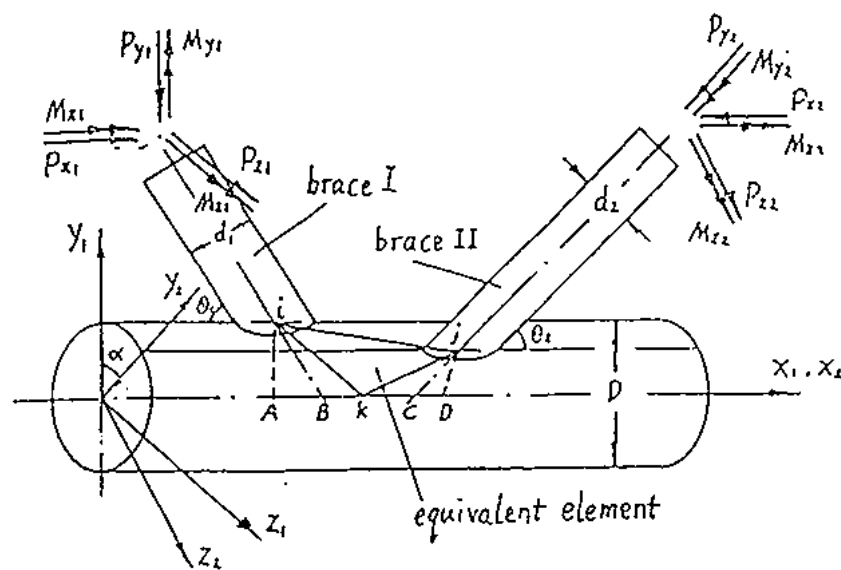


Figure 3.11 The equivalent element method by Chen (1993)

$$LJF_{Axial} = \delta/P = 1/P [ 1/4 \{ \Delta_a + \Delta_b + \Delta_c + \Delta_d \} - V_o] \sin \theta \quad (3.18)$$

Where  $\Delta_a + \Delta_b + \Delta_c + \Delta_d$  are the displacements at the two saddles and the crown positions (defined in the glossary in Appendix 1) and  $V_o$  is the transitional displacement at the mid-brace point on the chord due to the bending of the chord as a beam. Similarly, for the moment load cases, the joint flexibilities may be derived. By regression, analysis of the joint flexibility estimates from finite element analysis, the following formulae were derived:

$$LJF_{Axial} = 3.27 \gamma^{2.26} e^{-3.05\beta} \sin^{1.89} \theta / ED \quad (3.19a)$$

$$LJF_{OPB} = 52.19 \gamma^{2.48} e^{-3.95\beta} \sin^{2.01} \theta / ED^2 \quad (3.19b)$$

$$LJF_{IPB} = 132.49 \gamma^{1.70} e^{-4.32\beta} \sin^{1.22} \theta / ED^3 \quad (3.19c)$$

The equivalent element was proposed by Chen et al to represent the LJF behaviour by introducing a finite element (with LJF properties) into the tubular joint model. The equivalent element was formed from a triangle linking the intersection points on the chord surface under the two braces with the third point on the chord axis, see Figure 3.11. The resulting stiffness matrix [K], can be deduced such that

$$[K] = [B] [A]^{-1} [B]^T \quad (3.20)$$

Where [A] is the LJF matrix

And [B] gives the relative translational elements, thereby giving three force components and three moment components at each of the three points of the equivalent element.

No limitations were proposed on the range of application for these equations. For K-joints the relations between the local displacements are expressed in matrix form,

$$\{\delta\} = [F] \{P\} \quad (3.21)$$

Where  $\{\delta\}$  is a vector composed of the local displacements at the intersections between the braces and the chord wall.

And  $\{P\}$  is the vector composed of the external loads.

$$\{\delta\} = [ \delta_1, \varphi_{01}, \varphi_{11}, \delta_2, \varphi_{02}, \varphi_{12} ]^T \quad (3.22)$$

$$\{P\} = [P_1, M_{01}, M_{11}, P_2, M_{02}, M_{12}]^T \quad (3.23)$$

And the 6x6 local flexibility matrix [F] can be reduced to only eleven independent variables to include:

$$\begin{pmatrix} f_{11} & \blacksquare & \blacksquare & \blacksquare & \blacksquare & \blacksquare \\ 0 & f_{22} & \blacksquare & \blacksquare & \text{SYM} & \blacksquare \\ 0 & 0 & f_{33} & \blacksquare & \blacksquare & \blacksquare \\ f_{41} & 0 & f_{43} & f_{44} & \blacksquare & \blacksquare \\ 0 & f_{52} & 0 & 0 & f_{55} & \blacksquare \\ f_{61} & 0 & f_{63} & 0 & 0 & f_{66} \end{pmatrix} \quad (3.24)$$

Again, formulae for each element in the matrix were developed from the finite element analysis. By performing a regression analysis on these results, simple LJF equations for symmetric and non-symmetric K-joints were developed:

#### a) Empirical Formulae for Symmetric K-Joints

$$f_{11} = f_{44} = 3.66 \gamma^{2.19} e^{-2.74\beta} \sin^{2.11} \theta / ED \quad (3.25a)$$

$$f_{22} = f_{55} = 49.59 \gamma^{2.48} e^{-3.80\beta} \sin^{2.10} \theta / ED^3 \quad (3.25b)$$

$$f_{33} = f_{66} = 111.49 \gamma^{1.73} e^{-3.98\beta} \sin^{1.42} \theta / ED^3 \quad (3.25c)$$

$$f_{41} = 1.37 \gamma^{2.43} e^{-2.22\beta} \sin^{3.00} \theta / ED \quad (3.25d)$$

$$f_{43} = -4.76 \gamma^{1.84} e^{-2.23\beta} \sin^{1.61} \theta / ED^2 \quad (3.25e)$$

$$f_{52} = 5.61 \gamma^{2.81} e^{-1.84\beta} \sin^{3.43} \theta / ED^3 \quad (3.25f)$$

$$f_{61} = 4.76 \gamma^{1.84} e^{-2.22\beta} \sin^{1.61} \theta / ED^2 \quad (3.25g)$$

$$f_{63} = -26.33 \gamma^{1.33} e^{-3.44\beta} \sin^{0.29} \theta / ED^3 \quad (3.25h)$$

#### b) Empirical Formulae for Non-Symmetric K-Joints

$$f_{11} = 4.54 \gamma^{2.16} e^{-2.85\beta} \sin^{2.48} \theta / ED \quad (3.26a)$$

$$f_{22} = 55.37 \gamma^{2.45} e^{-3.82\beta} \sin^{2.22} \theta / ED^3 \quad (3.26b)$$

$$f_{33} = 115.57 \gamma^{1.74} e^{-4.08\beta} \sin^{1.52} \theta / ED^3 \quad (3.26c)$$

$$f_{44} = 3.55 \gamma^{2.21} e^{-2.85\beta} \sin^{0.03} \theta / ED \quad (3.26d)$$

$$f_{55} = 58.07 \gamma^{2.43} e^{-3.85\beta} \sin^{0.03} \theta / ED^3 \quad (3.26e)$$

$$f_{66} = 170.02 \gamma^{1.62} e^{-4.43\beta} \sin^{-0.01} \theta / ED^3 \quad (3.26f)$$

$$f_{41} = 1.30 \gamma^{2.55} e^{-2.68\beta} \sin^{2.44} \theta / ED \quad (3.26g)$$

$$f_{43} = -2.78 \gamma^{1.99} e^{-1.97\beta} \sin^{0.43} \theta / ED^2 \quad (3.26h)$$

$$f_{52} = 5.56 \gamma^{2.86} e^{-2.10\beta} \sin^{2.64} \theta / ED^3 \quad (3.26i)$$

$$f_{61} = 3.96 \gamma^{1.91} e^{-2.10\beta} \sin^{1.97} \theta / ED^2 \quad (3.26j)$$

$$f_{63} = -20.90 \gamma^{1.44} e^{-3.21\beta} \sin^{0.59} \theta / ED^3 \quad (3.26k)$$

Chen's formulae were developed for symmetrical K-type joints and later developed for non-symmetric K-type joints and later to include the axial and in-plane bending for T and Y-joints. Chen used twenty-one points from a structural database, which is not referenced, and the finite element models are developed from this undisclosed source. He develops all terms in the flexibility matrix for K-type joints only and ignores the terms for other joint configurations. The inclusion of an equivalent element to represent an element displaying joint flexibility behaviour is a forward step in modeling the effects of LJF in tubular joints. This work was used by future researchers, including Buitrago, to develop the short beam (flex) element. The work by Chen et al focuses on the finite element method and there is no attempt to benchmark and compare results with experimental work or with other existing LJF formulations available at the time. With the above mentioned shortcomings on Chen's equations, they are rarely used due to lack of confidence in the benchmarking and completeness of the structural database used to develop the equations.

### 3.9 Buitrago, Healy and Chang (1993)

In 1993, Buitrago, Healy and Chang reviewed local joint flexibility of tubular joints. They considered the shortcomings from previous research on LJF and attempted to improve upon them. Buitrago's equations considered single-braced, cross and gapped and overlapping K-type joints. Apart from developing a suite of LJF equations, Buitrago et al compared the use of the spring element vs a short beam (flex) element. The short beam (flex) element is a beam finite element incorporated in the frame analysis to demonstrate the effects on LJF, by having the effects of axial, IPB and OPB in terms of moments of inertia and cross-sectional area and length of the element. Buitrago's work built on the then recent work done by Chen et al on their equivalent element to represent LJF behaviour. Buitrago provided simple expressions for the short stub (flex) element in Equations 3.27 and 3.28 for bending (IPB, OPB) and axial loading respectively. The Area,  $A$ , and the moments of Inertia,  $I$ , of the short beam (flex) element are calculated as follows:

$$I = L / E (LJF_m) \quad (3.27)$$

$$A = L / E (LJF_p) \quad (3.28)$$

Where

- $L$  is the length of the flex-element
- $LJF_m$  is either the in-plane or out-of-plane local joint flexibility
- $LJF_p$  is the axial loading local joint flexibility

In the work comparing short beam (flex) elements to spring elements, Buitrago reported values are within 10% of each other, but the main limitation of the spring element is that it doesn't lend itself easily to be included in most modern finite element computer packages.

Buitrago's paper introduced new parametric equations to calculate the local joint flexibility (LJF) of tubular joints. The parametric joint flexibility equations have been derived from finite element analysis work, which are expressed as a function of the conventional tubular joint parameters, apply to planar

single brace, cross, and gapped and overlapped K-joints. He considers each of the direct or cross terms developed as influence functions. Direct terms are the LJF terms derived from the brace that is directly loaded. Cross terms are those from the unloaded brace. These influence functions when combined provide the overall LJF of the joint.

Using the PMBSHELL finite element program generally employing thick shell elements with some brick elements at the weld region, a total of 192 joints were analyzed: 30 T/Y, 30 X and 63 K Gap and 69 K overlap joints. The joints considered showed a strong dependency on the  $\beta$  and  $\gamma$  parameters with a lesser influence from the  $\tau$  and  $\theta$  parameters. Comparisons of new joint flexibility derived from these data with other equations suggested similar trends, although some differences in IPB LJFs were attributed to the modeling of  $\beta = 1$  joints. For the X and K-joints, direct and cross terms were derived to allow an influence function approach to be adopted. The direct term relates to the reference brace and the cross term being the effect of loading the second brace. The general terminology used by Buitrago for joint definitions are provided within Figure 3.12.

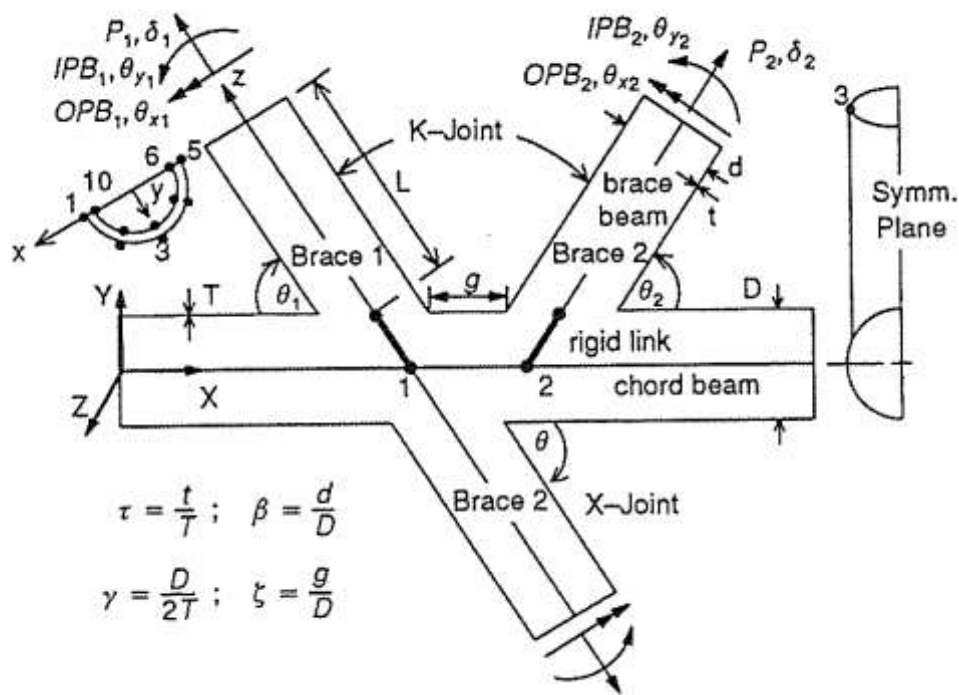


**Figure 3.12 General Joint Geometry, Loads and Degrees of Freedom (Buitrago 1993)**

The LJF formulae and range of applicability for T/Y and X-joints are:

### T/Y-joints

$$\text{LJF}_{\text{Axial}} = 5.69 \tau^{-0.111} \exp(-2.251\beta) \gamma^{1.898} \sin^{1.769\theta} / \text{ED} \quad (3.29a)$$

$$\text{LJF}_{\text{OPB}} = 55.0 \tau^{-0.22} \exp(-4.076\beta) \gamma^{2.417} \sin^{1.883} \theta / \text{ED}^3 \quad (3.29b)$$

$$\text{LJF}_{\text{IPB}} = 1.39 \tau^{-0.238} \beta^{-2.245} \gamma^{1.898} \sin^{1.240} \theta / \text{ED}^3 \quad (3.29c)$$

### X-Joints (Direct terms)

$$\text{LJF}_{\text{Axial}} = 8.94 \tau^{-0.198} \exp(-2.759 \beta) \gamma^{1.791} \sin^{1.700} \theta / \text{ED} \quad (3.30a)$$

$$\text{LJF}_{\text{OPB}} = 73.95 \tau^{-0.300} \exp(-4.478 \beta) \gamma^{2.367} \sin^{1.926} \theta / \text{ED}^3 \quad (3.30b)$$

$$\text{LJF}_{\text{IPB}} = 67.60 \tau^{-0.063} \exp(-4.056 \beta) \gamma^{1.892} \sin^{1.255} \theta / \text{ED}^3 \quad (3.30c)$$

### X-Joints (Cross terms)

$$\text{LJF}_{\text{Axial}} = \tau^{-0.1} (-353 + 1197 \beta - 1108 \beta \sin \theta - 40 \beta \gamma + 50 \gamma \sin \theta) / \text{ED} \quad (3.31a)$$

$$\text{LJF}_{\text{OPB}} = \tau^{-0.1} (2249 + 5879 \beta + 5515 \beta \sin \theta + 221 \beta \gamma - 358 \gamma \sin \theta) / \text{ED}^3 \quad (3.31b)$$

$$\text{LJF}_{\text{IPB}} = \tau^{-0.1} (26 - 75\beta^2 - 8.5\beta^2 \sin \theta + 85 \beta^2 - 7.4 \gamma \sin \theta) / \text{ED}^3 \quad (3.31c)$$

A total of sixty-three gapped K-joints and thirty-nine overlapping K-joints were considered again with direct and cross terms.

### Gap K-Joints (Direct Terms)

$$\text{LJF}_{\text{Axial}} = 5.90 \tau^{-0.114} \exp(-2.163\beta) \gamma^{1.869} \zeta^{0.009} \sin^{1.869} \theta_1 \sin^{-0.089} \theta_2 / \text{ED} \quad (3.32a)$$

$$\text{LJF}_{\text{OPB}} = 49.7 \tau^{-0.251} \exp(-4.165\beta) \gamma^{2.449} \zeta^{0.004} \sin^{1.865} \theta_1 \sin^{0.054} \theta_2 / \text{ED}^3 \quad (3.32b)$$

$$\text{LJF}_{\text{IPB}} = 52.2 \tau^{-0.119} \exp(-3.835\beta) \gamma^{1.934} \zeta^{0.011} \sin^{1.417} \theta_1 \sin^{-0.108} \theta_2 / \text{ED}^3 \quad (3.32c)$$

### Gap K-Joints (Cross Terms)

$$\text{LJF}'_{\text{Axial}} = 3.93 \tau^{-0.113} \exp(-2.198\beta) \gamma^{1.847} \zeta^{-0.056} \sin^{0.837} \theta_1 \sin^{0.784} \theta_2 / \text{ED} \quad (3.33a)$$

$$\text{LJF}'_{\text{OPB}} = 4.37 \tau^{-0.295} \exp(-3.814\beta) \gamma^{2.875} \zeta^{-0.149} \sin^{0.885} \theta_1 \sin^{1.109} \theta_2 / \text{ED}^3 \quad (3.33b)$$

$$\text{LJF}'_{\text{IPB}} = \text{LJF}_{\text{IPB}} - 1.83 \tau^{-0.212} \beta^{-2.102} \gamma^{1.872} \zeta^{0.020} \sin^{1.249} \theta_1 \sin^{0.060} \theta_2 / \text{ED}^3 \quad (3.33c)$$

### For Overlapping K braces (Direct Terms)

$$\text{LJF}_{\text{Axial}} = 3.91 \exp(-2.265\beta) \gamma^{2.010} \zeta^{-0.009} \sin^{1.811} \theta_1 \sin^{-0.029} \theta_2 \quad (3.34a)$$

$$\text{LJF}_{\text{OPB}} = 54.2 \exp(-3.959\beta) \gamma^{2.403} \zeta^{0.001} \sin^{1.856} \theta_1 \sin^{-0.009} \theta_2 \quad (3.34b)$$

$$\text{LJF}_{\text{IPB}} = 1.86 \beta^{-2.093} \gamma^{1.766} \zeta^{-0.029} \sin^{0.711} \theta_1 \sin^{0.036} \theta_2 \quad (3.34c)$$

**For Overlapping K braces (Cross Terms)**

$$\text{LJF}_{\text{Axial}} = 0.48 \beta^{-1.269} \gamma^{2.032} \zeta^{0.072} \sin^{0.949} \theta_1 \sin^{0.954} \theta_2 \quad (3.35a)$$

$$\text{LJF}_{\text{OPB}} = 1.16 \beta^{-2.068} \gamma^{2.550} \zeta^{0.117} \sin^{1.090} \theta_1 \sin^{1.089} \theta_2 \quad (3.35b)$$

$$\text{LJF}_{\text{IPB}} = 0.75 \beta^{-3.000} \gamma^{2.063} \zeta^{1.079} \sin^{0.533} \theta_1 \sin^{0.586} \theta_2 \quad (3.35c)$$

The range of applicability of these formulae are:

$$\begin{aligned} 10 \leq \gamma \leq 30, & \quad 0.25 \leq \tau \leq 1.00, & \quad 30^\circ \leq \theta \leq 90^\circ \\ -0.5 \leq \zeta \leq 0.5, & \quad 0.3 \leq \beta \leq 1.0, & \quad (\leq 0.9 \text{ for overlap K-joints}) \end{aligned}$$

Buitrago considered the use of a gap parameter  $\zeta$ , in his LJF formulations. He reported that for gap sizes above 50mm, the K-joint begins to display properties of a Y-joint. Further work included in ISO 19902 disproved Buitrago's view on the gap parameter. ISO 19902 (2007) considers that for good joint detailing of a gapped uni-planar joint, the minimum distance (gap) between both braces at the chord is 50mm. Therefore the joint can display K-type properties beyond 50mm. Buitrago did not perform a gap sensitivity study to test his hypothesis and this is a limitation on the work he has performed. A major improvement on the work done by Buitrago in this thesis will be to perform a gap sensitivity study to determine the range of applicability of the suite of RK-LJF equations.

To validate the LJF equations, Buitrago compared the finite elements results to the database Fessler used to develop his LJF equations. Fessler's limited data base included 27 Y-type joint and only 3 K-type joints. This comparison exercise is insufficient as it does not consider a variety of geometric parameters to adequately validate the LJF equations. In this thesis, a larger database reflective of all the geometric parameters of uni-planar K-type joints will be used to validate the RK-LJF equations.

Buitrago concluded that the inclusion of local joint flexibility in the global structural analysis of offshore structures can lead to significant redistribution of calculated member-end forces and moments, which in turn may result in lesser structural demands on the tubular joints. In particular, joints to which relatively short members are attached, as in the case of horizontal conductor bracing,

tend to benefit the most. In the re-analysis of existing structures, accounting for LJF may obviate the need of costly, underwater strengthening schemes. To use LJF, however, it is necessary that numerical values for the LJFs be calculated and the plausible models be implemented in the frame analysis software. Incorporating LJF in structural frame models can be done using a short beam (flex) element which displays the properties of LJF and inserted into the joint. This is now a well-established procedure based on Buitrago's work, with many offshore structural software such as USFOS (Ultimate Strength Finite Element Software) and SACS (Structural Analysis Computer Software) having adopted this approach to simulate LJF behaviour in frame structures.

### **3.10 MSL - JOINT Module (2002)**

MSL Engineering (1994, 1998) proposed new joint capacity equations for tubular joints in fixed offshore structures. These were derived from finite element analysis and were validated through databases on tubular joints from Boone et al (1982) and Makino and Kurobane (1986). BOMEL Engineering (1995) published the results of the large scale testing of structural frames, also called the BOMEL frames tests, around the same time. Both projects were conducted on behalf of OGPs. These OGPs in the UK then considered the linkages between the MSL new joint formulations and large scale testing of frames. The MSL joint formulations would later be developed in to the MSL-ISO joint equations and included in the ISO 19902 (2007) Fixed Steel Offshore Structures 1st Edition.

The development of the MSL-JOINT module was achieved in a Joint Industry Project (JIP), which encompassed two phases. In Phase I, all test and numerical data on the load behaviour of tubular joints were collated and carefully screened. From the screened database, robust static strength provisions were derived. From those data where full load deformation ( $P\delta$  or  $M\theta$ ) curves were reported, formulations were developed whereby the load deformation curve, (against  $P\delta$  or  $M\theta$ ) could be recreated from all joint geometry and material properties. These formulations were developed from a range of simple joints which occur in practice.

The success of the new load deformation formulations in predicting  $P\delta$  and  $M\theta$  responses compared to the previous joint capacity equations, gave confidence in moving the JIP to the second phase. Phase II developed the Phase I load deformation formulations to address pertinent influencing factors such as: interaction with chord, joint classification of axial loads, interaction (coupling) between  $P\delta$  and  $M\theta$ , ductility limits and unloading behaviour, which were lacking from previous joint capacity formulations.

The studies resulted in a set of mathematical formulations or algorithms which were then coded up in a series of sub-routines leading to a joint module (MSL-JOINT). The module was tested to ensure correct function against individual joint test/numerical data then calibrated against test data for steel frames. The SINTEF analysis package, USFOS, was the vehicle used to develop, test and calibrate the module.

In 2002, Adrian Dier (MSL Engineering) and Oyvind Hellan (SINTEF) proposed this non-linear tubular joint response model for pushover analysis. The work reported concerned the development, testing and calibration of an efficient analysis tool (a joint module called MSL-JOINT) that allows the behaviour of tubular joints within a space frame structure to be appropriately accounted for. Since the MSL-JOINT represents the overall performance of the joint, then the effects of LJF has been accounted for its load displacement responses under axial, IPB and OPB.

The attention was directed at representing the  $P\delta$  curve by a single continuous function with coefficients related to the joint geometric parameters  $\beta$ ,  $\gamma$  and  $\tau$  and material properties. Following trials with a few mathematical functions, an exponential expression was selected. In its simplest form, this can be written as

$$P = d - a (1 - b \cdot \exp \{-c \delta\})^2 \quad (3.36)$$

Where a, b, c and d are constants (or more correctly, functions of joint geometry) to be fitted. The more important findings for the analysis were noted as

- The constant ‘d’ is directly associated with  $P_u$  the maximum constant load
- The constant ‘a’ is the magnitude of the drop in load following the peak
- The initial stiffness of the  $P\delta$  curve (at the origin) is given by:

$$K = 2 a b c (b-1) \quad (3.37)$$

Fitting to the experimental data was performed with a non-dimensional form of the Equation (3.36).

Taking into account the dependency of one of the constants on the others, the final  $P\delta$  and  $M\theta$  formulations from Phase I were:

$$P = P_u (1-A [1- (1+1 (A)^{-2}) \exp\{-B\delta/f_y d\}]^2) \quad (3.38)$$

$$M = M_u (1-A [1- (1+1 (A)^{-2}) \exp\{-B\theta/f_y d\}]^2) \quad (3.39)$$

Where:

$P, M$  = joint load

$P_u, M_u$  = joint mean strength

$\delta$  = joint deformation (aligned to an individual brace)

$\theta$  = joint rotation (radians)

$D$  = chord diameter

$F_y$  = chord yield stress (N/mm<sup>2</sup>)

$A, B$  = fitted “constants” for any joint geometry and load type.

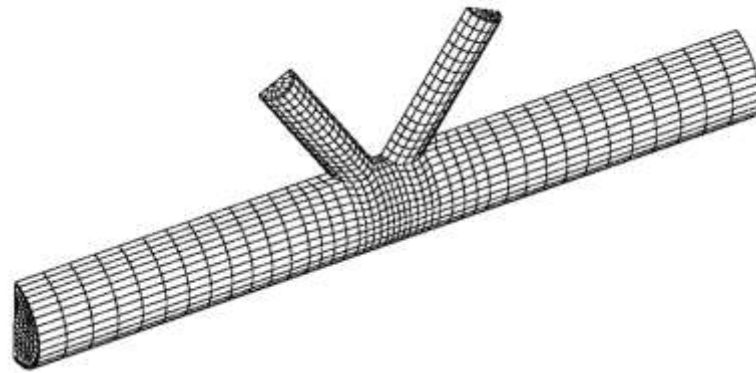


**Figure 3.13 FE Mesh for K-Joint  $\beta = 0.4$**   
(Dier 2002)

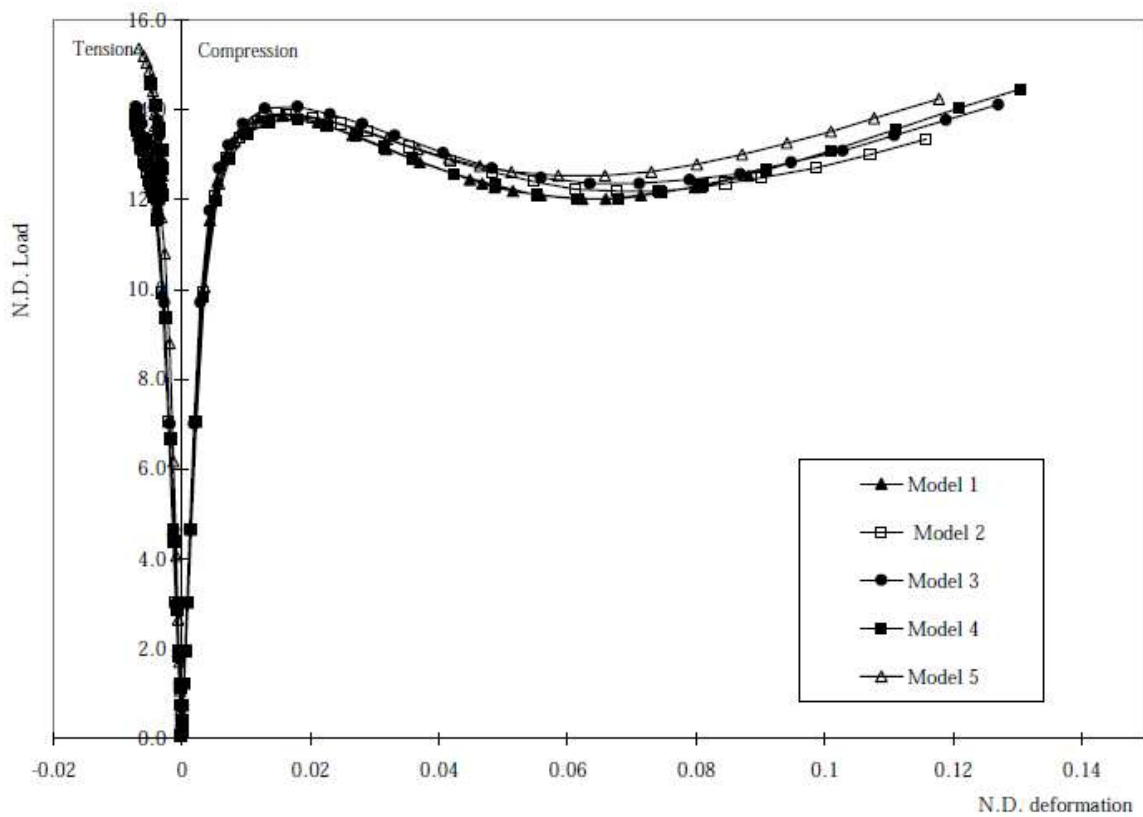


**Figure 3.14 Pδ curves for K-Joint  $\beta = 0.4$ ,  $\gamma = 15$ ,  $\tau = 0.81$**   
(Dier 2002)

MSL performed the Phase II work building on their own MSL formulation and benchmarking the formulation against the BOMEL frame tests; however, Dier et al still investigated the role of joint classification on joint stiffness, or its reciprocal the Local Joint Flexibility (LJF). He performed a series of pushover analyses for rigid joints, MSL formulations and BOMEL tests to compare the results (Figure 3.15).

For predicting frame behaviour, the MSL-JOINT must necessarily be used in conjunction with a frame analysis finite element package. The frames are modeled as beam-column elements. When performing the frame analysis, only the joint of interest was selected to be analyzed with the MSL-JOINT and the remaining joints were treated as rigid. Despite the good performance of capturing individual joint behaviour in order to have more accurate simulations of frame behaviour, certain adjustments were made to the module. These adjustments are mainly concerned with the value of the chord stress factor ( $Q_f$ ). It should be noted that the  $Q_f$  factor is one of the least researched areas in tubular joint technology.

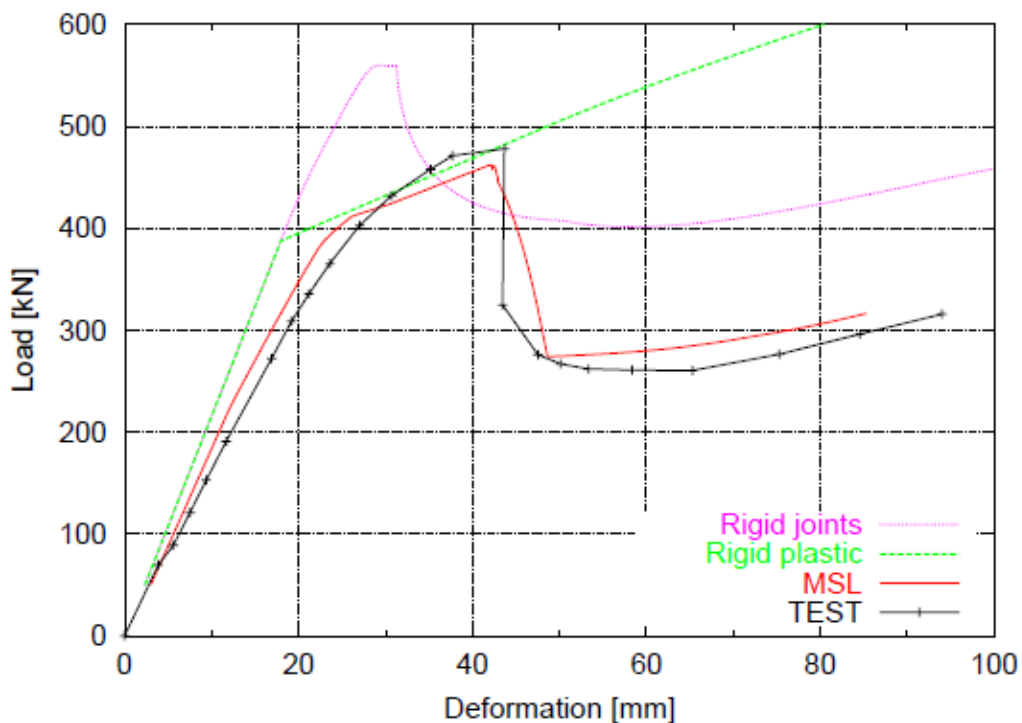


**Figure 3.15 BOMEL Frame Tests VII behaviour compared to test measurements**

MSL reported that the MSL JOINT frame is about 4 times more flexible than the rigid frame and is in good agreement with the BOMEL Frame test data. Dier then concluded that since the Local Joint Flexibility (LJF) for a given joint will change during a complete pushover analysis e.g. due to load redistribution following non-linear behaviour, it will be necessary to apply platform loads incrementally. For the initial increment or increments, the structure will be elastic and member loads generally small. During this phase of the LJFs for axial, in-plane bending (IPB) and out-of-plane

bending (OPB), behaviour will be uncoupled and the effects of the load negligible. There is difficulty with the selection of the axial LJFs for the first increment, as the axial LJF for each brace is dependent on the joint classification which, in turn, is dependent on the loads in all braces at the joint, which are unknown at the outset of the analysis. The difficulty does not arise with the moment LJFs as, in common with the moment capacity, these are not dependent on joint classification. The mean joint capacities for use in the  $P\delta$  and  $M\theta$  Equations are provided in Table 3.2. Dier et al concluded that the testing and calibration exercises have demonstrated that in general the MSL-JOINT is successful, leading to more accurate analyses than the traditional approach of using rigid joint assumptions. Better correlation with the test data is achieved with respect to initial global stiffness, component failure sequence, peak global load and post-peak global response. Dier et al further concluded that in addition to the global system response, use of the MSL-JOINT will lead to increased accuracy of member/joint loads with attendant benefits for component checking, including fatigue life estimation.

Joint Type	Load Type	$P_u$ or $M_u$
T/Y	Compression	$1.27 (1.9 + 19\beta) Q_\beta^{0.5} Q_f F_y T^2 / \sin\theta$ (3.40a)
	Tension	$(42.3 \beta + 17.6) Q_f F_y T^2 / \sin\theta$ (3.40b)
	IPB	$5.5 \beta \gamma 0.5 Q_f F_y T^2 d / \sin\theta$ (3.40c)
	OPB	$4.2 \gamma^{(0.5 \beta^2)} Q_f F_y T^2 d / \sin\theta$ (3.40d)
DT/X	Compression	$1.16 (2.8 + 14\beta) Q_\beta Q_f F_y T^2 / \sin \theta$ (3.40e)
	Tension <sup>(4)</sup>	$(37.3\beta + 6.6) Q_f F_y T^2 / \sin \theta$ for $\beta \leq 0.9$ (3.40f)
		$[40 + (\beta - 0.9) (37.6 \gamma - 364)] Q_f F_y T^2 / \sin \theta$ for $\beta > 0.9$ (3.40g)
	IPB	$5.5 \beta \gamma 0.5 Q_f F_y T^2 d / \sin\theta$ (3.40h)
	OPB	$4.2 \gamma^{(0.5 \beta^2)} Q_f F_y T^2 d / \sin\theta$ (3.40i)
K	Balanced Axial <sup>(5)</sup>	$1.30 (1.9 + 19\beta) Q_\beta^{0.5} Q_g Q_{yy} Q_f T^2 / \sin \theta$ (3.40j)
	IPB	$5.5 \beta \gamma 0.5 Q_f F_y T^2 d / \sin\theta$ (3.40k)
	OPB	$4.2 \gamma^{(0.5 \beta^2)} Q_f F_y T^2 d / \sin\theta$ (3.40l)

$$1. Q_{\beta} = 0.3 / (\beta (1.0 - 0.833\beta)) \quad \text{for } \beta > 0.6 \quad (3.40m)$$

$$= 1.0 \quad \text{for } \beta \leq 0.6$$

$$2. Q_g = 1.9 - (g/D)^{0.5} \quad \text{for } g/T \geq 2.0 \quad (3.40n)$$

$$= 0.13 + 0.65 \varphi \gamma^{0.5} \quad \text{for } g/T \leq -2.0$$

Where  $\varphi = t F_{yb} / (TF_y)$

$$3. Q_{yy} = 1.0 \quad \text{when } \theta t \leq 4\theta_c - 90^\circ \quad (3.40o)$$

$$= (110^\circ + 4\theta_c - \theta_t) / 200^\circ \quad \text{when } \theta t > 4\theta_c - 90^\circ$$

4. The expression for tension loaded X-joints when  $\beta > 0.9$  should only be applied when the braces are reasonably co-linear (say  $e/D \leq 0.2$ ). If the braces are not reasonably co-linear, the expression for  $\beta \leq 0.9$  should be invoked.

5. The expression for a K-Joint under balanced axial loading relates to the compression brace. For the tension brace, increase the calculated value of  $P_u$  by 10%.

**Table 3.2 Mean joint capacities for use in P $\delta$  and M $\theta$  Equations  
(MSL, 2002)**

While the MSL Joint formulation can be used for frame behaviour for ultimate strength, it does not explicitly demonstrate and measure the contribution of LJF to ultimate strength. Furthermore, no guidance is provided on MSL-JOINT in the calculation of fatigue life prediction of tubular joints. The primary objective of Phase II study was to provide a basis for adopting the MSL-JOINT formulation as a joint strength equation considering both linear and non-linear behaviour of tubular joints. The main focus was on benchmarking against large scale testing, but additional work by Dier revealed that the LJF is considered in the MSL-JOINT formulation. It does not draw on previous studies on LJF with no reference to LJF considerations for multi-planar joints or the effects of cross and direct terms. In frame analysis, the MSL-JOINT module has to make certain adjustments (within the USFOS software, selection tool) to account for the Qf factor and is therefore reliant on the software package to

be effectively used. With regards to this research, the RK-LJF parametric equations is a major improvement of the MSL-JOINT module, as it can be used for fatigue life predictions as its basic inputs are geometric properties of tubular joints. The RK-LJF equations are effectively benchmarked to large scale frame testing and can be used to determine the ultimate strength results of the K-joints without any adjustment to the chord stress factor.

### 3.11 Qian, Zhang and Yoo Sang (2013)

Developed with similar intent as the MSL formulations, Qian et al seeks to benchmark its formulations for ultimate strength with the BOMEL 2D Frames Tests. The lists of specimens used in the finite element and experimental work were the ones provided by Vegte (1995) and Kurobane (1986). These specimens do not represent an exhaustive list of in-service tubular joints. The load deformation formula provides responses to CHS X and K-type joints.

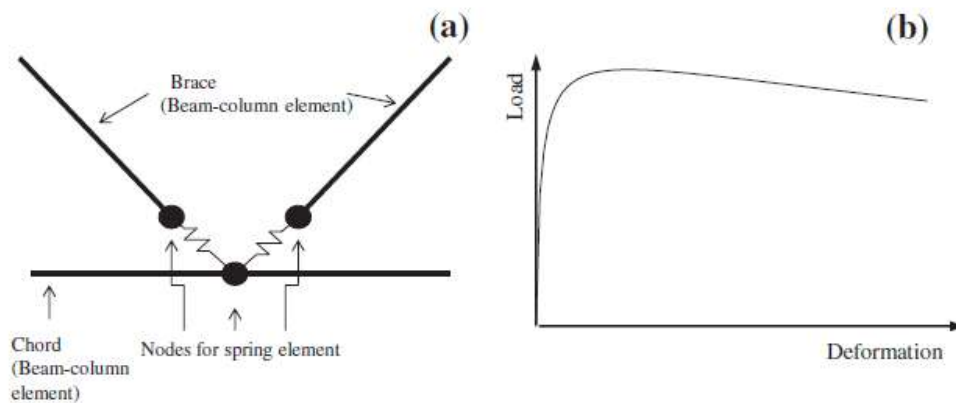


**Figure 3.16 (a) Joint Spring representation in the global frame analysis  
(b) Load deformation characteristics of the joint spring (for axial and bending)**

Spring elements were used to simulate the joint behaviour in the structural models (Figure 3.16). Figure 3.17 shows the FE mesh and the load deformation curves of the joint tests performed at National University of Singapore. Figure 3.16 presents the BOMEL Frames I, II and III that were used to benchmark the FE work and joint test results against. The parametric FE analysis covers a  $\beta$  range of 0.30 to 1.0 and a  $\gamma$  range from 7 to 25. The finite element models have been developed without joint cans (thickened sections) included as the BOMEL Frames tests did not include these sections.

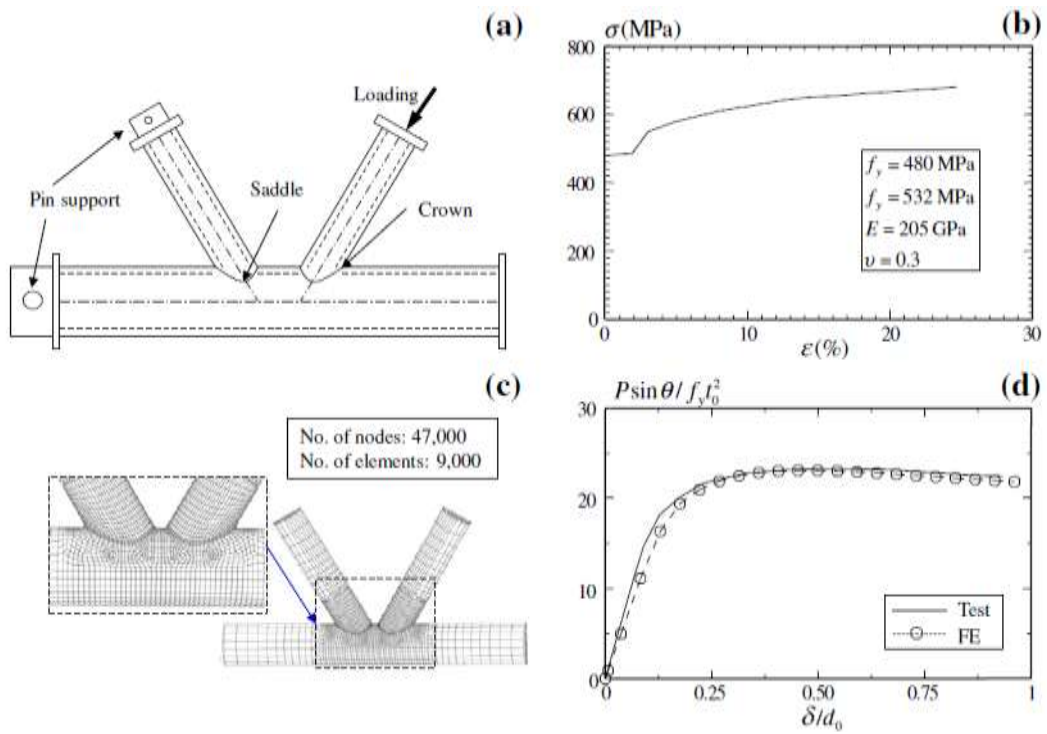


Figure 3.17 CHS K-Joint Test

- (a) loading and boundary conditions
- (b) uni-axial true stress and true strain curve
- (c) FE Mesh
- (d) Comparison of the load deformation of the tests and FE analysis (with LJF)

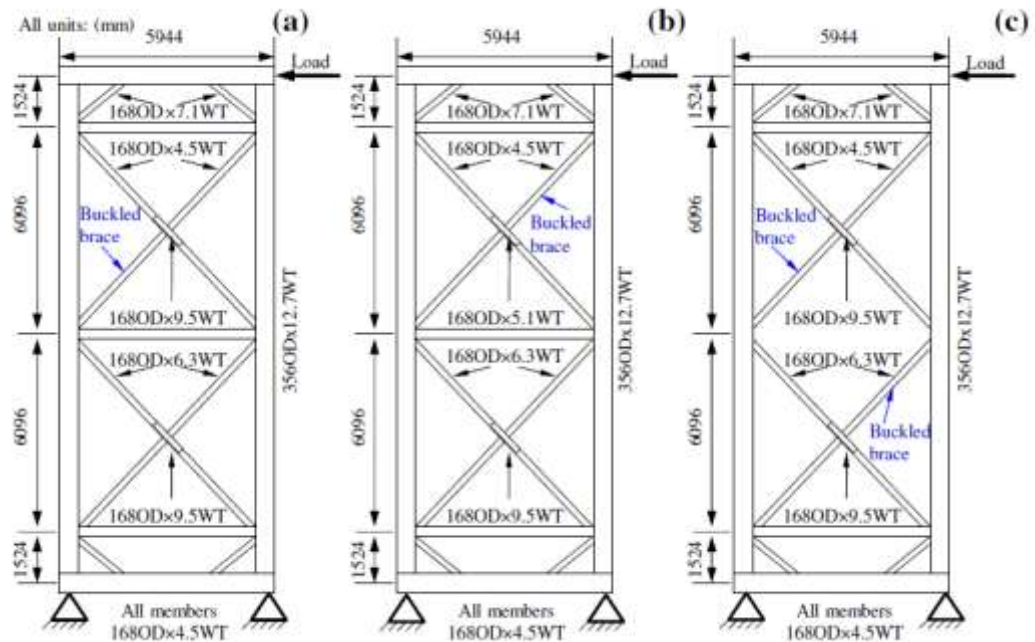
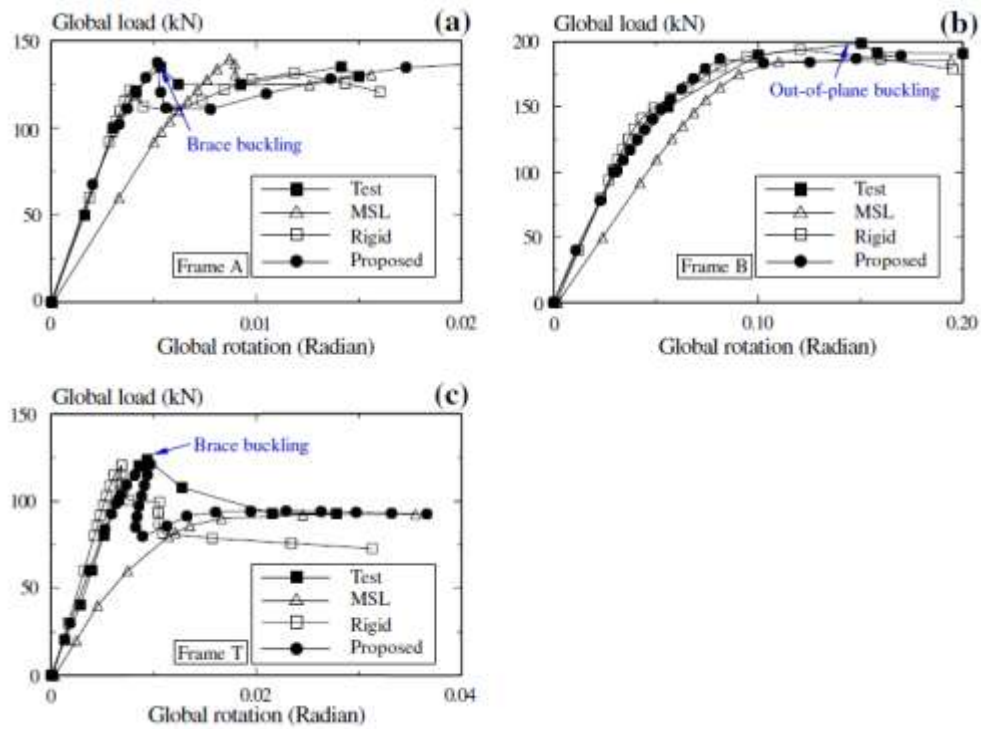


Figure 3.18 Configuration of BOMEL 2D Frames

- (a) Frame I
- (b) Frame II, and
- (c) Frame III



**Figure 3.19 Comparison of the Global load deformation response between numerical analysis and experimental records**

**(a) Frame I (b) Frame II, and (c) Frame III**

Coefficient	Formulation
A	$(0.075\gamma^2 - 1.5\gamma + 26.4)e^{(-0.0017\gamma^2 + 0.014\gamma + 1.47)\beta} / 1000$
B	$2267e^{-1.9\beta}$
C	1.13

**Table 3.3 Coefficient in the proposed formulation for K-joints**

Further work was undertaken to incorporate in the BOMEL 3D frames and perform ultimate strength analysis (pushover analysis) and the MSL formulations (Figure 3.20). The proposed Qian joint formulations incorporate LJF implicitly as part of the load displacement curve generated from the formulation. As with MSL formulations, they do not call out the contributions made by axial compression or tension, in-plane and out-of-plane bending impacts. Additionally, they cannot be used in the contribution to enhanced fatigue life predictions and only used as part of joint strength equations for ultimate strength.

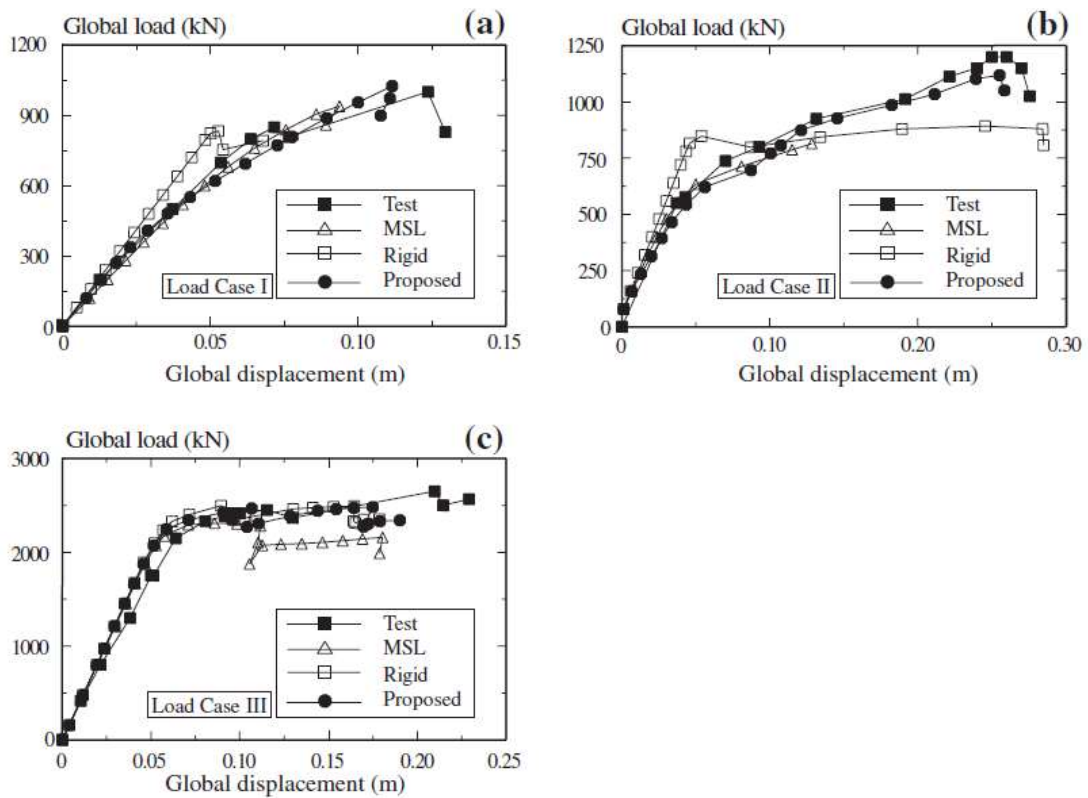


**Figure 3.20 Comparison of the Global load deformation response between numerical analysis and experimental records for BOMEL 3D Tests**  
**(a) Load Case I (b) Load Case II, and (c) Load Case III**

From Figure 3.20, the rigid joint assumption leads to a different failure mechanism in the frames because some joint capacities show higher utilizations and even failure, because stresses are unable to be re-distributed to other parts of the framework and concentrated at the tubular joint level. In the flexible joint analysis, moments are often re-distributed appropriately throughout the frame via LJF. In such cases, this would lead to a more realistic understanding of joint capacities and a more realistic representation of frame failure mechanisms.

The good relationship with the 2D frames, 3D BOMEL model and the MSL equations, provide sufficient evidence that the Qian formulations can be used appropriately for joint ultimate capacity of X and K-type joints. It, however, does not add anything new to the body of knowledge on LJF that MSL has reported.

### 3.12 Asgarian, Mokarram and Alanjari (2014)

In 2014, Asgarian et al provided an up-to-date set of LJF equations called the AMA-LJF equations. Based primarily on finite element analysis, it investigates the work done by previous researchers, including Fessler, Chen and Buitrago, and concludes that the key element for the AMA equations (Equation 3.41) being an improvement of the previous work is that AMA investigated the gap length and the interaction between braces to improve on the previous equations. Asgarian et al provides little or no basis on the joint database used in the analysis, but does state that the AMA-LJF equations were developed from regression analysis of a given database. Furthermore, the equations (Equation 3.41) represent the flexibility matrix coefficients for isolated joints for uni-planar multi-brace Y-T and K-type joints. There is little evidence to suggest that AMA would give a satisfactory result when included in a large scale Frame Test under ultimate strength or fatigue life prediction. Such formulations as AMA requires proper benchmarking against large scale tests to verify its validity to frame system performance. As with most researchers, Asgarian ignores the inclusion of joint cans or thickened sections in the finite element modeling.

$$\begin{aligned}
 f_{11} &= 3.501(\sin \theta_1)^{1.898} (\sin \theta_2)^{-0.114} \gamma^{2.129} \exp(-2.302\beta_1) \exp(-0.412\beta_2) \exp(0.221\zeta) \\
 f_{21} &= -10.070 + 0.408 \left[ (\sin \theta_1)^{2.457} (\sin \theta_2)^{1.375} \gamma^{2.458} \exp(-5.581\beta_1) \exp(2.761\beta_2) \exp(-2.492\zeta) \right] \\
 f_{31} &= 2.789(\sin \theta_1)^{0.949} (\sin \theta_2)^{0.949} \gamma^{2.225} \exp(-1.636\beta_1) \exp(-1.636\beta_2) \exp(0.256\zeta) \\
 f_{41} &= 10.116(\sin \theta_1)^{0.716} (\sin \theta_2)^{1.033} \gamma^{1.710} \exp(-3.064\beta_1) \exp(-0.863\beta_2) \exp(-0.295\zeta) \\
 f_{22} &= 102.164(\sin \theta_1)^{2.411} (\sin \theta_2)^{0.042} \gamma^{2.166} \exp(-6.255\beta_1) \exp(0.003\beta_2) \exp(0.491\zeta) \\
 f_{32} &= -10.116(\sin \theta_1)^{1.033} (\sin \theta_2)^{0.716} \gamma^{1.710} \exp(-0.863\beta_1) \exp(-3.064\beta_2) \exp(-0.295\zeta) \\
 f_{42} &= -40.793 - 953.641 \left[ (\sin \theta_1)^{2.016} (\sin \theta_2)^{2.016} \gamma^{1.500} \exp(-6.317\beta_1) \exp(-6.317\beta_2) \exp(-3.955\zeta) \right] \\
 f_{33} &= 3.501(\sin \theta_1)^{-0.114} (\sin \theta_2)^{1.898} \gamma^{2.129} \exp(-0.412\beta_1) \exp(-2.302\beta_2) \exp(0.221\zeta) \\
 f_{43} &= 10.070 - 0.408 \left[ (\sin \theta_1)^{1.375} (\sin \theta_2)^{2.457} \gamma^{2.458} \exp(2.761\beta_1) \exp(-5.581\beta_2) \exp(2.492\zeta) \right] \\
 f_{44} &= 102.164(\sin \theta_1)^{0.042} (\sin \theta_2)^{2.411} \gamma^{2.166} \exp(0.003\beta_1) \exp(-6.255\beta_2) \exp(0.491\zeta)
 \end{aligned} \tag{3.41}$$

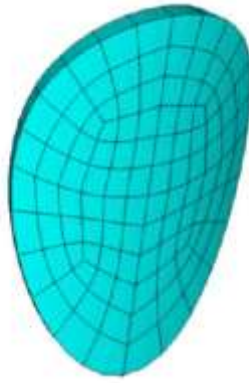


**Figure 3.21 Mesh generation for the intersection areas between chord and braces  
(ANSYS model)**

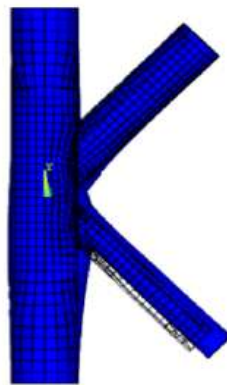


**Figure 3.22 Deformed and undeformed shape of a model under loading  
(ANSYS model)**

### **3.13 Summary and Conclusions**

Joint flexibility parametric equations have been published by Det Norske Veritas (DNV), Fessler, Efthymiou, Ueda, Kohoutek, Chen, Buitrago, MSL, Qian and Asgarian. There are considerable differences in their range of application and in their estimations of joint flexibilities for joint configurations. Given the significant differences that can occur for different boundary conditions, such differences between empirical formulae are not unexpected. From Table 3.3, the existing parametric equations for local joint flexibility do not cover the full range of loading conditions and joint parameters and some are limited in their applicability.

While the Buitrago parametric equations seem applicable to most loading applications, they have been predominantly derived from finite element analysis alone and it should be noted that these equations

should all be benchmarked against measured test data for joint flexibility. Considering gapped K-type joints, only Fessler, Efthymiou, Buitrago and Chen provide formulations that are applicable, although MSL and Qian cannot be used to calculate LJF explicitly, as they are only benchmarked to large scale frame testing for ultimate strength. Only Fessler and Buitrago considers all three loading effects of axial, in-plane bending and out-of-plane bending, while Asgarian does not address the axial loading condition. With the exception of Asgarian, none of the researchers above have a considered gap study to determine the applicability of their proposed formulations. None of the researchers have considered the effects of joint cans (thickened sections) in their LJF formulations as these thickened sections improve on joint rigidity and therefore the effects of LJF are often misleading.

Fundamentally, none of the above mentioned LJF equations addresses a standardized methodology for the derivation and validation of their parametric equations. In this thesis, a benchmarking study is undertaken on the best available large scale testing to develop a finite element model, small scale laboratory testing has been undertaken to develop a deeper understanding on the in-plane condition, finite element modeling is performed on an in-service database of K-type joints to demonstrate applicability across all parametric ranges, gap parameter study and finally, validation of the derived RK-LJF equations against large scale test results where LJF have been incorporated within the failure and collapse mechanisms. All of these represent a refinement to the existing methodology for the development of LJF parametric equations of uni-planar K-type joints.

Source	Ref	Basis	Single Brace			Cross			Gapped K			Overlapped K			Gap Study
			AXL	IPB	OPB	AXL	IPB	OPB	AXL	IPB	OPB	AXL	IPB	OPB	
DNV	1977	Not applicable		X	X										
UEG	1985	Epoxy Models 27 points	X	X	X										
Fessler et al	1986	Epoxy Models 27 T & Y joints	X	X	X	X	X	X	X	X	X				
Efthymiou	1985	FE PMBSHELL 12 T Joints 3 Y Joints 9 (90-45) K Joints		X	X						X	X		X	
Ueda et al	1990	FE 11 points	X	X											
Chen et al	1990	FE 21 points							X	X					
Kohoutek	1992	FE and Lab Tests 11 steel models		X											
Buitrago	1993	FE Analysis	X	X	X	X	X	X	X	X	X	X	X	X	
MSL	2002	FE Analysis	The formulations for MSL address ultimate strength considerations												
Qian et al	2009	Lab Tests & FE Analysis	Similar to MSL Study, the formulations are based on ultimate strength considerations												
Asgarian	2014	FE Analysis		X	X		X	X		X	X		X	X	X

**Table 3.4 Summary of the applicability of Local Joint Flexibility Equations**

## CHAPTER 4

### Literature Review: Local Joint Flexibility Studies

#### 4.1 Introduction

This Chapter provides the few experimental and application studies that have been conducted on Local Joint Flexibility, some based on the LJF parametric equations discussed in Chapter 3. The Chapter focuses primarily on developments in experimental testing, LJF application studies and analytical methods. The key application studies are focused on fitness for purpose (FFP) and asset life extension studies (ALE) for aging structures for fatigue and ultimate strength considerations.

#### 4.2 Laboratory Testing

Laboratory testing in the area of LJF has been limited. The main tests include Wimpey offshore tests (1982), work on araldite models by Fessler at Nottingham University, AMOCO K-Joint tests (1983), BOMEL Frames tests, where LJF was not measured explicitly but included in the collapse mechanism and recent small scale testing by Da Silva to investigate the in-plane condition of LJF. The Da Silva tests (2015) were performed to have a deeper understanding of the in-plane condition with regards to the findings of the AMOCO K-Joint tests. Both tests and their results are discussed in more detail in Chapter 5.

In his 1982 Offshore Technological Conference (OTC) paper on the behaviour of grouted joints in offshore structures, Tebbett (1982), at Wimpey Offshore Laboratories, stated that joint flexibility coefficients had been measured on all steel joints. However, while some sixty tests were performed, only sample joint flexibility results have been published. Joint Flexibilities on five 90° joints have been reported and the results from these tests in both the as-welded and grouted states are presented in Table 4.1. The results show a significant reduction in LJF with increasing  $\beta$  values, and expected a

significant reduction in flexibility due to the addition of grout. The results are expressed coefficients and no units for each of the LJF are reported.

Geometry			Local Joint Flexibility Coefficients							
Conf.	$\gamma$	$\beta$	Axial Tension x ED		Axial Compression x ED		OPB x ED <sup>3</sup>		IPB x ED <sup>3</sup>	
			Weld	Grout	Weld	Grout	Weld	Grout	Weld	Grout
T	32	0.59	-	-	-	-	22060	2910	4280	2725
T	20	0.33	900	480	825	-	25870	-	5320	-
T	20	0.54	575	392	333	-	-	-	3125	-
T	20	0.92	154	10	142	-	-	-	-	-
X	48	0.53	1685	272	1970	127	11295	1545	5580	3270

**Table 4.1 Measured LJF coefficients for as-welded and grouted tubular joints by Wimpey (1982)**

In 1986, Fessler et al of Nottingham University, reported joint flexibility results from a series of 27 T/Y and non-symmetric KT joint tests using precision cast epoxy resin tubes. All models had  $D = 132\text{mm}$  and  $L = 838\text{mm}$  (i.e.  $\alpha > 12$ ). The araldite models were clamped between sturdy steel supports with the loading rig used to apply pure tension, in-plane and out-of-plane bending to the brace end. At any cross section of the chord, twenty-one linear displacement transducers, evenly spread around  $270^\circ$  of the circumference measured the displacements of the chord. Measurements were taken at thirty equally spaced sections covering most of the length of the chord. Polynomial functions were fitted to the test data to allow the flexibility of the joint to be determined at all locations. Thus the twenty-seven uni-planar joints covered all combinations of  $\gamma = 10, 15$  and  $20$ ;  $\beta = 0.33, 0.53$  and  $0.76$  and  $\theta = 35^\circ, 50^\circ$  and  $90^\circ$ . A further six multi-brace models were tested to examine the validity of Fessler multi-brace LJF formulae derived from uni-planar brace models.

Reference No	Joint Type	$\gamma$	$\beta$	$\theta$	e/D
1	KT	20	0.53/0.33/0.76	50°/90°/35°	0.11/0.21
2	KT	20	0.53/0.53/0.33	50°/90°/35°	0.21/0
3	KTKT	20	0.53/0.33/0.53	50°/90°/35°	0.11/0.25
4	KY	15	0.53/0.33/0.76	50°/90°/35°	0.11/0.21
5	N	20	0.53/0.33	50°/90°	0.11
6	N	20	0.53/0.53	50°/90°	0

**Table 4.2 Fessler’s Tests on Multi-brace Joints**

The parametric values presented of these six joints are given in Table 4.2. Four KT joints were tested with variation in  $\gamma$ ,  $\beta$ ,  $\beta_c$ ,  $\theta$  and gap (e/D), where “e” is the brace eccentricity (i.e. the gap between brace centerlines on the chord axis). One KT joint (denoted KTKT) had identical braces in both the 0° and 90° brace planes. The remaining two joints were non-symmetrical K joints (N joints) with the braces overlapping in one case.

Fessler concluded at this time that the parameter  $\tau$  ( $= t/T$ ) was not considered significant and was not reported. However, in an accompanying paper on experimental technique, he demonstrated the stock of tube sizes used in these tests allows the  $\tau$  values to be reduced. These tests are the basis for Fessler’s improved LJF equations documented in Chapter 3.3. More work in the area of large scale tests are required on tubular joints and also on the effects of LJF on the overall framing of the jacket structure.

### 4.3 Analytical Methods

The key work done in analytical methods include the work by Bijlaard (1955), Kellogg (1956), Tebbett (1982), Holmans (1985, 1987), Soussi (1989) and Romeyn (1991, 1992). Kellogg (1956) and Bijlaard (1955) used similar methods to model tubular joints. Kellogg replaced the brace load of the joint with an equivalent distributed load based on elastic foundation theory. Kellogg derived the stress under the equivalent load which provided approximate stress values for the chord and ignored the brace (Figure 4.1). A major drawback of this method is that it considers the axial load and/or in-plane bending on the brace alone. It does not consider full interaction between the brace and the chord.

Bijlaard (1955) work used a double Fourier series to show the displacement field of the cylinder subjected to a rectangular distributed field. However, for this method to be accurate, a substantial number of terms is required for the Fourier series (Figure 4.2). It is highly impractical and only provides an approximate solution. It does not consider a full tubular joint with both chord and brace interactions.

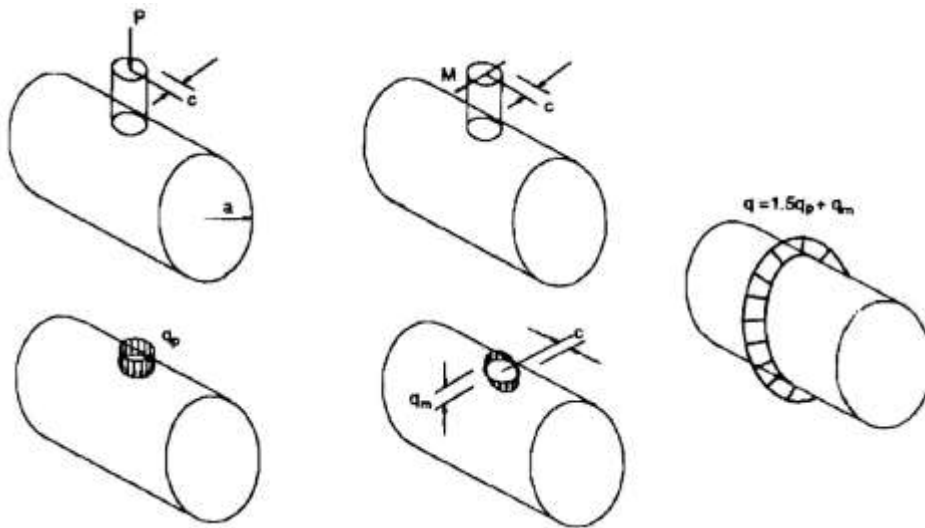


**Figure 4.1 Tubular joint model**  
(Kellogg, 1956)

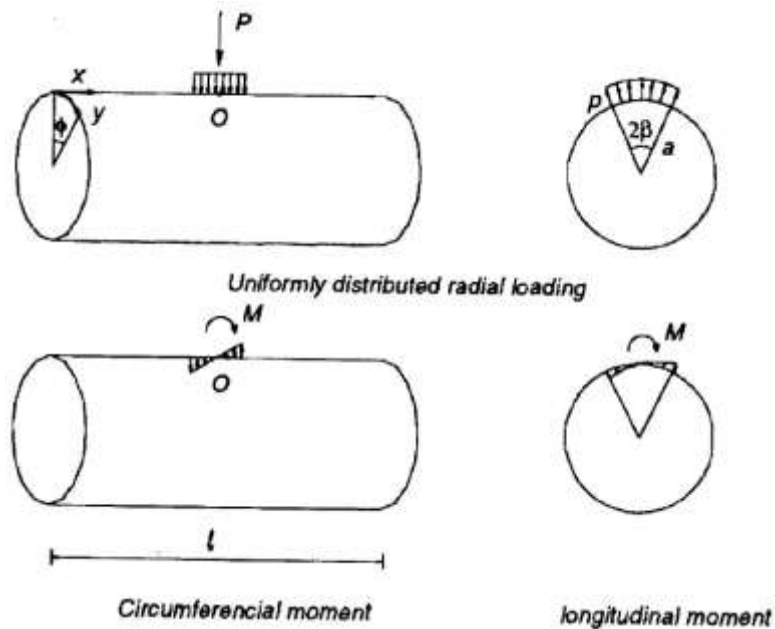


**Figure 4.2 Cylindrical vessel model**  
(Bijlaard, 1955)

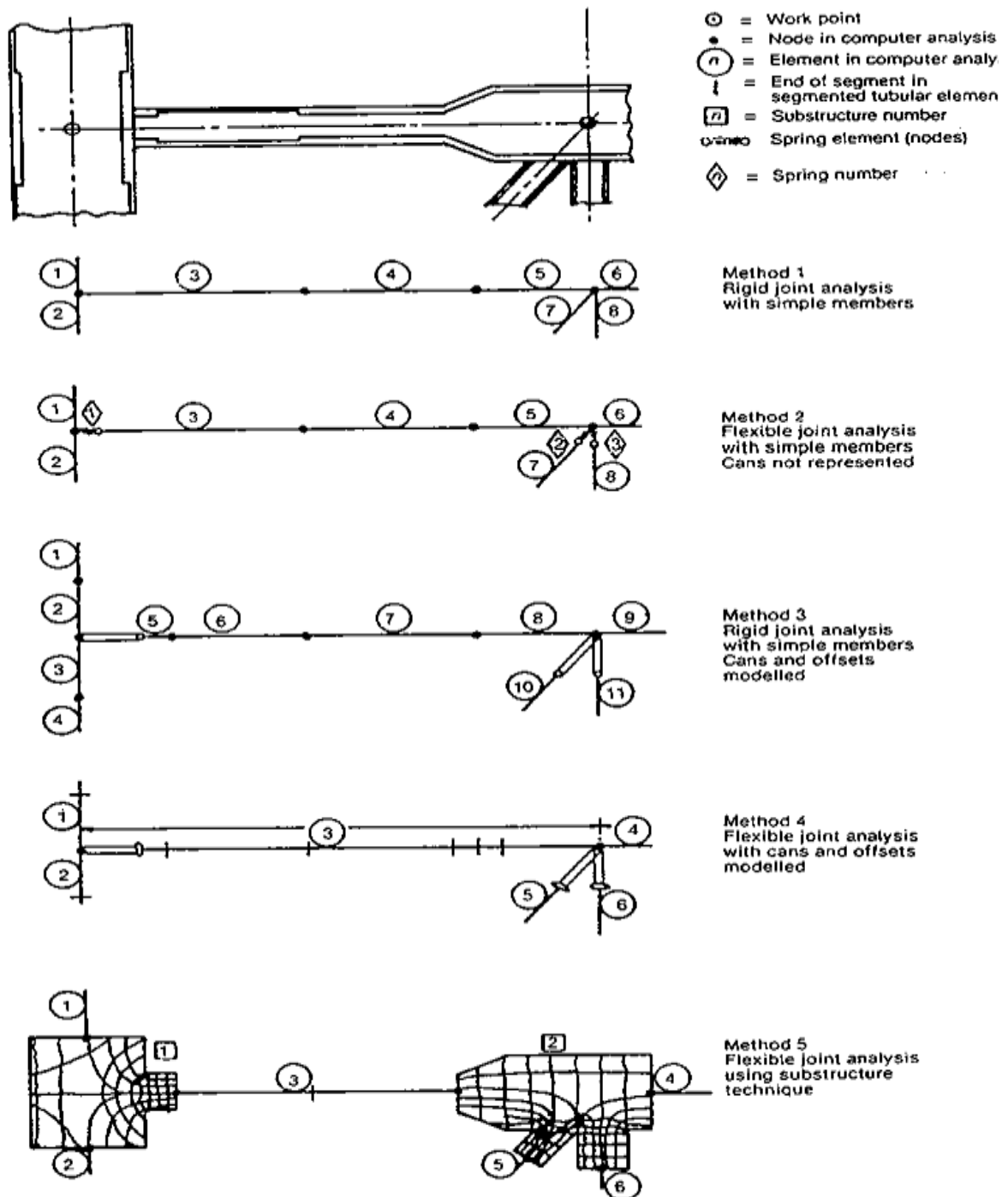


Figure 4.3 Alternative Methods for modeling joints  
(Adapted from Tebbett 1982)

Tebbett (1982) proposed five alternatives, covering a wide range of possible requirements for the inclusion of joint cans in plane-frame structural analysis programs. These are shown on Figure 4.3. It consists of a horizontal member joining a vertical leg at each end, framing into vertical diagonal

braces at mid-point. The main leg has a local joint can with a thick wall stub for the brace. The brace wall changes wall thickness along its length and tapers close to the centerline.

The methods are:

1. Rigid joints with cans not represented. This uses simple tubular members of uniform cross-section and requires nodes in the analysis at each change in section.
2. Flexible joint cans not represented. Method 1 is modified to include local joint flexibility by the addition of spring elements. This involves additional nodes or degrees of freedom.
3. Rigid joints and cans as offsets. The basic tubular element is provided with optional offsets at either end so that brace lengths for wave loading calculation and member stability checks are correct so that joint forces are generated at the chord wall.
4. Flexible joints with cans and offsets. A segmented tubular element which eliminates the need for nodes along a variable section can be used. In this example, this reduces the number of nodes from seven to two, a considerable saving. This can in the main leg can also be modeled by segments. The element is also provided with the offset capability and an in-built spring element into which the LJF coefficients can be entered.
5. Flexible joint using substructures. A substructure consisting of an internally generated finite element mesh is added to the overall analysis.

Three of the five methods include joint flexibility. Method 4 provides the most economical solution and the LJF can be included with a relatively small increase in computing cost and reduced modeling effect. Care must be exercised in the implementation of the above LJF representations, in particular Method 4 requires a LJF matrix for joints with more than one brace.

The methods employed by Tebbett (1982) above are fundamental to how tubular joints have been modeled over the past thirty years and in essence are still used today. The common drawback on the limitation of Tebbett's studies is the lack of experimental studies to adequately support the finite

element results. The offshore industry has benefitted tremendously from the work by Tebbett in that the LJF represented as a matrix can be used in most finite element software packages through the direct stiffness method of structural analysis. Both Tebbett and Lalani (1986) concluded that LJF should be incorporated in all joint modeling but suggested a more standardized approach to joint modeling be adopted.

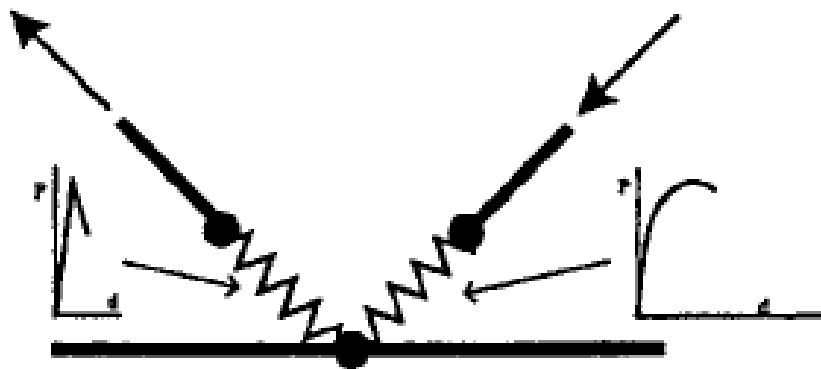


**Figure 4.4 LJF as a spring element in K-Joints**  
(Ultigude, 1999)

The concept of including LJF equations (in Chapter 3) into a structural framework has often been the concern for many practicing offshore engineers. An early attempt to model global structural behaviour used the concept of spring elements (Figure 4.4) to consider the effects of axial, in-plane and out-of-plane bending effects.

As computing power increased in the late 1980s, it was expected that the use of spring elements was not an easily practicable exercise for most finite element software packages. To consider the use of finite element software, special purpose finite elements have been developed by Holmans (1985, 1987) using classical shell theory. In Figure 4.5, the shell is represented as a shell property element between the chord-brace interface and the chord interface node. Buitrago (1993) used a similar approach to Holmans in developing a flex-beam type element to consider the effects of LJF within a tubular joint. Hellan (1995) also used this approach and claims good agreement with the parametric equations for ultimate strength.

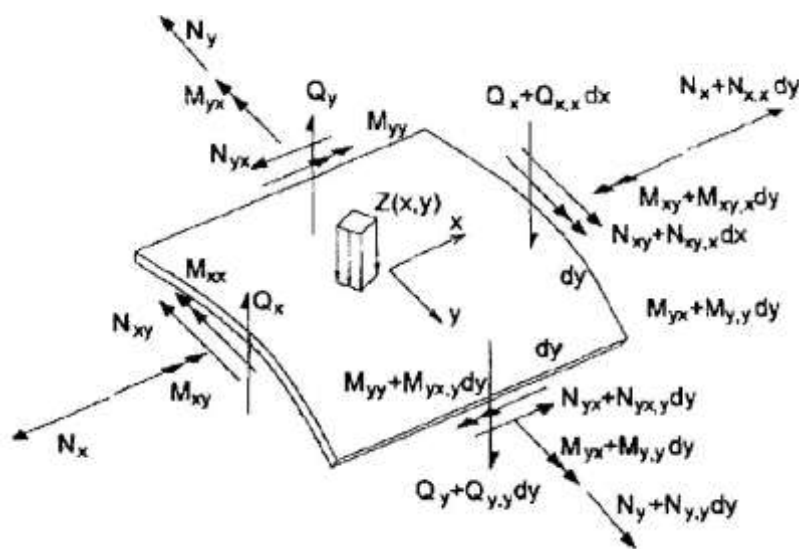


**Figure 4.5 Shell Element**  
(Holmans, 1985, 1987)

In the Ultimate Strength Finite Element Software (USFOS), the software developers, SINTEF used the flex-beam element for non-linear behaviour, (Figure 4.6), similar to Buitrago. It is an approach that is currently being used today and provides the basis for incorporating the effects of LJF for global frame analysis. The flex-element is modeled as an interaction between the brace and chord. The properties of the flex-element are representative of the effects of axial, IPB and OPB of the LJF equation used.

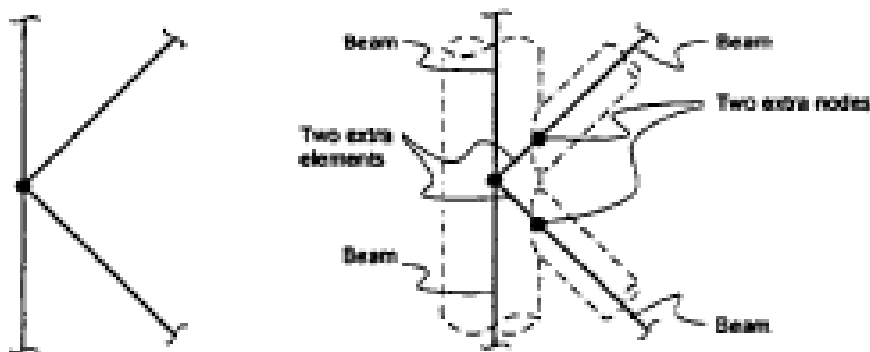


**Figure 4.6 Joint Flexibility Model**  
(Adapted from Holmans, 1985, 1987)

Souissi (1989) also presented the local joint coefficients of eighteen T-joints under the three loading modes. Following the work by Efthymiou, Souissi modeled the joints using the finite element method with specimens having a chord length six times the chord diameter (i.e.  $\alpha = 12$ ), thereby eliminating the ovalization effects of tubular sections. He established a super-element to model a joint. It can be

assumed that the weld region was not well modeled. Souissi provided no details of the finite element program that was used.

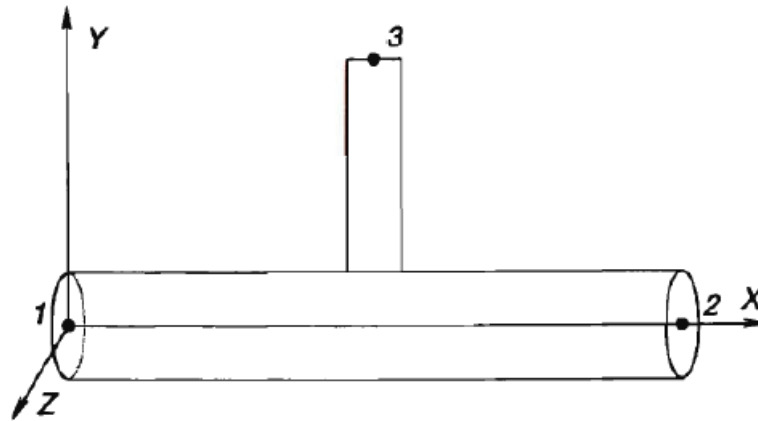


**Figure 4.7 Joint super element used by Souissi (1989)**

Souissi considered the LJF effects IPB, OPB and axial loading and reported that the results were in good agreement with Efthymiou's work. This is not entirely unexpected as the finite element models are similar. He also reported that correction factors to each loading case are required to consider the  $\tau$  parameter.

In 1990, Romeyn et al, of the Delft University of Technology, investigated the flexibility of multi-planar K (KK) and multi-planar X (XX) joints. By 1991, the results of numerical work on uni-planar T/Y and K-joints and multi-planar KK gap and KK overlap joints were presented, the KK joints being identical K-joint configurations for  $0^\circ$  and  $90^\circ$  planes. Romeyn et al (1991) stated that three approaches may be used for defining joint stiffness coefficients in a beam model, where joint stiffness (K) is the inverse of the joint flexibility. Stiffness coefficients for sixteen T-joints are given for the three modes of loading, derived using the three analytical approaches summarized by:

In Approach A, joint stiffness coefficients are determined from the difference between the displacements at the brace member end of a joint modeled with beam elements and thin shells at unit load. For Approach B, joint stiffness coefficients are determined in an identical way to Approach A; however the restraint condition is different from Approach A as the brace and the chord ends are always fixed against translation and rotation (i.e. fully clamped).

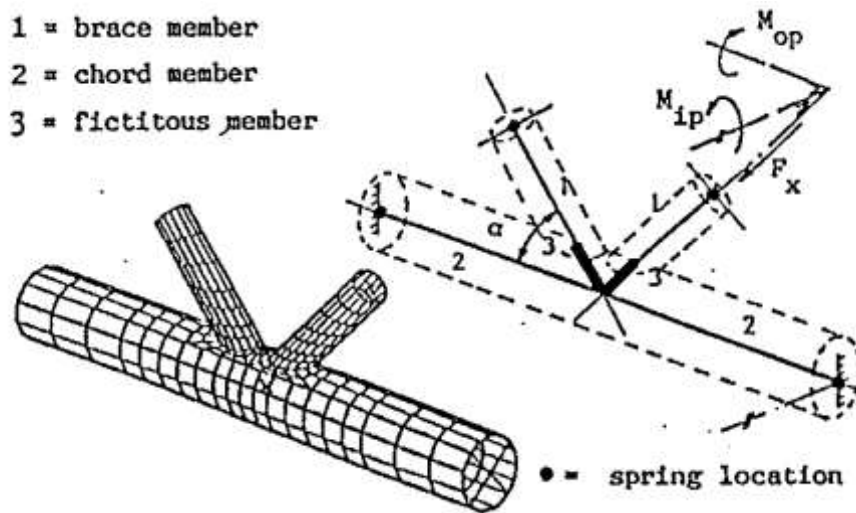


**Figure 4.8 Joint Definitions**  
 (Adapted from Romeyn 1991)

For Approach C, it is based on classical theory of thin shells and the finite element methods. Romeyn (1991) concluded that this was theoretically the correct approach since no approximations are used.

The results from these three analyses indicate that for a T-joint under axial load ( $0.2 \leq \beta \leq 0.65$ ), differences between Approaches A to C is less than 10%. However, under out-of-plane bending and in-plane bending, coefficients for Approach C are 50-600 times larger than Approach A and 10-150 times larger than Approach B. Romeyn states that *“although Approach C is theoretically the correct approach, it is found to be cumbersome to use, because of excessive matrix handling that is necessary. Approach B, in spite of it being an approximation of Approach C, has been found to give better stiffness coefficients for general use than Approach A,”* which has been used by others including UEG, Fessler, Efthymiou and DNV. In the X-joint models, the approach is not specified. This subsequent work covering Y-joints, K-joints and multi-planar KK gap/overlap joints is presented in pictorial form. The following points from Approach A results were noted:

- For  $0.2 \leq \beta \leq 0.65$ , LJF reduces with increasing  $\beta$  value.
- LJF increases with increasing  $\gamma$  values.

LJF values under axial load reduce from T-joints to Y-joints to K-joints to multi-planar K-joints, although it should be assumed that the K-joint is under balanced loading.

In 1992, Romeyn et al considered the method of finite element modeling and displacements for sixty multi-planar XX joint configurations (i.e. braces in 0°, 90°, 180° and 270° planes). These displacements are converted to joint flexibilities based on a shell model with solid elements at the weld (Model 4). The research was an attempt to standardize the use of FE modeling to joint behaviour to obtain results better than approximate values. The following FE models were used in Romeyn's study.

FE model	Description
Model 1	Joint modeled with four (4)-noded quadrilateral linear shell elements and weld shape not included.
Model 2	Joint modeled with eight (8)-noded quadrilateral quadratic shell elements and the weld shape not included.
Model 3	Joint modeled with twenty (20)-noded hexahedral quadrilateral quadratic shell elements and the weld shape included.
Model 4	Joint modeled with eight (8)-noded quadrilateral quadratic shell elements and the welded shape included by twenty (20)-noded hexahedral quadratic solid elements. Between the shell and the solid elements, thirteen (13)-noded quadrilateral quadratic transition elements were used.
Model 5	Joint modeled with two (2)-noded beam elements and all member ends rigidly connected.

**Table 4.3 Joint model criteria  
(Romeyn, 1992)**

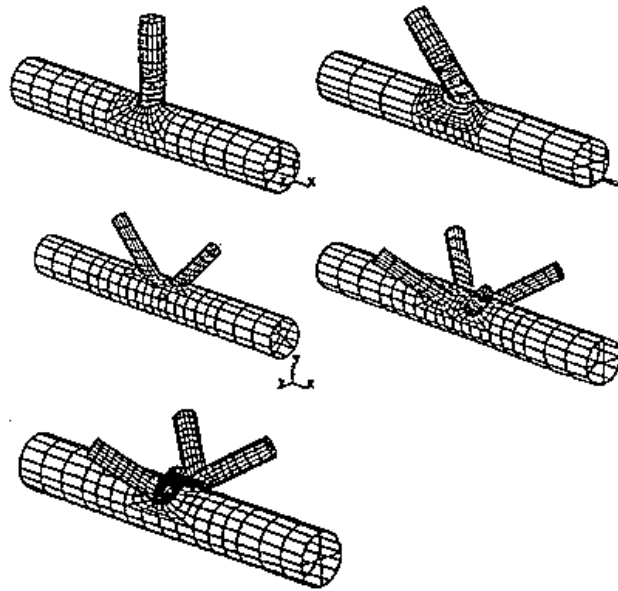


**Figure 4.9 Finite Element Models 1-5**  
(Adapted from Romeyn 1992)

For each model, four mesh refinements ranging from fine mesh to coarse mesh was considered. In addition, four integration schemes were reviewed:  $2 \times 2 \times 2$ ,  $2 \times 2 \times 3$ ,  $2 \times 2 \times 5$  and  $3 \times 3 \times 3$ .

Romeyn (1992) concluded that:

- The use of eight (8)-noded shell elements exhibit more flexible behaviour than the four (4)-noded shell elements and are considered more accurate.
- No general conclusion can be made on the accuracy of twenty (20)-noded solid elements against eight (8)-noded shell elements because this depends entirely on the geometry and type of loading.
- When using integration scheme  $3 \times 3 \times 3$ , a large decrease of joint flexibility occurs.
- Integration scheme  $2 \times 2 \times 2$  is preferred for joint flexibility behaviour and integration scheme  $2 \times 2 \times 3$  is preferred when the results are obtained directly from the nodes for obtaining Stress Concentration Factors (SCFs), compared to other integration schemes.
- The joint flexibility increases with mesh density but after a certain mesh refinement, the joint flexibility converges to an optimum.

- A finite element model with the weld shape included, behaves more stiffly than a finite element model without the weld shape included. Differences up to 20% have been found for some X-joints. DNV (2011) concluded that when performing analytical work (where nodal displacements are the objective) the weld has negligible effect on the overall displacements of the joint. For tubular joints where the ratio of the chord thickness (T) to brace thickness (t) is low and in the region of 1 -2, then the DNV statement is applicable. For higher T/t ratios (for the OPB condition), the weld is more likely to contribute to the overall stiffness of the tubular joint.

The work by Romeyn provides a standardized approach to modeling tubular joints. Software developers have used this work as a pioneering work in their development of finite element packages to this day. For the design of tubular joints, the Structural Analysis Computer Software (SACS) is generally used. Embedded in the joint code check, is the ability to activate a LJF module. The module incorporates Fessler, Buitrago and MSL's equations. Limited guidance is provided in the SACS manuals on the applicability of these equations and their use. The Ultimate Strength Finite Element Offshore Software (USFOS) suite of software has also adopted the MSL formulations as part of the pushover analysis. This feature is also optional and is dependent of the user needs. From Romeyn's studies, thin shell elements are generally preferred and are widely adopted by engineers and analysts today.

Apart from the use of the appropriate finite elements and mesh refinement, decisions on the number of brace/chord intersections to be separately modeled are often a compromise between increased accuracy (i.e. whether secondary moments will be significant) and the cost/time penalty of defining extra nodes, are often required.

The UEG Report (1982) on the determination of the effect of LJF has shown that working point eccentricities of D/4 have a significant effect on the load distribution when coupled with the effect of local joint flexibility. The need to model working point offsets, i.e where distance between the

centerline of node to node connects and the face to face lengths of the brace and chords depend primarily on the diameter of the chord and the effect of the change in stiffness to the brace member. The effect of modeling an offset is to ensure that wave and current loading on the member are not overestimated.

It is generally accepted that offsets must be specified on short members framing into chords with diameters greater than 1.5m. The inclusion of all thickened sections (joint cans) in a computer grid can be time consuming and does not necessarily improve accuracy in calculating the LJF. Most of the major computing packages available to engineers are now fully equipped with appropriate mesh refinement tools and host a series of finite elements that can be used to represent LJF behaviour.

#### **4.4 Fatigue Studies**

Prior to the early 2000s, it was generally accepted that the effects of fatigue was the key driver in the remaining life assessments of fixed offshore structures. Gibstein, Baehem and Osean (1990) reported a refined fatigue analysis approach for the Veslefrikk jacket, where the jacket and the deck structure was modeled using beam elements with the capability of including tubular joint super-elements at selected locations. These super-elements are finite elements which exhibit the axial, IPB and OPB effects due to LJF. Local finite element analyses were performed with the joint stiffness concentrating at nodes at the center of each tube end. The reduced joint stiffness matrices were included as separate super-elements in the global beam-frame model. Therefore, local flexibilities are properly accounted for in the global finite element model. Adoption of this approach, including estimation of stress concentration factors (SCFs) from the mesh, rather than one of the generally conservative SCF equations, and the more accurate determination of the location of the hot-spot stress that results, led to the calculated fatigue lives 5-10 times larger than from conventional analysis due to the effects of LJF. While only selected joints were studied, the most appropriate approach was to include LJF on all joints but this would be time consuming. Through LJF, moments at the joints are redistributed to other

members and joints, thus reducing the stresses at any one joint. This reduced moments and thus stresses at the joint allow for greater fatigue lives to be predicted.

MSL (2001) investigated the effects of LJF on fatigue life inspections and adopted these findings to develop a more in-depth underwater inspection plan. The platform chosen was a structure in-service for thirty years and a 3D structural model (Figure 4.10) was developed to perform the spectral fatigue analysis. To implement LJF, a flex-element was introduced at the fatigue susceptible joints based on the Buitrago’s formulations. A factor of life is determined using the LJF which is a ratio of the life calculated using LJF to the life calculated using the rigid joint analysis. Typically the average factors on life were reported and summarized in Table 4.4. Figure 4.11 shows the comparison of the fatigue life predictions using rigid joint analysis and flexible joint analysis at one of the jacket frames.

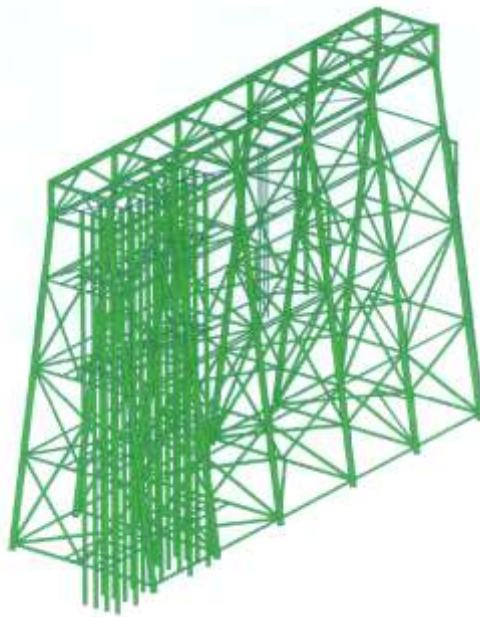


**Figure 4.10 3D Isometric Structure  
(Adapted from MSL 2001)**

<b>Location</b>	<b>Average Factor on life</b>
Transverse frames (A to F)	19.3
Longitudinal Frames (1 & 2)	9.2
Horizontal framing (-24' elevation)	8.0

**Table 4.4 Average Factor on Fatigue Life (MSL 2001)**

The results have led to a more detailed review of the inspection whereby the following inspection categories were determined based on the LJF analysis.

- Category 1 – Highest Priority, predicted fatigue lives of less than 10 years
- Category 2 – High Priority, predicted fatigue lives between 10 and 30 years
- Category 3 – Medium Priority, predicted fatigue lives 30 and 60 years
- Category 4 – Inspection not justified on the basis of fatigue assessment.

MSL concluded that for Category 1 and 2 joints included in the periodic inspections, the implementation of LJF has reduced the requirement for underwater inspection by approximately 75%.

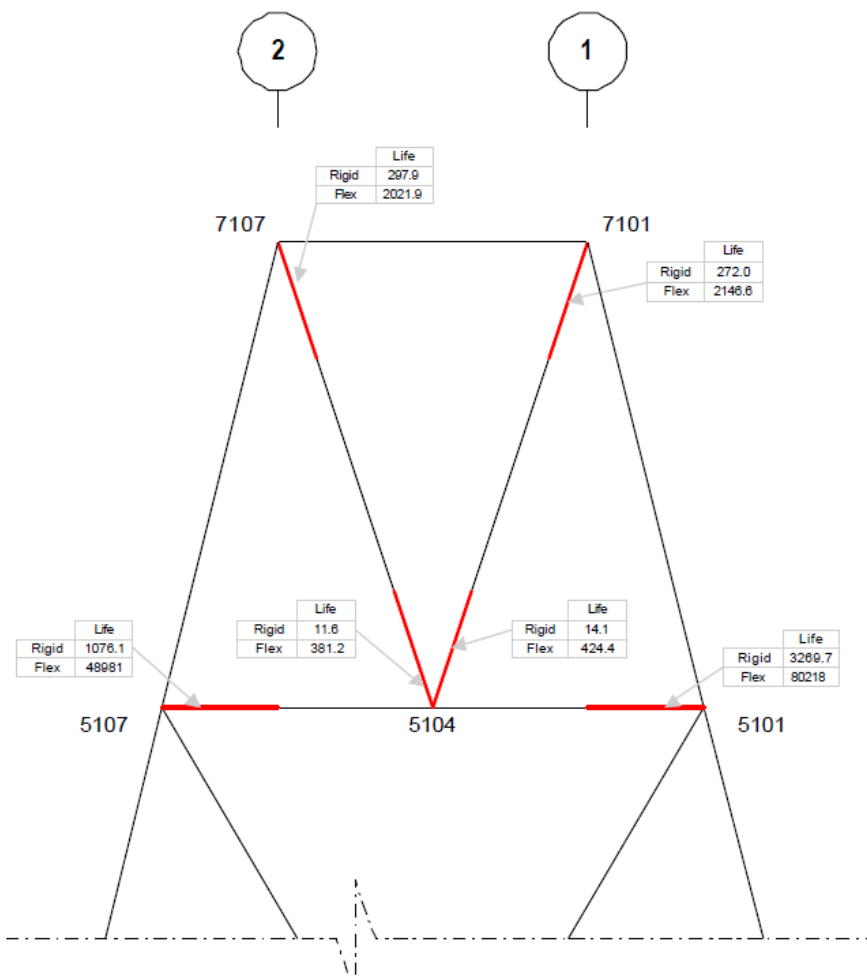


**Figure 4.11 Joint Fatigue Life Comparison  
(MSL engineering 2001)**

Nichols (2006) adopted a similar approach to another offshore platform located in South East Asia. The platform was approximately thirty years old at the time. The Buitrago LJF joint flex model was

also included in the SACS model and average fatigue life comparison between the rigid joint and the flexible joint analysis were determined. Nichols reported that the average factors on life for each of the framing components were typically as follows - Transverse frames: >10, Longitudinal frames: >5, Horizontal framing: >5. To complete the study, a further categorization similar to that of MSL was also adopted and by extension incorporated into the long term inspection planning of that platform.

O'Connor et al (2005) undertook fitness for purpose assessments on the Cassia A platform. He demonstrated that the platform has sufficient reserve capacity in terms of a Reserve Strength Ratio (RSR) for ultimate capacity. O'Connor (2005) et al also demonstrated the numerical benefits of having used local joint flexibility analysis for a platform exceeding design fatigue lives at critical joints. Table 4.5 provides the results of the Cassia A LJF Study and how the use of joint flexibility was used to justify increase in the fatigue lives when using the assessment approach as outlined in Section 2.2. The design approach identifies eleven joints with fatigue lives less than the target eighty years (2x by required platform life extension). The shortest fatigue life is 0.3 years at the time of the study and the structure has been in operation for twenty years at this stage. When using the assessment approach, including the application of joint flexibility analysis, the shortest fatigue life is 106 years.

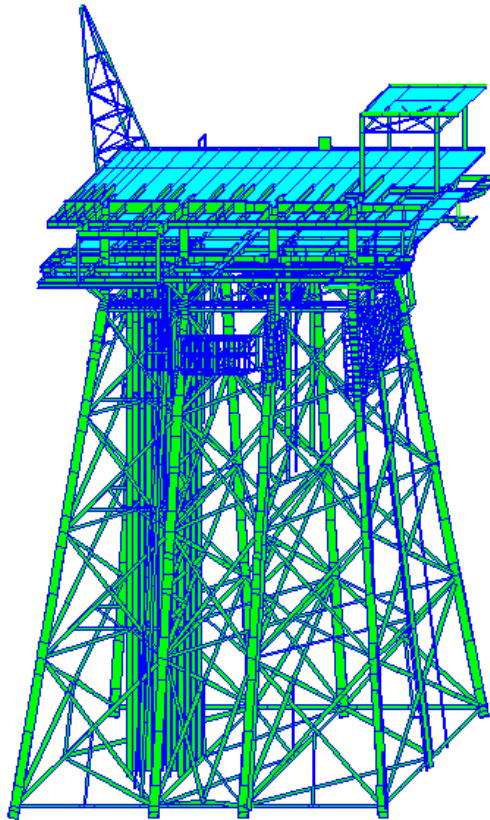


**Figure 4.12 bpTT Cassia A platform**  
(O'Connor et al, 2005)

Joint Can	OD (in)	WT (in)	Joint Type	Member Type	Fatigue Lives (years)		
					Design Approach	Modified Approach	Assessment Approach
1643	16.00	0.500	Y	BRC	0.3	0.7	106.3
	58.50	1.000	Y	CHD	0.3	0.5	
1421	14.00	0.375	Y	BRC	1.8	394.0	6685.1
	19.50	0.562	Y	CHD	7.5	79.8	

**Table 4.5 bpTT Cassia A Comparison of Fatigue Life Assessments**

The results of this LJF study was a game changer on the way British Petroleum (bp) conducted their fitness for purpose in the future for aging assets. LJF has demonstrated that aging facilities can remain operating, provided that an adequate structural integrity management program is in place for the facility. This is especially so in the North Sea operations, where some of bp assets are older facilities from heritage AMOCO (in the 1970s) before both companies merged to form one major operator.

Chakrabarti et al (2005) performed similar type of studies on over twenty platforms in the Bay of Campeche, Mexico. He reported having used Buitrago's LJF equations for the fatigue assessments and

having used a short flex-element at the end of the brace to represent the axial and bending stiffness at the joint. While Chakrabarti et al (2005) used LJF in their analyses they did not perform a comparison of joint behaviour without the LJF. As expected, the assessed joints performed well under fatigue LJF analysis with design fatigue lives exceeding the required 2 times fatigue life requirement of the API RP 2A. Figure 4.13 shows a typical frame in one the structures analyzed and its calculated fatigue life of some joints.

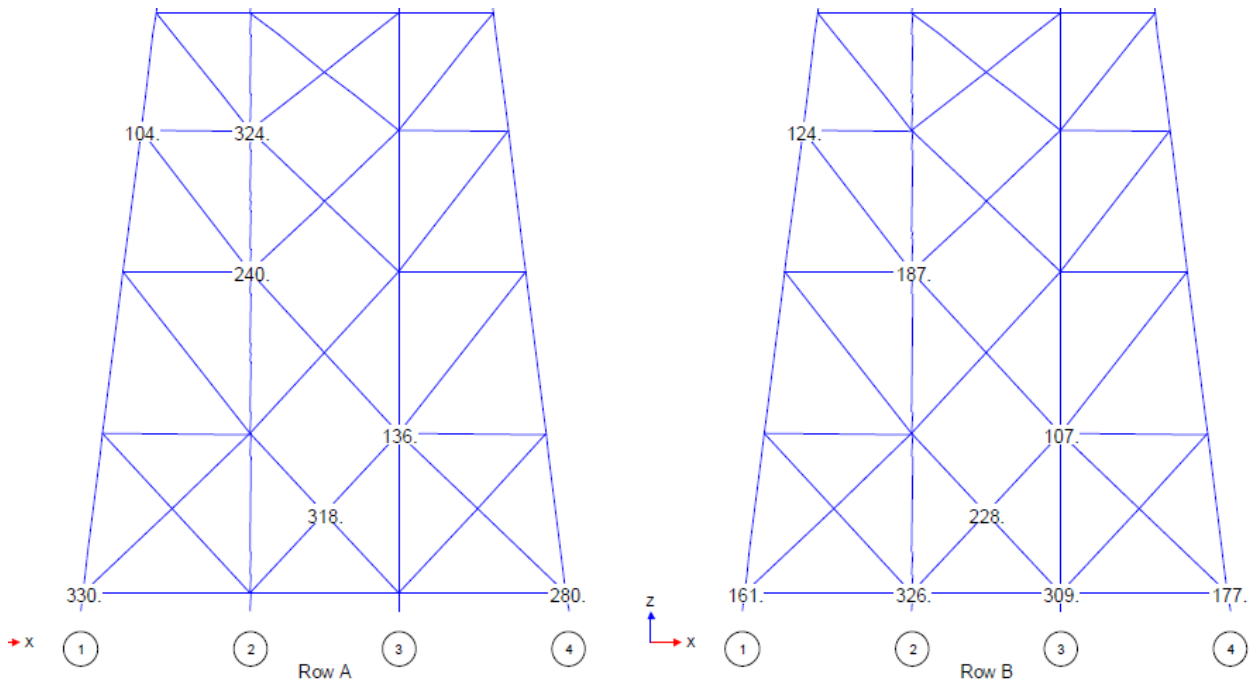


**Figure 4.13 Calculated Fatigue Lives of Joints**  
(Chakrabarti, et al, 2005)

Samandani et al (2009) conducted a study on two older structures to compare the effects of LJF on the structures to demonstrate the significance of joint cans. For fatigue assessments, the structures without joint cans tend to provide larger values of fatigue life predictions than those with cans. This is expected as the thickened sections provide a stiffer section with less ability to “flex” and also increased stress concentrations at sectional changes from joint can to tubular adversely affect the performance of joints for fatigue life predictions. These structures are typical of pre-1979 API structures. In many cases, these older structures perform quite well for fatigue driven assessments but may need to be strengthened for continuous operations for ultimate strength.

## 4.5 Global Effects of LJJ on Frame Structures

The earliest type of studies to determine the global effects of LJJ on frame structures were performed by Bouwkamp et al (1980) who sought to determine the joint flexibility effects on the overall response of a 2-D tower structure. Chord and brace substructures were referenced to a master node located at the axis of the member (Figure 4.14). The FACTS package was employed to determine the local joint flexibilities. Bouwkamp reported the use of the nine (9)-node doubly curved iso-parametric degenerate shell elements, using quadratic Lagrange polynomials. In the degeneration concept, the displacements and rotations of the shell mid-surface are independent variables.

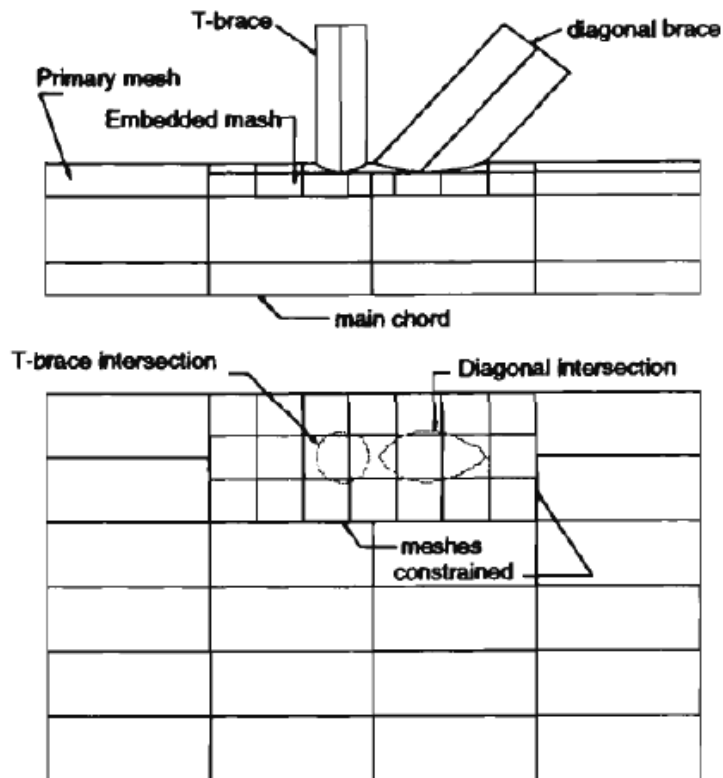


**Figure 4.14 Model of Joint Substructures  
(Bouwkamp 1980)**

The 2-D tower frame considered by Bouwkamp and reproduced in Figure 4.15 was analyzed using the usual super-element approach and a simple rigid joint analysis where the local joint was not modeled. Wave and dead load including the deck load and effective jacket weight were considered with displacements initially assessed for a flexible pile-supported base versus a rigid base configuration.

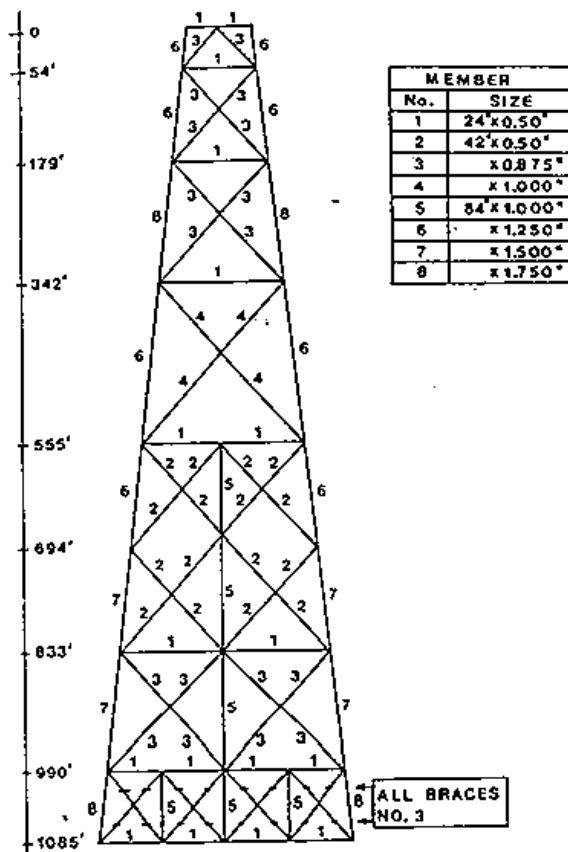


**Figure 4.15 Tower Frame  
(Bouwkamp, 1980)**

Bouwkamp showed that the inclusion of LJF can lead to:

- Up to 30% larger calculated displacements at the lower framing levels, although at upper levels the calculation deflections were within 1% of rigid joints nodal predictions. Bouwkamp suggests that this is due firstly to the effect of longer brace members at upper levels which reduces the axial stiffness of the members and secondly to the modeling of increased joint can thickness which increases the relative stiffness.
- Slight increases in calculated leg axial forces (up to 2% higher) and considerable reductions in calculated brace axial forces (up to 20%).

WS Atkins and Partners, under contract to the Underwater Engineering Group, UEG (1982) carried out a project to determine the effects of LJF on the three 2-D frames shown in Figures 4.17, 4.18 and 4.19 with regard to:

1. Member axial force and bending moment distribution

2. Member Buckling
3. Natural Frequencies

Furthermore, the effects of local joint flexibility corresponding to joint geometric variations (i.e.  $\tau$ ,  $\beta$ ,  $e$ ) were examined. The approach used differs from that used by Bouwkamp in that the test data obtained by Fessler et al were used to generate the flexibility matrix. The frames were analyzed using the general purpose stiffness method program 'ASAS' (Atkins Structural Analysis System). Each frame was the subject of at least two analyses: the first is of the conventional type where no allowance is made for joint flexibility. The second analysis allows for joint flexibility.

Flexibility coefficients were determined in the model tests, for only three degrees of freedom for each brace of a joint - those freedoms where local joint flexibilities are considered to be most interesting. The study only addressed the axial and in-plane flexibility effects. A tubular joint is more flexible under out-of-plane loads and the effects could therefore be more significant.

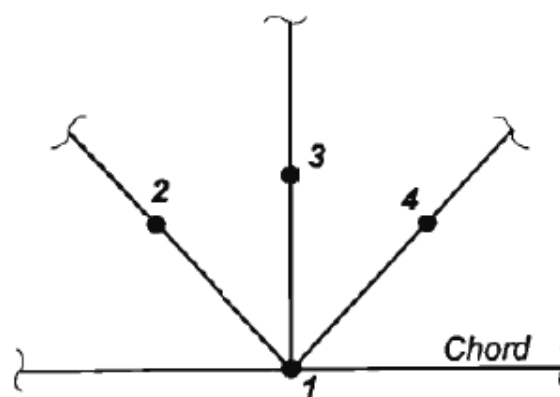


**Figure 4.16 Nodal points considered for UEG Study**

A simple representation of the joints was selected for the study with one nodal point provided on the chord and one on the brace. The nodal points 2, 3, and 4 were all connected by a stiffness matrix derived from the flexibility matrices by Fessler (Figure 4.16).

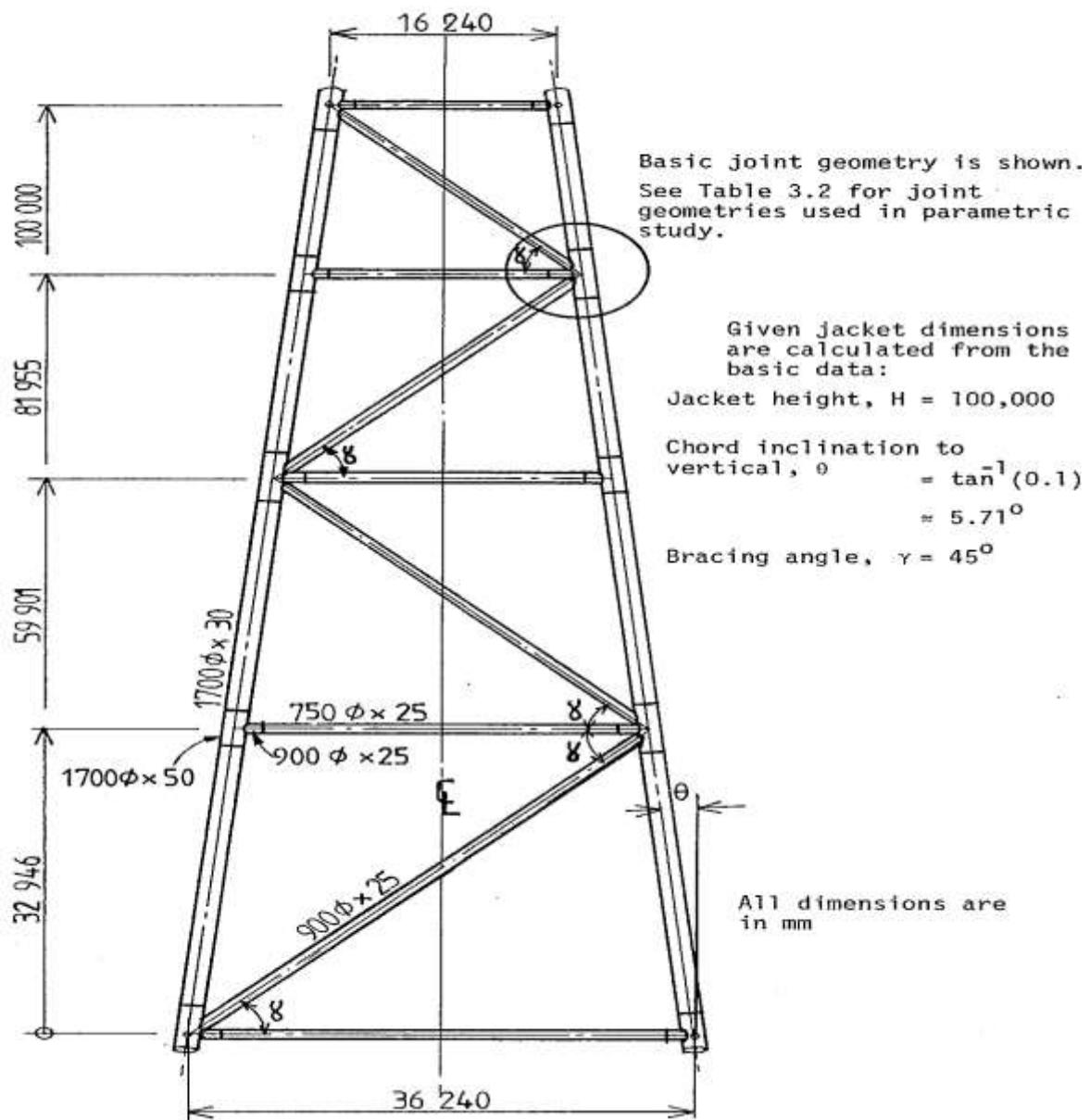


Figure 4.17 Structure 1

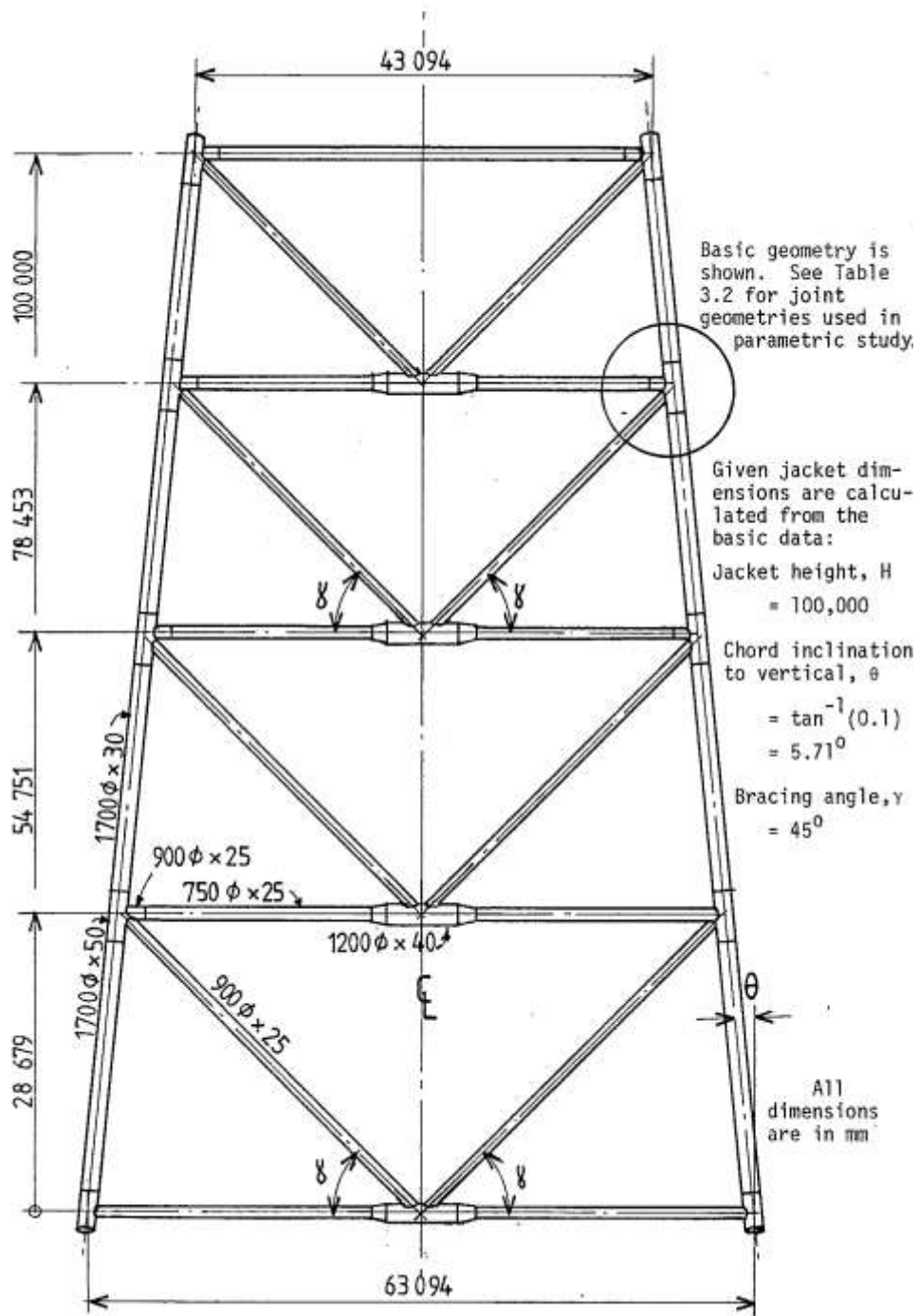
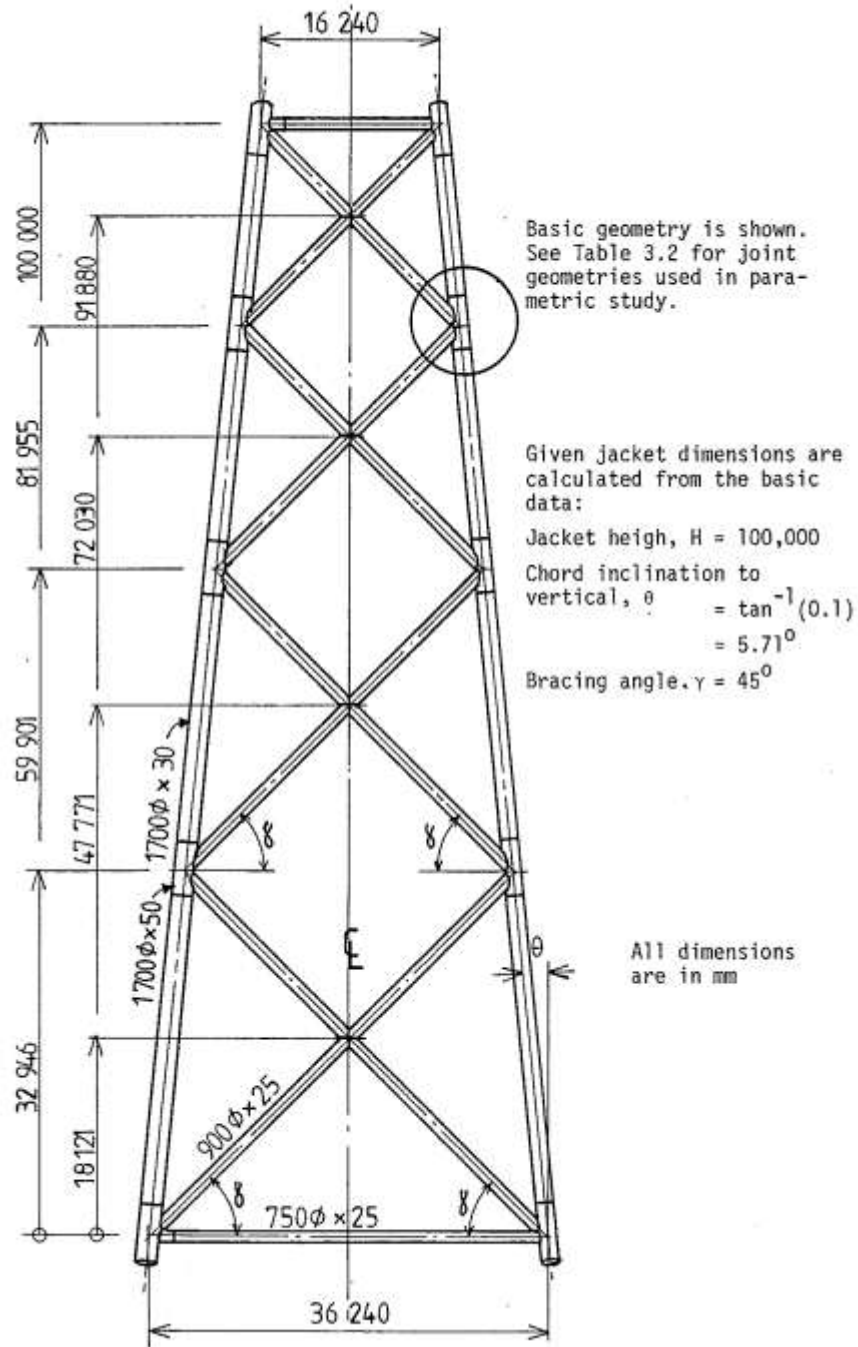


Figure 4.18 Structure 2



**Figure 4.19 Structure 3**

The authors concluded that:

- Deflection changes are significant on Structure 2 partly because of the large number of flexible joints ( $\gamma = 25.3$  and  $\beta = 0.53$ ) and partly because of the small height-to-width ratio of the frame. The deflection increases for the structures ( $\gamma = 25.3$  and  $\beta = 0.53$ ) range from 1 and 3, to 13% for Structure 2 with respect to conventional rigid-frame analysis.

- In terms of percentage change for in-plane moment effects, Structure 1 shows the largest increase in the horizontal braces at the KT joints. The 90° brace member is rotated by opposite axial forces in the adjacent 45° braces. An increase of 34N/mm<sup>2</sup> resulted, which represents an increase of 200% on the conventional rigid frame analysis.
- The greatest changes in natural frequency of similar modes between the conventional and most flexible ( $\gamma = 25.3$  and  $\beta = 0.53$ ) analyses is 82% and occurred for Structure 3.

O'Connor et al (2005) also reported ultimate strength analysis on the bpTT Cassia A as a part of the fitness for purpose assessments. The analysis included LJF and the USFOS package was used in the analysis. The results of the analysis indicate that the structure has an unusually high safety factor (reserve strength) with a capacity of over 5 times the design capacity load, with all members intact. Figures 4.20 and 4.21 illustrate the USFOS ultimate strength model and load displacement curves for bpTT Cassia A platform and the load deformation curves from the series of analysis performed.

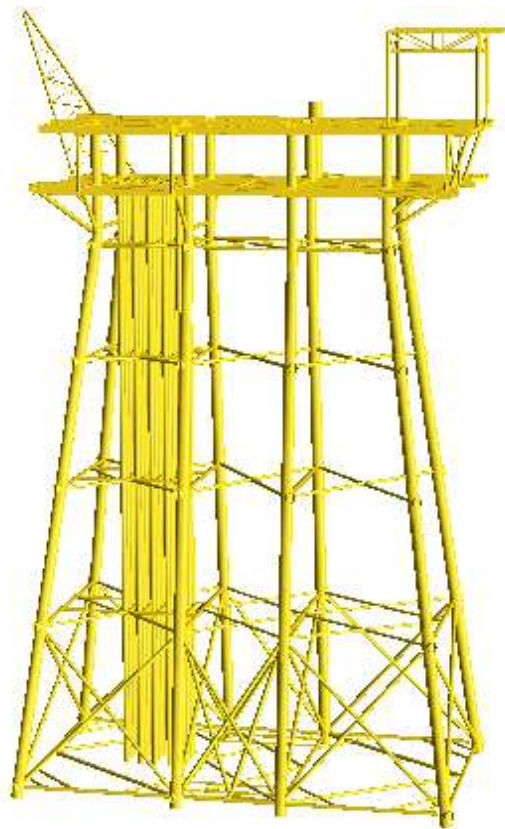


**Figure 4.20 bpTT Cassia A Platform  
(USFOS model)**

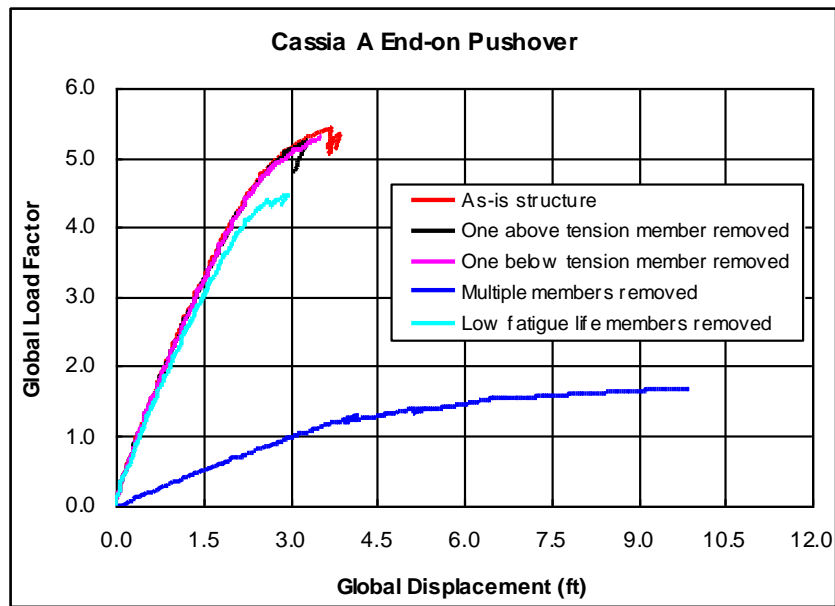


**Figure 4.21 bpTT Cassia A Platform, Load Deformation curves**

In 2009, Mirtaheri et al investigated the effects of joint flexibility of tubular joints based on the finite element method. In this study, in analogous to Bouwkamp (1980), individual full scale tubular connections are modeled with the aid of multi-axial shell elements and loaded to reach moment-rotation relations. Two types of offshore connections which are frequently used in the offshore platforms are examined, namely T and Y connections and loaded to test their rotations in comparison with the fully rigid assumption (Figure 4.22).

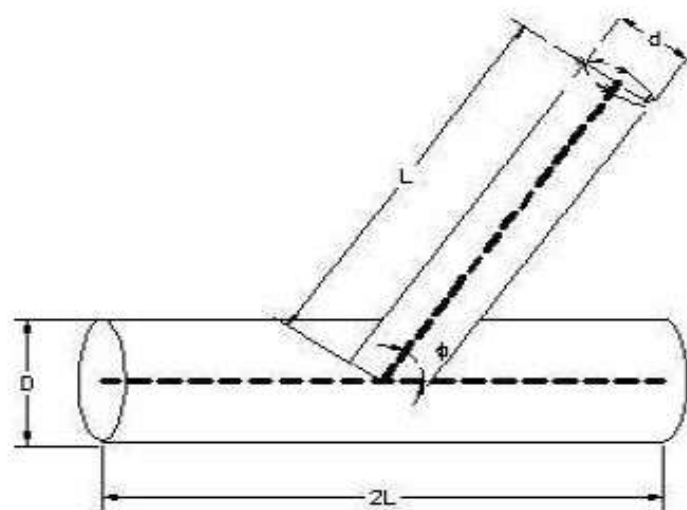


**Figure 4.22 Y-type Tubular Joint Model  
(Mirtaheri, 2009)**

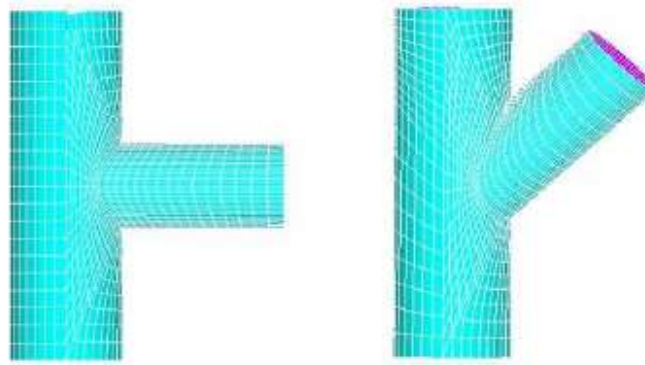


**Figure 4.23 Finite Element model and mesh discretization for Y and T type connections**

Figure 4.23 illustrates the finite element model of typical connections generated through the use of shell elements and dense mesh discretization in intersection region to capture nonlinear strains as accurately as possible. After performing nonlinear static analyses, one can obtain moment-rotation relationships of several connections with different intersection angles. Two finite element models of a 2D frame of an offshore platform are designed, and generated analytically and studies comparatively to gain insights about performance of platforms with rigid and flexible connections. The first model is made by means of uniaxial beam-column elements in which connections are assumed to be fully rigid, whereas the second model is generated through the use of 3D shell elements in which case, joint flexibility are accounted for automatically.

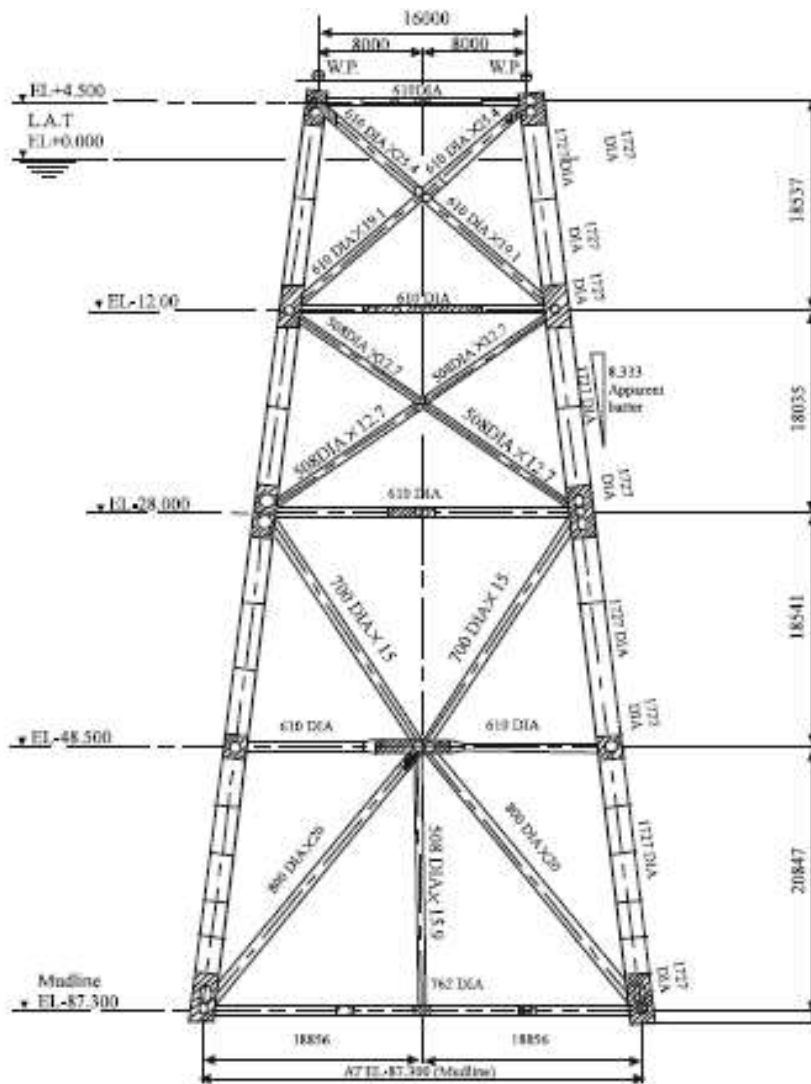


Figure 4.24 General configuration and member sizes for 2D frame

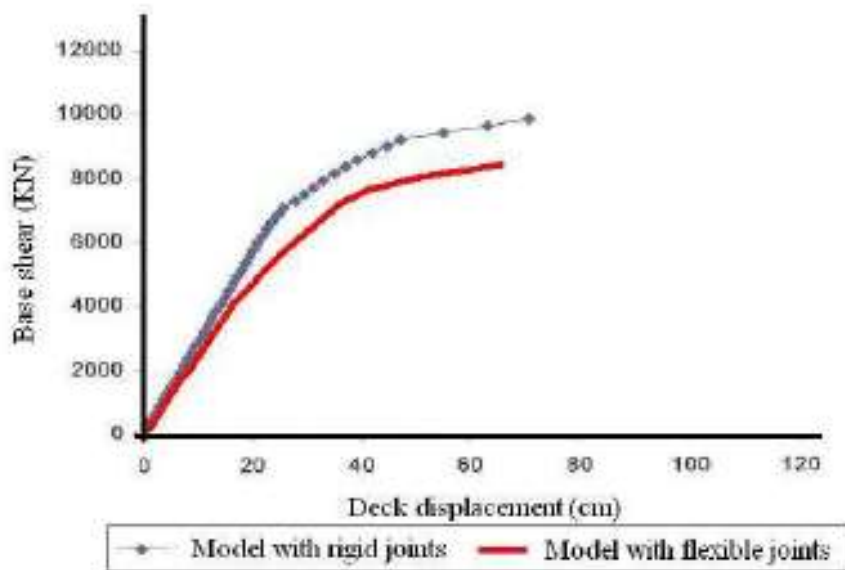


Figure 4.25 Results of Ultimate Strength Analysis

Mitaheri et al concluded that:

- Tubular connections used in the offshore industry are intrinsically flexible. These flexible joints are able to dissipate energy when subject to cyclic forces.
- Compressive axial forces in struts reduces the strength of the end connections as they increase the susceptibility of local buckling of joints unlike the tensile forces which assist the strength of the connections and prevent local buckling occurrence.
- Results of pushover analysis (ultimate strength) indicate that effect of joint flexibilities become more apparent when the structure undergoes strain beyond the elastic region and shows nonlinear behaviour.

## **4.6 Summary and Conclusions**

The variations of the results in Table 4.6 indicate that joint flexibilities have different results on the analysis results of tubular structures. The effects vary with structural geometry, loading, configuration and height of the structure. For ultimate strength studies, the global effects of LJF are determined in terms of global collapse and deflection of the structure. For fatigue life predictions, these are more localized effects as the main concern is at the tubular joint level. While fatigue life prediction is a localized effect, to ensure moment redistribution of loads due to LJF, all joints in the frame must be modeled with a flex-element or the super element to represent the overall effects of LJF in the frame structure.

Study	Loading	Global Deflection	Axial Load	Bending Moments	Natural Frequencies	Fatigue Life Prediction (Local)
<b>Bouwkamp (1980)</b>	Dead Load + Point Load at the top	+ 1% at the top 30% at lower framing levels	Leg axial forces 2% higher Reductions of 20% in brace axial forces			
<b>UEG (1982)</b>	Point Load + Wave Load	+13%	+1.5%	-90%	-45%	
<b>Soussi (1989)</b>	Dead Load + Point Load	+ 10%				
<b>Gibstein et al (1990)</b>	Dead Load + Wind, Wave and Current					+ 5-10%
<b>O'Connor (2005)</b>	Dead Load + Wind, Wave and Current					+ 212%

**Table 4.6 Maximum Responses when including LJFs compared to conventional design**

The finite element method offers the practicing engineer the capacity to model many joint configurations and to obtain accurate measurements of displacement under low nominal brace load. However, substantial differences in the joint flexibility analyses can be obtained depending on the boundary conditions, particularly under moment loading. Significant differences in joint flexibility results can also result from using an inappropriate mesh density, element type and integration scheme. The standardized approach to finite element modeling proposed by Romeyn has been adopted in many finite element software packages to model the effects of LJF.

For determining joint flexibilities from numerical methods, it is recommended that finite element methods should be benchmarked to physical tests whenever possible, particularly prior to comprehensive finite element analysis test programs being undertaken and shell type finite elements are preferred when developing FE models for LJF. For fatigue life prediction, there is considerable benefit in using LJF compared to the conventional design spectral approach. O'Connor on a full jacket

analysis predicted over 200% improvement to fatigue lives for high fatigue critical joints of an aging structure.

The oil and gas industry has been slow to incorporate this structural assessment tool LJF, and led to costly repairs and inspections. Since 2006, with the initiation of the API RP 2SIM, a global committee has now been educating each other with similar global operating experiences and the LJF concept and applications are becoming more popular. The concept of LJF also offers the practicing engineer the facility of employing a full assessment method when requiring fitness for purpose to continue operating beyond a design threshold.

In many cases, this FFP requires two key analyses, i.e. fatigue assessments and ultimate strength analyses. The use of one LJF formulation over another can be confusing, as the codes and standards do not explicitly spell out which formulation to use and when. For ultimate strength considerations, the use of MSL joint formulation in the USFOS software is the most appropriate, as it is benchmarked to large scale testing of the BOMEL frames. The RK-LJF equations developed within this research are validated against large scale frame tests and can be used for both fatigue life assessment and ultimate strength of gapped uni-planar tubular joints.

# CHAPTER 5

## Gapped K-Joint Testing and Local Joint Flexibility

### 5.1 Introduction

Gapped K-type tubular joint testing has been the subject of investigation with regards to offshore jacket structures since the early 1980s. In this Chapter, the main K-joint tests will be reviewed as they relate to LJF and accuracy of testing methods. The main experimental testing undertaken include:

1. The AMOCO K-Joint tests (1983)
2. BOMEL frame testing and isolated gapped K-joint tests (1994)
3. National University Singapore, (NUS) - large scale testing of grouted K-joints (2009)
4. Da Silva small scale testing to investigate LJF with a main focus on the IPB condition (2015)

The AMOCO K-Joint test represents the only large scale test results where LJF has been measured. The tests, while performed in the early 1980s, are limited by modern testing standards, but represent the best testing methods available to the offshore industry at that time. BOMEL Engineering Consultants (1994), while performing the BOMEL Frames Test as a Joint Industry Project (JIP), also provided a Specification for the testing of isolated K-joints. This specification provided an industry standard by which large scale testing of isolated joints should adhere to and forms the basis of subsequent work carried out by NUS in the late 2000s. From this specification the Amoco K-Joint tests are critically reviewed as to the applicability and accuracy of the testing methods.

The NUS large scale testing of gapped K-type joints is limited to grouted joints due to a limitation in funding to explore other concerns such as LJF. Although not discussed in this thesis with regards to LJF, it provides a consistent approach to large scale testing that adheres to the BOMEL specification for isolated joint testing. It should be noted that the experimental work and findings outlined in the Amoco K-Joint tests and the BOMEL frame testing and isolated gapped K-joint tests are not generally in the public domain. The author of this thesis has worked as a consultant within BP (formerly BP

AMOCO) and GL Noble Denton (an organization that acquired BOMEL in the 1990s), so was privy to these extensive studies and also had informal interaction with the personnel who were involved in developing these experimental works. Furthermore, the Da Silva small scale testing of IPB for the Y-type joint was initiated and developed by the author to further investigate any areas of concerns of the AMOCO joint tests.

## **5.2 AMOCO K-Joint Tests**

In 1983, Wimpey Laboratories, together with AMOCO UK Exploration Company, conducted joint flexibility tests on K-joints for full scale representation of existing joints on Amoco platforms in the southern North Sea, called the AMOCO K-Joint Tests. The principal objective of the tests was to determine the ultimate strength of the joints in the as-welded condition, under static loading for comparison with strengths predicted by existing design codes and parametric equations. In addition, stress concentration factors and local joint flexibilities, under elastic loading, were determined for the as-welded condition.

## **5.3 Rationale for the AMOCO K-Joint Study**

Detailed structural analysis using the then design codes show that some K-joints had become overstressed. Most of the design codes at that time provided joint strength formula for T and Y type steel tubular joints and can be applicable to K-joints with large gaps (large gap being  $g/D$  greater than 0.15) developed by Marshall et al (1970). Smaller gap joints under axial loading have strengths greater than the equivalent large gap joint. While the API RP 2A (used at that time) gave an enhancement factor of up to 1.3 for axial loading, work done at that time by Billington, Lalani and Tebbett (1982) shows an enhancement factor of 1.9 and Nakajima (1971) of 3.0 (albeit for very small joints, i.e. chords less than 150mm). The  $g/D$  parameter alone is insufficient to determine the strength of small gap K-joints. The design code at that time was conservative for its strength determination of small gap K-joints but no reliable data was available at that time to support this view. In performing the

AMOCO K-Joint study, the intention was to determine the parameters that affect the strength of small gap K-joint, stress concentrations associated with these parameters and any effects of local joint flexibility.

### 5.4 AMOCO K-Joint Geometry

The joints of principal concern were the non-overlapping K configuration and consist of 18 inch (457mm) Outer Diameter (OD) chords and 16 inch (406mm) Outer Diameter (OD) braces. The chord wall thicknesses are either 0.394 inch (10mm) or 0.375 inch (9.5mm) and the brace thickness is 0.394 inch (10mm). The angles of intersection vary but are, typically, in the range of 40° to 60°. It was Amoco’s intention that the tests should be carried out on the heavily loaded K-joint, which is the one with an intersection angle of 60° between the chord and the braces. The geometry of this joint is given in Figure 5.1. The Amoco jacket structures in the southern North Sea had many K-joints of similar geometries.

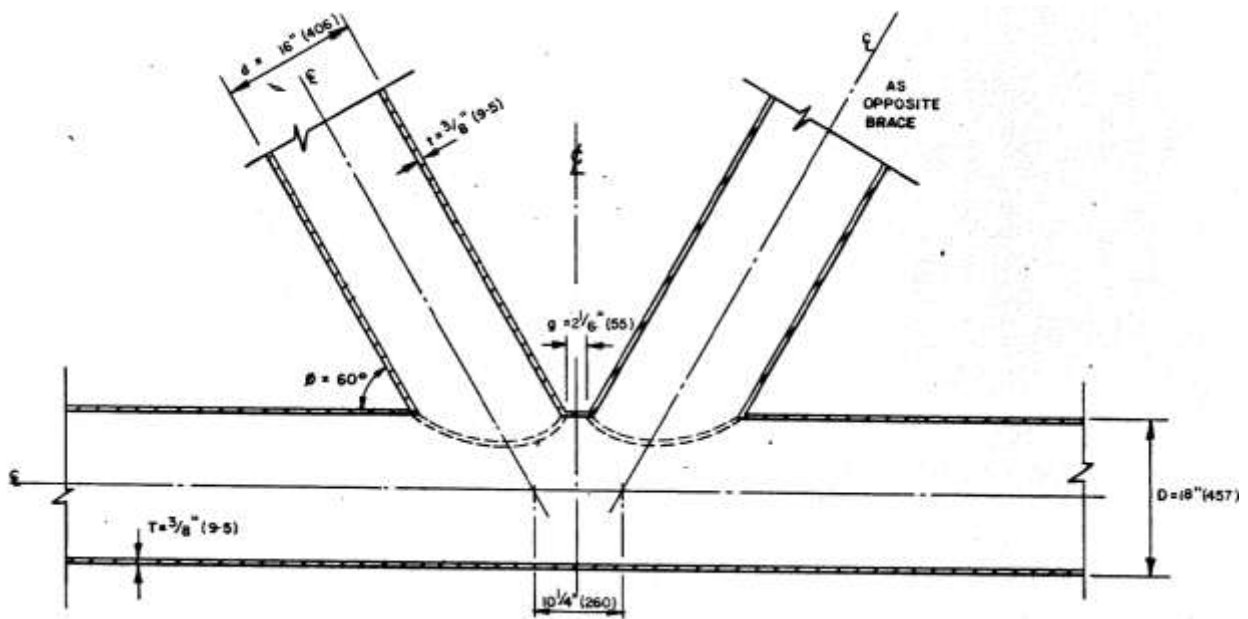


**Figure 5.1 Geometry of the Specimens  
(AMOCO K-Joint Tests, 1983)**

The geometrical parameters for the AMOCO K-Joints include the following:

$$\beta = d/D = 0.89$$

$$\gamma = D/T = 22.8$$

$$\zeta = g/D = 0.12$$

$$40^\circ \leq \theta \leq 60^\circ$$

## 5.5 Local Joint Flexibility Definition

Most structural analysis of the jacket structures at the time assumed that members were rigidly attached to each other at discrete points. This assumption was necessary because of the lack of published data relating to the flexible nature of the tubular joints. In essence, Local Joint Flexibility is a measure of the flexibility within the joint itself due to the local deformations of the chord under load. Local joint flexibility measurements have been made for the eleven load cases as shown on Figure 5.10. The definitions of local joint flexibility for axial load, in-plane bending and out-of-plane bending are given in Figures 5.2 through 5.4. The loading convention for the K-joint test is provided in Figure 5.5. These definitions are fundamental to all LJF calculations and are used to develop the LJF formulations discussed in Chapters 6 through 8.

### 5.5.1 LJF for Axial Brace Loads

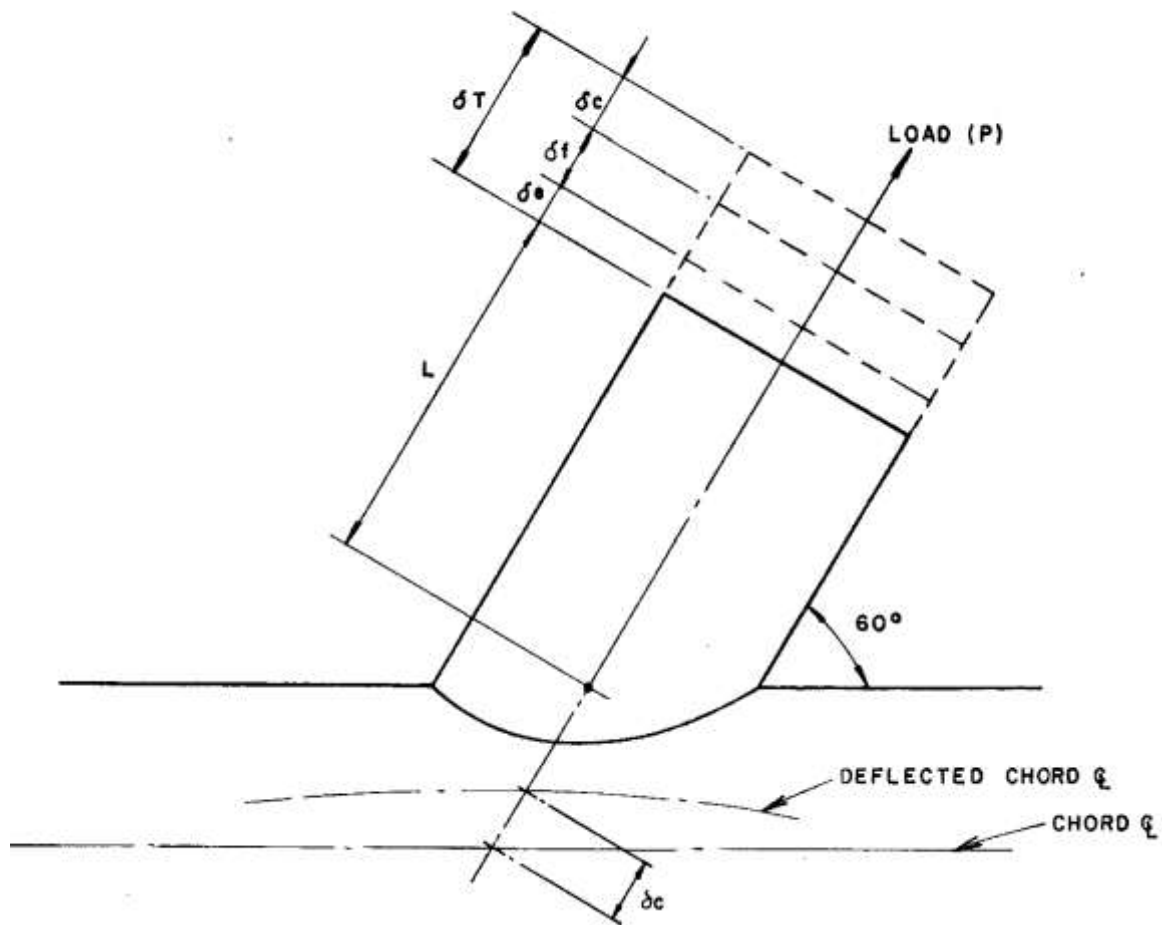


**Figure 5.2 Definition of Local Joint Flexibility for Brace Axial Loads  
(AMOCO K Joint Tests 1983)**

$$\delta T = \text{Total Measured Displacement} \quad (5.1)$$

$$\delta e = \text{Elastic Brace Displacement} = ML/AE \quad (5.2)$$

$$\delta c = \text{Chord Displacement} \quad (5.3)$$

$$\delta f = \text{Rigid Body Displacement} = \delta T - \delta c - \delta e \quad (5.4)$$

$$\text{Local Joint Flexibility} = \delta f/P \text{ (units: mm/KN)} \quad (5.5)$$

## 5.5.2 LJF for In-Plane Bending

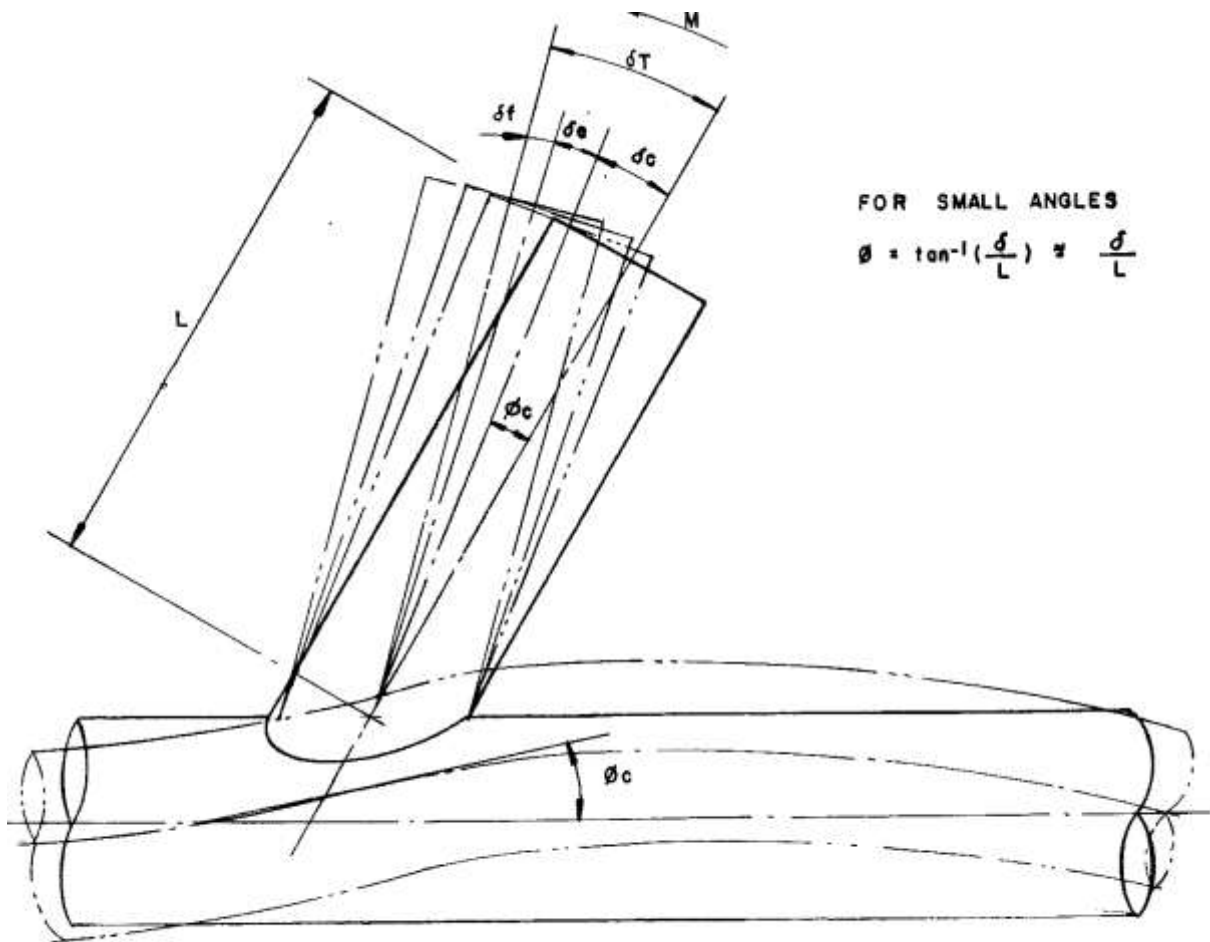


**Figure 5.3 Definition of Local Joint Flexibility for In-Plane Bending  
(AMOCO K-Joint Tests 1983)**

$$\delta T = \text{Total Measured Brace Displacement} \quad (5.6)$$

$$\delta e = \text{Displacement at the Brace due to Elastic Bending of brace} = ML^2/3EI \quad (5.7)$$

$$\delta c = \text{Displacement at Brace End due to Chord Rotation} \quad (5.8)$$

$$\delta f = \text{Rigid Body Displacement} = \delta T - \delta e - \delta c \quad (5.9)$$

$$\text{Local Joint Flexibility} = \phi f / M \text{ (units: Rad/KNm)} \quad (5.10)$$

### 5.5.3 LJF for Out-of-Plane Bending

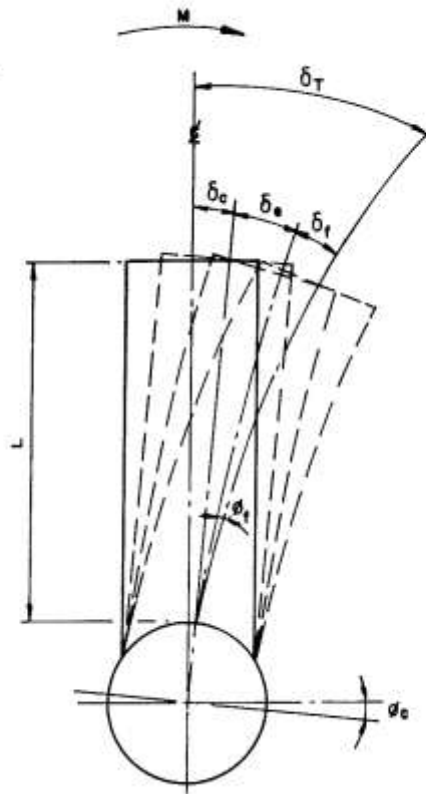


**Figure 5.4 Definition of Local Joint Flexibility for Out-of-Plane Bending  
(AMOCO K-Joint Tests 1983)**

$$\delta_T = \text{Total Measured Brace Displacement} \quad (5.11)$$

$$\delta_e = \text{Displacement at the Brace due to Elastic Bending of brace} = ML^2/3EI \quad (5.12)$$

$$\delta_c = \text{Displacement at Brace End due to Chord Rotation} \quad (5.13)$$

$$\delta_f = \text{Rigid Body Displacement} = \delta_T - \delta_e - \delta_c \quad (5.14)$$

$$\text{Local Joint Flexibility} = \phi_f/M \text{ (units: Rad/KNmm)} \quad (5.15)$$

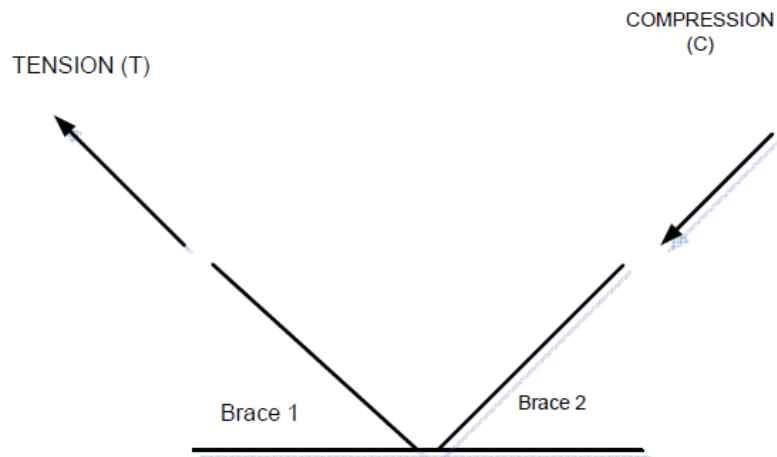


**Figure 5.5 K-Joint Loading Configuration**

## **5.6 Test Specimens**

The AMOCO K-Joint test specimens were fabricated by Research Models and Equipment Ltd at full scale from standard tubular sections conforming to API Specification 5L Grade B. The fabrication procedures were in conformance with AWS D1.1-82 which was used on fabrication work for steel structures in the North Sea at the time. Steel coupons were tested to determine the yield stress and ultimate strength of the material. A spectrographic analysis was carried out to determine the chemical composition of the steel. For fabrication QA, all work was witnessed by a representative from Lloyds Register of Shipping, signed and appended to the AMOCO K-Joint Test Report.

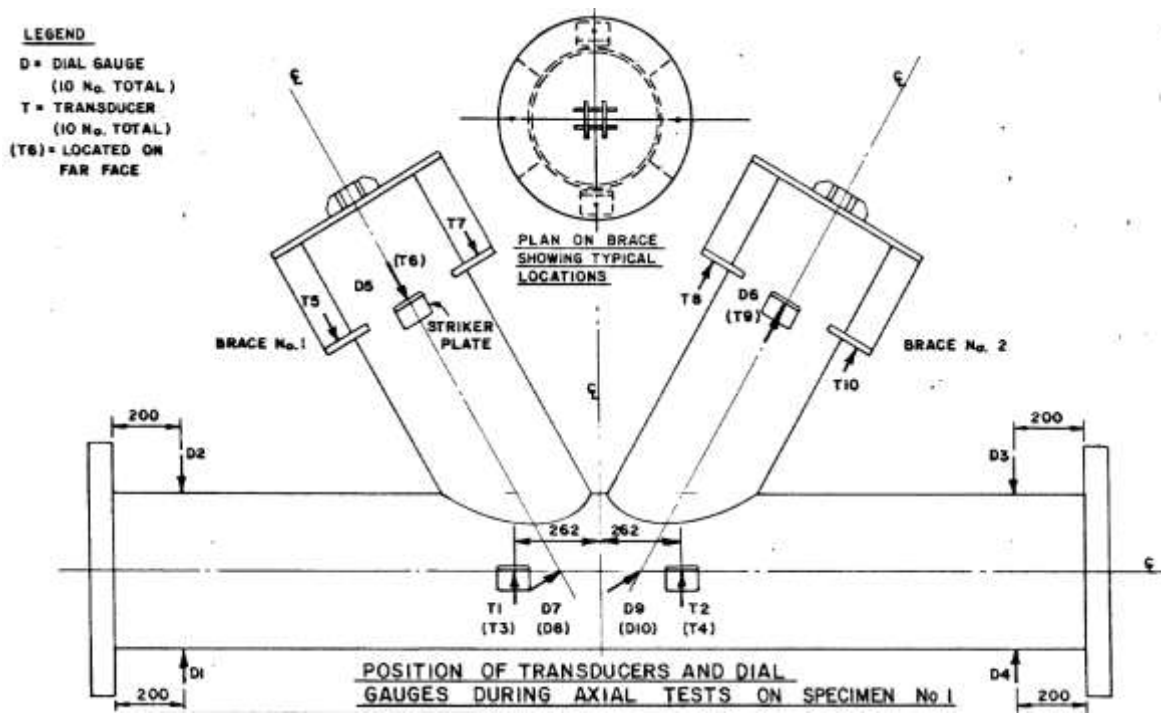


**Figure 5.6 Position of the Transducers and Gauges on Specimen 1, during Axial Loading (AMOCO K-Joint Tests 1983)**

Figure 5.6 shows the position of the transducers and strain gauges on one of the specimens. Compared to the arrangement prescribed by BOMEL one decade later (Figure 5.7), there is substantially more transducers at the chord region. It was understood at this time that both braces and chord interact together to contribute to the LJF on the joint. The gauges in the BOMEL joint tests provide a closer rosette arrangement to ensure the displacements across both chord and braces are adequately recorded.

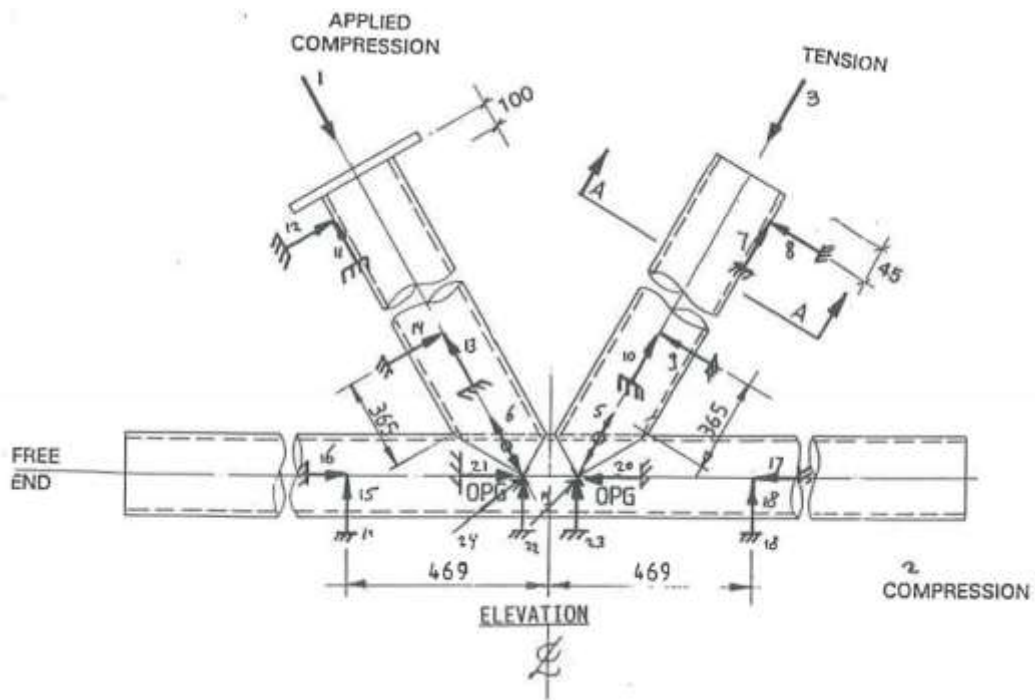


**Figure 5.7 Displacement transducer numbers  
(BOMEL Isolated K-Joint Tests, 1994)**

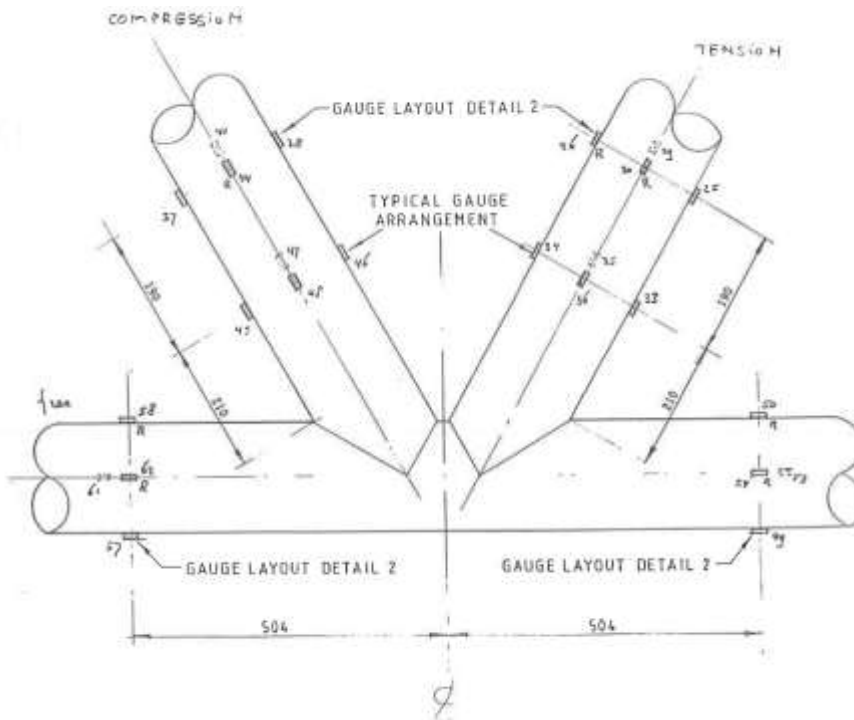


**Figure 5.8 Strain Gauge by number reference  
(BOMEL Isolated K-Joint Tests, 1994)**

## 5.7 Test Procedures

The test rig consists of two 36 inch x 16.5 inch (914mm x 419mm) universal beams, side by side, bolted together so to make a rectangular frame which is 181.1 inch x 114.2 inch (4.6m x 2.9m) internal size, (Figures 5.14, 5.15 & 5.16). At each end, the specimen chord is bolted to a hinge unit, which in turn, is bolted to the rig. The hinge unit cannot transfer moment, hence the chord can be considered to be pin ended. The rig takes the form of a closed rectangle, hence any loads applied to the specimen are reacted within the rig itself. The specimen is supported in the vertical plane with its chord horizontal. The combinations of loading which were used for the elastic tests on Specimen 1 and ultimate tests on Specimens 1 and 2 are given within Figure 5.10.



**Figure 5.9 Specimen 1 under Ultimate Strength  
(Amoco K Joint Tests 1983)**

The elastic load test on Specimen 1 used 4 No 300 kN jacks per brace, but the ultimate tests on Specimens 1 and 2 all use 4 No 900 kN jacks per brace. The 300 kN jacks were used for elastic tests to obtain greater sensitivity for loading within the elastic load range which was much smaller than the range of loading for the ultimate tests. On the compression brace, the jacks were placed directly onto the brace top hat and reacted against the rig through ball seatings to get axial load. A load cell of 0.1% accuracy was placed on one of the jacks applying load to the brace, this load cell was used to

accurately monitor the loads being applied by the hydraulic loading cabinet. To put tension into a brace, it is necessary to place the hydraulic jacks on the outside face of the rig and connect the jack to the specimen with Macalloy bars. A load cell was placed on one of the jacks to monitor the load being applied to the brace. The jacks reacted through cross beams which had adjustable mountings onto the rig so that they could be accurately positioned at the start of the test. Bending load is applied to the end of each brace by a nominal 4.4 tonne jack acting in the appropriate direction. The jack acts on the small rectangular frame on the end of the brace producing a force perpendicular to the axis of the brace.

Electrical resistance strain gauges were bonded to the chord member and both brace members to determine the strain and stress distributions and obtain estimates of stress concentration factors (Figure 5.16). Displacement measurements were taken with a combination of self-temperature compensating transducers with a nominal accuracy of  $\pm 0.025\text{mm}$  and dial gauges with a nominal accuracy of  $\pm 0.01\text{mm}$ . For the accuracy, BOMEL prescribed  $\pm 0.025\text{mm}$  for all gauges as well, so the AMOCO tests results adhered to this. BOMEL prescribed that all transducers and strain gauges be connected to a computer controlled data logging system which will record and reduce all readings. In this case, AMOCO tests are reliant on more manual recording of readings and are more prone to errors.

Local Joint Flexibility measurements were made for the eleven load cases shown in Figure 5.10. The measured and predicted values for local joint flexibility under axial load, in-plane and out-of-plane bending are shown in Table 5.1. The LJF calculations have been developed from the UEG (1982) report for Y-type joints. The UEG used then unpublished work by Fessler and Spooner (1981) as a basis to develop the LJF calculations. The Fessler and Spooner, then unpublished work, was the most current methodology at the time for developing the effects of LJF and was later developed further into the Fessler equations (1983) and improved Fessler (1986) a few years later.

Load Case	Brace 1	Brace 2	Units
	Local Joint Flexibility	Local Joint Flexibility	
1-Axial	1.7	3.8	$\times 10^{-3}$ mm/kN
2-Axial	-1.2	1.4	$\times 10^{-3}$ mm/kN
3-Axial	2.6	2.5	$\times 10^{-3}$ mm/kN
4-Axial	8.4	6.7	$\times 10^{-3}$ mm/kN
5-Axial	1.6	3.9	$\times 10^{-3}$ mm/kN
6-In Plane Bending	2.7	2.3	$\times 10^{-5}$ rad/kNm
7-In Plane Bending	0.8	3.7	$\times 10^{-5}$ rad/kNm
8-In Plane Bending	4.1	4.9	$\times 10^{-5}$ rad/kNm
9-Out of Plane Bending	17.4	16.3	$\times 10^{-5}$ rad/kNm
10-Out of Plane Bending	11.2	12.1	$\times 10^{-5}$ rad/kNm
11-Out of Plane Bending	26.3	3.0	$\times 10^{-5}$ rad/kNm

**Table 5.1 Local Joint Flexibility for Specimen 1  
(AMOCO K-Joint Test Results 1983)**

To derive the LJF values for specimen 1, detailed calculations have been performed to determine the contributions made by the chord and brace deflections based on expressions 5.6 through 5.15. The total displacements for the joint have been extracted from measured results from the transducers and recordings from the tests. The detailed calculations for the LJF for all eleven load cases in specimen 1 have been included in Appendix 3 for the axial, in-plane bending and out-of-plane bending conditions and included in Table 5.1.

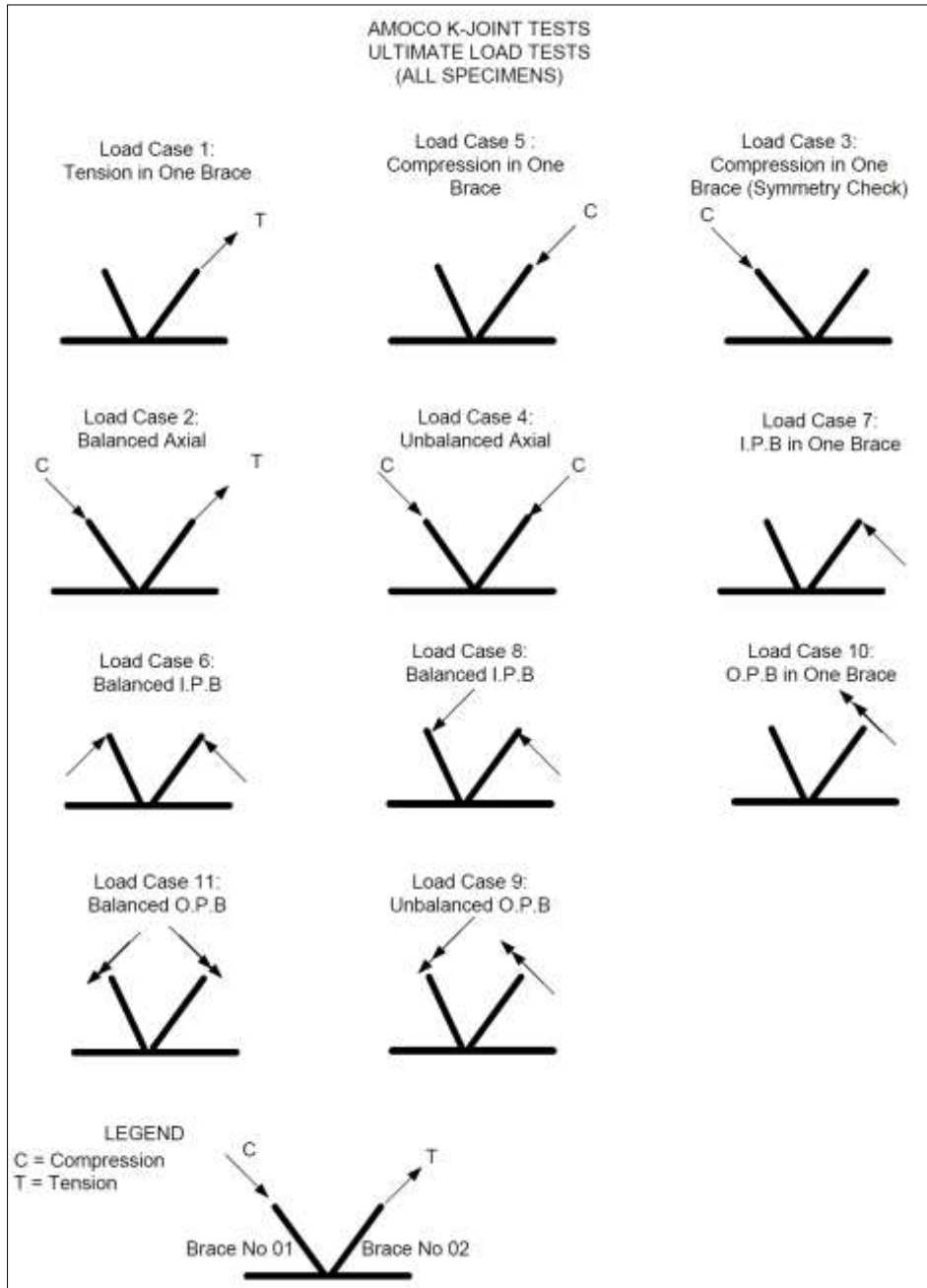


**Figure 5.10 Loadings on Specimens 1 & 2  
(AMOCO K-Joint Tests 1983)**

## 5.8 Loading

The test loading frame and arrangements shown in Figures 5.11 through 5.13 are in good agreement with that prescribed by BOMEL in Figure 5.14. All external load cells have been calibrated within 12 months and have an accuracy of better than  $\pm 0.005$ , but no record exists if the calibration was performed directly before and after the Amoco test results.

### 5.8.1 Axial Load

Axial Load was applied to the braces in the arrangement shown on Figure 5.11. The compression brace is on the left hand side of the drawing and the tension brace is on the right hand side. The elastic load test on Specimen 1 used 4 No 30 tonne jacks per brace, but the ultimate strength tests on Specimens 1 and 2 all used 4 No 90 tonne jacks per brace.

### 5.8.2 Compression Loading

On the compression brace, the jacks were placed directly onto the brace top hat and reacted through the rig through ball seatings. The ball seatings allow rotation of the brace to occur during the test without bending moments being set up in the brace. This arrangement is shown on Figure 5.11.

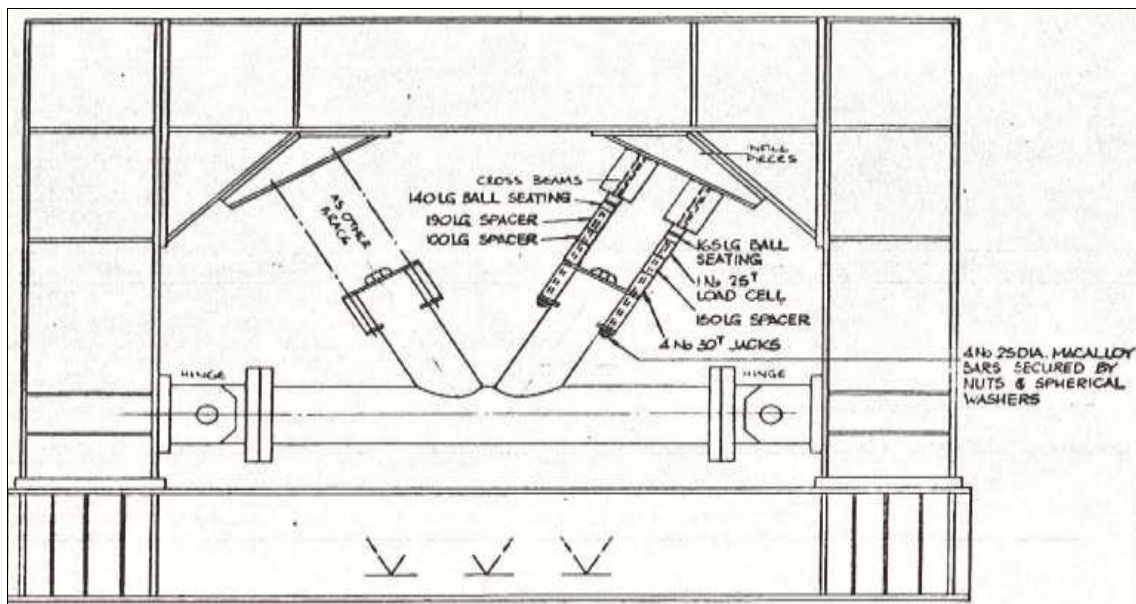


**Figure 5.11 Brace Compression only**  
(AMOCO K-Joint Tests 1983)

### 5.8.3 Tension Loading

To put tension into a brace, it was necessary to place the hydraulic jacks on the outside face of the rig and connect the jacks to the specimen with Macalloy bars. Ball seatings were not required since the bending stiffness is sufficiently low that they will not restrain rotational movement of the brace. This arrangement is shown on Figure 5.12.

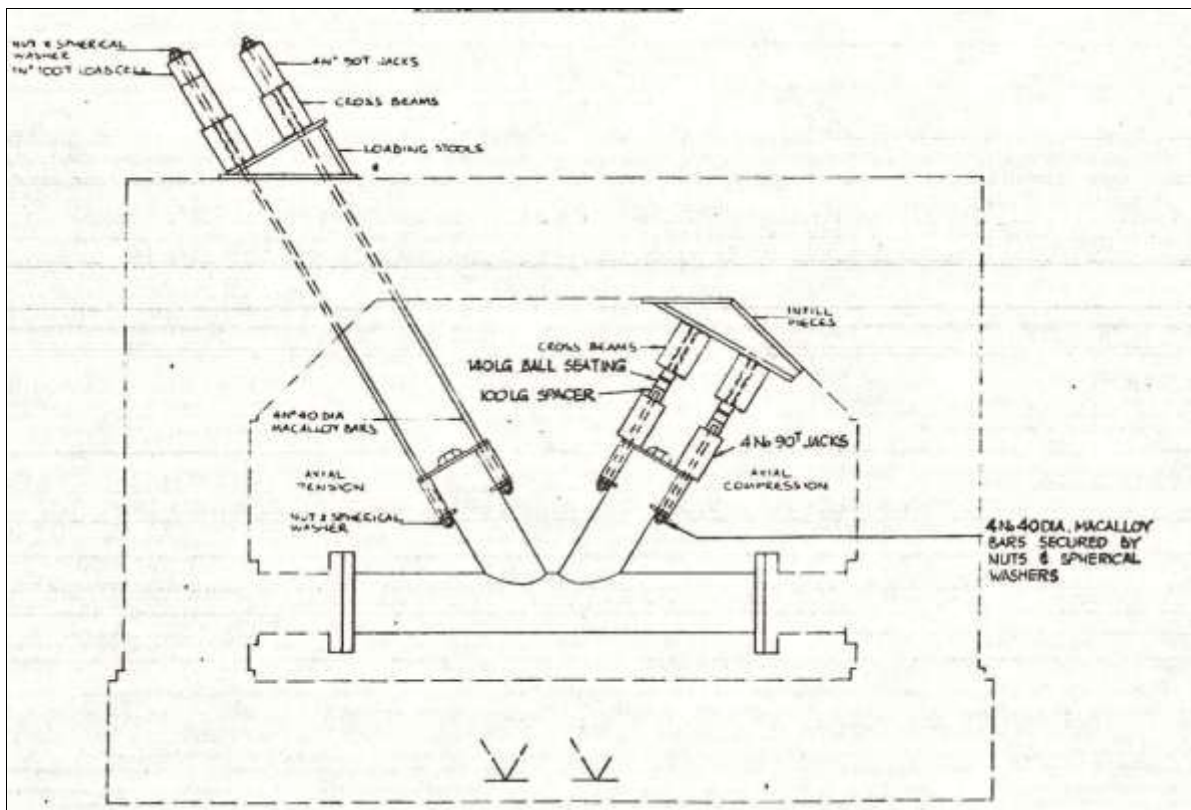


**Figure 5.12 Brace Tension only or Tension and Compression  
(AMOCO K-Joint Tests 1983)**

#### **5.8.4. Bending Load**

Bending load is applied to the end of each brace by a nominal 4.4 tonne jack acting in the appropriate direction. The jack acts on the small rectangular frame on the end of the brace producing a force perpendicular to the axis of the brace. The jack force is multiplied by the lever arm of the jack from the joint to give the applied bending moment. Two identical arms are used which can apply in-plane or out-of-plane bending. This arrangement is found on Figure 5.13.

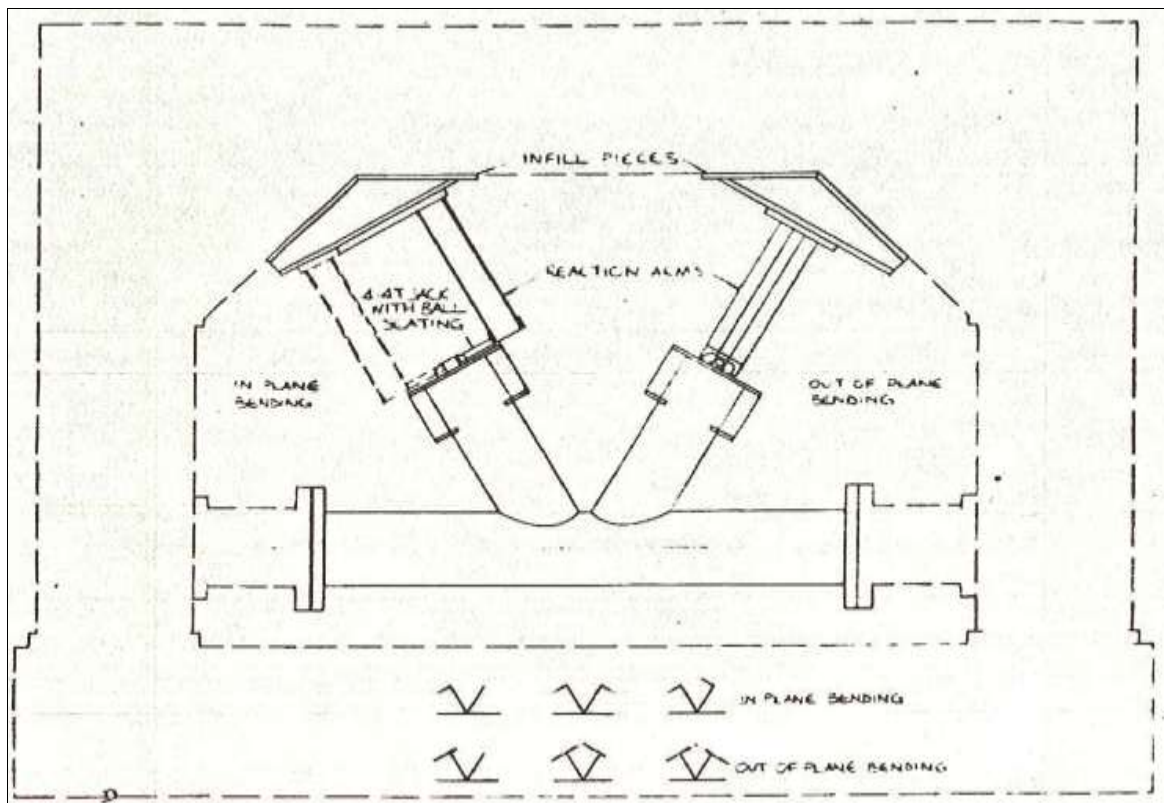


**Figure 5.13 Bending**  
**(AMOCO K-Joint Tests 1983)**

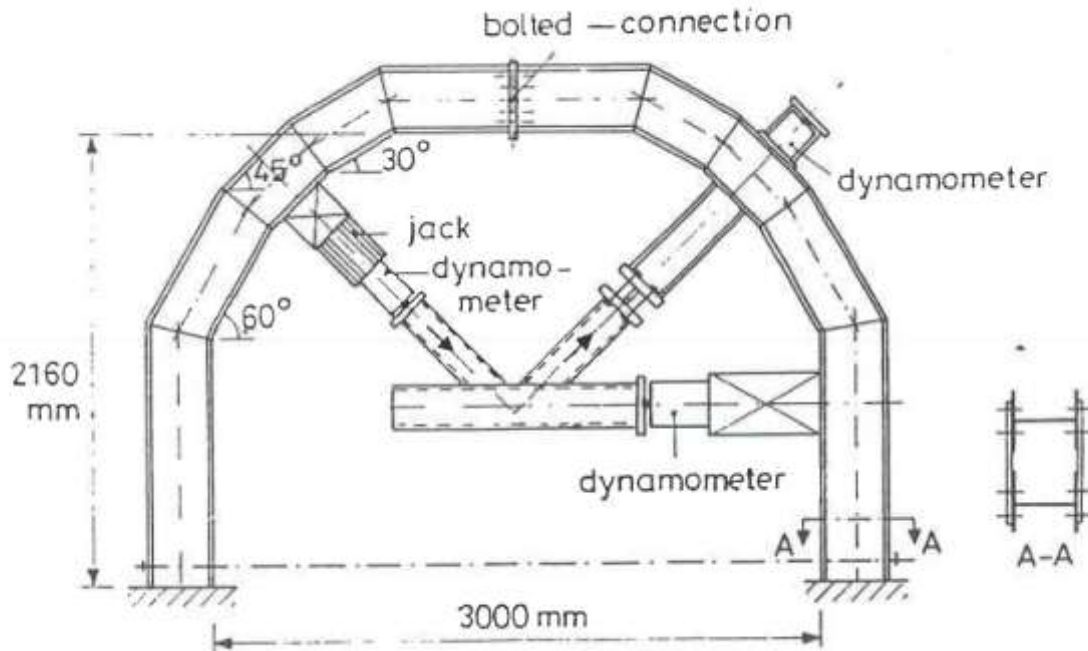


**Figure 5.14 Schematic Drawing of Test Rig**  
**(BOMEL Isolated K-Joint Tests, 1994)**

*Note: The actual angle of the braces was 60° instead of 45°*



**Figure 5.15 General Arrangement of Test Rig and Specimen  
(AMOCO K-Joint Tests 1983)**



**Figure 5.16 Compression and Tension Loading Arrangement  
(AMOCO K-Joint Tests 1983)**



**Figure 5.17 Details of Strain Gauges  
(AMOCO K-Joint Tests 1983)**

### **5.9 Da Silva LJF Small Scale Tests**

In 2015, Da Silva conducted LJF tests on a small scale model to address the in-plane bending condition (IPB). The results of the tests and findings are reported in an MSc thesis by Da Silva (2015). The author of this thesis (Riaz Khan) was responsible for setting up the research statement and the test procedures for the Da Silva tests. The testing of the in-plane condition was selected on the basis that the major source of ambiguity in the AMOCO K-Joint tests was in the comparison of the in-plane condition experimental results and the finite element results. It should be noted that a scaling factor of  $\frac{1}{4}$  the size of the dimensions of the large scale specimen was used which is deemed acceptable, as a rule of thumb, by former Lloyds Register's laboratory researcher Nigel Nichols. Through his many conversations with Nichols, the author (Riaz Khan) was able to obtain an insight on the IPB condition as it has proven difficult to measure appropriately, especially on a small scale. The main source of difficulty in measuring IPB stems from an inability to appropriately position the transducers at the brace and chord to simulate the chord distortion, especially when ultimate capacity has been achieved, but more importantly for the LSBU tests, is that they were able to show similar deformed shape to that

of the Amoco K-Joints for IPB. This was quite useful as it indicated consistency between both tests in terms of their modes of failure.

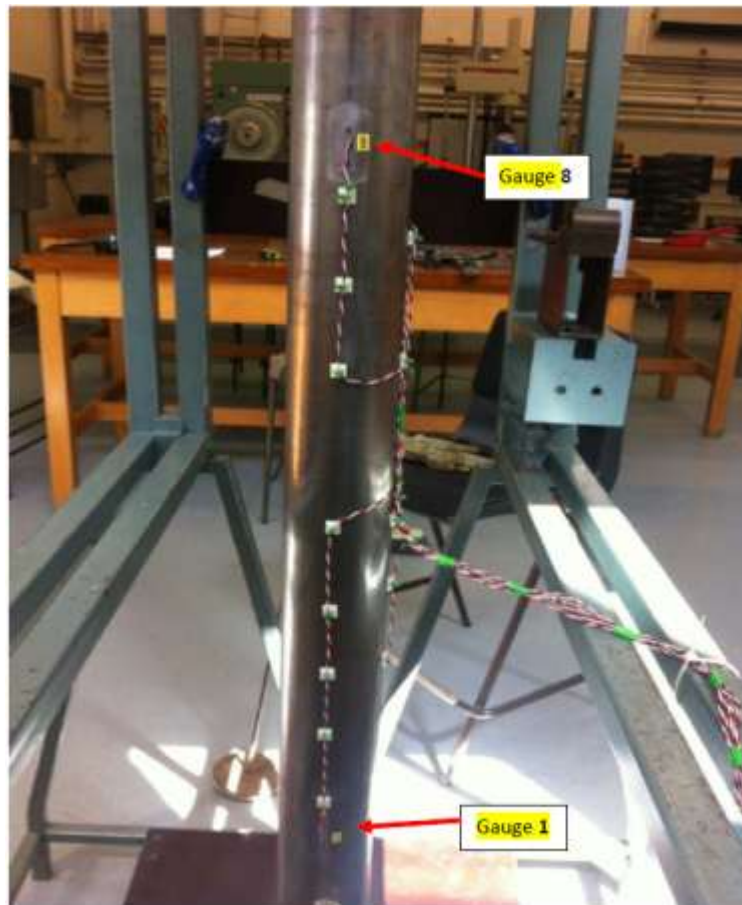


**Figure 5.18 Transducer position  
(LSBU, 2015)**

Using a series of the Mitutoyo 543-690 transducers, their arrangement shown on Figure 5.18, Da Silva was able to record a good relationship between the loaded brace and the applied bending moment for the IPB condition.

When calculating the effects of LJJ using a comparison with the experimental tests results and Buitrago's equations, LSBU reported a 185% difference. There are many reasons for the possible differences in the experimental work vs the finite element modeling. Da Silva used the STRAND 7 software to perform the finite element work which does not carry the LJJ module as with other offshore structures software such as SACS and USFOS. In such a case, it is expected that the STRAND 7 model represents a slightly more rigid joint compared to the measured values in the LSBU

tests. In many cases, the gap size in modern design of tubular joints is generally greater than 50mm (based on ISO 19902) thus K-joint configurations begin to exhibit behaviour of Y-type joints. The Da Silva tests, while based on Y-type joints, provide a good reference for the performance of K-joints with very large gap sizes or those based on modern design criteria. From the experiments, it was noted that linear strain gauges were used, but the use of rosette strain gauges to properly record the rosette deflections around the chord and brace would have been ideal to calculate LJF.

## 5.10 Summary and Conclusions

The AMOCO K-Type joint tests *represent the only published test results for local joint flexibilities for large scale tests*. To derive the RK-LJF equations, they will serve as a basis for experimental work for finite element benchmarking. The following should be noted:

- The AMOCO K-Joint tests were subjected to rigorous test specimen preparation and the rig configuration for load testing, which proved consistent with the BOMEL specification for large scale testing. However, AMOCO K-Joint tests gauges and transducers were not connected to a computer logging system to record displacements and were subject to manual error at times when recording data.
- Furthermore, the LJF values for all eleven load cases are determined through test data and calculations using the methods outlined in the UEG report (1982). The predictions of LJF were based on unpublished Fessler and Spooner (1981) work, which was subsequently updated to reflect the Fessler (1983) and improved Fessler equations (1986). The results of the measured LJF should be treated as indicative values for LJFs and any benchmarking is to consider accuracy in the values as outlined by the constraints in testing and calculation at the time. There is also no clear information on whether calibration of the load cells was performed before and after the AMOCO tests.
- The current work by Da Silva (with Riaz Khan) demonstrated that there is still limited testing and understanding on the IPB condition on tubular joints and presents an opportunity for the

offshore oil and gas industry to lead more large scale testing on tubular joint behaviour. However, the tests did provide a consistent mode of failure to the AMOCO K-Joints test for the IPB and so validates the failure mechanism of the AMOCO K-Joints for IPB. When compared with STRAND 7 results, the measured values demonstrated some degree of joint flexibility compared to the stiffer finite element joint analysis.

## CHAPTER 6

# Finite Element Modeling of Uni-Planar Tubular K-Type Tubular Joints, Results and Comparison with Experimental Data

### 6.1 Background

Accounting for joint flexibility in structural analysis of tubular joints will correctly have the effect of reducing the member end moments i.e. the members shift from being *fixed-ended* to somewhere between *fix-ended* and *pin-ended* depending on the degree of flexibility. At a simple level, joint flexibility causes members to act less as *fix-ended* and more as *pin-ended*.

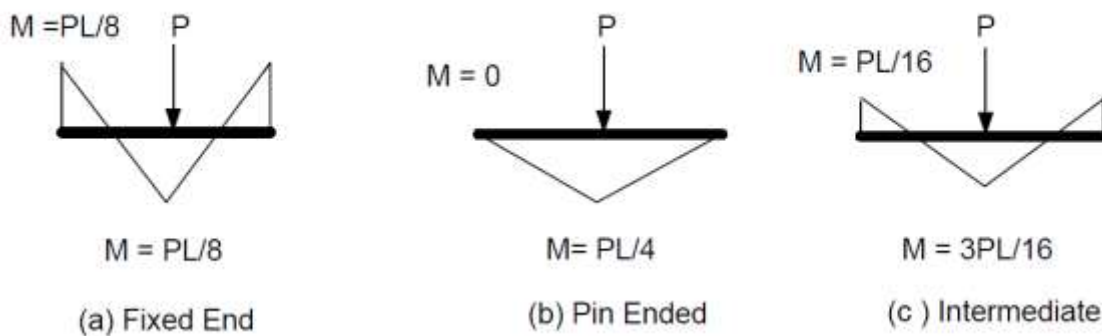


**Figure 6.1 Beam Bending Moments for the fixed, pinned and intermediate end conditions**

From structural analysis principles, the simple illustrations shown in Figure 6.1 show that for a simple beam loaded with a point load,  $P$ , at the center of its span, the bending moments are shed from the ends to mid-span as the *fixed end* conditions change from more rigid to *more pinned* connection. Therefore, the actual stress at the member end is substantially reduced, which in turn leads to a large increase in estimated and actual fatigue life of the joint. The structural behaviour of the intermediate end connection is very similar to the structural behaviour of local joint flexibility of a tubular joint connection.

At the tubular joint level, the local joint flexibility that is inherent in the brace to brace connection, tends to relax the member end forces and moments, increase deflections, redistribute the stresses,

reduce the buckling loads and change the natural frequencies, as well as mode shapes of an offshore platform, compared to the original design approach using rigid joint frame analysis. To demonstrate the action of joint flexibility, the stiffness method is often used to perform the structural analysis and dictates that the load deflection relationships for joints to be included in the analyses in the form of a local stiffness matrix  $k$ , relating applied loads at nodes of the joint,  $p$  to deflections,  $\delta$  where:

$$p = k \delta \quad (6.1)$$

Fessler et al (1982) produced a set of flexibility matrices  $f'$  for several tubular joints of different geometric configurations, relating deflections  $\delta'$  in response to applied loads  $p'$  where

$$\delta' = f' p' \quad (6.2)$$

A tubular joint with two braces serves to illustrate the method, but the equations used may be extended to accommodate any number of braces. Flexibility coefficients were determined in model tests conducted by Fessler et al (1982), in Equation (6.2), for only three degrees of freedom for each brace of a joint. These freedoms do not correspond with the three degrees of freedom required in Equation (6.1) and the local stiffness matrix must now be derived by providing flexibility data and basic engineering bending theory. A procedure to derive the joint local stiffness matrix is now described (Fessler et al 1982).

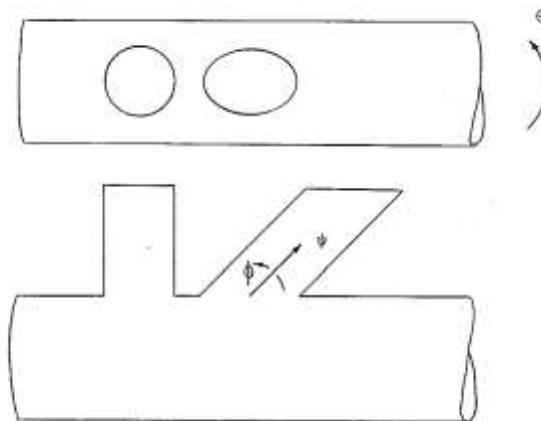


**Figure 6.2 The degrees of freedom provided by Fessler's experimental work  
(Adapted from Fessler et al 1982)**

Figure 6.2 shows the directions of the three degrees of freedom  $\psi$ ,  $\theta$ ,  $\phi$ , used for loads and displacements relating to the flexibility matrices (Fessler et al, 1982). The brace axial displacements are given by the measured displacements, these being perpendicular to the chord axis. The flexibility matrix must be converted from these skewed axes into a rectangular Cartesian system also eliminating the out-of-plane degree of freedom from the equations. Figure 6.3 shows the degrees of freedom  $x$ ,  $y$ ,  $\phi$  of interest to the plane frame problem.

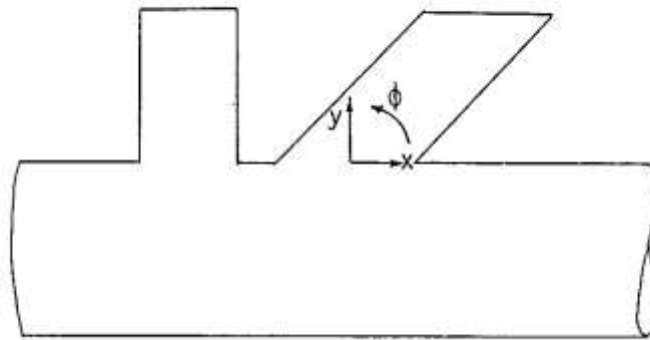


**Figure 6.3 The degrees of freedom required in the Joint Stiffness Matrix**  
(Adapted from Fessler et al, 1982)

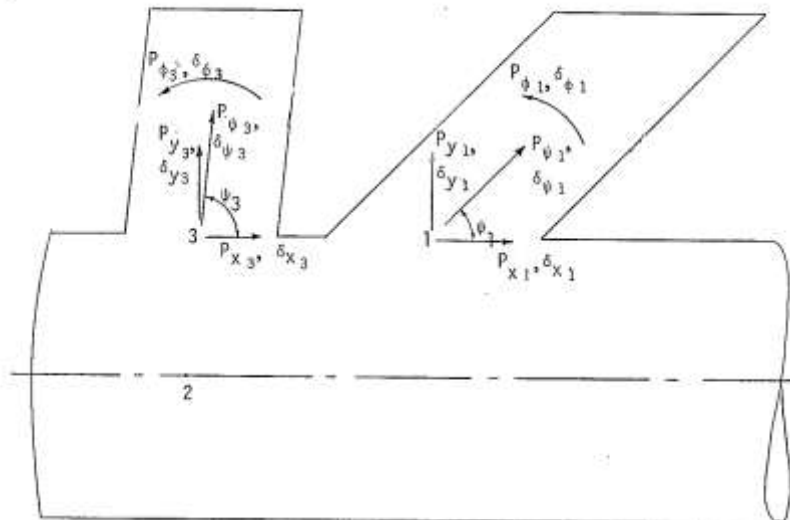


**Figure 6.4 Loads and relative displacements of a two braced joint**  
(Adapted from Fessler et al 1982)

The complete system of loads and displacements for degrees of freedom in the plane of the two braced joints is shown in Figure 6.4. The flexibility of a tubular joint is considered to be the difference between the displacements at the member ends at unit load. It is conventionally assumed in structural

analysis that tubular joints can effectively be represented as a discrete point to which members are rigidly attached. Therefore, in the traditional design (using computer-based analyses) of fixed offshore structures, the effect of joint flexibility is generally not considered. However, in the limited studies undertaken thus far, the inclusion of joint flexibility in the analysis of offshore structures has been identified as having an effect on both the global static and dynamic responses to the structure. For such a joint (Figure 6.4), a flexibility matrix  $f^*$ , is provided below, where, all deflections  $\delta$ ' are measured relative to the chord axis.

		$P\psi_1/ED^2$	$P\theta_1/ED^3$	$P\phi_1/ED^3$	$P\psi_3/ED^2$	$P\theta_3/ED^3$	$P\phi_3/ED^3$
Node 1	$\delta_{\psi_1/D}$	$f_{\psi_1\psi_1}$	$f_{\psi_1\theta_1}$	$f_{\psi_1\phi_1}$	$f_{\psi_1\psi_3}$	$f_{\psi_1\theta_3}$	$f_{\psi_1\phi_3}$
	$\delta_{\theta_1}$	$\times$	$f_{\theta_1\theta_1}$	$f_{\theta_1\phi_1}$	$f_{\theta_1\psi_3}$	$f_{\theta_1\theta_3}$	$f_{\theta_1\phi_3}$
	$\delta_{\phi_1}$			$f_{\phi_1\phi_1}$	$f_{\phi_1\psi_3}$	$f_{\phi_1\theta_3}$	$f_{\phi_3\phi_3}$
Node 3	$\delta_{\psi_3/D}$				$f_{\psi_3\psi_3}$	$f_{\psi_3\theta_3}$	$f_{\psi_3\phi_3}$
	$\delta_{\theta_3}$					$f_{\theta_3\theta_3}$	$f_{\theta_3\phi_3}$
	$\delta_{\phi_3}$						$f_{\phi_3\phi_3}$

**Figure 6.5 Flexibility Matrix for Uni-Planar Two Braced Joint (global representation)**  
 (Adapted from Fessler et al 1982)

Fessler (1982) et al provided the following stages in the derivation of the local stiffness matrix:

1. Firstly the values of Young's modulus, E, the chord diameter, D, appropriate to the application of the joint are used to dimensionalize the flexibility matrix  $f^*$ .
2. The flexibility matrix is then transformed to rectangular Cartesian system, shown in Figure 6.4. A reference point (Node 2), is chosen on the chord axis and considered fixed in translation and rotation, so that deflections may be conveniently taken as absolute for the purposes of this transformation. The flexibility matrix in Cartesian co-ordinates required is:

		Node 1			Node 3		
		$p_{x_1}$	$p_{y_1}$	$p_{\phi_1}$	$p_{x_3}$	$p_{y_3}$	$p_{\phi_3}$
Node 1	$\delta_{x_1}$	$f_{x_1x_1}$	$f_{x_1y_1}$	$f_{x_1\phi_1}$	$f_{x_1x_3}$	$f_{x_1y_3}$	$f_{x_1\phi_3}$
	$\delta_{y_1}$		$f_{x_1y_1}$	$f_{y_1\phi_1}$	$f_{y_1x_3}$	$f_{y_1y_3}$	$f_{y_1\phi_3}$
	$\delta_{\phi_1}$			$f_{\phi_1\phi_1}$	$f_{\phi_1x_3}$	$f_{\phi_1y_3}$	$f_{\phi_1\phi_3}$
$f =$							
Node 3	$\delta_{x_3}$				$f_{x_3x_3}$	$f_{x_3y_3}$	$f_{x_3\phi_3}$
	$\delta_{y_3}$					$f_{y_3y_3}$	$f_{y_3\phi_3}$
	$\delta_{\phi_3}$						$f_{\phi_3\phi_3}$

**Figure 6.6 Flexibility Matrix in Cartesian Co-ordinate Form**  
(Adapted from Fessler, 1982)

3. Matrix Inversion is performed on the transformed flexibility matrix,  $f$  (Figure 6.6), to produce the local stiffness matrix  $k^*$ , relating deflections,  $\delta$  of Nodes 1 and 3, relative to the reference point Node 2, as shown on Figure 6.4, so

$$P = f^{-1} \delta = k^* \delta \quad (6.3)$$

4. Provision is now made in the stiffness matrix for any arbitrary absolute displacement at any of the nodal points on the joint to be equated with loads at these points, thus a further transformation takes place on  $k^*$  to produce  $k$ , the final joint stiffness matrix of Equation (6.1).

Within the Benchmarking Study outlined in this Chapter, a flexibility matrix is derived comparing the coefficients of finite element analysis and measured test data for a uni-planar K-type tubular joint, in the form of Equation (6.1).

## 6.2 Shell Finite Elements

The ABAQUS suite of software (Version 6.11) is used for the mesh sensitivity study, benchmarking study and the generation of the coefficients of the parametric study to model the K-joint in finite element analysis Romeyn et al (1992) proposed the use of shell type elements exhibiting thin bending shell theory behaviour. Three dimensional shell elements in ABAQUS are named as follows:

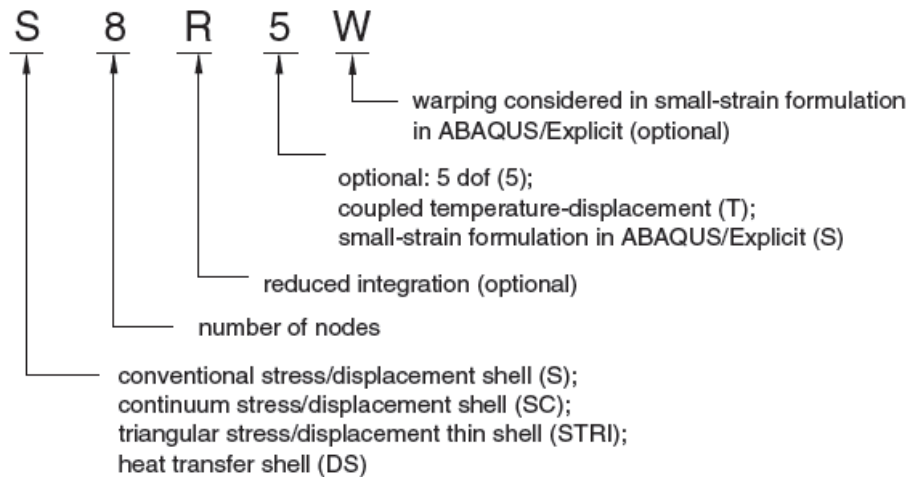


**Figure 6.7 Naming Convention for three-dimensional shell elements  
(ABAQUS Manual, 2011)**

For example, S4R is a 4-node, quadrilateral, stress/displacement shell element with reduced integration and a large-strain formulation, and a SC8R is an 8-node, quadrilateral, first-order interpolation, stress/displacement continuum shell element with reduced integration. ABAQUS includes general-purpose, conventional shell elements as well as conventional shell elements that can be used for both thick and thin shell problems. The 8-node quadrilateral elements in ABAQUS while they do not hourglass, they are prone to *locking*: both shear and volumetric locking. Shear locking can occur in first order fully integrated 8-noded elements subjected to bending. The numerical formulation of the elements gives rise to shear strains that do not really exist, the so called parasitic shear. These elements become too stiff in bending in particular if the element is of the same order of magnitude or greater than the wall thickness.

As stated in the ABAQUS manual (2011), *“The general-purpose conventional shell elements provide robust and accurate solutions to most applications; however in certain cases, enhanced performance may be obtained with the thin or thick shell elements, for example if only small strains occur and five degrees of freedom of modes are required.”*

Conventional shell elements allow transverse shear deformation. They use thick shell theory as the thickness increases and become discrete Kirchhoff thin shell elements as the thickness decreases. Element Types include S3/S3R, S3RS, S4R, S4RS, S4RSW, SAX1, SAX2, SAX2T, SC6R and SC8R. Although Romeyn (1982) proposed the use of the 8-noded shell elements, as he concluded that they demonstrate *“flexible”* behaviour better than 4-noded elements, ABAQUS argues the use of the 4-noded quadrilateral thin shell elements (S4R) can be used just as well when used to determine very small nodal displacements.

According to the ABAQUS Manual (2011), the S4 is a fully integrated, general purpose, finite-membrane strain element where, *“The element’s membrane response is treated with an assumed strain formulation and gives accurate solutions to in-plane bending problems, is not sensitive to element distortion and avoids parasitic locking. The S4 element can be used for problems prone to membrane or bending mode hour-glassing, in areas where greater solution accuracy is required or for problems where in-plane bending is expected.”*

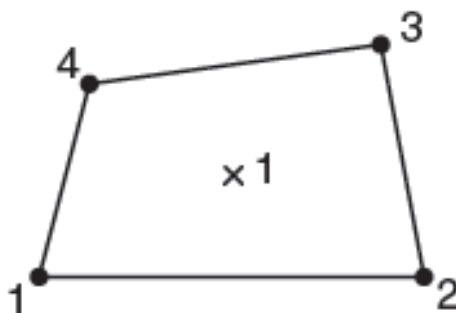


**Figure 6.8 4-Noded Reduced Integration Element, Numbering of Integration points for output, Stress/Displacement Analysis ( ABAQUS Manual, 2011)**

Although the 8-noded quadrilateral element can provide accurate results in most loading solutions, ABAQUS also noted that because of their constant bending and membrane strain approximations, high mesh refinement may be required to capture pure bending deformations or solutions to problems involving high strain gradients. The ABAQUS suite of software is one of the world's leading finite element packages for structural analysis. The finite elements included with ABAQUS have been appropriately benchmarked.

For the above-mentioned reasons, the 4-noded (S4R) quadrilateral shell element has been selected as the finite element best suited to model the K-joint behaviour. The general behaviour and characteristics of the S4R element is provided in Appendix 1.

### **6.3 Finite Element Mesh Analysis**

Prior to the Benchmarking Study, a mesh size and refinement study was performed which shows that the 4-noded General Purpose Shell Element (S4R) would yield convergent displacement results with that obtained from the experimental data. The use of shell type elements has the added advantage of not having to model the weld profile and details, as per the recommendations provided in DNV RP 203 (2010). The main reason for DNV stating this is because the LJF FE analysis is primarily focused on obtaining displacement values rather than stress analyses which require more accurate finite element modeling and mesh refinement. As such, FE stress concentration models which are generally sensitive to mesh refinement and element type, FE displacement models are not as sensitive to element type and mesh refinement, provided the FE mesh generated, is reasonably refined. The Mesh Generator in ABAQUS serves as a building model tool and is used in this study compared to the tedious manual mesh generation. The application of the mesh generator was verified against test data provided in the AMOCO test joint for LJF for axial compression, tension and out-of-plane and in-plane bending.

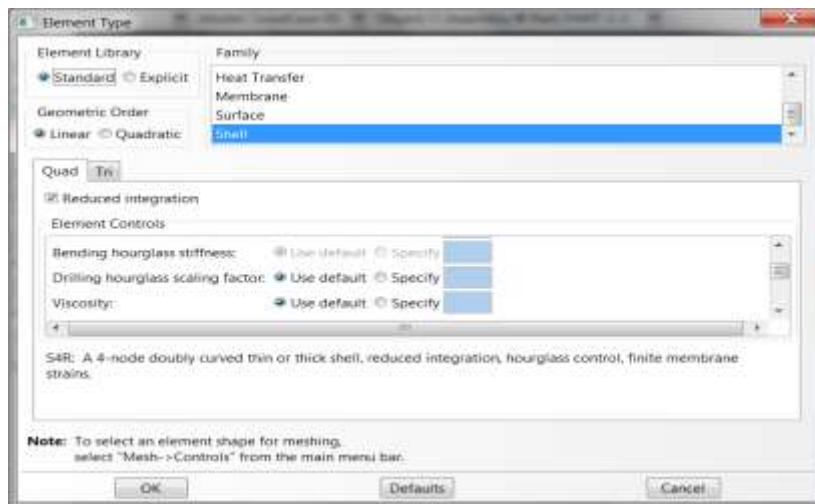


**Figure 6.9 Setting Element Type, 4-Noded Quadrilateral Thin Shell Elements**

The first step in the meshing process is to *Assign Mesh Properties and Set Mesh Controls*. For this, we need to set mesh control in the form of mesh density, element shape and element size. After these are included, the mesh can now be generated. To refine the mesh, ABAQUS provides a series of techniques and tools including the *Seeding Tool*, which allows adjustment to the mesh density in selected areas. *The Partition Toolset* allows partition of complex models into simpler regions. *The Virtual Topography Toolset* allows the simplification of the model by combining small faces and edges with adjacent faces and edges. Both these tools are very useful as they allowed the tubular joint to be modeled as a 2D model in plan representation and then combined to represent the complete tubular joint. *The Edit Mesh Toolset* allows minor adjustments in the mesh. The mesh can now be verified by using the *Verification Tool* on the suitability of elements for use in the mesh. Figure 6.9 shows the selection of the proposed element and Figure 6.10 illustrated the refined mesh in the un-rendered format, in ABAQUS and Figure 6.11 shows the refined mesh with the elements.

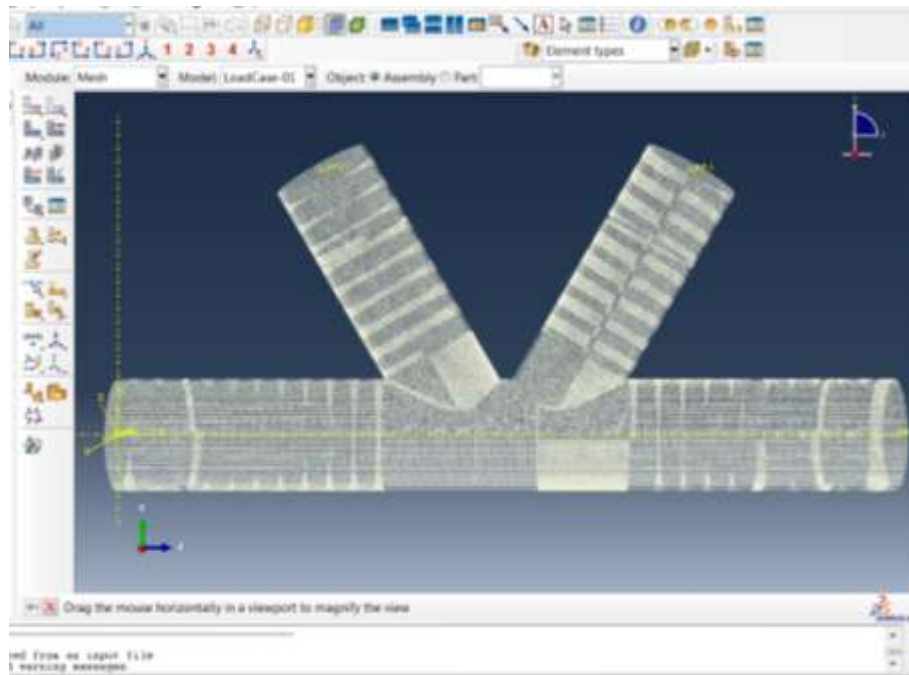


**Figure 6.10 Refined Mesh in Mesh Generator**

The values for the total deflections for finite element analyses were compared with those measured from the AMOCO tests. The total deflections from the FE analysis were extracted from the nodal deflections obtained from the results files after post-processing. The average nodal deflections were considered for chord and brace displacements. To calculate  $\delta T$  (Total deflection) from the FE Analysis, the average nodal deflection was divided by the applied loading i.e. 300KN ( $\delta T/P$ ). The  $\delta T$  obtained from the AMOCO K-Joints were abstracted from those measured by the transducers and gauges and calculated in the AMOCO K-Joint Test Report.

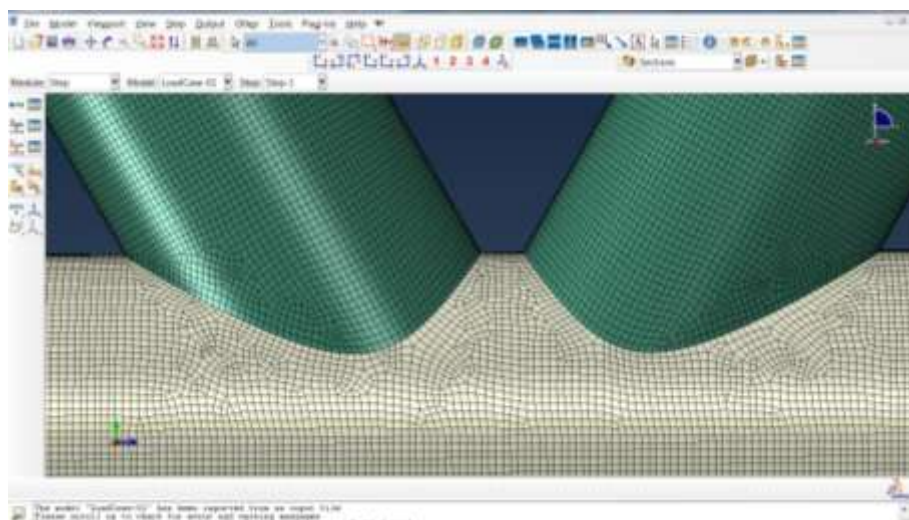


**Figure 6.11 Refined Mesh with Elements**

Results in Table 6.1 indicate that the refined mesh together with the use of 4-noded general purpose shell element (reduced integration with hourglass control, finite membrane strains) provide results within 1-2% compared with test data for in-plane and out-of-plane bending and within 10% for axial loading. The basis for determining the structural strength of tubular joints is not to consider them individually as axial, in-plane bending and out-of-plane bending. In fact, all three load effects are generally combined for tubular joint code design checks and structural assessments are performed based on system performance within the frame structure and expressed as an interaction ratio. Therefore, due to limitations in the test results at the time and the good performance of the in-plane and out-of-plane results of FEA vs test results the refinement to the FEA model is deemed as adequate, without any compromise to the strength requirements of the joint.

The structural model (FEA) provided in the finite element sensitivity study can be used for the benchmarking study for all the load cases in the AMOCO K-Joint Study and the determination of the local joint flexibilities at chords and braces from the total deflections obtained. The ABAQUS (2011) provides the following explanation for the use of the SR4 element using reduced integration and hourglass control: *“The advantage of the reduced integration elements is that the strains and stresses are calculated at the locations that provide optimal accuracy. A second advantage is that the reduced number of integration points decreases CPU time and storage requirements. The disadvantage is that the reduced integration procedure can admit deformation modes that cause no straining at the integration points. These zero-energy modes make the element rank-deficient and can cause a phenomenon called “hourglassing”, where the zero energy mode starts propagating through the mesh, leading to inaccurate solutions.”* The structural model provided in the finite element sensitivity study can be used for a benchmarking study for all the load cases in the Amoco K-Joint study and the determination of the local joint flexibilities at chords and braces from the total deflections obtained.

Load	Amoco K-Test Results	FE Results Refined Mesh	% Difference
Total Displacement (Axial) - Load Case No 2 - Tension Brace only	<b>0.0031</b> (mm/kN)	<b>0.0028</b> (mm/kN)	9.67%
Total Displacement (Out-of-Plane Bending) - Load Case No 11, Brace 1 only	<b>3.90 E-05</b> (rad/kN-m)	<b>3.917 E-05</b> (rad/kN-m)	0.43%
Total Displacement (In-Plane Bending) - Load Case No 06, Brace 1 only	<b>3.21 E-05</b> (rad/kN-m)	<b>3.164 E-05</b> (rad/kN-m)	1.43%

**Table 6.1 Mesh Sensitivity Results**

#### **6.4 Benchmarking Study of FE Model and the AMOCO K-Joint Tests**

Eleven finite element (FE) models were created in ABAQUS to represent the geometry and loadings of the specimens (Figure 5.8). The main objective of the FE model generation was to benchmark the AMOCO test data by providing a finite element gapped K-joint model that best represents the results of the eleven load cases. FE models for Load Case 10 are shown on Figures 6.12 through 6.14, while Figures 6.15 and 6.16 show various stages in the model creation in the pre-processing mode. Figure 6.17 illustrates the deformed and stress plot, post processing, for Load Case 10.



**Figure 6.12 AMOCO K-Joint Finite Element Benchmark Model, Y-Z plane view  
(generated in ABAQUS for Load Case 10)**



Figure 6.13 AMOCO K-Joint Finite Element Benchmark Model, X-Y plane view  
(generated in ABAQUS for Load Case 10)



Figure 6.14 AMOCO K-Joint Finite Element Benchmark Model, X-Y-Z plane view  
(generated in ABAQUS for Load Case 10)

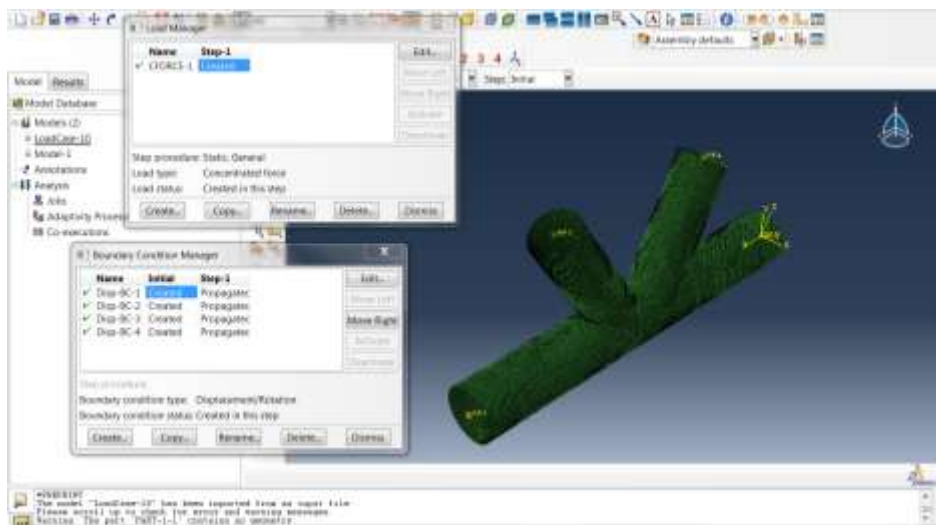
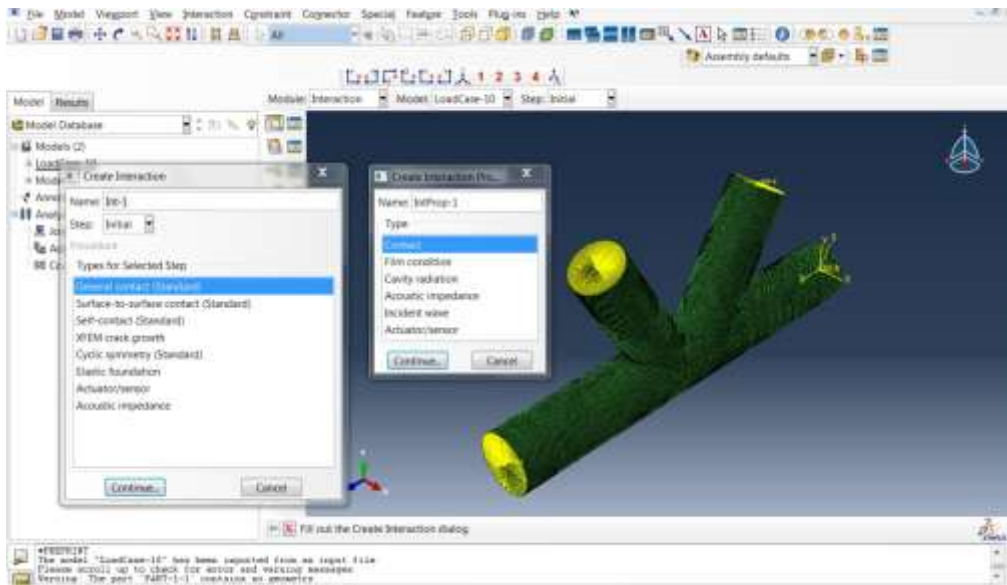
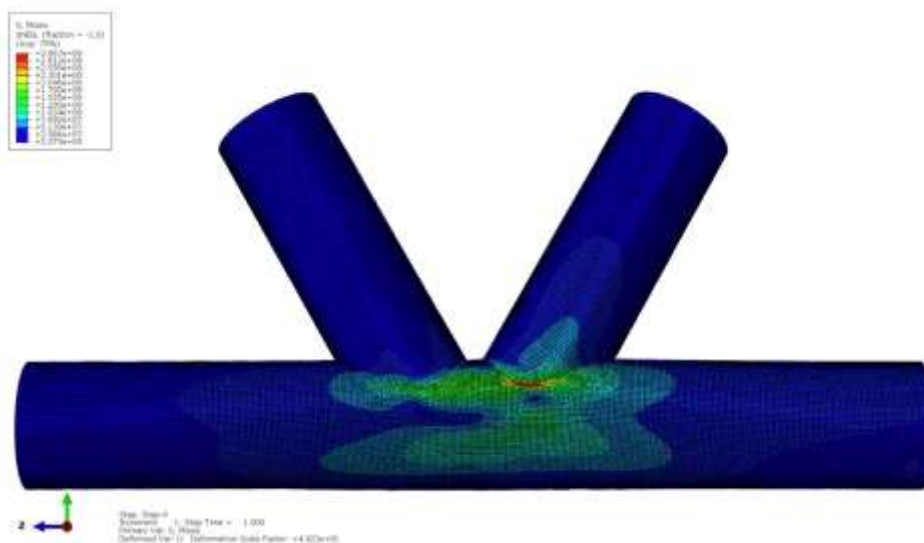


Figure 6.15 AMOCO K-Joint Finite Element Benchmark Model, Applying Boundary Conditions  
(generated in ABAQUS 6.11)



**Figure 6.16 AMOCO K-Joint Finite Element Benchmark Model, Creating Load Step  
(generated in ABAQUS 6.11)**

The chord walls at the supports in the FE model were restrained from translation in the x and y directions to maintain the roundness of the chord section (Figure 6.15). The joint is modeled as part of a structure where the beam theory is no longer valid and must be replaced by shell theory, to derive the benefits of the FE model. In the FE model, the end cross sections behave as rigid planes with no ovalization (Figure 6.16). The contribution made by chord rotations are calculated on spreadsheets and added to the overall LJJ of the joint.



**Figure 6.17 AMOCO K-Joint Finite Element Benchmark Model, Deformed Mesh & Stress Contours  
(generated in ABAQUS for Load Case 10)**

## 6.5 Benchmarking Study Results

A complete set of calculated and measured values for LJJ to include the effects of in-plane bending, out-of-plane bending and axial compression and tension loadings (Figure 5.8) based on the AMOCO K-Joint tests and finite element modeling of the steel tubular joint are provided in Table 6.2. A procedure to determine the LJJ effects due to Axial, OPB and IPB is provided on Figure 6.18. Joint Flexibility calculations to support this procedure from the FE modeling are provided in Appendix 2. It should be noted that the only published large scale testing of tubular joints for LJJ has been the Amoco K-type joints.

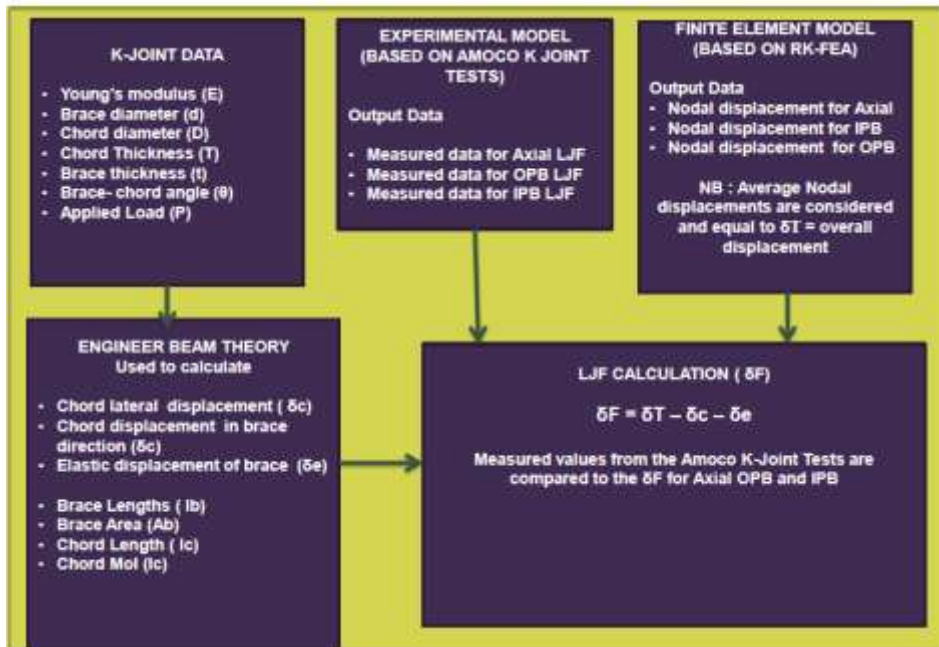


Figure 6.18 Procedure for the calculation of LJJ for Axial, OPB and IPB

Load Case	Measured (AMOCO K-Joint Test Results)		Finite Element Analysis (Benchmarking Study)		Units	Flexibility matrix coefficients	
	Brace 1	Brace 2	Brace 1	Brace 2		Brace 1	Brace 2
1	1.7	3.8	1.6	3.2	$\times 10^{-3}$ mm/kN	$f_{14}$	$f_{44}$
2	-1.2	1.4	-2.5	2.5	$\times 10^{-3}$ mm/kN	$-f_{11}+f_{14}$	$-f_{41}+f_{44}$
3	2.6	2.5	3.2	1.6	$\times 10^{-3}$ mm/kN	$f_{11}$	$f_{41}$
4	8.4	6.7	4.8	4.8	$\times 10^{-3}$ mm/kN	$f_{11}+f_{14}$	$f_{41}+f_{44}$
5	1.6	3.9	1.6	3.2	$\times 10^{-3}$ mm/kN	$f_{14}$	$f_{44}$
6	2.7	2.3	2.8	2.8	$\times 10^{-5}$ rad/kNm	$-f_{33}+f_{36}$	$-f_{63}+f_{66}$
7	0.8	3.7	0.35	3	$\times 10^{-5}$ rad/kNm	$f_{36}$	$f_{66}$
8	4.1	4.9	3.3	3.3	$\times 10^{-5}$ rad/kNm	$f_{33}+f_{36}$	$f_{63}+f_{66}$
9	17.4	16.3	19	19	$\times 10^{-5}$ rad/kNm	$f_{22}+f_{25}$	$f_{52}+f_{55}$
10	11.2	12.1	7.4	11.2	$\times 10^{-5}$ rad/kNm	$f_{25}$	$f_{55}$
11	2.6	3	3.1	3.1	$\times 10^{-5}$ rad/kNm	$f_{22}-f_{25}$	$-f_{52}+f_{55}$

**Table 6.2 Comparison of AMOCO K-Joint Tests and FE Modeling Results**

A comparison is shown between the flexibility coefficients derived from the finite element analysis and the measured test results in Table 6.2. The flexibility matrix developed by Fessler (1982) and outlined in Figure 6.5 to represent uni-planar two brace joint can be simplified to represent the flexibility coefficients in the form outlined in Figure 6.19.

$$\begin{bmatrix} \delta_1 \\ \Phi_{o1} \\ \Phi_{i1} \\ \delta_2 \\ \Phi_{o2} \\ \Phi_{i2} \end{bmatrix} = \begin{bmatrix} f_{11} & & & & & \\ & f_{22} & & & & \\ & & f_{33} & & & \\ f_{41} & & & f_{44} & & \\ & & & & f_{55} & \\ & & & & & f_{66} \end{bmatrix} \times \begin{bmatrix} P_1 \\ M_{o1} \\ M_{i1} \\ P_2 \\ M_{o2} \\ M_{i2} \end{bmatrix}$$

**Figure 6.19 Flexibility Coefficients in the Matrix Form**

		<b>RK-FEA Results</b>	<b>Measured (AMOCO K-Joint Tests)</b>	<b>Units</b>
f <sub>11</sub> =	f <sub>44</sub> =	<b>3.2</b>	<b>3.8</b>	x10 <sup>-3</sup> mm/kN
f <sub>14</sub> =	f <sub>41</sub> =	<b>1.6</b>	<b>1.7</b>	x10 <sup>-3</sup> mm/kN
f <sub>22</sub> =	f <sub>55</sub> =	<b>11.2</b>	<b>12.1</b>	x10 <sup>-5</sup> rad/kNm
f <sub>25</sub> =	f <sub>52</sub> =	<b>7.4</b>	<b>11.2</b>	x10 <sup>-5</sup> rad/kNm
f <sub>33</sub> =	f <sub>66</sub> =	<b>3.0</b>	<b>3.7</b>	x10 <sup>-5</sup> rad/kNm
f <sub>36</sub> =	f <sub>63</sub> =	<b>0.3</b>	<b>0.8</b>	x10 <sup>-5</sup> rad/kNm

**Table 6.3 Flexibility Matrix Coefficients from AMOCO K-Joint Tests and FE Modeling**

While the test results may have limitations as outlined in Chapter 5, the results generated from the RK-FEA model based on classical theory, finite element modeling and the use of established FE software provide a good validation of the limited test results and provide a basis to extend the research to other K-joint geometric ranges. The AMOCO K-Joint is a high  $\beta$  joint (approaching  $\beta = 1.0$ ) which many researchers, including Woodsworth (1983) and Billington (1994), agree display unique behaviour as the effects of the chord brace interactions are generally not well represented. In the context of LJF, high  $\beta$  joints are stiffer than those with lower  $\beta$  values. This is well represented in the RK-FEA model and other finite element analysis discussed in Chapter 7. As  $\beta$  values increase, a reduction in LJF values is expected but a greater sample of the results from varying  $\beta$  values is therefore needed to be considered when addressing LJF comparison. It should also be noted that the RK-FEA has been created using a very fine mesh and a simple joint model so the possibility of an inaccurate model is remote, whilst the possibility of errors from the AMOCO tests are more likely and are discussed in Chapter 5. From this perspective any variations from the test results and the RK-FEA model are not entirely unexpected.

## 6.6 LJF Comparison Study with AMOCO K-Joint Tests

The existing formulations applicable to uni-planar gapped K-type joints are the Fessler, Efthymiou, Chen, Buitrago, Asgarian and MSL equations. However, Efthymiou's equations are only applicable

for in-plane and out-of-plane bending. MSL-Joint formulations are not considered in the comparison study, as joint flexibility is considered as implicit to the MSL equation for ultimate strength. Due to results provided by the AMOCO K-type joint tests confined to the elastic range, the comparison with the RK-FEA model will be confined to the elastic LJJ behaviour of the K-type joint.

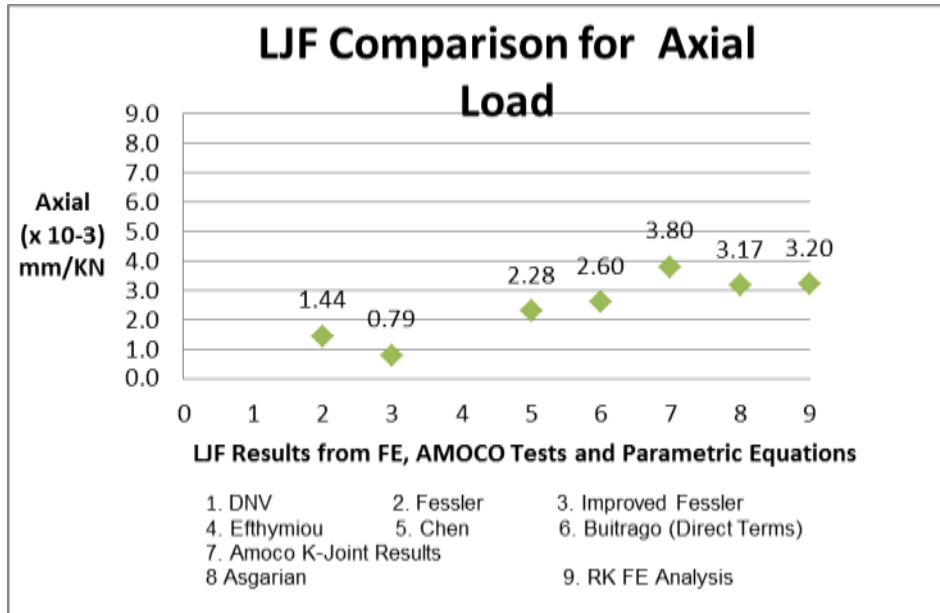


**Figure 6.20 LJJ Comparison for Axial Loading (Direct Terms)**

For axial loading (Figure 6.20), the results from the direct terms associated with the RK-FE modeling and the AMOCO K-Joint tests are within 20% of each other. Improved Fessler’s equations under-predicts LJJ by approximately 80%. Fessler’s equations under-predicts LJJ by approximately 60% and Buitrago and Chen under-predict by 30%, compared to the AMOCO K-Joint test results. The RK-FEA model provides the closest agreement with the AMOCO K-Joint tests results.

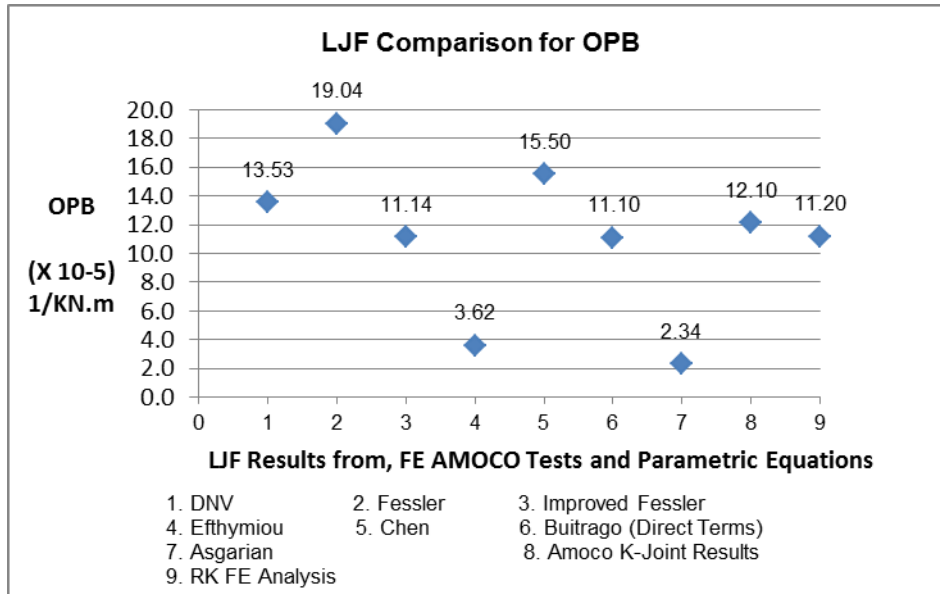


**Figure 6.21 LJF Comparison for Out-of-Plane Bending**

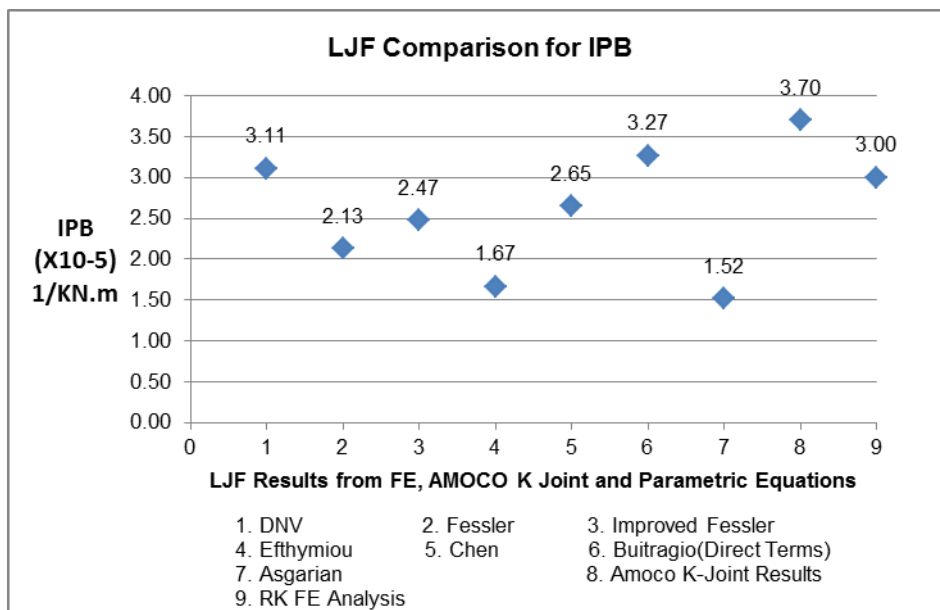


**Figure 6.22 LJF Comparison for In-Plane Bending**

For out-of-plane bending, the Improved Fessler, Buitrago, RK-FEA modeling results are within 10% of the K-joint test results (Figure 6.21). Efthymiou’s equations under-predict the LJF by 73% and Asgarian by 80%, while DNV, Fessler and Chen over-predicts LJF for out-of-plane bending by 20%, 42% and 13% respectively. For in-plane bending (Figure 6.22), DNV, Chen, Buitrago and RK-FEA results are within 20% of the AMOCO Test results. Chen and Buitrago are closer to the AMOCO K-Joint tests than RK-FEA. For joints where  $\beta$  values are approaching 1.0 ( $\beta = 0.89$  for AMOCO joint)

IPB conditions for the effects of the loaded brace (cross terms) on the overall LJF must be further examined so small variations between RK-FEA and AMOCO tests are expected. In this research, both cross and direct terms will be provided for both the IPB and OPB condition. Furthermore, varying  $\beta$  values for joints are required to have a better assessment rather than one  $\beta$  data point evaluation. Efthymiou's equations under-predict by 77%, Asgarian by 61% and Fessler and Improved Fessler's equations under-predict in the range of 30-45%.

## **6.7 Summary and Conclusions**

The 4-node non-linear quadrilateral thin shell finite element (with reduced integration and hourglass control) is suitable to model flexible joint behaviour in ABAQUS when used to determine nodal displacements used for LJF calculations. Furthermore, the mesh sensitivity tests provide a good FE mesh which convergences well with the AMOCO K-Joint test displacement values.

The comparison exercise should be treated with caution. While the RK-FEA model provides reasonable agreement with the AMOCO K-Joints, the K-joints test values should be considered as indicative rather than absolute values. As discussed in Chapter 5, there are possible sources of errors in the AMOCO K-Joint tests results, so for a finite element model results to be within 10-20% of the tests may be considered as reasonable. The main results are summarized in Table 6.4. Consistently the RK-FEA model provides the closest results for axial, OPB and IPB compared with the AMOCO large scale test results. It should be noted that varying  $\beta$  points need to be assessed when performing the comparison exercise as varying values of  $\beta$  display different behaviour to the overall LJF of the joint as their variations change. In this Chapter, the comparison of the AMOCO K-type joint and other LJF equations is only used to provide a basis for the RK-FEA as a benchmarking model to perform more detailed LJF analysis. In Chapter 7, after the derivation of the RK-LJF equations, a more detailed comparison study is performed to further evaluate the derived RK-LJF equations compared to other LJF equations for varying geometric ranges. The RK-FEA model was used to extend the research to other geometric parameters for in-service K-type joints.

<b>LJF Equation Comparison Study Summary</b>												
	<b>Axial</b>				<b>Out-of-Plane Bending</b>				<b>In-Plane Bending</b>			
	< 10%	10% - 20%	20% - 30%	> 30%	< 10%	10% - 20%	20% - 30%	> 30%	< 10%	10% - 20%	20% - 30%	> 30%
RK-FEA		<b>X</b>			<b>X</b>					<b>X</b>		
DNV							<b>X</b>			<b>X</b>		
Fessler				<b>X</b>	<b>X</b>							<b>X</b>
Improved Fessler				<b>X</b>	<b>X</b>							<b>X</b>
Efthymiou								<b>X</b>				<b>X</b>
Chen				<b>X</b>						<b>X</b>		
Buitrago				<b>X</b>	<b>X</b>			<b>X</b>		<b>X</b>		
Asgarian				<b>X</b>								<b>X</b>

**Table 6.4 LJF Comparison Study Results Summary**

# CHAPTER 7

## Developing an Improved Suite of LJF Parametric Equations

### 7.1 Introduction

Having established the methodology for the calculation of the LJF from numerical methods, this Chapter will further develop this methodology by introducing a step-by-step process to develop improved LJF parametric equations for all in-service K-type steel joints. Furthermore, a gap sensitivity study was performed to demonstrate the applicability of the improved equations as the gap increases from the prescribed 50mm between braces for K-type joints.

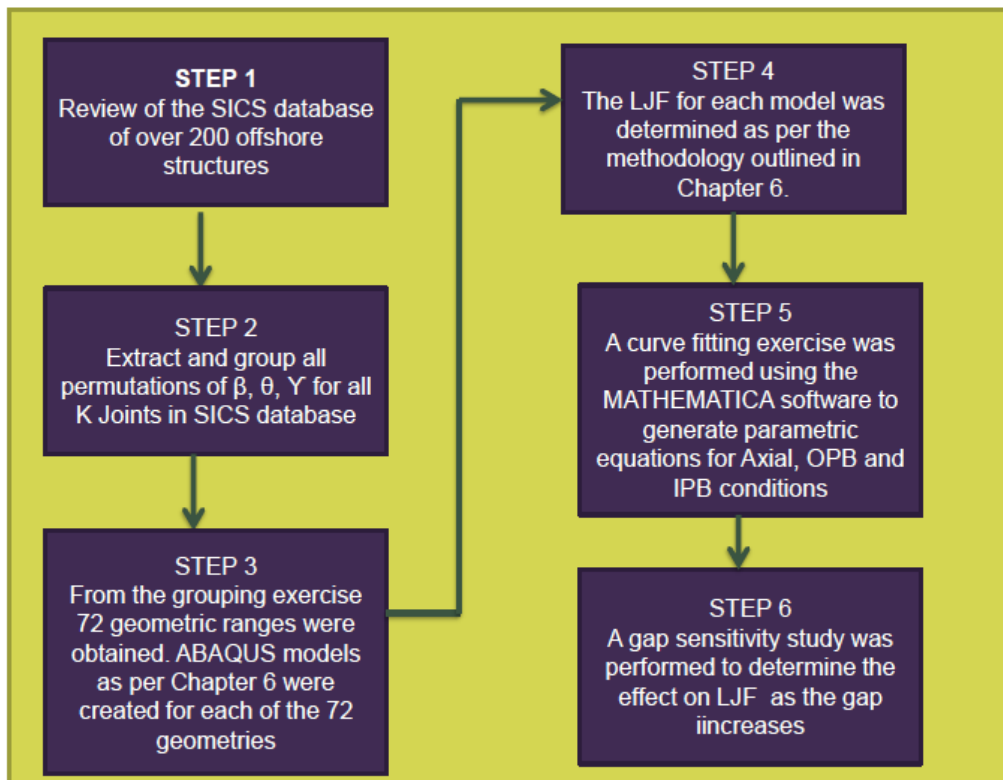


**Figure 7.1 Six Step Work Flow Process to develop the RK-LJF Parametric Equations**

Figure 7.1 illustrates the six step process for LJF parametric equation development and validity of the parametric ranges with increases in the gap value.

## 7.2 Database of In-Service Fixed Offshore Structures

A data collection exercise was embarked upon, using an offshore structures database and associated drawings to catalogue the geometrical properties of in-service K-type joints. The Structural Integrity Compliance System (SICS) database is used for the structural integrity management of over 200 fixed steel offshore structures in South East Asia and has been developed by Nichols and Khan (2015) and maintained by a major oil and gas operator. The offshore platforms in the structural database are of various vintages, ranging from pre-API RP 2A structures to those designed to modern API RP 2A code of practice.

The screenshot shows the 'Platform Document Register' interface. At the top, there are filter options for 'Filter by Type' (Reports, Drawings, Presentations, Permits, Waivers), 'Filter by System' (General, Jacket, Topsides, Foundations), and 'Filter by Category' (Design, Assessment, Inspection, Maintenance). Below these are search fields for 'Asset' and 'Reference'. The main table has columns for 'Format', 'Reference', 'Asset', and 'Rev'. A context menu is open over a row, showing options like 'Open', 'Open in New Tab', 'Save Target As...', 'Print Target', 'Cut', 'Copy', 'Copy Shortcut', 'Paste', 'Blog with Windows Live', 'E-mail with Windows Live', 'Translate with Bing', 'All Accelerators', 'Add to Favorites...', 'Send to OneNote', and 'Properties'.

Platform Document Register			
Filter by Type	<input checked="" type="checkbox"/> Reports	<input type="checkbox"/> Drawings	<input type="checkbox"/> Presentations
Filter by System	<input type="checkbox"/> General	<input type="checkbox"/> Jacket	<input type="checkbox"/> Topsides
Filter by Category	<input type="checkbox"/> Design	<input type="checkbox"/> Assessment	<input type="checkbox"/> Inspection
Free Search	Asset	Reference	
:ports			
Appurtenance			
Format	Reference	Asset	Rev
pdf	OFF/92-044/18	SMJT-F	SMJT-F - 110 Days Riser Ins No.OFF/92-044/18
pdf	OFF/92-262/7	SMJT-F	SMJT-F - Riser Re-Visit Insp
pdf	OFF/94 -022	SMJT-F	SMJT-F - Riser Inspection R
pdf	OFF/92-044/18	SMJT-E	SMJT-E - 110 Days Riser Ins No.OFF/92-044/18
pdf	OFF/93-131/5	SMJT-E	SMJT-E - Riser Inspection R
pdf	OFF/94-018	SMJT-E	SMJT-E - Riser Inspection R
pdf	OFF/92-262/8	SMP-A	SMP-A - Riser Re-Visit Insp
pdf	OFF/93-180	SMP-A	SMP-A - Riser Inspection R

Figure 7.2 Structural Integrity Compliance System (SICS) Document Register

From the platforms that have been selected through a thorough platform screening process, as a representative sample of existing structures (Figure 7.3), over one thousand K-type joints were recorded and compiled. A total of 38 groups of variations of  $\beta$ ,  $\gamma$ ,  $\zeta$ , Gap  $g$  and Brace – Chord Angle  $\theta$ , were established for constant chord diameters. Fessler (1983, 1986) concluded that it is very rare for tubular joints to be outside of the following ranges:

$$10 \leq \gamma \leq 20,$$

$$0.30 \leq \beta \leq 0.80,$$

$$30^\circ \leq \theta \leq 90^\circ$$

But this was based on a limited database. A further K-joint data collection and screening using a SICS database was undertaken to ensure that the geometric ranges proposed by Fessler were initially considered. There are a number of K-type joints, where  $\gamma < 10$  and  $\beta > 0.80$  so these K-joint geometric parametric ranges are included in this study in addition to Fessler’s recommendations.

3-D View of SACS Analysis Model	Description	Parameters
	<b>Design Criteria – API RP 2A WSD 21<sup>st</sup> Edition</b>	
	Water Depth (MSL)	60.7 m
	Highest Astronomical Tide (HAT)	1.33 m
	Lowest Astronomical Tide (LAT)	-1.27 m
	100-year Return Storm Surge	0.60 m
	100-year Return Wave $H_{max}$ and $T_{ass}$	10.8 m, 10.0 sec
	100-year Return Wind (hourly mean)	32 m/s
	100-year Return Wind (1 min mean)	40 m/s
	100-year Return Current Profile	Surface 1.1 m/s Mid-depth 1.0 m/s Bottom: 0.57 m/s
	<b>Design Analysis Results</b>	
	Maximum Base Shear	10,635 kN
	Maximum Overturning Moment	545,371 kN-m
	Maximum Member Unity Check	0.869
	Maximum Joint Unity check	0.863
Max Foundation Pile Unity Check	0.819	
Min Foundation Pile Factor of Safety	1.820	

**Figure 7.3 Typical Fixed Jacket Structure (from SICS database)**

A total of 72 K-joint geometric ranges were considered from the platform screening and K-joint study that can adequately provide a full range of data points for determining improved local joint flexibility parametric equations. Table 7.1 provides the full set of geometric ranges.

Geometric Range No	$\gamma = D/2T$	$\beta = d/D$	$\theta$	Geometric Range No	$\gamma = D/2T$	$\beta = d/D$	$\theta$	Geometric Range No	$\gamma = D/2T$	$\beta = d/D$	$\theta$
1	8	0.30	30	31	20	0.50	30	61	15	0.89	30
2	8	0.30	45	32	20	0.50	45	62	15	0.89	45
3	8	0.30	60	33	20	0.50	60	63	15	0.89	60
4	8	0.50	30	34	20	0.70	30	64	20	0.89	30
5	8	0.50	45	35	20	0.70	45	65	20	0.89	45
6	8	0.50	60	36	20	0.70	60	66	20	0.89	60
7	8	0.70	30	37	25	0.30	30	67	25	0.89	30
8	8	0.70	45	38	25	0.30	45	68	25	0.89	45
9	8	0.70	60	39	25	0.30	60	69	25	0.89	60
10	10	0.30	30	40	25	0.50	30	70	30	0.89	30
11	10	0.30	45	41	25	0.50	45	71	30	0.89	45
12	10	0.30	60	42	25	0.50	60	72	30	0.89	60
13	10	0.50	30	43	25	0.70	30				
14	10	0.50	45	44	25	0.70	45				
15	10	0.50	60	45	25	0.70	60				
16	10	0.70	30	46	30	0.30	30				
17	10	0.70	45	47	30	0.30	45				
18	10	0.70	60	48	30	0.30	60				
19	15	0.30	30	49	30	0.50	30				
20	15	0.30	45	50	30	0.50	45				
21	15	0.30	60	51	30	0.50	60				
22	15	0.50	30	52	30	0.70	30				
23	15	0.50	45	53	30	0.70	45				
24	15	0.50	60	54	30	0.70	60				
25	15	0.70	30	55	8	0.89	30				
26	15	0.70	45	56	8	0.89	45				
27	15	0.70	60	57	8	0.89	60				
28	20	0.30	30	58	10	0.89	30				
29	20	0.30	45	59	10	0.89	45				
30	20	0.30	60	60	10	0.89	60				

**Table 7.1 K-Joint Geometric Ranges (input for ABAQUS Analysis)**

The data from Table 7.1 is presented on Figure 7.4 to represent all the geometric ranges for  $\gamma$ ,  $\beta$  and  $\theta$  used for 72 models to perform detailed analysis. The data set represents a complete range of geometric ranges that are typical of in-service K-type uni-planar joints. Whilst these ranges have been extracted from a database on fixed offshore platforms, they are also applicable for wind energy structures whose substructures include a variety of tubular members and joints of varying geometric ranges.

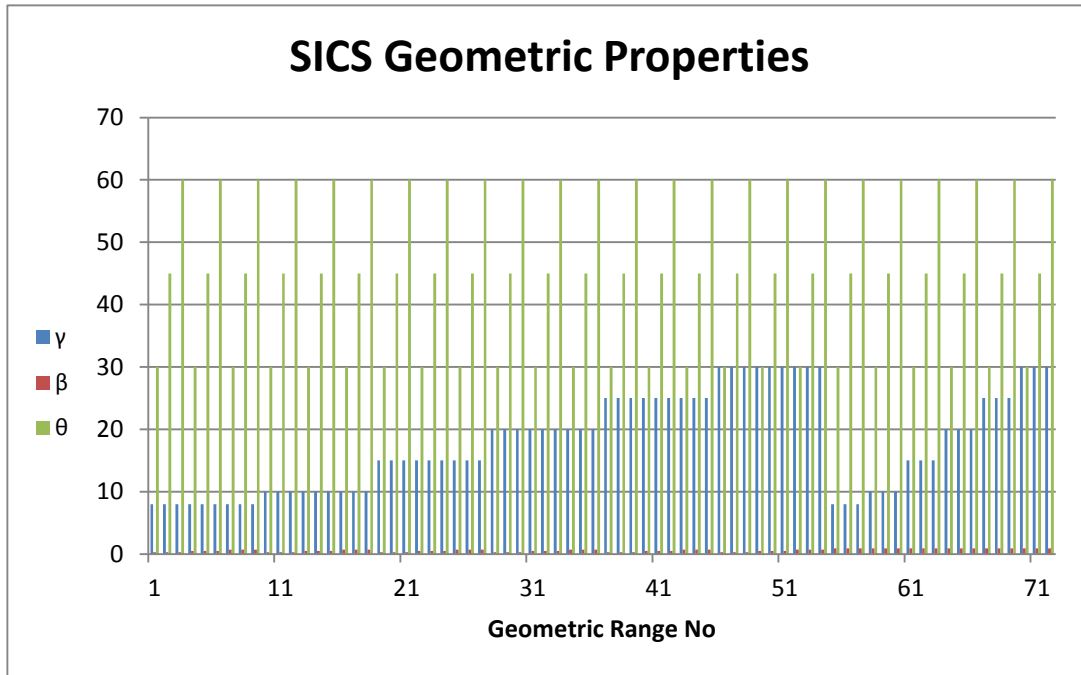


Figure 7.4 Geometric Ranges of Tubular K-Joints (input for ABAQUS)

### 7.3 Finite Element Modeling of Database of K-Type Joints

#### 7.3.1 Developing the Structural Models

ABAQUS structural analytical models are created for each of the seventy-two geometric ranges in Table 7.1 and Figure 7.4. The structural models have been created based on the ABAQUS benchmarking model methodology. Typical ABAQUS models varying geometric ranges are shown on Figures 7.5 to 7.7. For each of the 72 models, Axial Balanced, In-Plane Bending (IPB) and Out-of-Plane Bending effects are calculated based on the Excel spread-sheet structural calculations. Five load cases were applied to each of the 72 ABAQUS models. These are provided in Tables 7.2 and 7.3.

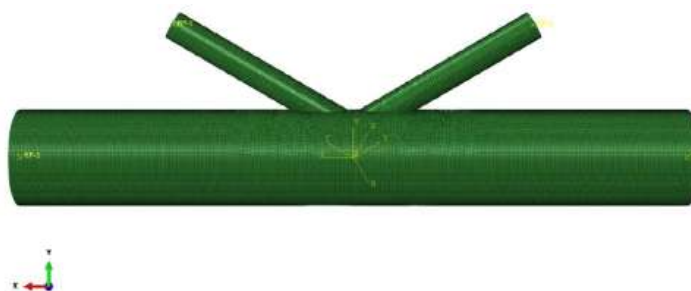
Young's Modulus of Elasticity (E)	Diameter (D)	$\beta = d/D$	$\theta$	$\gamma = D/2T$
210 KN/mm <sup>2</sup>	457 mm	0.3, 0.5, 0.70, 0.89	30°, 45°, 60°	8, 10, 15, 20, 25,30

Table 7.2 Basic Input parameters

Load Case	Condition	Loading – Brace 1	Loading – Brace 2	Comments
LC1	Axial Balanced	1 KN Compression on Brace 1	1 KN Compression on Brace 2	
LC2	IPB (22)	-	1KN-m moment applied on brace 2	LJF calculated on Brace 2
LC3	OPB (22)	-	1KN-m moment applied on brace 2	LJF calculated on Brace 2
LC4	IPB (21)	-	1KN-m moment applied on brace 2	LJF calculated on Brace 1
LC5	OPB (21)	-	1KN-m moment applied on brace 2	LJF calculated on Brace 1

**Table 7.3 Loading System for all geometric models**

The 72 geometric ranges in Table 7.1 will be used to develop ABAQUS structural models to determine LJF for the Balanced Axial, IPB and OPB conditions. The results of the LJF values for the loading effects due to axial balanced, IPB and OPB for  $\beta$  values of 0.3, 0.5, 0.7 and 0.89 are calculated using the same methodology as the benchmarking study.



**Figure 7.5 K-Type Tubular Joint model:  $\beta = 0.3, \gamma = 10, \theta = 30^\circ$**

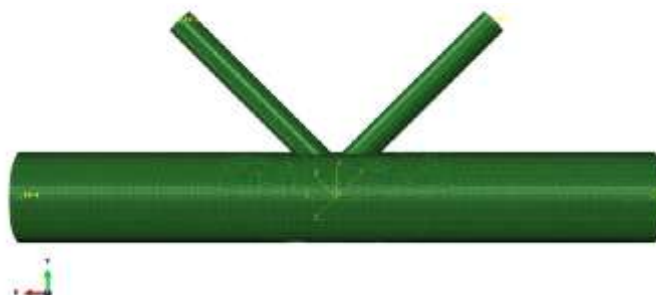


**Figure 7.6 K-Type Tubular Joint model:  $\beta = 0.3, \gamma = 10, \theta = 45^\circ$**



**Figure 7.7 K-Type Tubular Joint Model:  $\beta = 0.5$ ,  $\gamma = 15$ ,  $\theta = 60^\circ$**

### **7.3.2 Finite Element Analysis Results**

The finite element analysis results are reported on Axial, IPB and OPB in Tables 7.4, 7.5, 7.6 and 7.7 for  $\beta = 0.30$ , 0.50, 0.70 and 0.89 respectively. Graphs were generated on each of the results on Figures 7.8 through 7.11 to illustrate the relationship between  $\beta$ ,  $\theta$ ,  $\gamma$  and joint flexibility for  $\beta = 0.30$ . The relationships suggest that equations can be established to cover the calculated stiffness values for IPB, OPB and Axial loading conditions. The results indicate some of the LJF values may be negative (-ve) and some may be positive (+ve). This represents the deflected form of the chord in relation to its original unloaded position. In principle, this phenomenon is primarily for the axially balanced condition, which demonstrates that the unloaded brace deforms in the opposite direction to the loaded brace with similar magnitude, which is expected. Detail calculations for the LJF results for one sample case are provided within Appendix 5.

	$\beta = 0.30$			0.30	0.30	0.30
	$\theta$	$\gamma$		Axial Balanced	IPB brace2	OPB brace2
1	30	8	brace1	-2.1179E-04	2.6972E-06	1.8211E-05
2	30	8	brace2	2.1180E-04	1.5925E-05	3.4764E-05
3	30	10	brace1	-2.9714E-04	4.4532E-06	3.4874E-05
4	30	10	brace2	2.9714E-04	3.5448E-05	8.4046E-05
5	30	15	brace1	-5.3835E-04	1.0086E-05	1.0893E-04
6	30	15	brace2	5.3835E-04	9.4602E-05	2.6847E-04
7	30	20	brace1	-8.1272E-04	1.6846E-05	2.3658E-04
8	30	20	brace2	8.1273E-04	1.6581E-04	5.4127E-04
9	30	25	brace1	-1.1183E-03	2.4502E-05	4.2413E-04
10	30	25	brace2	1.1183E-03	2.4782E-04	9.0300E-04
11	30	30	brace1	-1.4575E-03	3.3179E-05	6.7722E-04
12	30	30	brace2	1.4575E-03	3.4066E-04	1.3588E-03
13	45	8	brace1	-2.3056E-04	-1.0454E-06	4.9593E-05
14	45	8	brace2	2.3051E-04	4.2556E-05	1.1731E-04
15	45	10	brace1	-3.4385E-04	-6.7645E-07	9.0532E-05
16	45	10	brace2	3.4333E-04	7.0561E-05	2.0929E-04
17	45	15	brace1	-6.8383E-04	1.2302E-06	2.6876E-04
18	45	15	brace2	6.8183E-04	1.5598E-04	5.6612E-04
19	45	20	brace1	-1.0929E-03	3.9616E-06	5.7040E-04
20	45	20	brace2	1.0891E-03	2.5860E-04	1.1092E-03
21	45	25	brace1	-1.5689E-03	7.4668E-06	1.0081E-03
22	45	25	brace2	1.5630E-03	3.7673E-04	1.8449E-03
23	45	30	brace1	-2.1155E-03	1.2006E-05	1.5930E-03
24	45	30	brace2	2.1073E-03	5.1063E-04	2.7861E-03
25	60	8	brace1	-2.5403E-04	-5.4369E-06	7.4543E-05
26	60	8	brace2	2.5404E-04	5.6931E-05	1.6670E-04
27	60	10	brace1	-3.9787E-04	-6.9815E-06	1.3497E-04
28	60	10	brace2	3.9787E-04	9.2012E-05	2.9302E-04
29	60	15	brace1	-8.4172E-04	-9.5555E-06	3.9695E-04
30	60	15	brace2	8.4164E-04	2.0028E-04	7.9032E-04
31	60	20	brace1	-1.3896E-03	-1.0776E-05	8.3944E-04
32	60	20	brace2	1.3894E-03	3.3060E-04	1.5572E-03
33	60	25	brace1	-2.0396E-03	-1.0843E-05	1.4812E-03
34	60	25	brace2	2.0391E-03	4.8028E-04	2.6060E-03
35	60	30	brace1	-2.7959E-03	-9.5417E-06	2.3379E-03
36	60	30	brace2	2.7952E-03	6.4954E-04	3.9556E-03

**Table 7.4 Uni-planar K-Joint LJFs for IPB, OPB and Axial Balanced for  $\beta = 0.3$**

	$\beta = 0.50$			0.50	0.50	0.50
	$\theta$	$\gamma$		Axial Balanced	IPB brace2	OPB brace2
1	30	8	brace1	-1.6915E-04	2.6325E-06	7.8115E-06
2	30	8	brace2	1.6915E-04	1.0788E-05	2.3329E-05
3	30	10	brace1	-2.3302E-04	3.8763E-06	1.6360E-05
4	30	10	brace2	2.3302E-04	1.7486E-05	4.3291E-05
5	30	15	brace1	-4.1507E-04	7.7959E-06	5.3122E-05
6	30	15	brace2	4.1509E-04	3.7124E-05	1.1604E-04
7	30	20	brace1	-6.2136E-04	1.2257E-05	1.1215E-04
8	30	20	brace2	6.2138E-04	5.9655E-05	2.1866E-04
9	30	25	brace1	-8.4858E-04	1.7003E-05	1.9320E-04
10	30	25	brace2	8.4862E-04	8.4656E-05	3.4918E-04
11	30	30	brace1	-1.0973E-03	2.2054E-05	2.9686E-04
12	30	30	brace2	1.0973E-03	1.1219E-04	5.0828E-04
13	45	8	brace1	-1.8591E-04	1.2411E-06	2.6501E-05
14	45	8	brace2	1.8592E-04	1.9277E-05	6.0750E-05
15	45	10	brace1	-2.6704E-04	2.0979E-06	4.8195E-05
16	45	10	brace2	2.6705E-04	2.8478E-05	1.0044E-04
17	45	15	brace1	-5.1014E-04	4.8799E-06	1.3823E-04
18	45	15	brace2	5.1018E-04	5.5188E-05	2.4844E-04
19	45	20	brace1	-8.0099E-04	8.0963E-06	2.8116E-04
20	45	20	brace2	8.0104E-04	8.5868E-05	4.6322E-04
21	45	25	brace1	-1.1349E-03	1.1614E-05	4.7749E-04
22	45	25	brace2	1.1349E-03	1.2013E-04	7.4339E-04
23	45	30	brace1	-1.5109E-03	1.5530E-05	7.2824E-04
24	45	30	brace2	1.5110E-03	1.5801E-04	1.0905E-03
25	60	8	brace1	-2.0028E-04	-5.8250E-07	4.0121E-05
26	60	8	brace2	2.0032E-04	2.4038E-05	8.3215E-05
27	60	10	brace1	-3.0043E-04	-2.9139E-07	7.1548E-05
28	60	10	brace2	3.0047E-04	3.5186E-05	1.3792E-04
29	60	15	brace1	-6.0920E-04	1.1512E-06	2.0155E-04
30	60	15	brace2	6.0926E-04	6.7515E-05	3.4402E-04
31	60	20	brace1	-9.8912E-04	3.1793E-06	4.0947E-04
32	60	20	brace2	9.8919E-04	1.0477E-04	6.4809E-04
33	60	25	brace1	-1.4328E-03	5.6610E-06	6.9741E-04
34	60	25	brace2	1.4329E-03	1.4647E-04	1.0503E-03
35	60	30	brace1	-1.9371E-03	8.6928E-06	1.0667E-03
36	60	30	brace2	1.9373E-03	1.9257E-04	1.5527E-03

**Table 7.5 Uni-planar K-Joint LJFs for IPB, OPB and Axial Balanced for  $\beta = 0.5$**

	$\beta = 0.70$			0.70	0.70	0.70
	$\theta$	$\gamma$		Axial Balanced	IPB brace2	OPB brace2
1	30	8	brace1	-1.2914E-04	2.6383E-06	2.1342E06
2	30	8	brace2	1.2915E-04	5.7343E-06	1.0600E-05
3	30	10	brace1	-1.7670E-04	3.5190E-06	6.2599E-06
4	30	10	brace2	1.7671E-04	8.7776E-06	1.9180E-05
5	30	15	brace1	-3.1477E-04	6.2049E-06	2.3912E-05
6	30	15	brace2	3.1478E-04	1.7402E-05	4.9795E-05
7	30	20	brace1	-4.7145E-04	9.1434E-06	5.0582E-05
8	30	20	brace2	4.7145E-04	2.6815E-05	9.1228E-05
9	30	25	brace1	-6.4102E-04	1.2117E-05	8.4918E-05
10	30	25	brace2	6.4102E-04	3.6857E-05	1.4172E-04
11	30	30	brace1	-8.2147E-04	1.5121E-05	1.2661E-04
12	30	30	brace2	8.2145E-04	4.7595E-05	2.0102E-04
13	45	8	brace1	-1.3808E-04	1.5136E-06	1.3646E-05
14	45	8	brace2	1.3808E-04	9.5867E-06	3.0907E-05
15	45	10	brace1	-1.9747E-04	2.1960E-06	2.4618E-05
16	45	10	brace2	1.9746E-04	1.3650E-05	4.8768E-05
17	45	15	brace1	-3.7728E-04	4.3064E-06	6.8055E-05
18	45	15	brace2	3.7726E-04	2.5115E-05	1.1279E-04
19	45	20	brace1	-5.9025E-04	6.5952E-06	1.3312E-04
20	45	20	brace2	5.9020E-04	3.7840E-05	2.0184E-04
21	45	25	brace1	-8.2739E-04	8.9243E-06	2.1838E-04
22	45	25	brace2	8.2728E-04	5.1577E-05	3.1404E-04
23	45	30	brace1	-1.0848E-03	1.1330E-05	3.2309E-04
24	45	30	brace2	1.0846E-03	6.6293E-05	4.4883E-04
25	60	8	brace1	-1.4596E-04	4.0906E-07	2.1036E-05
26	60	8	brace2	1.4596E-04	1.1497E-05	4.1758E-05
27	60	10	brace1	-2.1842E-04	8.0412E-07	3.6415E-05
28	60	10	brace2	2.1842E-04	1.6225E-05	6.6035E-05
29	60	15	brace1	-4.4367E-04	2.2026E-06	9.7261E-05
30	60	15	brace2	4.4365E-04	2.9619E-05	1.5398E-04
31	60	20	brace1	-7.1629E-04	3.8506E-06	1.9038E-04
32	60	20	brace2	7.1626E-04	4.4642E-05	2.7945E-04
33	60	25	brace1	-1.0233E-03	5.6208E-06	3.1481E-04
34	60	25	brace2	1.0232E-03	6.0931E-05	4.4099E-04
35	60	30	brace1	-1.3590E-03	7.5344E-06	4.6916E-04
36	60	30	brace2	1.3589E-03	7.8371E-05	6.3738E-04

**Table 7.6 Uni-planar K-Joint LJFs for IPB, OPB and Axial Balanced for  $\beta = 0.7$**

	$\beta = 0.89$			<b>0.89</b>	<b>0.89</b>	<b>0.89</b>
	$\theta$	$\gamma$		<b>Axial Balanced</b>	<b>IPB brace2</b>	<b>OPB brace2</b>
1	30	8	brace1	-9.7613E-05	2.8127E-06	-9.2929E-07
2	30	8	brace2	9.7610E-05	2.5865E-06	3.4190E-06
3	30	10	brace1	-1.3059E-04	3.5147E-06	6.3237E-07
4	30	10	brace2	1.3059E-04	4.0619E-06	6.8796E-06
5	30	15	brace1	-2.2760E-04	5.5073E-06	7.8671E-06
6	30	15	brace2	2.2760E-04	8.1639E-06	1.9158E-05
7	30	20	brace1	-3.3784E-04	7.6326E-06	1.8615E-05
8	30	20	brace2	3.3784E-04	1.2492E-05	3.5288E-05
9	30	25	brace1	-4.5482E-04	9.7799E-06	3.1835E-05
10	30	25	brace2	4.5481E-04	1.6985E-05	5.4203E-05
11	30	30	brace1	-5.7555E-04	1.1932E-05	4.7257E-05
12	30	30	brace2	5.7553E-04	2.1681E-05	7.5631E-05
13	45	8	brace1	-9.7214E-05	1.6387E-06	6.2560E-06
14	45	8	brace2	9.7209E-05	5.2135E-06	1.5839E-05
15	45	10	brace1	-1.3772E-04	2.1580E-06	1.1186E-05
16	45	10	brace2	1.3771E-04	7.3120E-06	2.3531E-05
17	45	15	brace1	-2.6093E-04	3.7077E-06	2.9884E-05
18	45	15	brace2	2.6092E-04	1.3081E-05	4.9762E-05
19	45	20	brace1	-4.0428E-04	5.3740E-06	5.6442E-05
20	45	20	brace2	4.0428E-04	1.9240E-05	8.4518E-05
21	45	25	brace1	-5.5849E-04	7.0441E-06	8.9861E-05
22	45	25	brace2	5.5849E-04	2.5635E-05	1.2675E-04
23	45	30	brace1	-7.1963E-04	8.7143E-06	1.2965E-04
24	45	30	brace2	7.1964E-04	3.2243E-05	1.7594E-04
25	60	8	brace1	-9.9743E-05	7.1076E-07	1.0453E-05
26	60	8	brace2	9.9737E-05	6.2908E-06	2.1336E-05
27	60	10	brace1	-1.4833E-04	1.0212E-06	1.7184E-05
28	60	10	brace2	1.4832E-04	8.6928E-06	3.1514E-05
29	60	15	brace1	-2.9860E-04	2.0520E-06	4.2455E-05
30	60	15	brace2	2.9859E-04	1.5296E-05	6.6464E-05
31	60	20	brace1	-4.7572E-04	3.2288E-06	7.9447E-05
32	60	20	brace2	4.7569E-04	2.2387E-05	1.1431E-04
33	60	25	brace1	-6.6795E-04	4.4447E-06	1.2743E-04
34	60	25	brace2	6.6791E-04	2.9758E-05	1.7420E-04
35	60	30	brace1	-8.7052E-04	5.6896E-06	1.8550E-04
36	60	30	brace2	8.7047E-04	3.7360E-05	2.4523E-04

**Table 7.7 Uni-planar K-Joint LJFs for IPB, OPB and Axial Balanced for  $\beta = 0.89$**

From the numerical results, the parameters  $\beta$  and  $\gamma$  have the greatest influence on LJFs. LJFs increase with increasing  $\gamma$  and LJF reduces with increasing  $\beta$ . Although  $\beta = 1$  normally exhibit unique behaviour,  $\beta = 0.89$  have been included as in-service K-joints fall within this range. For very low  $\beta$  (i.e.  $< 0.30$ ) for the in-plane condition, there is little effect on the LJF value for the unloaded brace. From this perspective, the  $\beta < 0.3$  is ignored from being included in curve fitting exercise for parametric equation development for the IPB<sub>21</sub> condition.

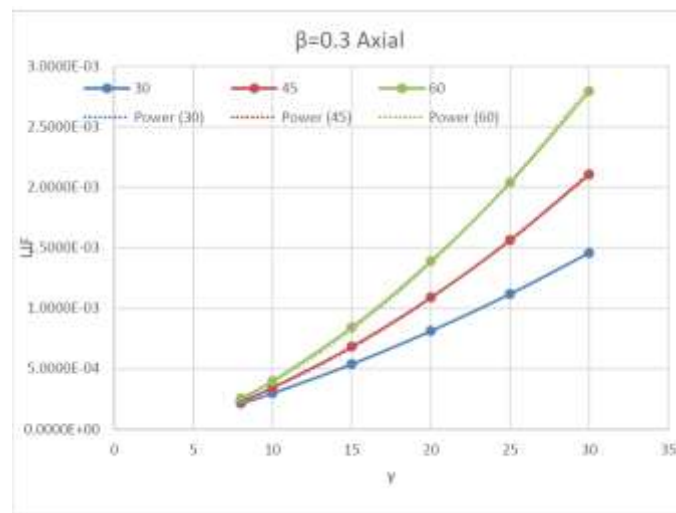


**Figure 7.8 LjF Results for Axial:  $\beta = 0.3$ ,  $\gamma = 8-30$ ,  $\theta = 30^\circ, 45^\circ, 60^\circ$**

*Note 1: LjF values are non-dimensional*

For the axial, IPB and OPB conditions, increasing  $\theta$  values together with increasing  $\gamma$  indicate and increase in the LjF values. Interestingly, as  $\gamma$  ( $D/2T$ ) values increase, the LjF values become more sensitive for axial, IPB and OPB. This is not unexpected as the thickness of the chord decreases, the joint is able to provide lesser internal resistance to the load effects that are now imposed on it and tends to redistribute these loads and moments to other members. The LjF behaviour for axial, OPB and IPB are provided on Figures 7.9 to 7.11 and Figures 7.12 to 7.15

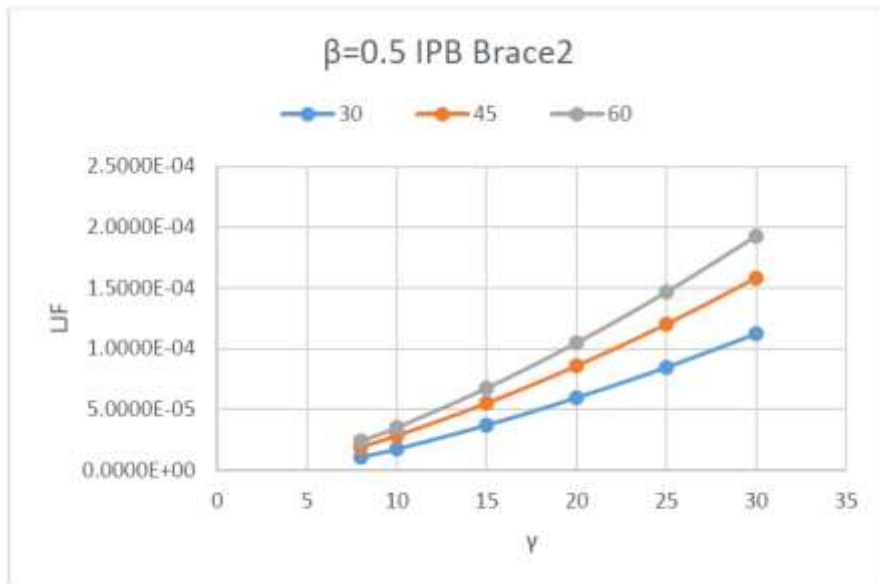


**Figure 7.9 LjF Results for IPB<sub>22</sub>: β = 0.3, γ = 8-30, θ = 30°, 45°, 60°**

*Note 1: LjF values are non-dimensional*

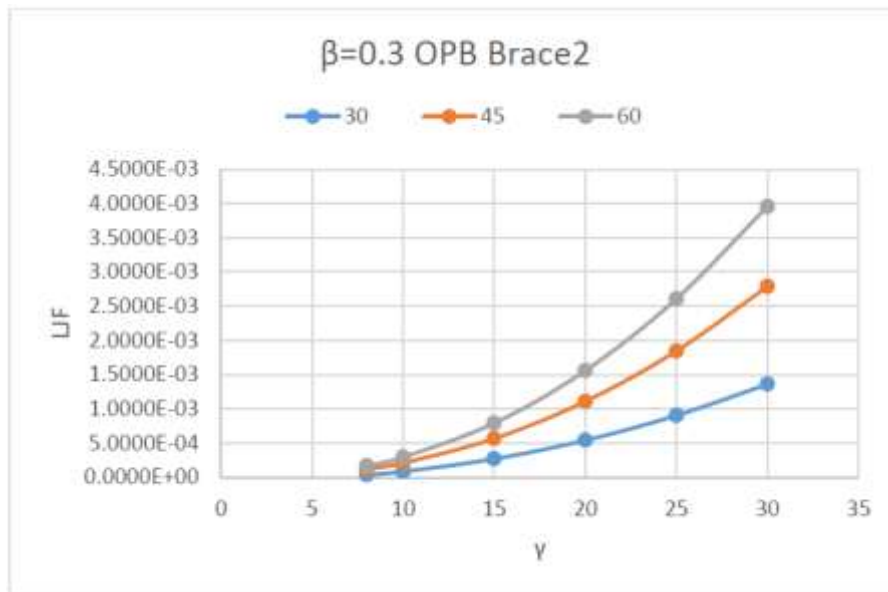


**Figure 7.10 LjF Results for OPB<sub>22</sub>: β = 0.3, γ = 8-30, θ = 30°, 45°, 60°**

*Note 1: LjF values are non-dimensional*

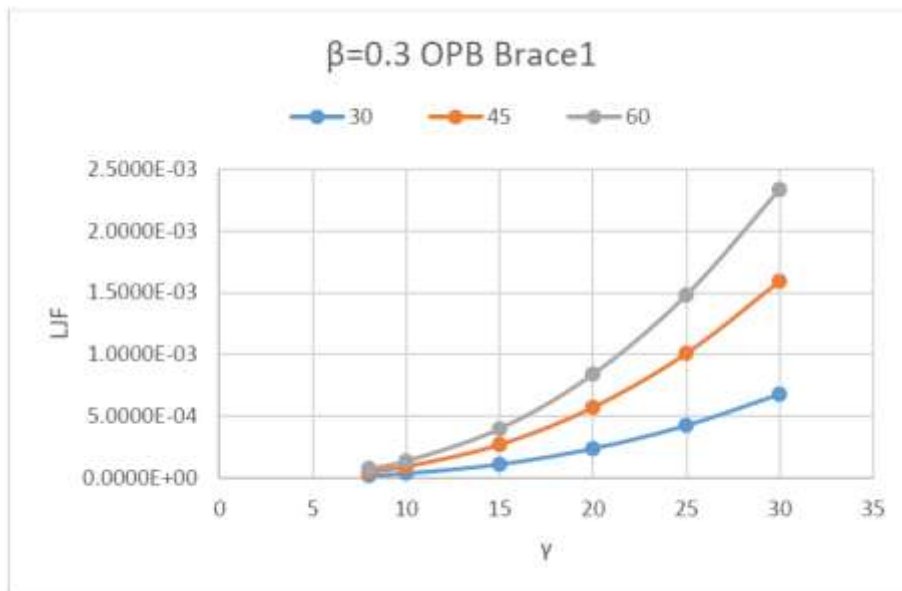


**Figure 7.11 LJF Results for OPB<sub>21</sub>: β = 0.3, γ = 8-30, θ = 30°, 45°, 60°**

*Note 1: LJF values are non-dimensional*

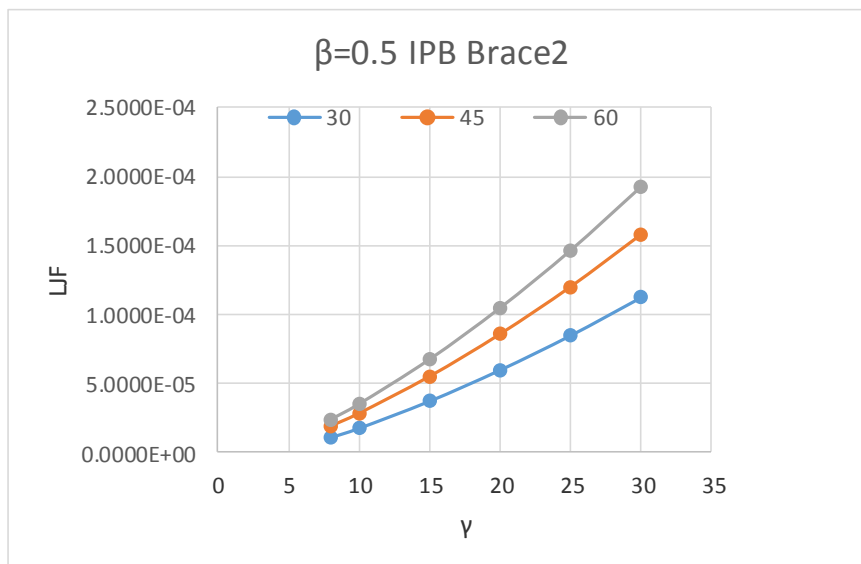


**Figure 7.12 LJF Results for IPB<sub>22</sub>: β = 0.5, γ = 8-30, θ = 30°, 45°, 60°**

*Note 1: LJF values are non-dimensional*

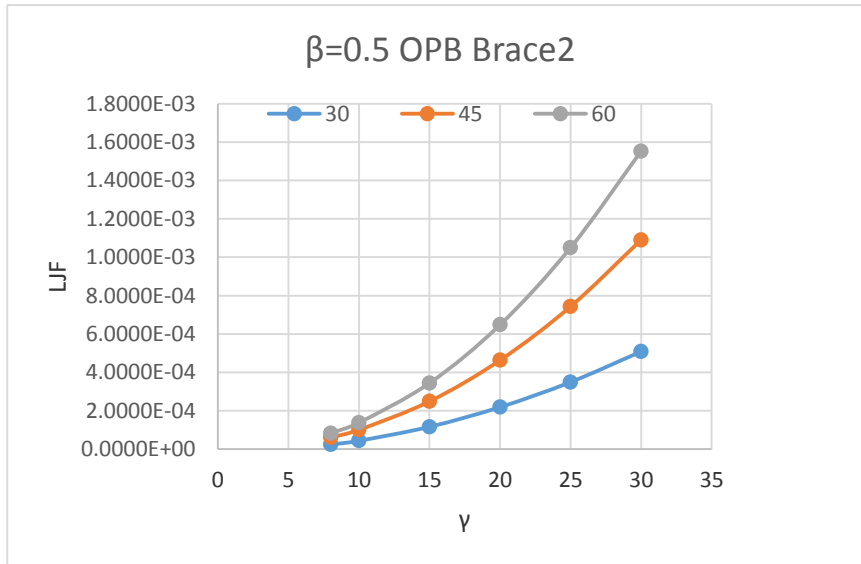


**Figure 7.13 L/JF Results for OPB<sub>22</sub>: β = 0.5, γ = 8-30, θ = 30°, 45°, 60°**

*Note 1: L/JF values are non-dimensional*

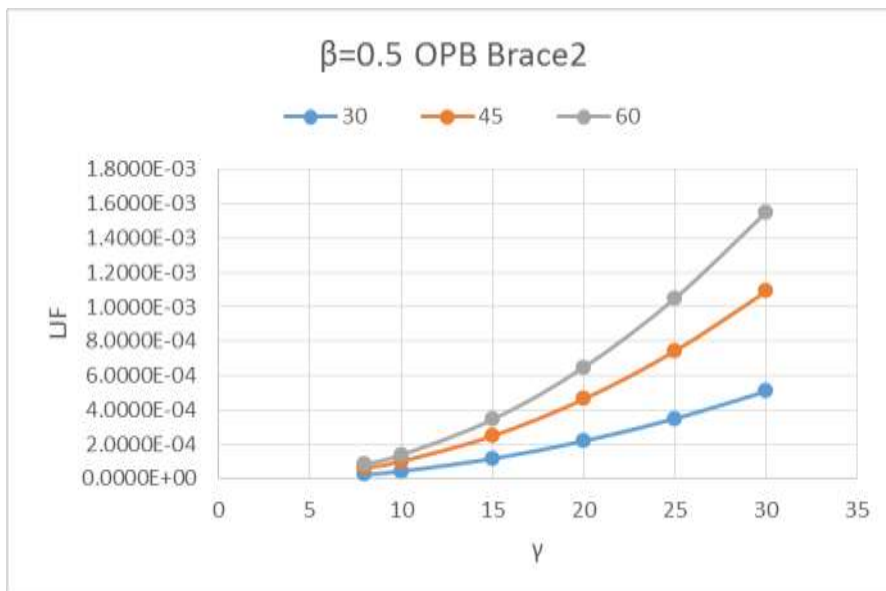


**Figure 7.14 L/JF Results for OPB<sub>22</sub>: β = 0.5, γ = 8-30, θ = 30°, 45°, 60°**

*Note 1: L/JF values are non-dimensional*

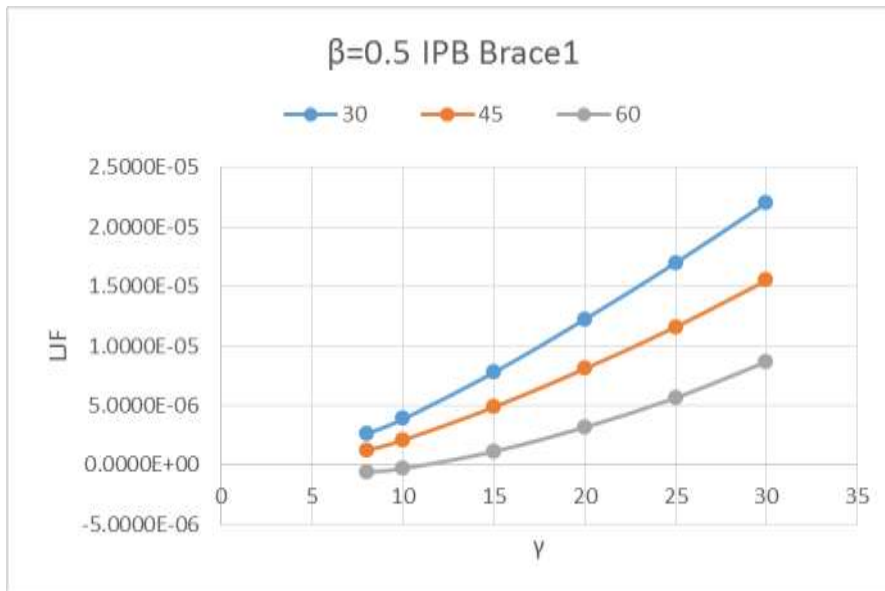


**Figure 7.15 LjF Results for IPB<sub>21</sub>:  $\beta = 0.5$ ,  $\gamma = 8-30$ ,  $\theta = 30^\circ, 45^\circ, 60^\circ$**

*Note 1: LjF values are non-dimensional*

For the IPB<sub>21</sub> condition, as  $\gamma$  increases for increasing values of  $\theta$ , the LjF value decreases. This is an interesting outcome as it differs from the IPB<sub>22</sub>, OPB<sub>22</sub>, OPB<sub>21</sub> and axial loaded conditions. This is because for the IPB condition for very large chord diameters, the contribution of the brace deformation and LjF is insignificant to the overall contribution to the LjF of the entire tubular joint. A very stiff chord must not be mistaken with the overall stiffness chord contribution to the overall structure, but rather as a local stiffness related to the particular joint. For very low  $\gamma$  values ( $\gamma$  in the range of 8-10) for larger angles, the LjF value approaches a negative value which indicates the joint rotation in the direction opposite to the sign convention for joint rotation. Therefore, to appropriately determine the LjF of a joint, the contributions direct and cross terms (from loaded and unloaded braces) and chord displacements need to be considered.

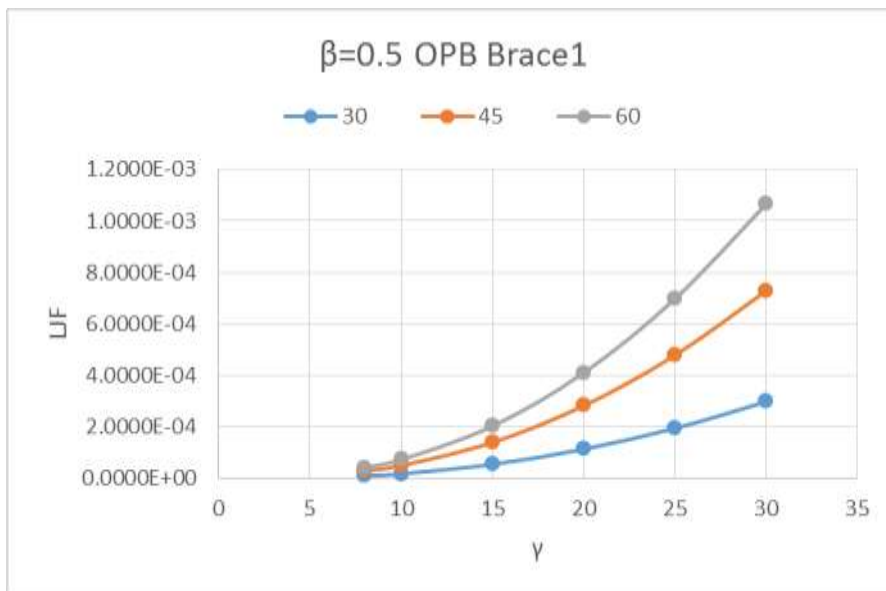


**Figure 7.16 LjF Results for OPB<sub>21</sub>: β = 0.5, γ = 8-30, θ = 30°, 45°, 60°**

*Note 1: LjF values are non-dimensional*

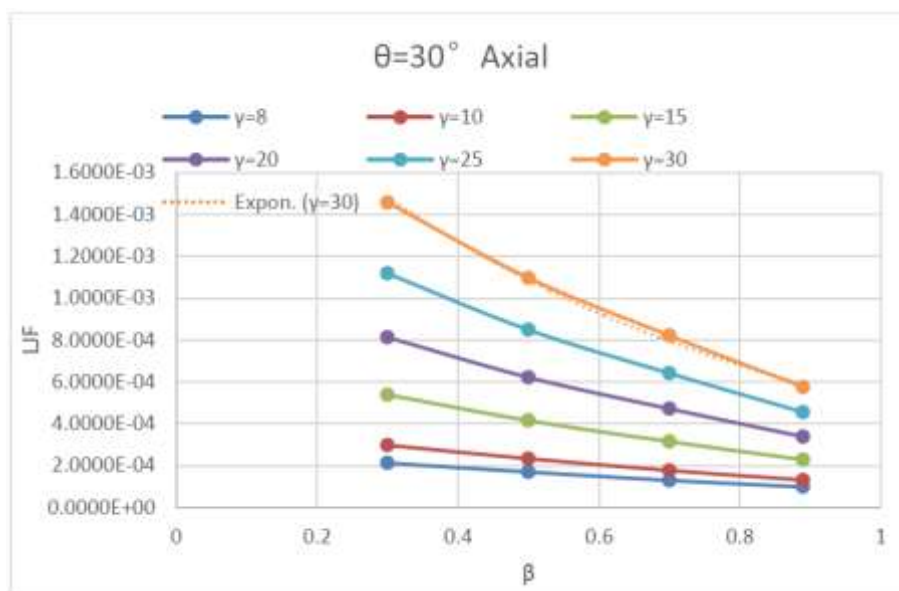


**Figure 7.17 LjF Results for Axial: β = 0.3-0.89, γ = 8-30, θ = 30°**

*Note 1: LjF values are non-dimensional*

The effects of LjF as the β and γ values changes are examined as the θ remains constant (Figure 7.17 to 7.21). For the axial condition, as β values increases LjF values decreases. Increasing γ values display increasing values of LjF.

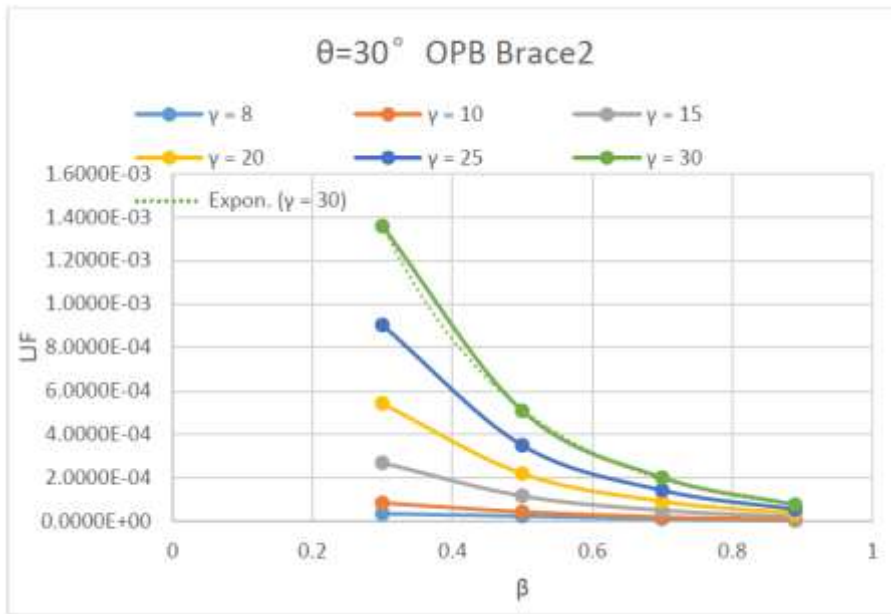


**Figure 7.18 LjF Results for IPB<sub>22</sub>: β = 0.3-0.89, γ = 8-30, θ = 30°**

*Note 1: LjF values are non-dimensional*

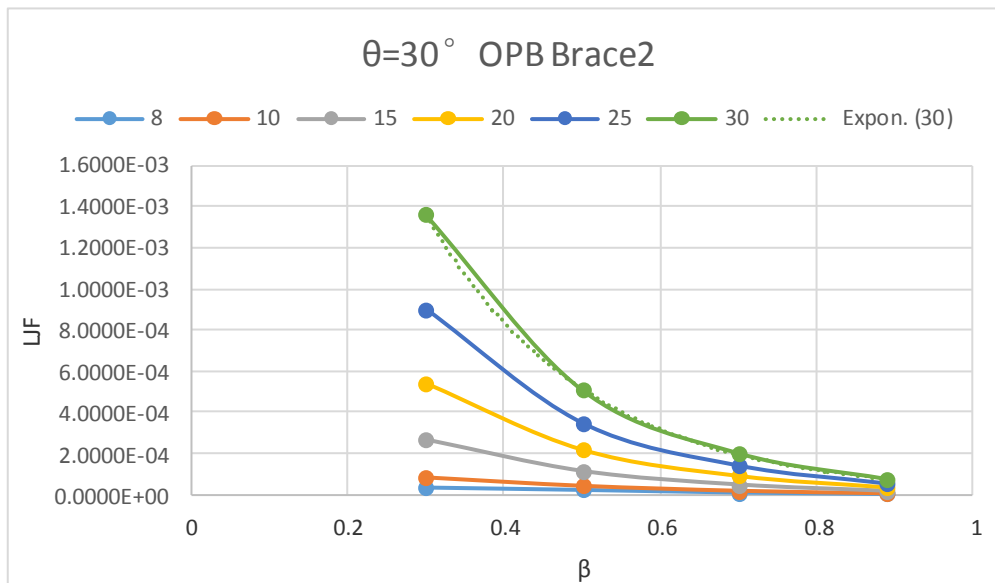


**Figure 7.19 LjF Results for OPB<sub>22</sub>: β = 0.3-0.89, γ = 8-30, θ = 30°**

*Note 1: LjF values are non-dimensional*

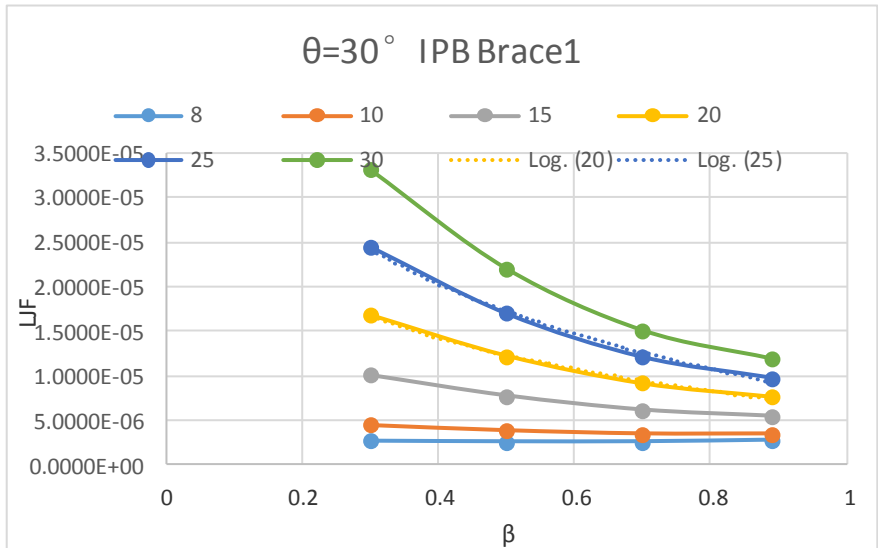


**Figure 7.20 LjF Results for IPB<sub>21</sub>:  $\beta = 0.5, \gamma = 8-30, \theta = 30^\circ$**

*Note 1: LjF values are non-dimensional*

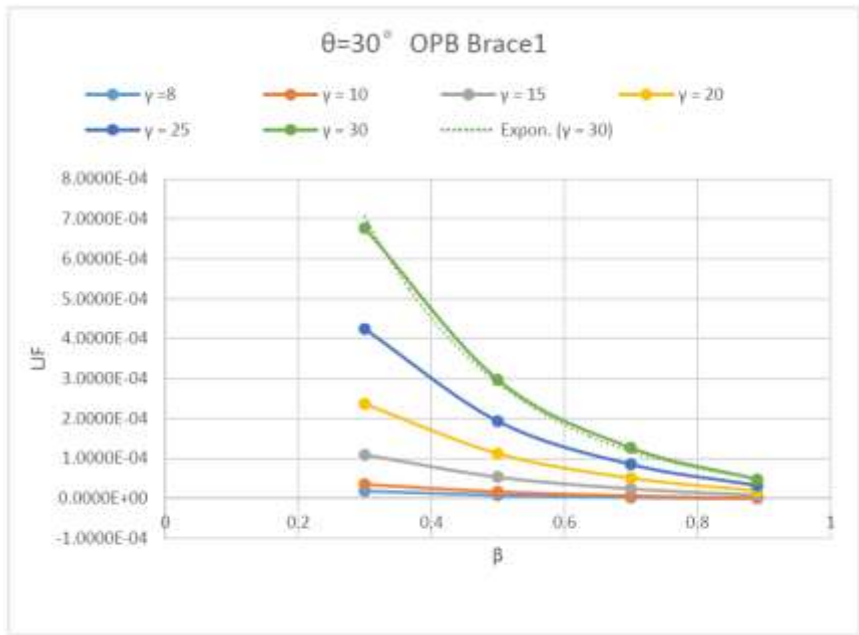


**Figure 7.21 LjF Results for OPB<sub>21</sub>:  $\beta = 0.5, \gamma = 8-30, \theta = 30^\circ$**

*Note 1: LjF values are non-dimensional*

Figures 7.17 to 7.21 indicate that as  $\beta$  ( $d/D$ ) values decreases and  $\gamma$  ( $D/2T$ ) increases the LjF values increase in sensitivity. This only reinforces the contributions made by chord diameter and chord thickness and the diameter of the brace to the overall LjF. If the chord diameter is too large compared to the brace diameter, the effects of the brace diameter is largely insignificant, and decreases in chord thicknesses ( $T$ ) only contributes to larger displacements and thus greater LjF values. The values of  $\beta$

( $d/D$ ) and  $\gamma$  ( $D/2T$ ) need to be put in the context of joint capacity and strength for the desired overall strength of the structure to withstand the loadings imposed on it and not just greater joint flexibility or deformation. MSL-ISO (1994, 1998) joint equations attempted to consider the joint capacities for variations of  $\beta$  and  $\gamma$  together with LJF. This is discussed in more detail in Chapter 8 of this thesis.

To develop a suite of equations to fully represent the relationship of the  $\beta$ ,  $\theta$ ,  $\gamma$  and joint flexibility for  $\beta = 0.30, 0.50, 0.70$  and  $0.89$ , a detail curve fitting exercise is required to fit the function that takes the list of points (IPB, OPB and Axial results), a list of expressions and a list of non-dimensional parameters and produce an expression as the best fit to the data sets.

## 7.4 Developing LJF Parametric Equations

The results generated from the calculations in Section 7.2 represent the performance of a full range of K-joint geometric parameters that can be used to accurately produce a suite of LJF equations for IPB, OPB and balanced axial loadings. To demonstrate the relationship between the joint stiffness and the non-dimensional parameters, the three dimensional plots of the stiffness of the LJF equations generated and are shown on Figures 7.22 to 7.26.

The *Mathematica* software was used to generate the LJF parametric equations. A major scientific tool in *Mathematica* is the manifold of plotting routines that helps to depict mathematical results graphically and is a good tool for making 3-dimensional graphs. Typically, the model will only contain a single variable while the parameters to be fit may be two or more items. The chord diameter is a constant throughout the FE analysis while the parameters include variations of  $\beta$ ,  $\gamma$  and  $\theta$ . A power regression method that is coded within the *Mathematica* software is used to derive the flexibility parametric formulae. *Mathematica* considers standard errors, test statistic (t-statistic) and parameter value (p-value) when determining the accuracy of the best fit parameters. In Figures 7.22 to 7.26, the *Estimate* column of these figures represents the best fit parameters. The t-statistic is the estimate divided by the standard errors. The standard error of an estimate is defined as the square root of the estimate error variance of the quantity. Each p-value is the two-sided p-value for the t-statistic which is

used to determine whether the parameter estimate is statistically significant. The curve fitting exercise demonstrated a very good fit with the analytical results with 99.8% for axial and 99.9% accuracy for both in-plane bending and out-of-plane bending conditions on the 3D plots.

#### **7.4.1 Axial Balanced Condition**

For the axially balanced condition, the analysis results of  $\beta = 0.3, 0.5$  and  $0.89$ ,  $\gamma$  ranging from 8 to 30 and  $\theta =$  from 30 to 60 degrees were considered. The flexibility of the K-joint under axial loading show decreasing trends when  $\beta$  ratio is increasing and they increase when the  $\gamma$  ratio is also increasing. The *Mathematica* model and the test data are within 99.8% agreement with each other. Figure 7.22 shows the analysis results and the LJF parametric expression. For mid-range  $\beta$  (0.5), there is a largely good agreement with the analytical results and parametric profile.

#### **7.4.2 In-Plane Bending Condition**

For the IPB condition, the analysis results of  $\beta = 0.3, 0.5$  and  $0.89$ ,  $\gamma$  ranging from 8 to 30 and  $\theta =$  from 30 to 60 degrees were considered. The in-plane condition considers two loading criteria, i.e. the effects of IPB on the loaded brace (Figure 7.23) and the effects on the unloaded brace (Figure 7.25). The first loading criterion is considered as  $IPB_{22}$  and the second,  $IPB_{21}$ . For  $IPB_{22}$ , the flexibility of the K-joint show decreasing trends when  $\beta$  ratio is increasing up to 0.5, with  $\theta$  ranging between 30 and 60 degrees. As  $\beta$  approaches 1.0 and  $\gamma$  increases, the overall flexibility of the K-joint is not affected. For  $IPB_{21}$ , the flexibility of the K-joint show decreasing trends when  $\beta$  ratio is increasing and they increase when the  $\gamma$  ratio is increasing. At very low  $\beta$  values ( $< 0.3$ ), the in-plane moment on the loaded brace has no effect on the unloaded brace, as the brace diameter is too small compared to the chord diameter. For mid-range  $\beta$  (0.5), there is a largely good agreement with the analytical results and parametric profile with the fitted model is required more in areas of higher and lower  $\beta$  values for both the  $IPB_{22}$  and the  $IPB_{21}$ .

### 7.4.3 Out-of-Plane Bending Condition

For the OPB condition, the analysis results of  $\beta = 0.3, 0.5$  and  $0.89$ ,  $\gamma$  ranging from 8 to 30 and  $\theta =$  from 30 to 90 degrees were considered. As with the in-plane condition, the out-of-plane considers two loading criteria, i.e. the effects of OPB on the loaded brace (Figure 7.24) and the effects on the unloaded brace (Figure 7.26). The first loading criterion is  $OPB_{22}$  and the second,  $OPB_{21}$ . For both  $OPB_{22}$  and  $OPB_{21}$ , the flexibility of the K-joint show decreasing trends when  $\beta$  ratio is increasing up to 0.5, with  $\theta$  ranging between 30 and 60 degrees. As  $\beta$  approaches 1.0 and  $\gamma$  increases, the overall flexibility of the K-joint is not affected. The flexibilities for OPB also show an increasing trend as the  $\gamma$  ratio is increasing. For mid-range  $\beta$  (0.5), there is a largely good agreement with the analytical results and parametric profile with the fitted model is required more in areas of higher and lower  $\beta$  values for both the  $OPB_{22}$  and the  $OPB_{21}$ .

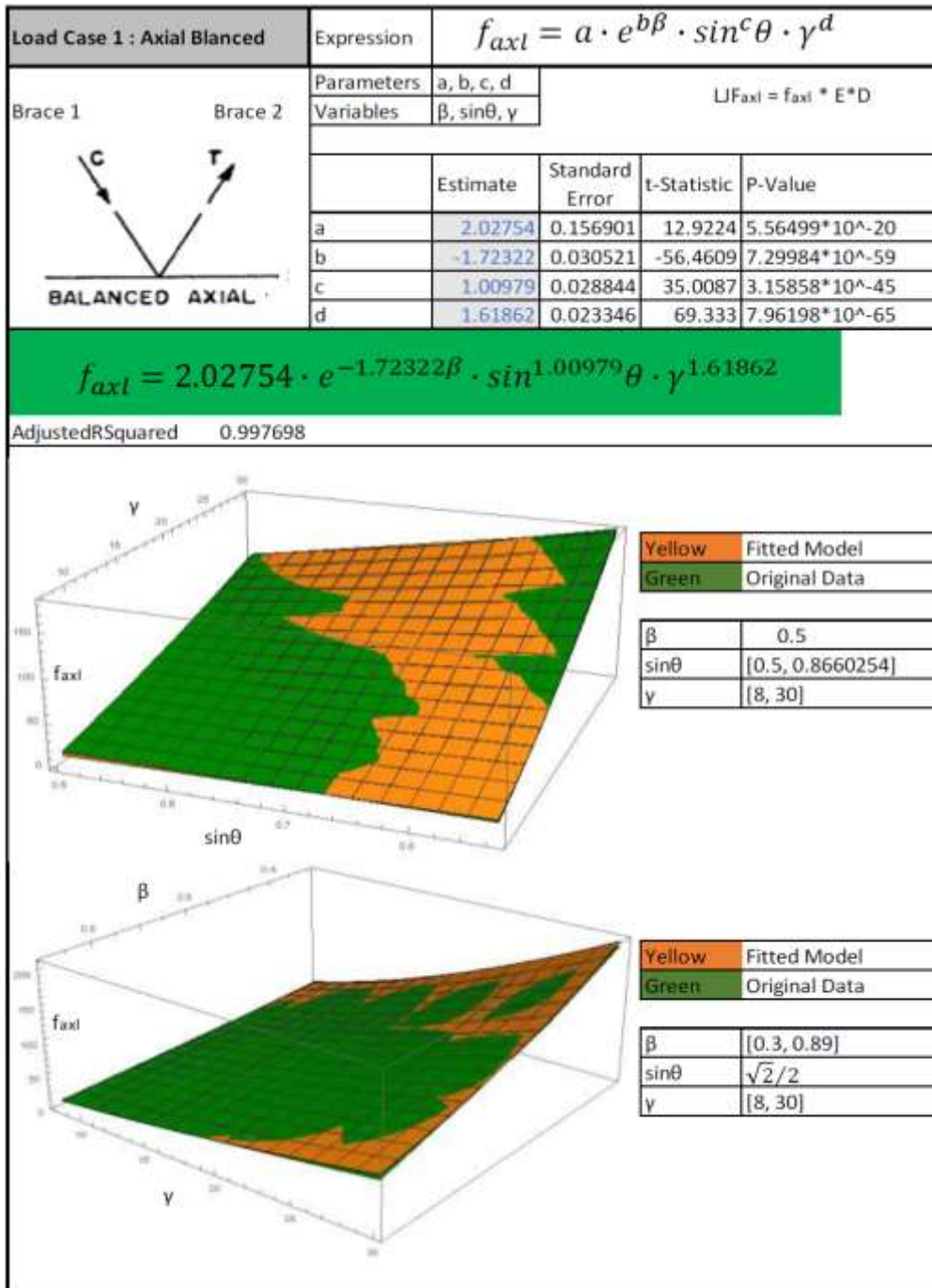


Figure7.22 LJF Expression for the Axially Balanced Condition

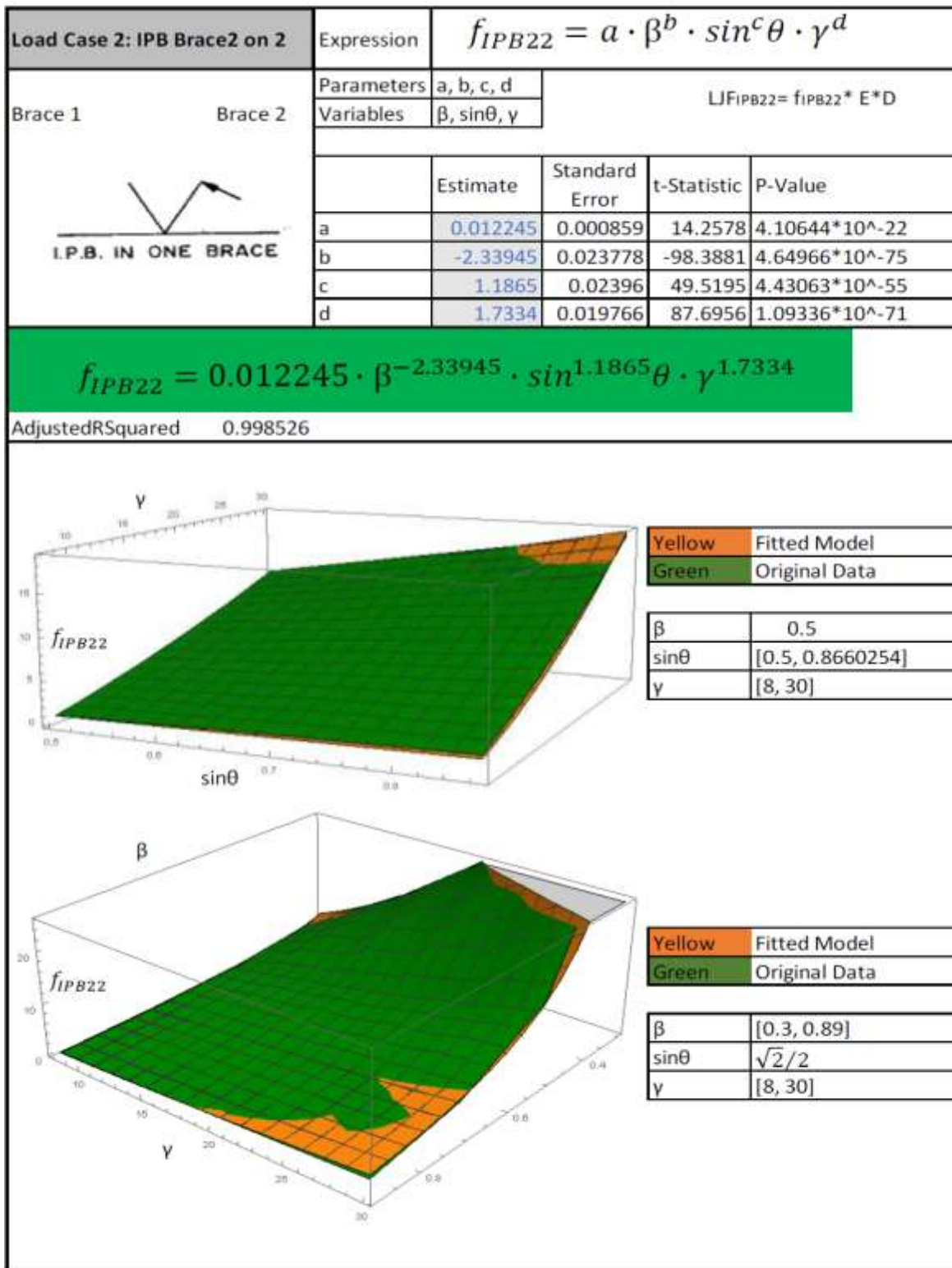


Figure 7.23 LJF Expression for the IPB for the loaded Brace (IPB<sub>22</sub>)

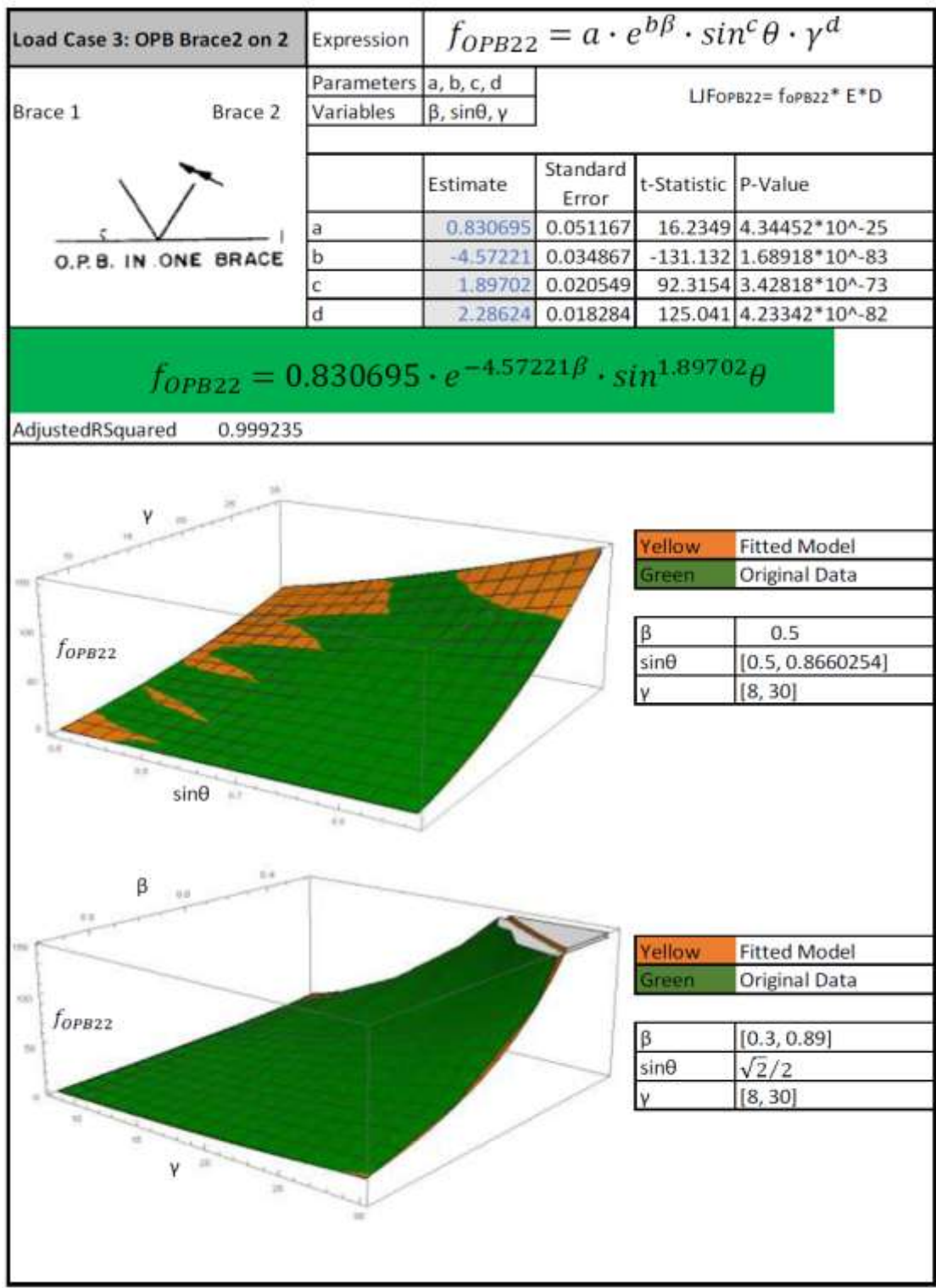


Figure 7.24 LJF Expression for the OPB for the loaded Brace (OPB<sub>22</sub>)

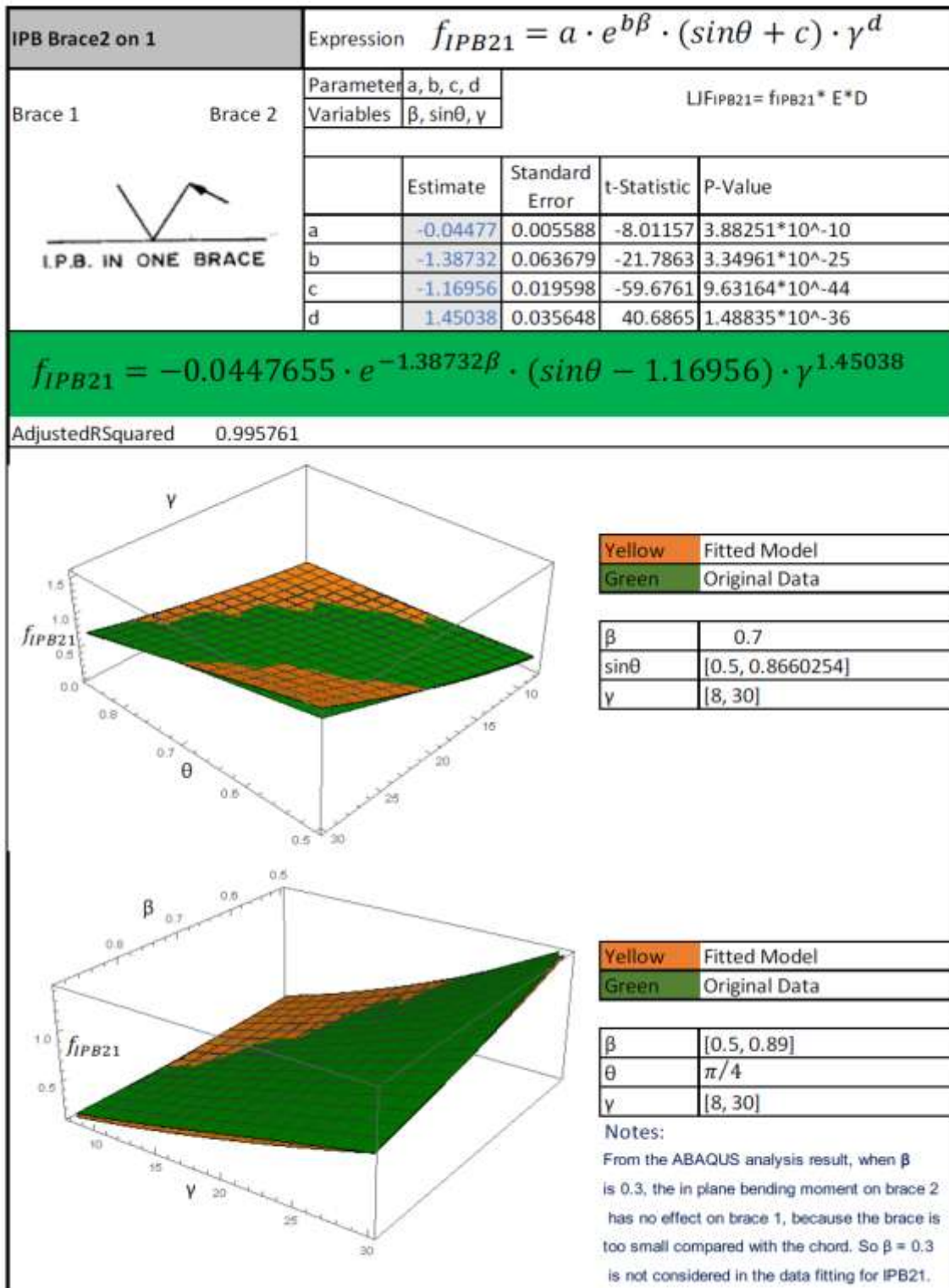


Figure 7.25 LJF Expression for the IPB for the unloaded Brace (IPB<sub>21</sub>)

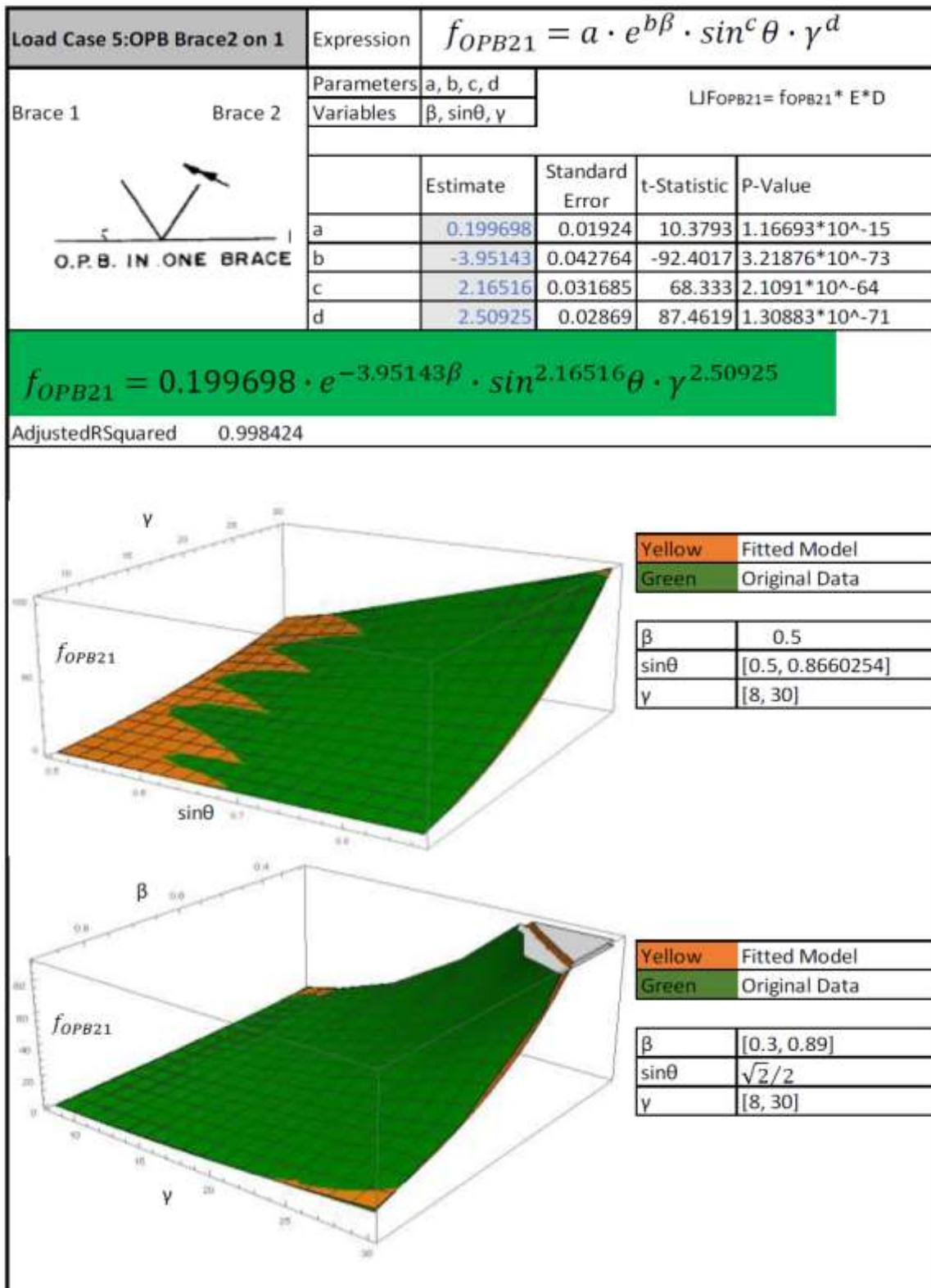


Figure 7.26 LJF Expression for the OPB for the unloaded Brace (OPB<sub>21</sub>)

## 7.5 RK Suite of LJF Equations for Gapped Uni-planar K-type Tubular Joints

The local joint flexibility values, which were calculated by using finite element analysis, indicate an established relationship between the non-dimensional geometric parameters of  $\beta$ ,  $\gamma$  and  $\theta$ . Formula can now be derived for each mode of deformation i.e. axial balanced, in-plane bending (IPB) and out-of-plane bending (OPB) on the K-type joint. The parametric equations derived for LJF can take form and not confined to any specific format. The results of the curve fitting exercise in *Mathematica* yield Equation 7.1 for the axially balanced condition, 7.2 and 7.3 for the in-plane condition and 7.4 and 7.5 for the out-of-plane condition. These equations are dependent on the ranges of data used for the input and the detailed curve fitting used to represent the data in parametric form in *Mathematica*.

Condition	RK- LJF Parametric Equation	Equation No.
Axially Balanced	$f_{axl} = 2.0275 \cdot e^{-1.7232\beta} \cdot \sin^{1.0098}\theta \cdot \gamma^{1.619}$	(7.1)
IPB Brace 2 on 2	$f_{IPB22} = 0.0122 \cdot \beta^{-2.3395} \cdot \sin^{1.1865}\theta \cdot \gamma^{1.7334}$	(7.2)
OPB Brace 2 on 2	$f_{OPB2} = 0.8307 \cdot e^{-4.5722\beta} \cdot \sin^{1.8970}\theta \cdot \gamma^{2.2862}$	(7.3)
OPB Brace 2 on 1	$f_{OPB21} = 0.1997 \cdot e^{-3.9514\beta} \cdot \sin^{2.1652}\theta \cdot \gamma^{2.5093}$	(7.4)
IPB Brace 2 on 1	$f_{IPB2} = -0.04478 \cdot e^{-1.3873\beta} \cdot (\sin\theta - 1.1696) \cdot \gamma^{1.4504}$	(7.5)

Table 7.8 RK-LJF Parametric Equations for Axial, IPB and OPB

These equations are applicable for the following range of uni-planar K-type joints.

$$8 \leq \gamma \leq 20,$$

$$0.30 \leq \beta \leq 0.89,$$

$$30^\circ \leq \theta \leq 60^\circ$$

By observation, Eqs 7.1, 7.3 and 7.4 for the axial balanced and the OPB conditions are of the form

$$F_{ij} = a \cdot e^{b\beta} \cdot (\sin^c \theta) \cdot \gamma^d$$

Where a,b, c and d are constants

And the IPB formulae do not necessarily conform to that standard form. It should be noted as in the case of previous researchers, the form of the equations may vary considerably and there is no fixed form for LJF. The RK-LJF equations are those derived from *Mathematica* as the best fit to the data input from Tables 7.4 through 7.7.

## 7.6 Gap Sensitivity Study

Many researchers have included the gap parameter within their formulations. A gap sensitivity study was performed to examine the effects of the gap size for the Axial, IPB and OPB. Figures 7.27 to 7.29 and Table 7.9 provides the results of the gap study.

B	$\theta$	$\gamma$	g		Axial Balanced	Axial Balanced Average	Axial Unbalanced 22 - 21 - Axial Balanced	Axial Unbalanced brace2	IPB brace2	OPB brace2
0.89	60	25	55	brace 1	-6.6795E-04	6.6793E-04	-2.0952E-08	1.7807E-03	4.4447E-06	1.2743E-04
				brace 2	6.6791E-04			2.4486E-03	2.9758E-05	1.7420E-04
			75	brace 1	-6.9783E-04	7.0032E-04	-3.4287E-06	1.7667E-03	4.4208E-06	1.2426E-04
				brace 2	7.0282E-04			2.4636E-03	2.9797E-05	1.7433E-04
			100	brace 1	-7.3217E-04	7.3216E-04	-1.7113E-08	1.7517E-03	4.1936E-06	1.2042E-04
				brace 2	7.3214E-04			2.4838E-03	2.9753E-05	1.7505E-04

**Table 7.9 Gap Sensitivity Study for IPB, OPB and Axial Balanced for  $\beta = 0.89$**

*Note 1: LJF values are non-dimensional*

### 7.6.1 Gap Size and the Axial Condition

For the axial balanced condition, the LJF values within 5% to both loaded and unloaded braces as the gap increases from 55mm to 100mm. However, the effects of LJF on average (as a combination of both braces) show a negligible increase (5%) as the gap size increases from 55mm to 75mm and a further 5% as gap increases from 75 to 100mm. For the effects of the axial unbalanced condition, LJFs are higher than the balanced condition, with a small decrease in the value of LJF of the unloaded brace as the gap size increases from 55mm to 100mm. The unbalanced axially loaded condition for the

loaded brace exhibits the largest LJF values compared to the unloaded (unbalanced) and the balanced conditions, while the LJF values show a constant value as they increase from 55mm to 100mm.

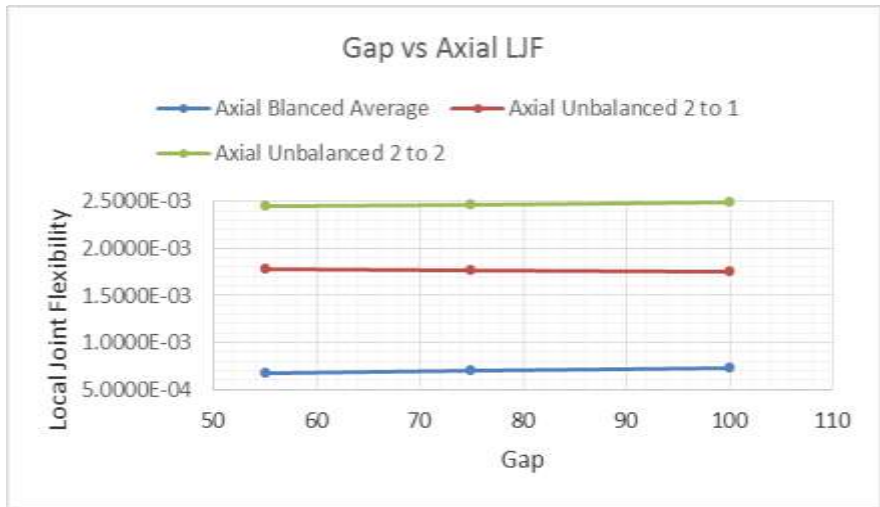


**Figure 7.27 Gap Sensitivity Analysis – Gap vs Axial LJF**

*Note 1: LJF values are non-dimensional*

### 7.6.2 Gap Size and the In-Plane Condition

For the in-plane condition, the LJF on the loaded brace is considerably higher than that of the unloaded brace.



**Figure 7.28 Gap Sensitivity Analysis – Gap vs IPB LJF**

*Note 1: LJF values are non-dimensional*

The LJF for the loaded brace shows a negligible increase in LJF values as the gap size increases from 55mm to 100mm. For the unloaded brace condition, the LJF exhibit a decreasing trend as the gap size

increases. The unloaded brace appears to have little or no effect on the overall effect on the LJF. In terms of calculating the LJF for the entire joint, the cross terms from the unloaded brace for the in-plane condition can be largely ignored.

### 7.6.3 Gap Size and the Out-of-Plane Condition

For the out-of-plane condition, the LJF on the loaded brace is considerably higher than that of the unloaded brace. The LJF for the loaded brace shows a negligible increase as the gap size increases from 55mm to 100mm. For the unloaded brace condition, the LJF exhibit a decreasing trend as the gap size increases. In the case of OPB, the cross terms from the loaded brace cannot be ignored and will contribute to the overall LJF of the joint.

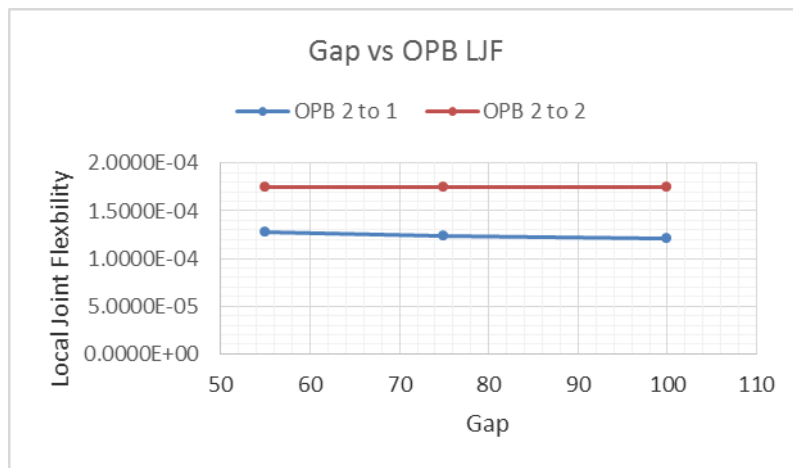


**Figure 7.29 Gap Sensitivity Analysis – Gap vs OPB LJF**

*Note 1: LJF values are non-dimensional*

### 7.7 LJF Comparison Study for varying $\beta$

A comparison study was performed on the basis of the AMOCO K-Joint Tests for varying  $\beta$  values ( $\beta = 0.30, \beta = 0.50, \beta = 0.70, \beta = 0.89$ ) and existing LJF formulations. The AMOCO K-Joint tests are represented below for  $\beta = 0.89$ .

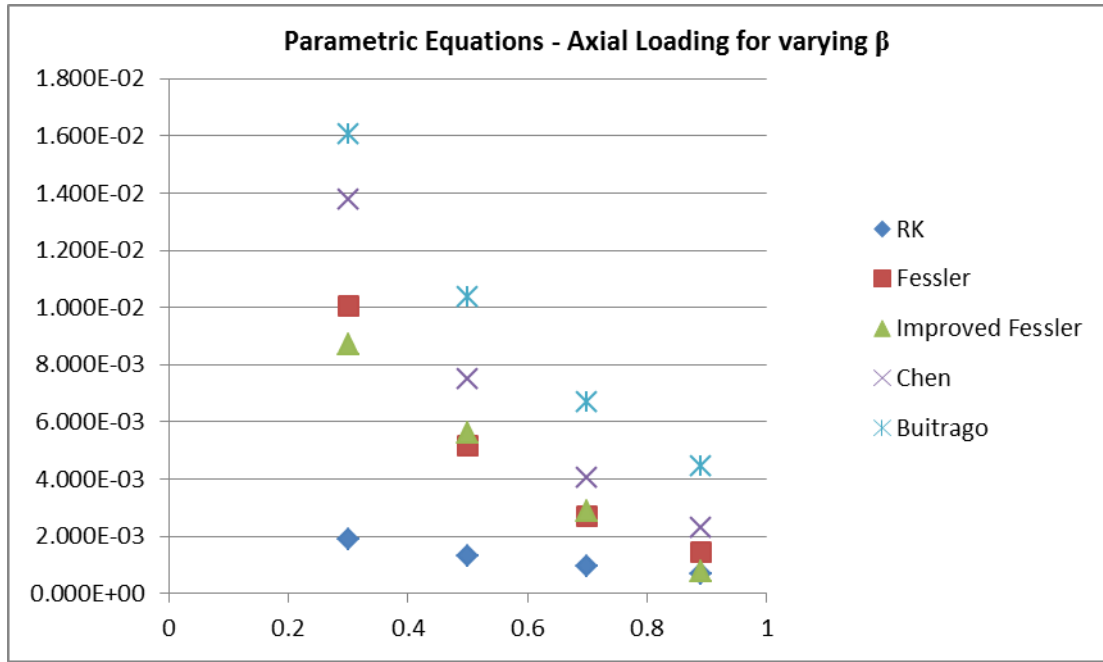


**Figure 7.30 LJF Comparison for Axial loading vs varying  $\beta$**

*Note 2: LJF units for Axial Loading: mm/kN*

For the axially loaded condition, Figure 7.30 shows that previous LJF formulations have overestimated these loading effects. With the advancement of computing power and the extensive database, RK-LJF formulation represents best LJF formulation for uni-planar gapped K-type joints based on current methods. For the OPB condition (Figure 7.31), both cross terms and direct terms have been included. All LJF equations show an increasing trend as  $\beta$  values decreases. This is highly expected with RK-LJF formulations providing more flexibility than the others. This is not unexpected as the other LJF equations have all been a derivative of each other in terms of the limited and similar database of joints used in the past twenty years. RK-LJF formulations are based on an up-to-date database of in-service K-type joints. Increased flexibility would mean in the case of fatigue life predictions, these are expected to be increased with the RK-LJF formulation and reported in Chapter 8. The RK-LJF equations will be validated against large scale testing and the MSL equations to show a good agreement for ultimate strength in Chapter 8.

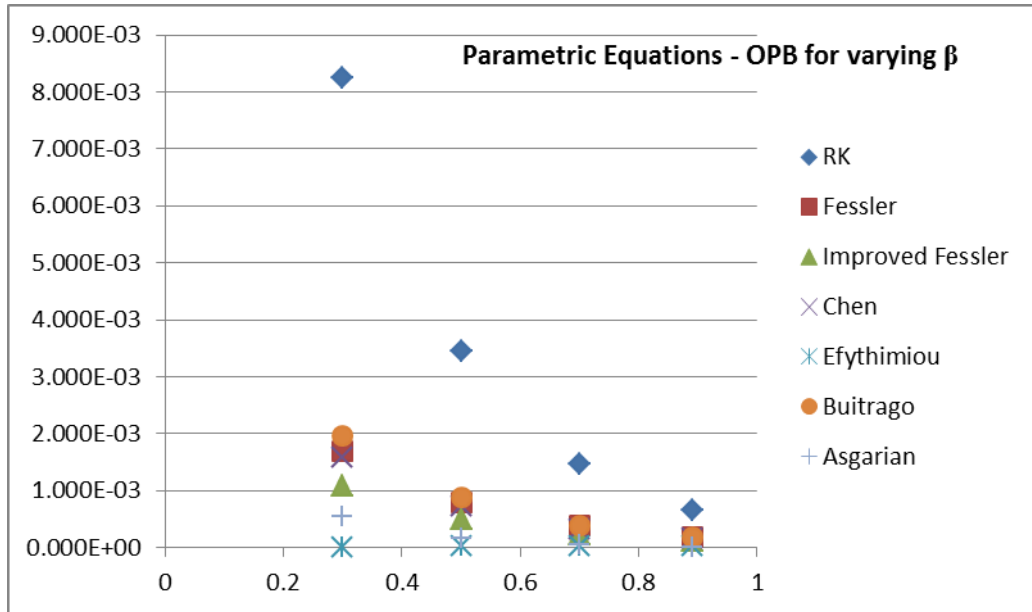


**Figure 7.31 LJF Comparison for OPB vs varying  $\beta$**

*Note 3: LJF units for OPB: 1/kN.m*

For the in-plane condition (IPB), Figure 7.32, the unloaded brace has little effect on the overall LJF of the K-joint system. This is only applicable for gapped K-type joints and may not be applicable for overlapping K-type joints and other T-Y-X joint configurations. This is expected in the case of the IPB condition. As with OPB, the increased flexibility provided by the RK formulations are expected to show a significant improvement on the fatigue life predictions of uni-planar gapped K-type joints. Similarly, as with the OPB, ultimate strength validation is required to determine the performance of the RK-LJF equations in a frame system, which is done in Chapter 8 of this thesis.

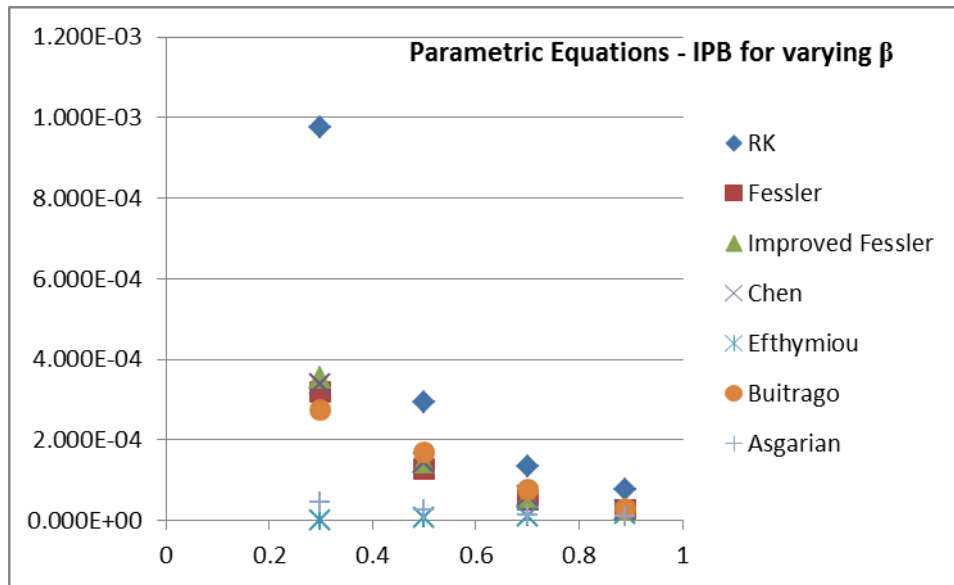


**Figure 7.32 LJF Comparison for IPB vs varying  $\beta$**

*Note 4: LJF units for IPB: 1/kN.m*

## 7.8 Summary and Conclusions

The results outlined in this Chapter signify a significant improvement to the body of work on LJF. A paper entitled “*Improved Joint Flexibility Equations for uni-planar gapped K-type tubular joints of fixed offshore structures*” has been accepted for the Journal Of Marine, Engineering and Technology (JMET) publication, based on the new contribution in the area of joint flexibility and structural integrity management, within this Chapter.

The RK-LJF calculations are based on a robust methodology which uses an in-service database on K-type tubular joints with varying geometric parameters to determine the LJF. Considerable finite element models have been developed from this database to ensure that all geometric parameters have been considered. To develop the parametric equations for the *Mathematica* tool was used for the curve fitting exercise. The curve fitting exercise demonstrated a smooth, continuous function modeling the numerical results with 99.8% for axial and 99.9% accuracy for both in-plane bending and out-of-plane bending conditions on the 3D plots.

Furthermore, for the gap parameter, the results of the gap sensitivity indicate that as the gap size increases from 55mm to 75mm and finally 100mm, there is a 5-10% difference on the LJF results. At

the gap size of 100mm, the K-joint has begun to exhibit properties of the Y-joint with little or no effects from the unloaded braces to the overall LJF of the joint. From this basis, the RK-LJF equations are fully applicable to all gap size ranges for uni-planar K-type joints, with the gap parameter not being a critical parameter to include in the formulation.

While the RK-LJF formulation shows an improvement to LJF for IPB and OPB, further investigation is required to validate the applicability of this improvement in terms of ultimate strength and mechanism behaviour. The RK-LJF formulations are assessed in terms of a structural frame to determine the real behaviour of the effects of the LJF rather than on an isolated joint. This validation exercise is discussed in Chapter 8 of this thesis.

## CHAPTER 8

# Validation of the RK-LJF Formulations in Global Structural Assessments

### 8.1 Introduction

Zettlemoyer (2009), in his paper on life extension of fixed offshore structures, had a particular focus on fatigue life assessments and the ultimate strength analyses as being required to justify Asset Life Extension (ALE). This is also the general practice by most operators presently. While a spectral fatigue check is often performed at the design level and documented in most design codes, the ultimate strength analysis has, in the past, been restricted to assessment type codes and standards. In principle, the fatigue design life misnomer is often to be argued away by supporting inspection data and using assessment tools such as LJF. Most operators are now of the view that ultimate strength is a greater governing criteria for ALE and they require a baseline ultimate strength analysis performed at design stage to develop their SIM of that particular structure over its lifecycle. API RP 2A 22nd Edition (2014) has now adopted this approach to their design procedures.

The NORSOK Standard 004 (2004) makes particular reference to Fatigue Limit State (FLS) and Ultimate Limit State (ULS) in their design standard and in particular of the reassessment of offshore structures. According to NORSOK, *“The aim of fatigue design is to ensure that the structure has an adequate fatigue life. Calculated fatigue lives can also form the basis for efficient inspection programmes during fabrication and the operational life of the structure. The design fatigue life for the structure components should be based on the structure service life specified by the operator.”* Additionally NORSOK (2004) also stated that, *“To ensure that the structure will fulfill the intended function, a fatigue assessment, supported where appropriate, by a detailed fatigue analysis should be carried out for each individual member which is subjected to fatigue loading.”* For Ultimate Limit State (ULS) NORSOK reported that, *“ULSs are those associated with collapse, or with other forms of*

*structural failure which may endanger the safety of people. States prior to structural collapse which, for simplicity, are considered in place of the collapse itself are also classified and treated as ULSs."*

## **8.2 Ultimate Strength of Fixed Offshore Structures**

In 2000, MSL Engineering presented the JIP Rationalization and Optimization of Underwater Inspection Planning, consistent with API RP 2A Section 14 (2000), for key oil and gas operators in the Gulf of Mexico. One of the key findings of the MSL JIP involved the key source of joint failure. It was noted that those joints subjected to extreme loading were highly susceptible to damage. In recent times, De Franco et al (2004) have reported a series of hurricane driven incidents in the Gulf of Mexico, resulting in global structural failure of platforms of various vintages. The outcomes of these failures have led to revisions and update of current design codes and standards and the processes by which existing structures are assessed for extreme storm overloading.



**Figure 8.1 Global Structural Failure from Hurricane Lilli  
(De Franco, 2004)**

The ultimate strength analysis is performed on the jacket structures to determine its strength/capacity against the 100 year RP (Return Period) of the environmental loading. This 100 year RP is a minimum design criteria for fixed offshore structures in all design codes of practices (linear elastic check). In the

assessment approach, the engineer is allowed to exploit the inherent redundancy within the frame of the jacket structure (non-linear response). The ultimate strength or pushover analysis is measured through a RSR (Reserve Strength Ratio) or Load Factor that is above the 100 year design level at collapse at  $F_{max}$  (Figure 8.2).

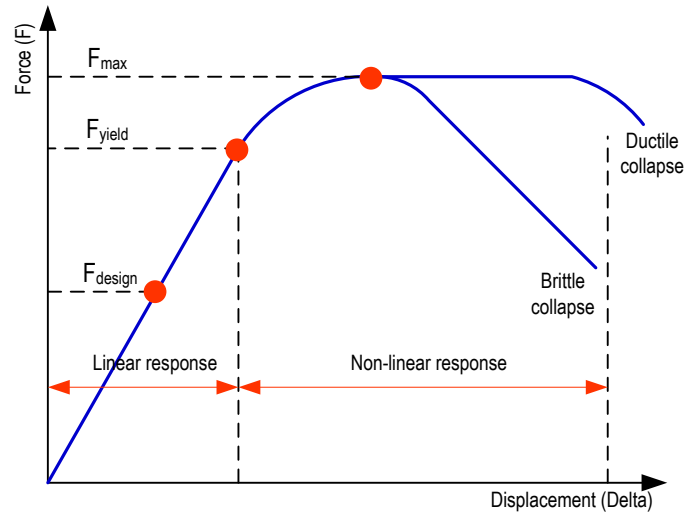


**Figure 8.2 Ultimate strength load displacement curve**

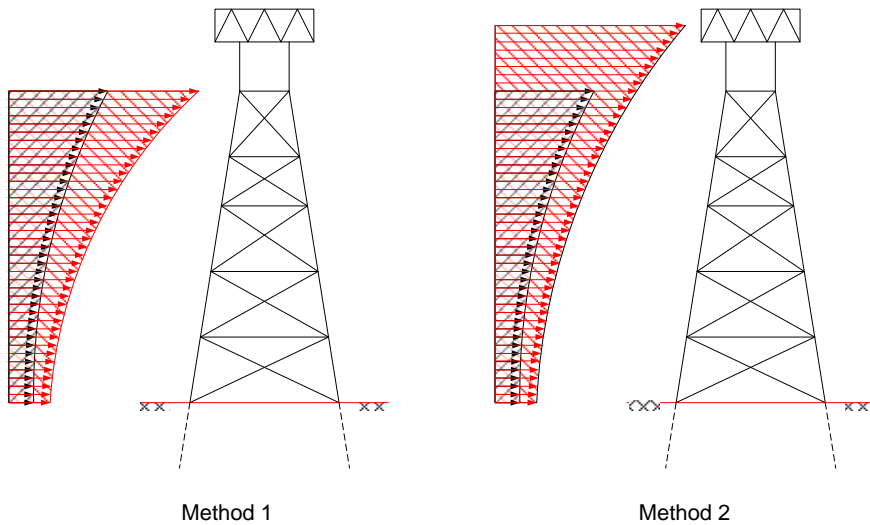


**Figure 8.3 Assessment approaches for ultimate strength  
(Method 1 Ramp up load & Method 2 Increased Wave approach)**

Figure 8.3 shows the two main approaches used in the ultimate strength analysis as it relates to the pushover of the environmental wave load. In Method 1, the environmental load (wind, wave and current) is ramped up and applied to the structure at collapse and the ratio of the collapse wave load to 100 design load is the RSR. In Method 2, the 100Yr RP wave is increased and applied to the structure

until it collapses. The ratio of the collapse wave to the 100 Yr design wave is considered as the RSR. Method 2 is the more accepted approach for aging structures where the effects of wave in deck loading (WiD) can be easily determined by the wave height hitting the lowest deck level. For older structures where, at the time of design, an air gap was not specified, due to it not being specified in the codes and standards, increased wave height due to metocean changes or subsidence of structures may lead to this air gap being compromised in the present operating conditions.

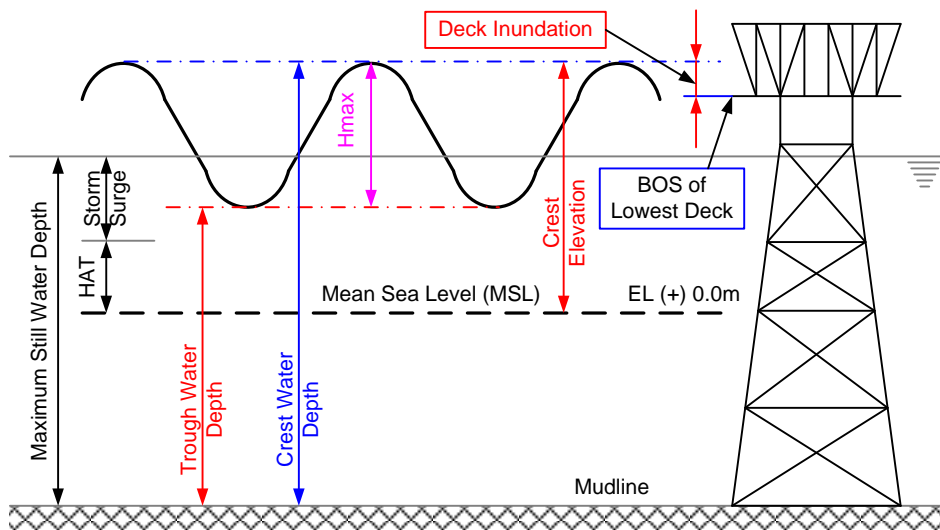


**Figure 8.4 Wave Loading on Fixed Offshore Structures**

Wave in Deck (WiD) loading increases the hydrodynamic loading that acts on the structure and contributes significantly to the collapse of structures under environmental loading. Ultiguide (1999) has recommended using LJJ in the ultimate strength analysis as it can contribute by 10-15% increase in RSR values. For aging structures, especially with those experiencing WiD loading, the use of LJJ can be an added advantage for continuing operations.

Since the early and mid-2000s, most of the work on local joint flexibility analyses and parametric equation development by MSL (2002), Miterhari (2009) and Qian et al (2013) have based their research on understanding the effects of LJJ on the frame or truss system to represent the jacket template of offshore structures. The most noteworthy benchmarking exercise that has been done was by MSL (1994, 1998) where revised formulations to the MSL-ISO joint strength formulae (2002) were

presented. These formulations were then benchmarked against the BOMEL frames test (1995) and provided a set of formulations that considered LJJ implicitly.

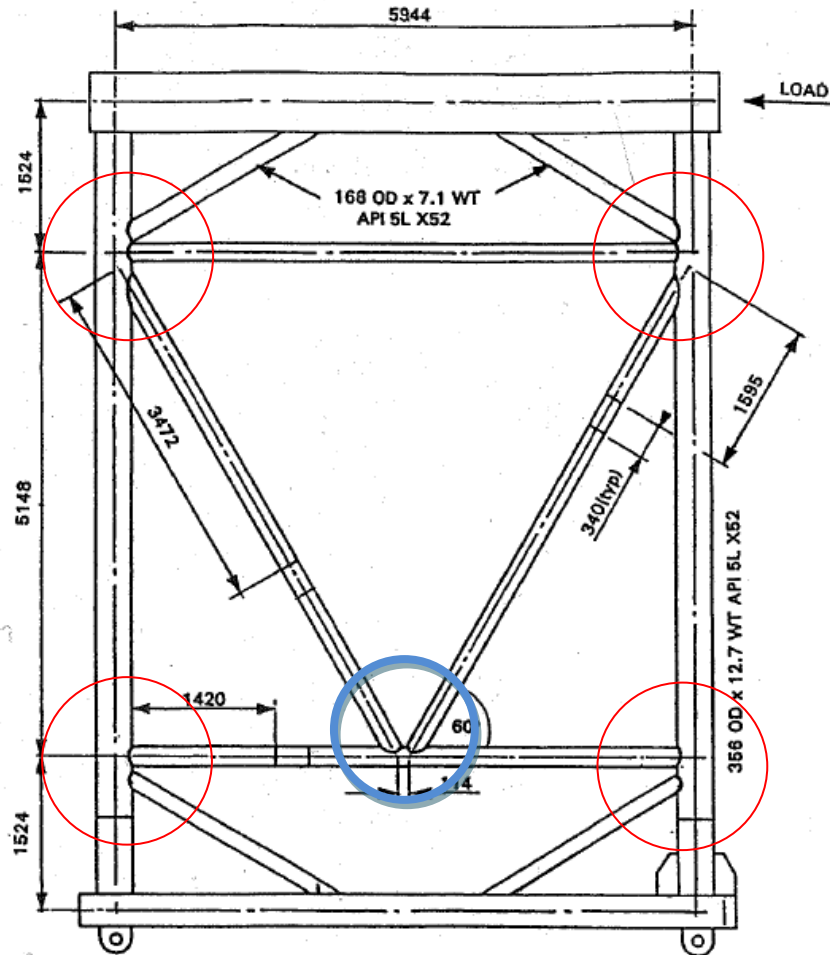


**Figure 8.5 Frame VII - Model Configuration**  
**(BOMEL Frame Tests, 1995)**

The BOMEL Frame VII (Figure 8.5) was the model used to calibrate gapped K-type joints for the MSL equations. The results generated from the benchmarking exercise included results for BOMEL test data, rigid joints and the MSL equations are presented in Figure 8.6.

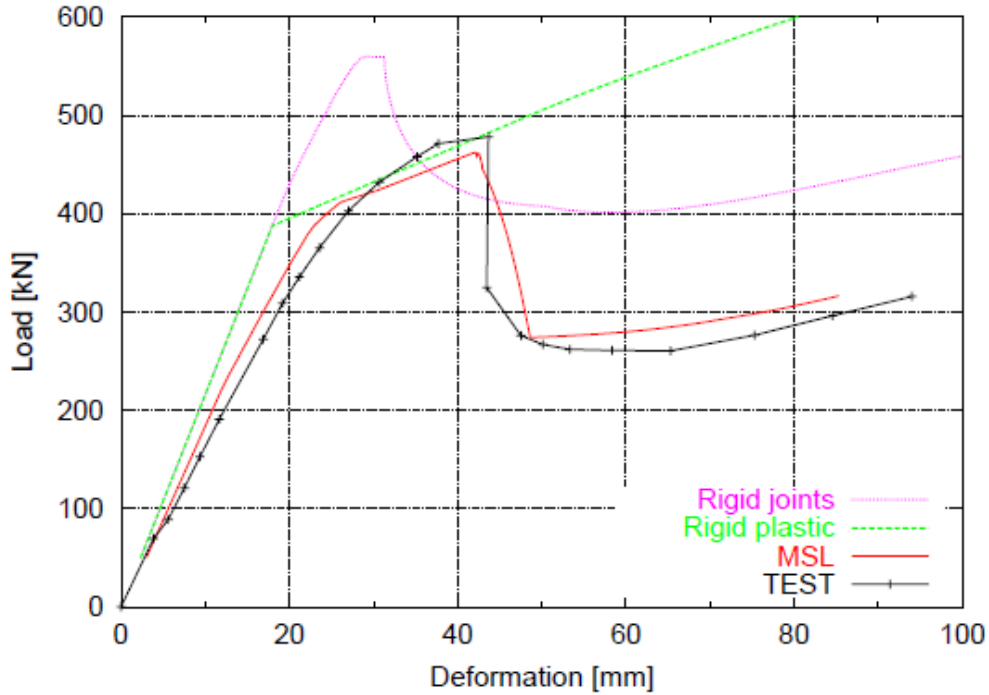


**Figure 8.6 Frame VII – Behaviour compared to Test Specimens  
(MSL, 2002)**

ISO 19902 (2007) reports that, “*full non-linear deformation curves for joints can be required for pushover analysis to determine a system ultimate strength, especially when joint failures participate in the sequence leading to system collapse. Such pushover analyses are common in studies for maintenance and life extension of structures.*”

Furthermore ISO 19902 (2007) provides a load displacement curve (Figure 8.6) similar to Figure 8.7, to present the curve-fitting exercise by MSL (1994, 1998).

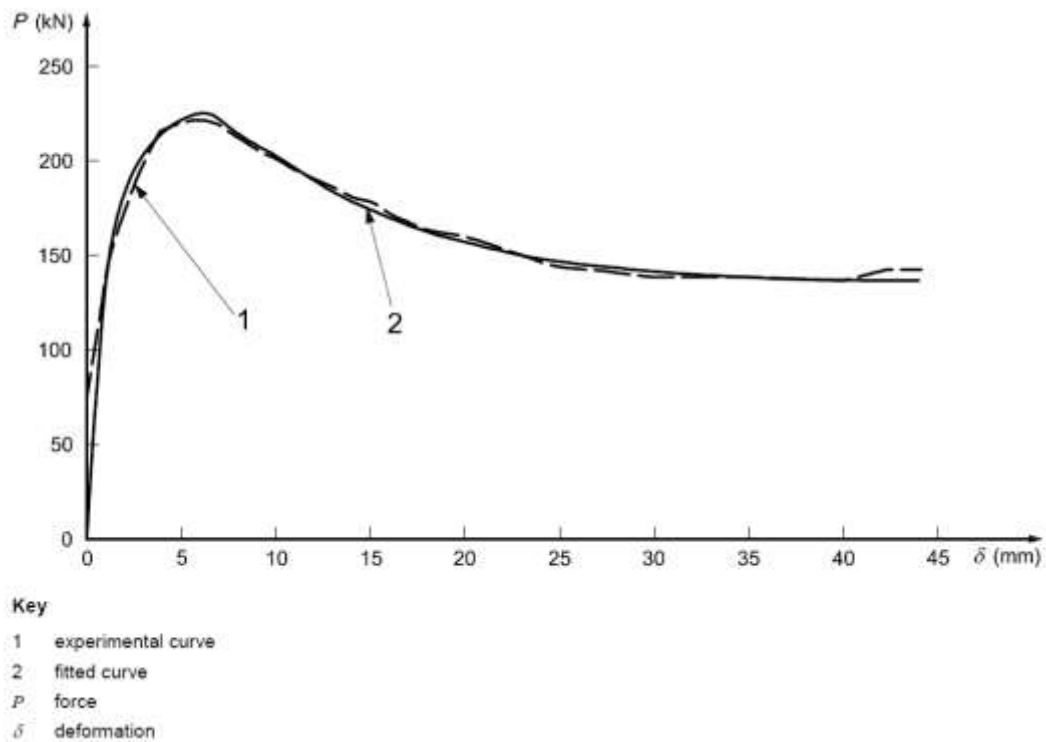


**Figure 8.7 Comparison of fitted curve to experimental data for force deformation behaviour of a simple tubular joint**

**(ISO 19902, 2007)**

ISO argues that with the MSL (1994, 1998) work, “*the understanding of linear elastic flexibility has been extended, through the analysis of an updated database and a range of closed-form expressions was established which permit the creation of non-linear load deformation curves in both loading and unloading regimes for simple joints across the practical range of load cases and geometries.*”

MSL has provided a robust methodology and study on benchmarking against large scale test results. As with Qian (2013), MSL does not explicitly mention the contribution to OPB, IPB or axial loading, but considers the overall system strength which relates to the overall ultimate strength. The RK-LJF formulations will be validated against the performance of the Frames VII for rigid, MSL-ISO equations and BOMEL test data to evaluate its performance in the 2D frame template.

### **8.3 Ultimate Strength Finite Element Software for Offshore Structures (USFOS)**

The USFOS is a finite element suite of software has been developed since 1985 and is primarily used for the collapse analysis of space frame structures, from initial yielding to the actual collapse of the structure. The program combines classical theory with accurate numerical procedures and conventional finite element formulations. It is generally accepted as the non-linear software of choice for most practicing engineers in the offshore structures industry. The key applications of USFOS include pushover analysis, ship collision, accidental loads and fire and blast assessments.

With the development of the MSL-ISO formulations (Table 3.2), USFOS developers have codified these formulations within the software, making it user friendly for the user to select the MSL formulations for respective joint configurations. The joint flexibility module has also been developed based on the procedure developed by Buitrago in Section 3.8.

### **8.4 Validation RK-LJF Equations in 2D Frame Tests**

The results obtained by MSL in Figure 8.5 provide the basis for this validation exercise. The RK-LJF was included in the Frames VII USFOS structural model and the load vs deflection results for the rigid joint, MSL-ISO joint, BOMEL test data and the RK-LJF formulations were compared.

To perform the analysis, the following procedure was followed:

- Create an USFOS model using the BOMEL Frame VII configuration, material properties and loading mechanisms.
- Use the USFOS pushover module to replicate the P-delta for the test data.

Four cases of analysis were performed, with the flexibility options in Table 8.1.

Case No.	Joint Flexibility Options	Comments
1	No LJF or joint strength check (Figure 8.8)	Rigid joint analysis
2	USFOS Joint check using MSL-ISO equations	All 5 K-type joints (one circled red and 4 circled blue) on Figure 8.5
3	USFOS Joint check using MSL-ISO equations	For the K-type joint circled in blue on Figure 8.5
4	RK-LJF using an updated model to Case 1 by inserting two short stub brace members (circled blue on Figure 8.5)	The properties for the short stub members were calculated based on the K-joint configuration

**Table 8.1 Joint Flexibility Options for RK 2D Frame validation study**

To develop the two short stub brace members, a similar approach is used to the one used by MSL (2001) in *The effects of local joint flexibility on the reliability of fatigue life estimates and inspection planning* for the HSE Executive. The methodology has been tailored to accommodate the element modeling capabilities of the USFOS program. The method involves inserting a short stub flex–element at the end of each brace. The short stub flex-element connects the brace to the chord. RK-LJF formulations give explicit formulae for the various uni-planar K-type joints based on their geometry. The Equations 7.1 – 7.5 (RK-LJF) are employed to calculate the LJF for the joint circled in blue on Figure 8.5. The result is then used to calculate the necessary area and inertial properties of the flex-element to represent axial, in-plane and out-of-plane bending. The flex-elements are represented as Elements 28 and 29 on Figure 8.9. The USFOS files and results for the RK-LJF validation are provided in Appendix 6.

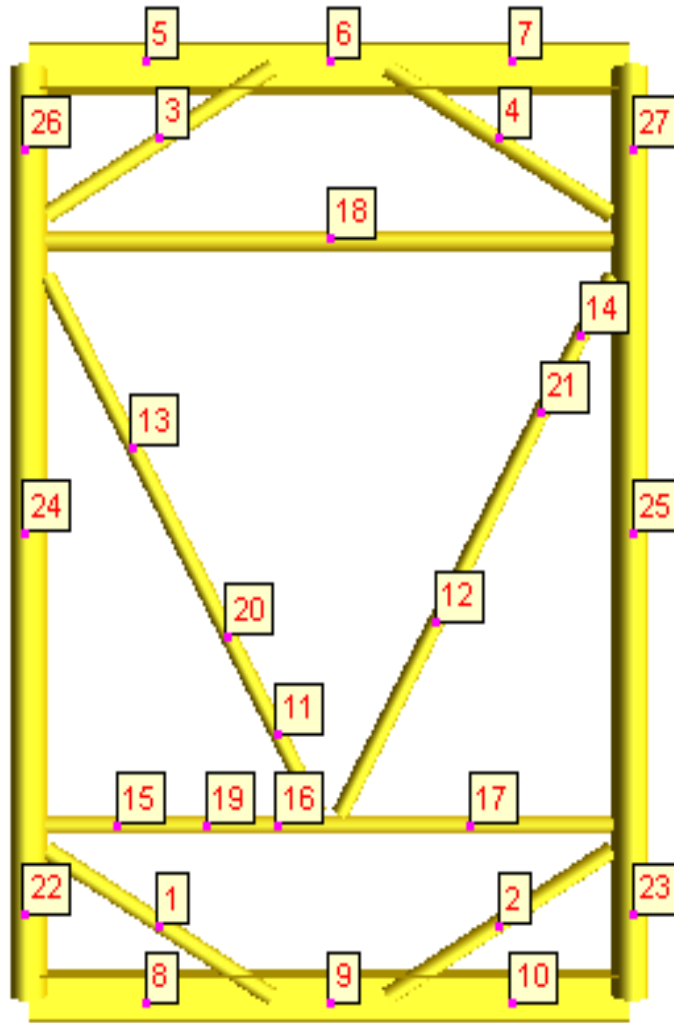


**Figure 8.8 BOMEL Frame VII modeled in USFOS (No LJF)**

The Area,  $A$ , and the moments of Inertia,  $I$ , of the flex-element are calculated as follows:

$$I = L / E (LJF_m) \quad (8.1)$$

$$A = L / E (LJF_p) \quad (8.2)$$

Where

- $L$  is the length of the flex-element
- $LJF_m$  is either the in-plane or out-of-plane bending local joint flexibility
- $LJF_p$  is the axial loading local joint flexibility

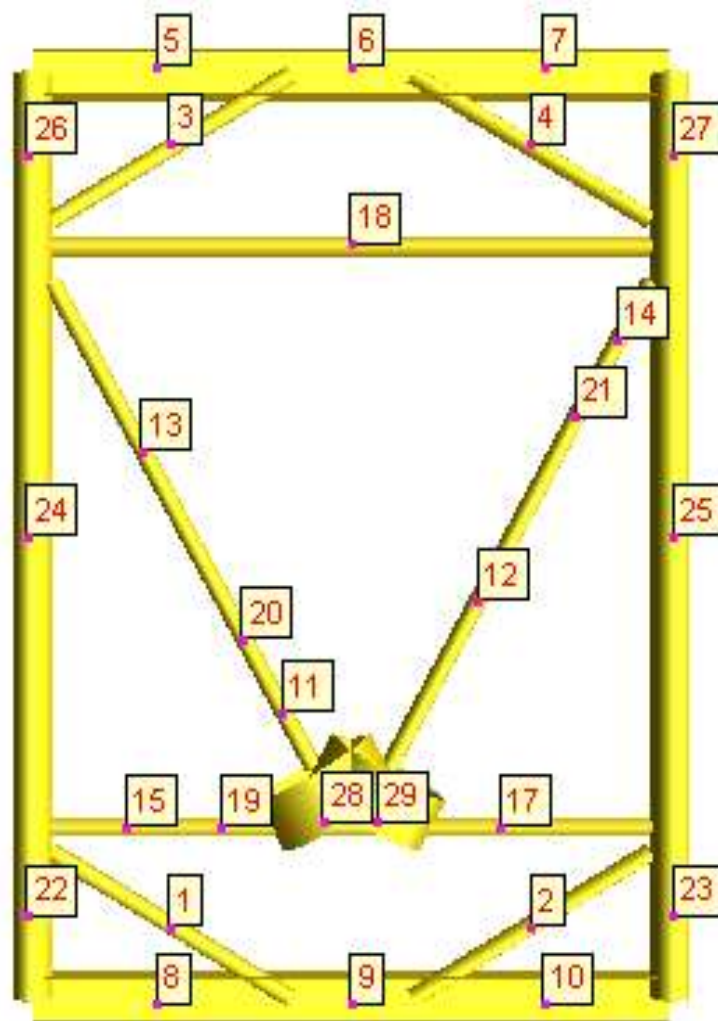


**Figure 8.9 BOMEL Frame VII modeled in USFOS (LJF included)**

Figure 8.10 provides the load displacement curves for all four cases outlined in Table 8.1. If no LJF is included in the analysis, the frame is much stiffer than the test data. If no LJF is included, the structure computer model behaves much stiffer than the prototype test data (compared results from analysis Case 1 with test results). The analysis results for Case 2 provides a good representation of the test data as the USFOS LJF or joint strength was calibrated against the large scale test data.

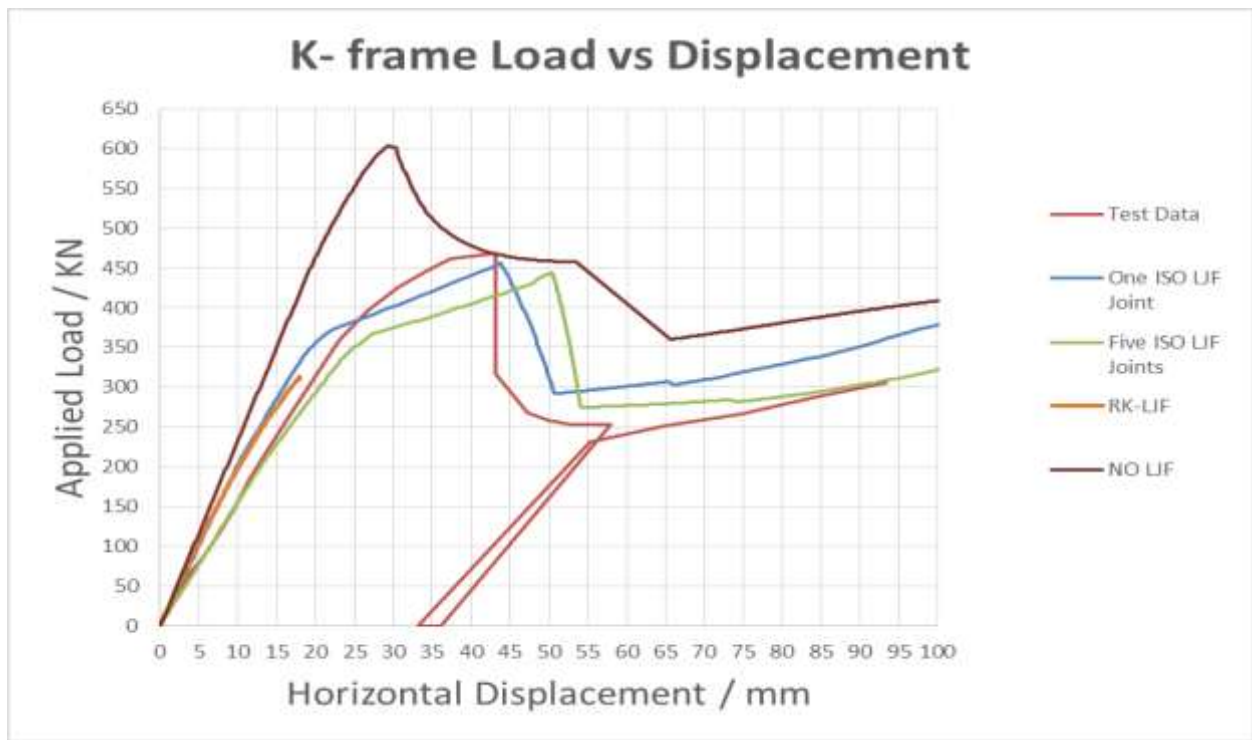


**Figure 8.10 Load vs Displacement Curve  
(RK-LJF included)**

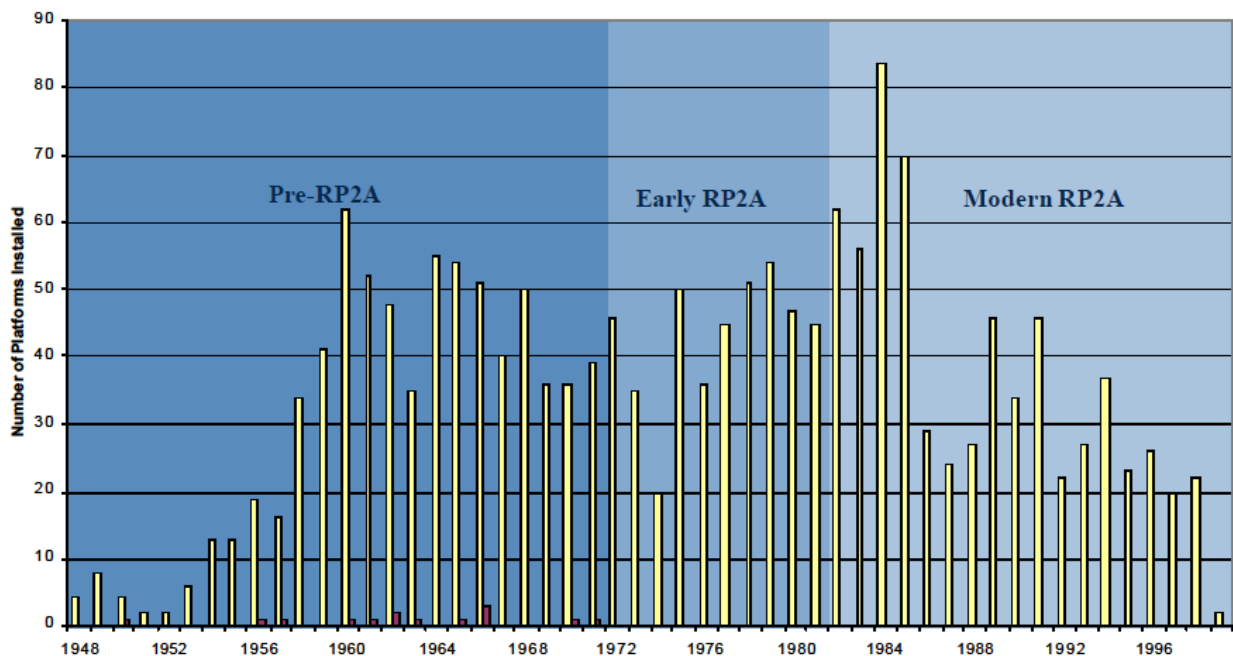
For the analysis from Case no 3, the results show stiffer than the results from 5 LJF joints being modeled (Case 2) but softer than the case without LJF (analysis results in Case 1). The analysis results in Case 4 (RK-LJF) derived from this study are similar to the results achieved from the analysis in Case 3 (MSL-ISO) above, which is expected. The RK-LJF results from this study using ABAQUS result in the frame that is slightly softer than the ISO formulation (which is of benefit and closer to the physical prototype model i.e. the BOMEL test results). The RK-LJF results are within 5% of the prototype tests results but are confined to the linear elastic region, as the RK-FEA benchmarking exercise was performed using linear elastic displacement values and the large scale AMOCO tests were performed in the linear elastic range. There is an opportunity in the future for researchers to develop the RK-LJF equations for the inelastic range of stress.

### **8.5 Recent understanding on the fatigue phenomena on fixed offshore structures**

Prior to the early 2000s, it was generally accepted that fatigue lives for existing structures was the governing criteria for asset life extension and continuous operations. With MSL Engineering

publishing a JIP Rationalization and Optimization of Underwater Inspection Planning consistent with API RP 2A Section 14 (2000), the general understanding of fatigue as it relates to fixed offshore structures would now be changed. This JIP considered a wide database of in-service structures in the Gulf of Mexico of various vintages to consider various degradation mechanisms. The pre-API structures ranged from 1948 to 1971. As fatigue is a time dependent phenomena, it would be expected that, all things being equal, fatigue cracks would be found in the older structures of the pre-API vintage. Figure 8.11 shows the contradiction where platforms installed towards the later part of the era show greater susceptibility to fatigue to general fatigue cracking.

The first platform in the Gulf of Mexico was installed in approximately 15m of water. By 1961, platforms were being installed in 200 feet of water and by the issue of the first API RP 2A (1969), platforms were being installed in over 300 feet of water (Figure 8.12). These platforms were designed without the benefit of modern joint design and did not include fatigue capacity checks. This is quite apparent in their joint make up which does not include the thickened can sections in their design.



Yellow (longer) bars show number of platforms installed  
 Red bars show number of platforms with multiple (>1) suspected general fatigue cracks

**Figure 8.11 Pre-API RP 2A Vintage Platforms with multiple fatigue cracks (MSL, 2000)**

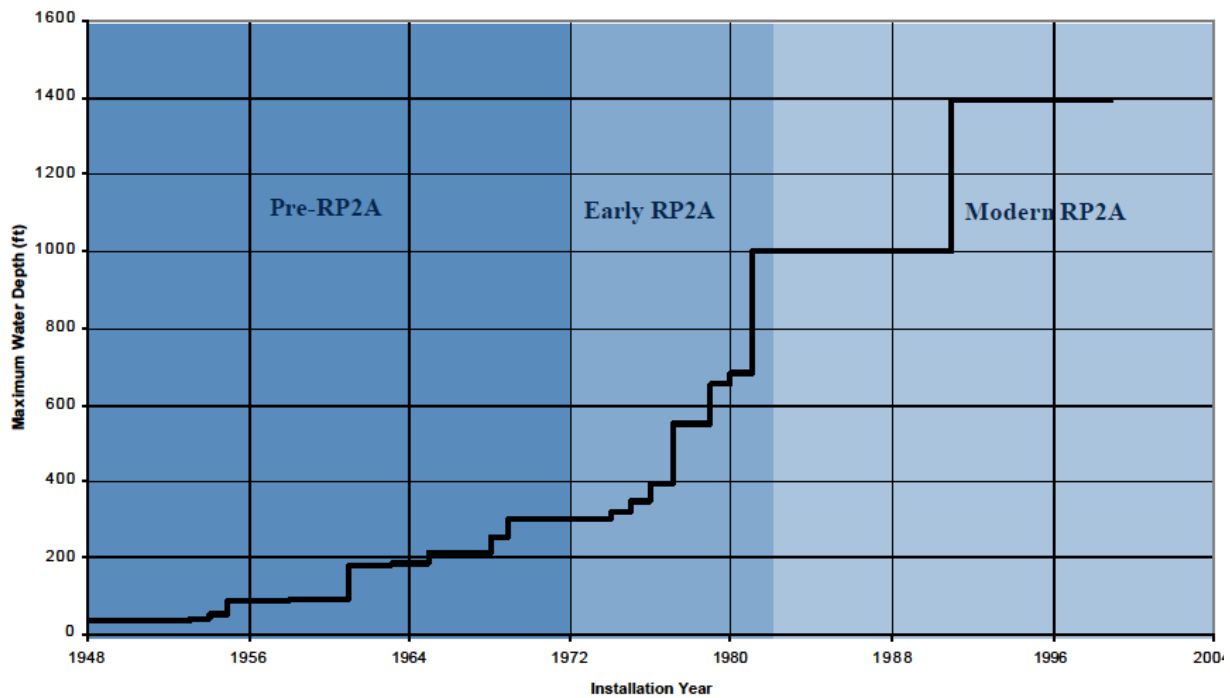


**Figure 8.12 Inspected Platforms, Water Depth increase with time (MSL, 2000)**

It is apparent that the joint design of the pre-API vintage was adequate for shallow waters but become more susceptible as the structures were being installed in deeper waters using the same joint capacity equations. In the modern API (after 1979), there is no issue of inadequate joint capacity equations. Modern API codes provide good guidance on tolerance, joint configurations and welds to ensure the effects of the fatigue issues are almost non-existent, but good quality control is required in fabrication yards to ensure that fatigue issues are appropriately considered.

With respect to fatigue, the JIP concluded the following, which enable operators to revisit their concept of fatigue damage and concentrate their efforts on other sources of damage to fixed offshore structures:

- Weld joint defects occur on less than 1% of modern-RP 2A vintage platforms and are associated with installation damage, fabrication defects and poor design/repair details.
- In both early RP 2A platforms and pre-RP 2A, approximately 80% of the weld/joint defects were a combination of fatigue damage and collateral damage from vessel collision.

- Fatigue damage in early RP 2A platforms is dominated by damage to the conductor framing guide at the first level of framing. This damage affected approximately 2% of the vintage population.
- General fatigue cracks were found in approximately 1% of the early RP 2A fleet.
- Early and pre-API RP 2A, where a failure is recorded in the cathodic protection (CP), has been recorded for some time in the service life, and are therefore more heavily corroded, and are at an increased risk of general fatigue damage.
- Conductor bay fatigue amongst the population of pre-API RP 2A platforms is consistent with early RP 2A vintage platforms. It occurs in a little over 3% of the vintage population.
- General fatigue damage is more widespread in pre-RP 2A platforms than it is in early vintage platforms, affecting 5% of the vintage population.
- Pre-RP 2A platforms most susceptible to general fatigue damage are those installed in the latter part of the era in relatively (for the vintage) deep water, generally of depths 100 feet or greater. The damage occurs mostly in the primary joints close to the mud-line.

For most oil and gas operators, this JIP revealed that the concept of fatigue considerations can be addressed within their Structural Integrity Management System (SIMS). Nichols and Khan (2015) demonstrated that embarking on a Risk Based Underwater Inspection (RBUI) approach, together with a good anomaly management program, and with platform CP functionality, platforms of all vintages can be managed effectively with limited resources. These practices have now been included in the API RP 2SIM (2014) and the ISO SIM (DIS) and adopted by many leading operators as global standards for managing fixed offshore structures. Where existing cracks are determined, the use of fracture mechanics has become a useful tool in predicting loss of capacity, crack growth and propagation over time. The operator will generally make a decision to employ a SMR scheme (Strengthening, Modification and Repair) such as using clamps or simply by introducing a pinhole in the crack path to arrest the propagation.

## 8.6 Summary and Conclusions

The RK-LJF suite of equations presented in Chapter 7 has been validated against large scale test results and the MSL-ISO equations that are included within the ISO 19902 (2007). The flexible behaviour when using the RK-LJF equations represents a considerable improvement on the rigid joint analysis and shows a closer relation (within 5%) to the MSL-ISO formulation. It displays a slightly softer behaviour than the MSL-ISO formulation which is closer to the real test data results. As for gapped uni-planar K-type joints, this represents an improvement on the current formulation and RK-LJF formulation should be used in the future for determining the LJF of this joint configuration. Furthermore, the RK-LJF formulation explicitly models the effects of axial, IPB and OPB, which makes it much more user friendly to calculate joint capacity for the uni-planar K-type joints. The concept of LJF is very important to ALE of fixed offshore structures in terms of the benefits derived by employing a flexible joint analysis compared to a rigid joint analysis. A paper on “*RK-LJF Formulations in Global Structural Assessments for Remaining Life Assessments of Fixed Offshore Structures*” for the 2017 ISOPE Conference in San Francisco. An Abstract on the paper has already been submitted for approval.

Recent researchers and code developers have aligned the ALE and work on LJF to be validated against the ultimate strength of the jacket structure. While spectral fatigue analysis is important in design, as it provides the basis for good joint configurations, offshore engineers have become less worried of the fatigue phenomena, as they can deal with it through a good structural integrity management program, which is now well documented in API RP 2SIM (2014) and the soon to be issued ISO 19901-09 SIM (DIS).

## **CHAPTER 9**

### **Concluding Remarks and Recommendations for Further Work**

#### **9.1 Concluding Remarks**

The research has successfully generated four peer reviewed publications, two of which are included within high impact journals and two are within highly esteemed structural engineering and integrity conferences.

The success of the work outlined in this research is also measured by the considerable feedback and interest that has been generated by many of the major operators including BP and PETRONAS, consulting engineering companies such as WS Atkins, IntelliSIMS, offshore code developers ISO and API and academic institutions such as LSBU and NUS, in this research. These companies and institutions all represent a wide variety of stakeholders in the offshore industry who are involved in ALE for themselves, their clients or for continued research and publication of recommended practice.

This research has a tremendous impact on the offshore industry as it allows the industry to continue to manage structures safely while exploiting the technology of LJF to consider ALARP principles to their operations. Fundamentally it has demonstrated, at least for uni-planar K-type joints, that it is closer to the prototype large test behaviour than the current MSL-ISO joints, so structures can now demonstrate greater ultimate strength than previously thought. In terms of economics, platform inspections can now be increased and the likelihood of some underwater repairs can be avoided. In terms of OGP, this can lead to reduction in their OPEX (operational expenditure) which can result in considerable savings.

In this research, the effects of LJF on uni-planar K-type joints were studied. This involved reviewing the development of LJF parametric equations from past researchers, a review of a series of LJF application studies and an understanding of the Structural Integrity Management (SIM) processes as it

relates to the fitness for purpose of fixed offshore structures and in particular, aging structures where, at the time of design, computational and modern code of practice considerations were not considered.

The SIM processes enable the OGP's to develop and make use of good data, technical expertise, maintenance plans, structural databases and effective implementation programmes, including inspections and repair, to effectively manage offshore platforms over their lifecycle. Structural assessment of an offshore structure is one such tool used by OGP's to demonstrate fitness for purpose and the concept of LJF is one method to be included in structural assessments. Over the past decade or so, it has become apparent to OGP's that they must codify best practices in operating offshore structures, which led to the development of the ISO 19902:2007, API RP2 SIM (2014) and the ISO 19901-09 SIM (DIS), currently being developed. These codes and standards are new for SIM and lack detail around more elaborate issues such as LJF. While they define LJF as being a good approach to be used for fitness for purpose assessments (including ultimate limit state and fatigue limit state), they do not recommend the use of one suite of LJF equations over another and do not comment on the limitations of each. This research critically examined the development and applicability of each of the ten existing LJF equations and improved upon them for the K-type uni-planar tubular joints. The ISO 19902 is currently being updated and the author is a member of the working committee, which has shown interest in including elements of this research in the new ISO 19902, to improve a deeper understanding of LJF and its applicability in offshore structures.

This thesis has made considerable improvements to the existing approaches of LJF behaviour and the derivation of existing equations. Firstly, this research provides a standardized approach to the development of LJF equations. It documents a six-step process (in Chapter 7) on how to appropriately develop the LJF equations. Previous researchers have used varying approaches including varying software, analytical methods, limited structural databases and small scale testing to derive their equations. In this research, an industry accepted structural analysis software, ABAQUS, was used together with a substantial in-service database (SICS) of tubular joints from over two hundred

operating structures. A detailed screening study to ensure that all permutations of geometric ranges are included in the research and is a fundamental improvement on all other LJF developers.

Secondly, the research provides a benchmarking model to large scale testing results on the AMOCO K-Joint tests. The AMOCO K-Joint tests are the only large scale testing of LJF available in the offshore industry and hitherto not available in academic literature. The RK-FEA model developed within this research consistently provides results within that of the AMOCO K-Joint tests results compared to other LJF formulations for axial, IPB and OPB. This can be deemed as an improved range due to limitations of the large scale test results (discussed in Chapter 5). This benchmarking exercise to large scale LJF tests has not been attempted previously so the RK-FEA model provides an original basis to develop the suite of LJF equations for K-type joints. The researcher was also directed and designed the replication of the AMOCO K-Joint tests by Da Silva at LSBU, on a smaller scale which proved useful in examining the modes of failure which were similar to those recorded by the AMOCO K-Joint tests.

Thirdly, the development of the RK-LJF equations considered over seventy-two geometric ranges for uni-planar tubular K-type joints. This provided a wide range of data for input into the *Mathematica* software to develop the parametric equations. The RK-LJF equations were developed with the data set from the finite element results. Previous LJF parametric equations fit accuracy have never been reported, so this is an encouraging outcome from the research as it justifies the use of an abundance of data points which is a significant improvement over other researchers. The RK-LJF equations were compared to other LJF equations and they showed considerable improvement on existing equations in terms of joint flexibility. This is not unexpected as the unique data set, analytical methods and RK-FEA (benchmarked to large scale testing) gave an improved result to other researchers.

The research also included a gap-sensitivity study to determine the applicability range of the RK-LJF equations as the gap size increases. The research indicates that the LJF is not sensitive to the gap size

for uni-planar K-type joints. This is another improvement to existing LJF researchers as neither of them has appropriately examined the effect of the gap size on their LJF equations.

MSL (2002) have benchmarked their LJF equations to the BOMEL frame tests. RK-LJF has been validated against the BOMEL Frame Test VII in the form of a pushover load displacement test and compared to MSL-ISO and original BOMEL test data. Results indicate that RK-LJF is very similar to the prototype test data and represents an improvement on the MSL-ISO test results for uni-planar K-type joints. This is also a fundamental improvement on the currently accepted practice where the MSL-ISO equations had previously represented the best fit to the prototype test results.

For the offshore industry, the use of the RK-LJF equations for the asset life extension will provide an improvement in the prediction of fatigue lives and ultimate capacity for fixed offshore jacket type structures, based on the close agreement with the prototype test results. It is also important to understand that an improvement at the tubular joint level may not be as significant as when the RK-LJF equations are employed over an entire frame structure to fully realize the redistribution of moments from one member, with the frame structure acting as a system rather than a set of isolated components. To successfully achieve this, the RK-LJF equations need to be incorporated into the SACS and USFOS suite of software to ensure that it is made accessible to practicing engineers for their use in structural assessments.

## **9.2 Recommendations for Further Work**

The research outlined in this thesis focuses on uni-planar K-type tubular joints. In reality, joints in offshore structures rarely are uni-planar in nature and they are often classified as multi-planar with many braces intersecting at a common chord. The methodology outlined in this thesis can be expanded to include the effects of multi-planar joints which can contribute further to the applicability to offshore structures.

As the gap size increases, the K-type joint begin to exhibit properties of a Y-joint configuration. Since the research has demonstrated that the gap size is not sensitive to LJF values, there is an opportunity to investigate if the RK-LJF equations are also applicable to Y and T type joint classifications as well.

A major finding from the research is the unavailability of large scale testing of tubular joints. Most modern research is centered around grouted tubular joints and the effects on ultimate strength but there is a considerable gap in the existing knowledge around LJF, especially the effects of the IPB condition. Another area of testing includes tubular joints where  $\beta$  approaches 1.0 where insufficient data on these joints are available in the industry.

The research in this thesis is confined to the elastic range as the LJF measured values by AMOCO and the benchmarking study has been limited to the elastic limit. Further improvement is required to consider the effects of the RK-LJF over the non-linear range of stress. Furthermore, apart from Hoshyari and Kohoutek (1993), there has been little research addressing the effects of LJF for dynamically sensitive structures or structures in seismic regions. This provides an opportunity to extend this research to include the effects of seismicity and dynamically sensitive structures.

With growing global demands for the provision of energy in recent times, the energy market has looked to alternative measures in addressing this demand. One such alternative to hydrocarbon based energy has been the use of wind energy generated by offshore wind turbine structures. In principle, offshore wind turbine structures behave primarily as fixed offshore structures, with similar engineering failure mechanisms of ultimate limit and fatigue limit states as fixed offshore structures. The application of local joint flexibility and the methodology outlined in this research is relevant to offshore wind turbines as well and should also be used to demonstrate the fitness for continued operations for these structures.

As a result of the current research outlined in this thesis, there is now a validated framework indicating that operating lifelines for OGPs can be safely extended, which can result in considerable economic benefits for the operator over the lifecycle of the offshore facility.

## REFERENCES

1. Abel, A. (1982). *Joints in Tubular Steel Structures*. Symposium, Research in Marine Structures, University of Sydney, April.
2. ABAQUS Theory Manual. *ABAQUS Suite of Documents*, 2011.
3. Alanjari P et al (2011). *Non-Linear Joint Element for the modeling of jacket-type offshore structures*. *App. Ocean Res.*, 33(2), 147-157.
4. American Welding Institute. *Structural Welding Code*. AWS D1.1-82, 1982
5. Analytical and Experimental Investigation of the Behaviour of Tubular Frames. Phase IIA. *Specification for the Testing an Isolated K Joint Specimen*. C6080505.02 Rev C. May 1994. BOMEL Engineering Limited.
6. API Recommended Practice for the *Planning, Designing and Constructing Fixed Offshore Platforms*. (1982) API RP 2A. American Petroleum Institute. 13th Edition.
7. API Recommended Practice for the *Planning, Designing and Constructing Fixed Offshore Platforms*. (2000) API RP 2A. American Petroleum Institute. 21st Edition.
8. API RP2 SIM *Recommended Practice for the Structural Integrity Management of Fixed Offshore Structures*. (2014). 1<sup>st</sup> Edition. American Petroleum Institute.
9. *A Review of the Ultimate Strength of Tubular Framed Structures*. Prepared by BOMEL for the HSE. Report No: OTO 92 365
10. Asgarian B et al (2014). *Local Joint Flexibility Equations for Y-T and K-type Tubular Joints*. *Ocean Systems Engineering*. Vol 4, No 2 (2014). 151-167
11. Atkins Research & Development (1977). *Dynamics of Marine Structures*. CIRIA UEG Report UR8
12. *Assessment Criteria, Reliability and Reserve Strength of Tubular Joints* (2000) MSL Engineering JIP C20400R014.
13. Aven, T. (2003). *Foundation of Risk Analysis, a knowledge and decision-oriented perspective*. John Wiley & Sons Limited. West Sussex. England.
14. Bathe, K.J (1982). *Finite Element Procedures in Engineering Procedures*. Prentice-Hall Inc.
15. Bea, R. and Craig, M.J.K (1993). *Developments in the Assessment and Requalification of Offshore Platforms*. Offshore Technological Conference. Houston. TX.
16. Billington, C.J., Lalani, M. and Tebbett, I.E. (1982). *Background to new formulae for the ultimate limit state of tubular joints*. Paper OTC 4189, Offshore Technological Conference, Texas.

17. Bijjard, P.P (1955). *Stresses from Radial in Cylindrical Pressure Vessels*. Welding Journal. Pp. 608s-617s.
18. Bolt, H.M, Billington, C.J and Ward, J.K (1994). *Non Linear Collapse of Offshore Jacket Structures*. Proceedings of the Structural Congress, ASCE, Atlanta, Georgia.
19. Bolt, H.M. (1995). *Results from Large Scale Ultimate Strength Tests of K-Braced Jacket Frame Structures*, OTC Paper 7783. Offshore Technological Conference, Houston, May 95.
20. Bolt, H.M., Seyed-Kebari, H., and Ward, J.K., (1992). *The Influence of Chord Length and Boundary Conditions on K-Joint Capacity*. Proceedings, 2nd International Offshore and Polar Engineering Conference, San Francisco.
21. Boone, T.J et al (1982). *Chord Stress Effects on the UTS of Tubular Joints*, Texas University Report PMFSEL No. 82-1. Dec 82
22. Bouwkamp, J.G. et al. (1980) *Effects of joint flexibility on the response of offshore towers*. OTC Paper 3901. Proceedings of the 12th Offshore Technological Conference, Houston, May 1980.
23. Buchholdt, H.A. (1997). *Structural Dynamics for Engineers*. 1st Edition. Thomas Telford.
24. Buitrago, J., Healy, B. E. and Chang, T.Y. (1993) *Local joint flexibility of tubular joints*, Offshore Mechanics and Arctic Engineering Conference, OMAE, Glasgow.
25. Cook, R.D (1995). *Finite Element Modeling for Stress Analysis*. John Wiley & Sons Inc.
26. Chakrabathi, P; et al (2005). *Effect of Joint Behaviour on the Reassessment of fixed offshore platforms in the bay of Campeche, Mexico*. Offshore 24<sup>th</sup> Proceedings to the Conference of Offshore Mechanics and Arctic Engineering, OMAE. Halkdiki. Greece
27. Chen, B., Hu, Y., and Tan, M., (1990) *Local Joint Flexibility of Tubular Joints of Offshore Structures*, Marine Structures, Vol. 3, pp. 177-197.
28. Da Silva, E.C. (2015). *Fatigue Life of Fixed Offshore Structures according to SCF and LJF Parameters*. MSc Thesis. London South Bank University.
29. DeFranco SJ et al (2004). *Eugene Island 322. A drilling platform decommissioning after Hurricane Lilli*. Proceedings to OTC. 04. May 3-6 2004. Houston TX. OTC 16801.
30. Dier, A.F., Hellan, O. (2002). *A non-linear tubular joint response for pushover analysis*. Proceedings of OMAE 2002-28634. 21st International Conference on Offshore Mechanics and Arctic Engineering.
31. Dier, A.F.,and Lalani, M. (1998). *New Code Formulations for Tubular Static Joint Strength*. Proceedings of the Eight International Symposiums on Tubular Structures. Published by Balkema.
32. DNV Technical Report. *Comparison of API, ISO and NORSOK Offshore Structural Standards*. For the Bureau of Ocean Energy Management, Regulation and Enforcement. TA&r No 677. Report No EP034373-2011-01 Rev 1. (2012).

33. DNV *Rules for the Design, Construction and Inspection of Offshore Structures* (1977). Det Norske Veritas.
34. DNV Recommended Practice DNV-RP- C203 (2011). *Fatigue Design of Offshore Steel Structures*. Det Norske Veritas
35. DNV Recommended Practice DNV-OS-J101 (2010). *Design of Offshore Wind Turbine Structures*. Det Norske Veritas.
36. Earl, C.P. and Teer, M.J. (1989) *A rational and economic approach to the calculation of K-factors*. Offshore Technological Conference, OTC 6162, Houston, Texas.
37. *Effects of local joint flexibility on the reliability of fatigue life estimates and inspection planning* Health and Safety Executive. Offshore Technological Report 2001/056, 2001
38. Ersdal, G. (2005). *Assessment of Existing Offshore Structures for Life Extension*. University of Stavanger. Doctoral Thesis.
39. Efthymiou, M. (1985) *Local rotational stiffness of unstiffened tubular joints*, Shell Report (KSEPL) RKER.85.199.
40. Efthymiou, M. et al (1985). *Stress concentrations in T/Y and gap/overlap K Joints*. BOSS 1985. Amsterdam.
41. Efthymiou, M. (1988). *Development of SCF formulae and generalized influence functions for use in fatigue analysis*. Offshore Tubular Joints Conference. OTJ'86, Egham, Surrey, UK.
42. Fatigue Guidance Review Panel. MaTSU. *Fatigue Guidance Background Document, An Offshore Technology Report*. HSE Books as an OTR, 1996.
43. Fessler, H. and Spooner, H. (1981). *Experimental determination of stiffness of tubular joints. Integrity of Offshore Structures*. Glasgow, UK. July 1981
44. Fessler H, Mockford P.B. and Webster J.J. (1986) *Parametric Equations for the flexibility matrices of multi-braced tubular joints in offshore structures*. Proceedings to the Institution of Civil Engineers. Part 2. 1986. 81. Dec. 675- 696. Paper 9124.
45. Fessler H, Mockford P.B. and Webster J.J. (1986) *Parametric Equations for the flexibility matrices of single-braced tubular joints in offshore structures*. Proceedings to the Institution of Civil Engineers. Part 2. 1986. 81. Dec. 679- 673. Paper 9089.
46. Gho, W (2009). *Local Joint Flexibility of tubular circular hollow section joints with complete overlap of braces*. Tubular Structures (pp 607-614). London CRC Press/Balkema
47. Gibstein, M., Baerheim, M. and Olsen, P. (1990) *Refined fatigue analysis approach and its application to the Veslefrikk jacket*. International Symposium of Tubular Structures, ISTS-3, Finland.
48. Graff, W.J (1981). *Introduction to Offshore Structures*. Gulf Publishing Company.

49. Grete, O. (1970). *Finite Element Analysis of tubular K-Joints*. PhD Thesis. University of Berkley California.
50. Holmans, T et al (1985). *Approximate Flexibility and Stress Analysis of Tubular Joints in Marine Structures*. Report STF71 F85045.SINTEF Concrete and Structures. Trondheim Norway.
51. Holmas, T (1987). *Implementation of Tubular Joint Flexibility in Global Frame Analysis*. Division of Structural Mechanics Report 87-1. The Norweigan Institute of Technology. Trondheim.
52. Hoshyari, I and Kohoutek, R (1991). *Flexibility of Tubular Joints in Offshore Structures*. The First International Offshore and Polar Engineering Conference, Edinburg. August 11-15. Pp 61-66
53. Hoshyari, I and Kohoutek, R (1993). *Rotational and axial flexibility of tubular T-joints*. Offshore and Polar Engineering Conference ISOPE, Singapore.
54. Hu, Y, Zhu J and Chen, B. (1993). Structural Analysis of offshore platforms considering local joint flexibility. Offshore Mechanics and Arctic Engineering Conference, OMAE, Glasgow, UK.
55. HSE (2002). OTO 2002-013. *Key Performance Indicators for Structural Integrity of Fixed Offshore Structures*. Health & Safety Executive, April 2002. HSE Books.
56. ISO 19902: 2007 *Fixed Steel Offshore Structures* British Standards International. 2007. 1st Edition.
57. ISO 19901-09 *Structural Integrity Management of Fixed Offshore Structures*. (DIS) Draft Industry Standard.
58. Kallaby J., O'Connor P.E. (1994) *An Integrated for Underwater Survey and Damage Assessment of Offshore Platforms*. Offshore Technological Conference, Paper 7487.
59. Kellogg, MW (1956). *Design of Piping Systems*. Second Edition. Wiley.
60. Khan R., Kraincanic I., Smith K., Gunn MJ. (2016). *The Role of Local Joint Flexibility (LJF) in the Structural Assessments of Aging Offshore Structures*. Proceedings to the 12th ISOPE Pacific/Asia Offshore Mechanics Symposium. Brisbane, Australia. 4-7 Oct.
61. Khan R., Kraincanic I., Smith K., Gunn MJ. (2016). *Improved Joint Flexibility Equations for uni-planar gapped K-type tubular joints of fixed offshore structures*. Journal of the Marine Engineering & Technology (JMET). (Under review).
62. Kreigier W.F, Banon H., Lloyd J.R. (1994), *Process for Assessment of Existing Platforms to determine their Fitness for Purpose*. Proceeding of the Offshore Technological Conference (OTC) 7482.
63. Lalani M., Bucknell J., O'Connor P.E. (2001) Chapter 14: Offshore and Subsea Facilities. Society of Petroleum Engineers (SPE) (2001), Offshore Handbook.

64. Lalani M. et al (1993). *New Large Scale Frame Data on the Reserve and Residual Strength of Offshore Structures*, 2nd International Conference on Offshore Structural Design against Extreme Loads, London, ERA Report 93-0843, November 93.
65. Lalani M et al (1986). *Improved Fatigue Life Estimation of Tubular Joints*. Offshore Technological Conference (OTC 5306), Houston Texas.
66. *Leman 49/27AD. K-Joint Tests* (1983). Final Report. Amoco (UK) Exploration Co. Report No ST 102/83A. May 1983.
67. Ma, S.Y. and Tebbett, I. E., 1988, *New Data on the Ultimate Strength of Welded Tubular K Joints Under Moment Loads*. OTC 5831, 20<sup>th</sup> Annual Offshore Technology Conference, Houston.
68. Marshall, P.W. et al (1984). *Basis for Tubular Joint Design Codes*. ASCE National Structural Engineering Meeting. San Francisco California. USA.
69. Marshall, P.W. (1974). *General consideration for tubular joint design*. Proceedings of Welding Institute on Welding in Offshore Construction, Newcastle, UK.
70. Makino, Y. et al. *Database of Test and Numerical Analysis Results for Unstiffened Tubular Joints*, IIW Doc XV-E-96-220, Kumamoto University, Kumamoto, Japan.
71. Makino, Y. et al. (1986). *Behaviour of T and K Joints under Combined Loads*. OTC 5133. Houston TX.
72. Mitaheri, M. et al. *Effect of joint flexibility on overall behaviour of jacket type offshore platforms*. American Journal of Engineering and Applied Sciences. 2(1): 25-30. 2009.
73. MSL Engineering Ltd. *JIP Phase II Final Report on Tubular Joint Non-Linear Modeling Algorithms for Frame Analysis*, Document No C20400R014. Nov 2000.
74. Nakajima, T et al. (1971). *Experimental study on the strength of thin wall welded tubular joints*. International Institute of Welding. Document No. XV-31-71.
75. Nichols, N.W. et al (2006). *Managing Structural Integrity for Aging Platform*. SPE-101000-PP.
76. Nichols, N.W and Khan, R (2015). *Structural Integrity Management System (SIMS) Implementation within PETRONAS' Operations*. Journal of Marine Engineering & Technology. Volume 14. Issue 2.
77. NORSOK Standard. N-004. *Design of Steel Structures*. Revision 2, October 2004.
78. NORSOK Standard. N-006. *Assessment of Structural Integrity of existing load-bearing structures*. Edition 1, March 2009.
79. O'Connor P., Bucknell J., Westlake H.S., Puskar F. (2005). *Structural Integrity Management (SIM) of Offshore Facilities*. Offshore Technological Conference, Paper 17545.

80. Pecknold, D.A, Park, J.B., Koppenhoeffter, K.C. (2001). *Ultimate Strength of Gap K Tubular Joints with Chord Preloads*. OMAE 2001/OFT- 1214
81. Puskar F, DeFranco S, O'Connor P., Bucknell J, Digre K (2010) *API RP 2SIM: Recommended Practice for Structural Integrity Management*. Proceeding of the Offshore Technological Conference (OTC) 20675.
82. Qian X et al (2013). *A Load-Deformation Formulation for CHS X and K-Joints in Pushover Analysis*. Journal of Constructional Steel Research 90 (2013). 108-119.
83. Rockley, K.C, Evans, H.R et al (1974). *A Basic Introduction to the Finite Element Method*. University College Cardiff. Department of Civil & Structural Engineering.
84. Romeyn, A., Puthli, R.S., and Wardenier, J., *Finite Element Modeling of Multi-planar Joint Flexibility in Tubular Structures*, Proceedings of the Second International Offshore and Polar Engineering Conference, Vol. IV, International Society of Offshore and Polar Engineers, pp. 420-429, 1992.
85. Romeyn, A., Puthli, R.S., and Wardenier, J. *The flexibility of uni-planar and multi-planar joints made up of circular hollow sections*. Offshore and Polar Engineering Conference (ISOPE), Edinburgh, UK, 1991.
86. Samadani, S. et al (2009). *Non-Linear analysis of offshore platforms subjected to earthquake loading considering the effects of local joint flexibility*. Proceedings of the ASME 2009, 28<sup>th</sup> International Conference Ocean, Offshore and Arctic Engineering, OMAE. Honolulu, Hawaii, USA.
87. Skallerud, Bjorn and Amdahl, Jorgen (2002). *Non Linear Analysis of Offshore Structures*. Research Studies Press Limited. Baldock, Hertfordshire, England.
88. SICS Database and Manual (2014). Copyright © Petronas Carigali Sdn Bhd.
89. SINTEF Civil and Environmental Engineering, *USFOS Theory Manual*, SINTEF, 1997.
90. Soussi, R. (1989) *Flexibility of tubular joints*. International Symposium on Tubular Structures, Finland.
91. *Stress Concentration factors for tubular complex joints* (1986). Final Report No.4. Unstiffened multi-planar K and KT joints. Lloyds Register of Shipping.
92. Tebbett, I.E. (1982) *The reappraisal of steel jacket structures allowing for the composite action of grouted piles*. Offshore Technological Conference, OTC 4194, Houston, Texas USA.
93. Turner, J.W, Wisch, D.J., Guynes, S.J., (1994). *A Review of Operations and Mitigation Methods for Offshore Structures*. Proceedings of the Offshore Technological Conference, Paper 7486.
94. Ueda, Y., Rashed, S. M. H., and Nakacho, K.,(1990) *An Improved Joint Model and Equations for Flexibility of Tubular Joints*, Journal of Offshore Mechanics and Arctic Engineering, vol. 112, pp. 157-168, 1990.

95. Ueda, Y et al (1968). *Elastic-plastic analysis of framed structures using the matrix method*. Journal of the Society of Naval Architects of Japan. Vol 124.
96. ULTIGUIDE. *Best Practice Guidelines for use of Non-Linear Analysis Methods in Documentation of Ultimate Limit States for Jacket Type Offshore Structures*. DNV-SINTEF-BOMEL, 1999.
97. Underwater Engineering Group (1982) *Design Guidance in tubular joints in steel offshore structures*, Part D.
98. Underwater Engineering Group (1984) *Node flexibility on the behaviour of jacket structures – pilot study on two dimensional frames*, UEG Report UR/22.
99. Wardenier, J (1982). *Hollow Sections Joints*. Delft University Press.
100. Wilson, J.F (2003). *Dynamics of Offshore Structures*. 2nd Edition. John Wiley & Sons Inc.
101. Wimpey Offshore. *SESAM Database Spectral Fatigue Analysis*, July 1990.
102. Wisch, D.J, Puskar, F.J., Laurendine, T.E., O'Connor, P.E., Versowsky, P.E., Bucknell, J., (2004) *An Update on API RP 2A Section 17 for the Assessment of Existing Platforms*, Proceedings of the Offshore Technological Conference, Paper 16820.
103. Wordsworth, A.C. (1981). *Stress Concentration Factors at K and KT Tubular Joints*. Fatigue in Offshore Steels. Institution of Civil Engineers. London, February 1981.
104. Young, W.C., Budynas, R.C. (2002). *Roark's Formulas for Stress and Strain*. Seventh Edition. McGraw Hill.
105. Zettlemyer N. *Life Extension of Fixed Platforms*. Tubular Structure XIII. 2010 3-13.
106. Zweremam, F.J, Digre, K (2010). *22nd Edition of API RP 2A Recommended Practice for Planning, Designing and Constructing Fixed Offshore Platforms - Working Stress Design*, Proceedings of the Offshore Technological Conference, Paper 20837.

## **APPENDICES**

## APPENDIX 1 - Glossary of Terms

Terms	Description
<b>Appurtenances</b>	These include structures that are appended to the main structures and required for the safe functioning of the structure. These include conductor and riser guards, boat landings etc.
<b>Assessment Engineering</b>	<p>Assessment engineering involves detailed analysis using finite element software to</p> <ul style="list-style-type: none"> <li>- determine the continued fitness for purpose of the structure in its present condition.</li> <li>- identify and optimize the extent of any required strengthening, repair or other mitigation and the associated urgency.</li> <li>- optimize the SIM strategy and update future inspection planning or condition monitoring as appropriate.</li> </ul> <p>It generally involves an ultimate strength analysis for fixed offshore structures, but fatigue, in-place analysis and seismic assessments are often required.</p>
<b>Bracing Configuration</b>	In the jacket structure of a fixed offshore platform, the frame type structure is typical of various bracing configurations. The most common types are the K-type, Diagonal (D), X (X) and the X with perimeter horizontal (XH) type framing configurations.
<b>Conductor</b>	The conductor is a large diameter pipe that is set into the ground to provide the initial stable structural foundation for a <u>borehole</u> or <u>oil well</u> . It can also be referred to as a drive pipe because it is often driven into the ground with a <u>pile driver</u> . In the <u>offshore drilling</u> industry, the conductor pipe is set in the seabed, and is a key structural foundation for the subsea <u>wellhead</u> .
<b>Continuous Improvement</b>	The process whereby up-to-date methodologies, current data trending, code improvements and training are incorporated with the SIMS. Periodic audits are required to assess the quality of these updates and make further recommendations for improvements.
<b>Database</b>	Historical data is a cornerstone of informed structural integrity assurance and a suitable system for referencing and archiving documents relating to the SIMS process shall be established and maintained.
<b>Dynamic response method</b>	In offshore structures, the applied loads (environmental loads) generally have a dynamic nature. To study the behaviour of these structures, free vibration and forced vibration must be considered in order to understand the actual (as possible) behaviour and response of the structure.

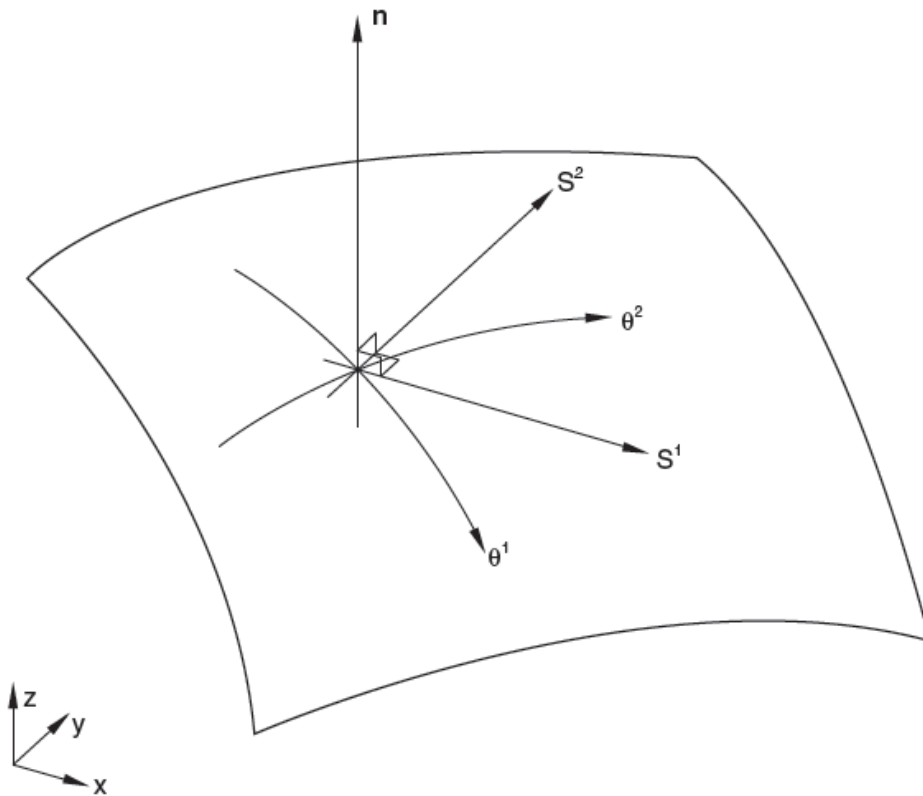
<b>Fatigue assessment</b>	The process by which the fatigue lives of tubular joints can be determined. Usually using a spectral fatigue approach and requires S-N curve selection, fatigue-life safety factors and techniques for improving/enhancing fatigue lives.
<b>Fitness for Purpose</b>	Each offshore facility is maintained safely for its designed purpose or an alternative purpose.
<b>Jacket</b>	The truss framework (substructures) below the highest water-level. It usually consists of tubular members with thickened sections at the tubular joints.
<b>Long Term Inspection Plan</b>	For offshore structures, both periodic inspections or the risk based underwater inspection program, can be mapped out for the lifecycle of the asset. If for example, a platform requires underwater inspections every five years and its last inspection was in 2010, the inspection plan should indicate that the next inspection is in 2015, then 2020, until decommissioning.
<b>Management of Change (MOC)</b>	Management of Change (MOC) is a system to evaluate, authorize and document changes before they are made and confirm proper closure after the changes have been made. Its purpose is to establish the measures necessary to confirm that HSE and operational risks arising from proposed temporary and permanent changes are managed to an appropriate level. It is also an important communication tool to inform people affected by the change about what is being considered or what is going to occur.
<b>Mitigation</b>	Mitigation is defined as modifications or operational procedures that reduce the consequence in the event of structural failure or reduce the likelihood of structural failure.
<b>Monitoring</b>	Structural Integrity Monitoring is considered to be the process whereby response characteristics of a fixed offshore jacket structure are measured (either continuously or at regular intervals) with a view to comparing the measured characteristics with a previously measured baseline or trend.
<b>Multi-planar tubular joints</b>	In the context of tubular joint framing for offshore structures, multi-planar joints are those with various bracing mechanism interacting with a common chord at the joint. The bracing are not within the same plane as the chord and be very complex in nature.
<b>Operations</b>	Refers to the maintenance and integrity management team that operates and ensures fitness for purpose throughout the operating life of an offshore facility.
<b>Projects</b>	Refers to the design team used for conceptual design, engineering, construction and commissioning of an offshore facility.

<b>Remaining Life Assessment (RLA)</b>	For offshore structures that have exceeded or approaching their design life span but are required to continue operating, are required to perform a RLA to determine its fitness for purpose. The RLA may take the form of more detailed fatigue analysis and ultimate strength assessments that may require assessment refinements such as LJF, to justify continued operations.
<b>RBUI</b>	Risk Based Underwater Inspection (RBUI) involves the inspection of substructures based on their susceptibility to damage and overloading including fatigue, strength, cathodic protection, corrosion etc. Structural Safety Critical Elements (SCEs) are usually identified in the assessments and more attention is paid to these during inspection campaigns.
<b>Risk Assessment</b>	Risk assessment is the analytical process that determines the types of adverse events or conditions that might impact the structural integrity, the likelihood that those events or conditions will lead to a loss of integrity, and the nature and severity of the consequences that might occur following a failure.
<b>Semi-Analytical Methods</b>	A combination of using numerical modeling, engineering judgment and rules of thumb that are generally associated with the offshore industry used in assessments.
<b>S-N Curve</b>	In high-cycle fatigue situations, materials performance is commonly characterized by an S-N curve, also known as a <u>Wöhler</u> curve. This is a graph of the magnitude of a cyclic stress (S) against the <u>logarithmic scale</u> of cycles to failure (N).
<b>Strengthening, Modifications &amp; Repair (SMR)</b>	The technique of restoring an offshore structure that has severe damage and is border-line with regards to fitness for purpose. SMR can involve grouting members, replacing full sections and repair to members and/or appurtenances.
<b>Stress concentration factors</b>	Stress concentration is where the stress is located. Stress Concentration Factors are those that have to be taken into consideration to better understand the stress distribution for various tubular joint configurations and geometries.
<b>Structural Integrity Management System (SIMS)</b>	A continuous integrity process applied throughout the design, operations, maintenance and decommissioning of a platform to ensure a platform is safely managed and is fit for its individual purposes.
<b>Structural Risk</b>	The cornerstone to successful implementation of SIM is the ability to effectively manage the structural risks associated with the platform operations is the adoption of a risk-based approach to managing the structural integrity for existing offshore structures. Within this context, structural risk is defined as the combination of the likelihood of some event

	<p>occurring during a time period of interest and the consequences, (generally negative) associated with the event. In mathematical terms, risk can be expressed as:</p> $\text{Risk} = \text{Likelihood} \times \text{Consequence}$
<b>Structural Safety Critical Elements (SCEs)</b>	<p>These are structural members within the platform that, if are severely damaged or damage goes unmitigated, can lead to a reduction in the performance of the structure and may lead to eventual collapse.</p>
<b>Substructures</b>	<p>The portion of the offshore structure that is below the highest expected water level. The most common substructure is the fixed steel structure. The substructure is connected to the seabed typically using long steel piles.</p>
<b>Ultimate strength analysis</b>	<p>Also called a “pushover analysis”, is a non-linear measure of the Reserve Strength Ratio (RSR) of the jacket structure. It is based on truss action and system strength rather than component strength. Ultimate Strength is performed using the USFOS suite of software.</p>

## APPENDIX 2 - Shear Flexible Small-Strain Shell Elements

The S4R5 Thin Shell Quadrilateral Finite Element, and the S8R5, S9R5, S8R and the 6-node triangle STR165 elements are considered as small strain shear flexible elements in ABAQUS/Standard. For these elements, the position of a point in the shell reference surface -  $\mathbf{x}$  - and the components of the vector  $\mathbf{n}$  - which is approximately normal to the reference surface - are interpolated independently. The kinematics of the shell theory then consist of measuring membrane strain on the reference surface from the derivatives of  $\mathbf{x}$  with respect to position on the surface and the bending strain from the derivatives of  $\mathbf{n}$ . The transverse strains are measured as the changes in the projections of  $\mathbf{n}$  onto tangents to the shell's reference surface.



Appendix 1 Figure 1 Shell Reference Surface (ABAQUS Manual, 2011)

$$\mathbf{N} = \frac{\partial \mathbf{X}}{\partial \theta^1} \times \frac{\partial \mathbf{X}}{\partial \theta^2} / \sqrt{\frac{\partial \mathbf{X}}{\partial \theta^1} \times \frac{\partial \mathbf{X}}{\partial \theta^2}}$$

$$\mathbf{T}_2 = \frac{\mathbf{N} \times \mathbf{i}}{\sqrt{\mathbf{N} \times \mathbf{i}}}$$

$$\mathbf{T}_2 = \frac{\mathbf{N} \times \mathbf{k}}{\sqrt{\mathbf{N} \times \mathbf{k}}},$$

$$\mathbf{T}_1 = \mathbf{T}_2 \times \mathbf{N}.$$

$$dS^\beta = \mathbf{T}_\beta \cdot \frac{\partial \mathbf{X}}{\partial \theta^\alpha} d\theta^\alpha$$

$$\frac{\partial}{\partial S^\alpha} = \frac{\partial \theta^\beta}{\partial S^\alpha} \frac{\partial}{\partial \theta^\beta}$$

$$\frac{\partial \theta^\alpha}{\partial S^\beta} = \begin{bmatrix} \mathbf{T}_1 \cdot \partial \mathbf{X} / \partial \theta^1 & \mathbf{T}_1 \cdot \partial \mathbf{X} / \partial \theta^2 \\ \mathbf{T}_2 \cdot \partial \mathbf{X} / \partial \theta^1 & \mathbf{T}_2 \cdot \partial \mathbf{X} / \partial \theta^2 \end{bmatrix}^{-1}.$$

## Displacements

The nodal variables for shell elements are the displacements of the shell reference surface,  $\mathbf{u} = \mathbf{x} - \mathbf{X}$ , and the normal direction,  $\mathbf{n}$ . Since  $\mathbf{n}$  is defined to be a unit vector, only independent values are needed to define  $\mathbf{n}$ , so that this type of shell element needs only five degrees of freedom per node. In ABAQUS, the issue is addressed in two ways. At nodes in a smooth shell surface in those elements that naturally have five degrees of freedom per node, ABAQUS stores the values of the projections of the change in  $\mathbf{n}$  projected onto two orthogonal directions in the shell surface at the start of the increment to define  $\mathbf{n}$ . Otherwise, ABAQUS stores the usual rotation triplet,  $\omega$ , at the node. The latter

method leaves a redundant degree of freedom if the node is on a smooth surface. A small stiffness is introduced locally at the node to constrain the extra degree of freedom to a measure of the same rotation of the shell's reference surface.

## Strains

The reference surface member strains are

$$\epsilon_{\alpha\beta} = \frac{1}{2}(g_{\alpha\beta} - G_{\alpha\beta}).$$

The curvature change is

$$\kappa_{\alpha\beta} = B_{\alpha\beta} - b_{\alpha\beta} + \frac{1}{2}(B_{\alpha}^{\gamma}\epsilon_{\gamma\beta} + B_{\beta}^{\gamma}\epsilon_{\gamma\alpha}).$$

The transverse shears are

$$\gamma_{3\alpha} = \mathbf{n} \cdot \mathbf{t}_{\alpha},$$

Where

$$\mathbf{t}_{\alpha} = \frac{\partial \mathbf{x}}{\partial S^{\alpha}} \bigg/ \sqrt{\frac{\partial \mathbf{x}}{\partial S^{\alpha}} \cdot \frac{\partial \mathbf{x}}{\partial S^{\alpha}}} \quad (\text{no sum on } \alpha)$$

Is a unit vector, tangent to the  $dS^{\alpha}$  line in the current surface.

In addition to these strains, when six degrees of freedom are used at the nodes of the elements, the extra rotation of freedom is constrained with a penalty as follows:

When such a node is the corner node of an element, define  $T_1, T_2, N_1, dS^1$  and  $dS^2$  in the element as above. These will be different in each element at the node, since the interpolated surface is not generally continuous. Then the strain to be penalized is defined as

$$\gamma_{SRC} = \frac{1}{2}(\mathbf{t}_1 \cdot \bar{\mathbf{t}}_2 - \mathbf{t}_2 \cdot \bar{\mathbf{t}}_1),$$

where

$$\bar{\mathbf{t}}_\alpha = \mathbf{C} \cdot \mathbf{T}_\alpha$$

is the rotated tangent direction, as defined by the rotation values at the node, and

$$\mathbf{t}_\alpha = \frac{\partial \mathbf{x}}{\partial S^\alpha} \Big/ \sqrt{\frac{\partial \mathbf{x}}{\partial S^\alpha} \cdot \frac{\partial \mathbf{x}}{\partial S^\alpha}} \quad (\text{no sum on } \alpha)$$

is the rotated tangent direction defined by the motion of the interpolated reference surface at the node.

At each mid-side node in the original configuration, define  $\mathbf{n}$  as the average surface normal for the elements of this surface branch at the nodes and  $\mathbf{T}$  as the tangent to the edge. Then define

$$\bar{\mathbf{t}} = \mathbf{C} \cdot \mathbf{T} \quad \text{and} \quad \mathbf{n} = \mathbf{C} \cdot \mathbf{N}$$

as the rotated values of  $\mathbf{T}$  and  $\mathbf{N}$ , as defined by the rotation values at the node. The vector

$$\mathbf{p} = \bar{\mathbf{t}} \times \mathbf{n}$$

is the normal to  $\mathbf{n}$  and to the edge.

The strain to be penalized at these mid-side nodes is then defined as

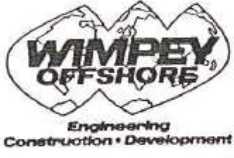
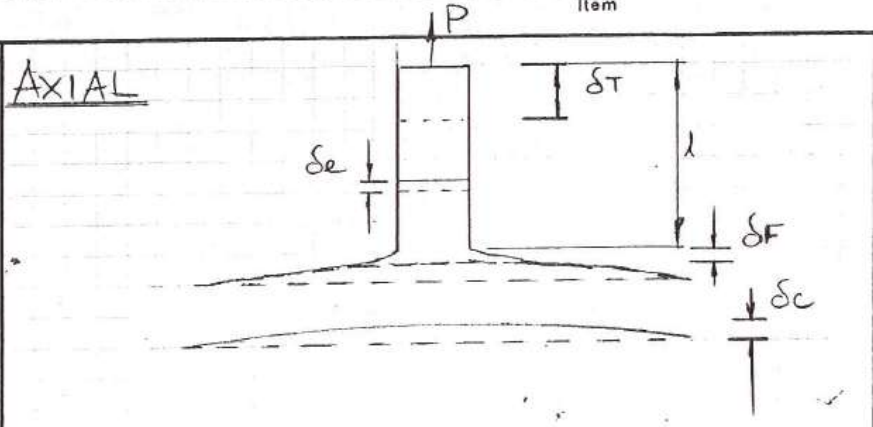
$$\gamma_{SRM} = \mathbf{t} \cdot \mathbf{p},$$

where

$$\mathbf{t} = \frac{\partial \mathbf{x}}{\partial S} \Big/ \sqrt{\frac{\partial \mathbf{x}}{\partial S} \cdot \frac{\partial \mathbf{x}}{\partial S}}$$

is the tangent to the edge of the element in the current position of the reference surface.

APPENDIX 3 - LJJ Calculations from the AMOCO K-Joint Test Results

 <p>Engineering Construction • Development</p>	<h2 style="margin: 0;">WIMPEY OFFSHORE LIMITED</h2> <h3 style="margin: 0;">CALCULATIONS</h3>	Date May 83 Made by SMR	Sheet 1a of 11 Checked by
Client AMOCO	Contract k joint tests		Account No.
LOCAL JOINT FLEXIBILITY			
Location	Item		
(A) <u>AXIAL</u>			
<p> <math>\delta_T</math> = overall displacement  <math>\delta_f</math> = displacement due to local joint flexibility  <math>\delta_c</math> = elastic displacement of chord (use component in direction of brace)  <math>\delta_e</math> = elastic displacement of brace.                 </p> <p style="text-align: center;"> <math>\delta_T = \delta_f + \delta_c + \delta_e</math>  <math>\therefore \delta_f = \delta_T - \delta_c - \delta_e</math> </p> <p>                     Brace = 406 <math>\phi</math> x 9.5 W.T.  <math>\Rightarrow</math> c/s area = 11833.6 mm<sup>2</sup> </p> <p style="text-align: center;"> <math>E = \frac{P/A}{\delta/l}</math> </p> <p style="text-align: center;"> <math>\therefore \frac{\delta_e}{P} = \frac{l}{AE}</math> </p> <p> <math>l = 1000 - 340 \quad \text{mm}</math> </p> <p style="text-align: center;"> <math>\therefore \frac{\delta_e}{P} = \frac{660}{11833.6 \times 0.21 \times 10^3} = \underline{\underline{0.0003 \text{ mm/kN}}}</math> </p>			



# WIMPEY OFFSHORE LIMITED

## CALCULATIONS

Date May 83 Sheet 2 of 11

Made by SMR Checked by

Client Amoco

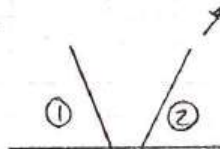
Contract k joint tests

Account No.

Location AMK 11

Item

LOAD CASE No. 1



GAGE	DISP/UNIT LOAD mm/kN
T2	+0.01125
T1	+0.01325
T4	+0.0128
T5	-0.0106
T6	-0.0115
T7	-0.0089
T8	+0.0114
T9	+0.0124
T10	
T3	
D6	+0.0165
D5	+0.0150

BRACE ②

$$\frac{\delta_C}{P} = \frac{(0.01125 + 0.0128) \sin 60}{2} \quad (T2, T4)$$

$$= 0.0104 \text{ mm/kN}$$

$$\frac{\delta_E}{P} = 0.0003 \text{ mm/kN}$$

$$\frac{\delta_I}{P} = \frac{(0.0124 + 0.0165)}{2} \quad (T9, D6)$$

$$= 0.0145 \text{ mm/kN}$$

$$\frac{\delta_F}{P} = 0.0145 - 0.0003 - 0.0104$$

$$= \underline{\underline{0.0038}} \text{ mm/kN}$$



# WIMPEY OFFSHORE LIMITED

## CALCULATIONS

Date May 83

Sheet 4 of 11

Made by SMR

Checked by

Client Amoco

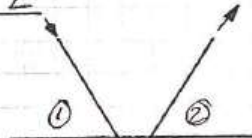
Contract K joint tests.

Account No.

Location AMK 12

Item

LOAD CASE NO. 2



GAUGE	DISP/UNIT LOAD.
T2	0.00214
T1	0.00245
T4	0.0010
T5	0.0017
T6	0.0008
T7	0.0011
T8	0.0023
T9	0.0024
T3	0.0015
T10	0.0033
D5	0.0007
D6	0.0044

mm/kN

BRACE ①

$$\frac{\delta_c}{P} = \frac{(0.00245 + 0.0015) \sin 60^\circ}{2} \quad (T1, T3)$$

$$= 0.0017 \text{ mm/kN}$$

$$\frac{\delta_e}{P} = 0.0003 \text{ mm/kN}$$

$$\frac{\delta_f}{P} = \frac{(0.0017 + 0.0008 + 0.0011 + 0.0007)}{4} \quad (T5, T6, T7, D5)$$

$$= 0.0011 \text{ mm/kN}$$

$$\frac{\delta_f}{P} = 0.0011 - 0.0017 - 0.0003$$

$$= \underline{\underline{-0.0009 \text{ mm/kN}}}$$



# WIMPEY OFFSHORE LIMITED

## CALCULATIONS

Date May 83 Sheet 5a of 11  
Made by SMR Checked by

Client Amoco

Contract K joint tests

Account No.

Location AMK12

Item

BRACE ②

$$\frac{\delta_c}{P} = \frac{(0.00214 + 0.0010)}{2} \sin 60 \quad (T2, T4)$$

$$= 0.0014 \text{ mm/kN}$$

$$\frac{\delta_T}{P} = \frac{0.0023 + 0.0024 + 0.0033 + 0.0044}{4} \quad (T8, T9, T10, D6)$$

$$= 0.0031 \text{ mm/kN}$$

$$\frac{\delta_R}{P} = 0.0003 \text{ mm/kN}$$

$$\frac{\delta_F}{P} = 0.0031 - 0.0014 - 0.0003$$

$$= \underline{\underline{0.0014 \text{ mm/kN}}}$$



# WIMPEY OFFSHORE LIMITED

## CALCULATIONS

Date May '83 Sheet No. of 11  
 Made by SMR Checked by

Client Amoco

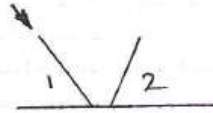
Contract k joint tests

Account No.

Location AMK 13

Item

### LOAD CASE No 3



GAUGE	DISP/UNIT LOAD mm/kN
T2	-0.0116
T1	-0.0119
T4	-0.0110
T5	+0.0105
T6	+0.0116
T7	+0.0126
T8	-0.0114
T9	-0.0109
T3	-0.0114
T10	-0.0105
D5	0.0174
D6	0.0163

BRACE ①

$$\frac{\delta_e}{P} = \frac{(0.0119 + 0.0114)}{2} \sin 60 \quad (T1, T3)$$

$$= 0.0101 \text{ mm/kN}$$

$$\frac{\delta_e}{P} = 0.0003 \text{ mm/kN}$$

$$\frac{\delta_T}{P} = \frac{0.0105 + 0.0116 + 0.0126 + 0.0174}{4}$$

$$= 0.0130 \text{ mm/kN} \quad (T5, T6, T7, D5)$$

$$\frac{\delta_F}{P} = 0.0130 - 0.0003 - 0.0101$$

$$= \underline{\underline{0.0026}} \text{ mm/kN}$$



# WIMPEY OFFSHORE LIMITED

## CALCULATIONS

Date May 83

Sheet 7 of 11

Made by SMR

Checked by

Client Amoco

Contract K joint tests

Account No.

Location AMK 13

Item

EFFECT IN ② OF COMP IN ①

$$\frac{\delta_c}{P} = \frac{(0.011 + 0.0116)}{2} \sin 60$$

$$= 0.0098 \text{ mm/kN (gauges T2 \& T4)}$$

$$\delta_T = \frac{0.0114 + 0.0109 + 0.0105 + 0.0163}{4}$$

$$= 0.0123 \text{ mm/kN (gauges T8, T9, T10, D6)}$$

$$\delta_f = 0.0123 - 0.0098$$

$$= \underline{\underline{0.0025 \text{ mm/kN}}}$$



# WIMPEY OFFSHORE LIMITED

## CALCULATIONS

Date May 83 Sheet 13 of 11  
 Made by SMR Checked by

Client Amoco

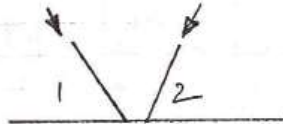
Contract K joint tests.

Account No.

Location AMK 14

Item

### LOAD CASE No. 4



GUAGE	DISP/UNIT LOAD
T2	0.0225
T1	0.0210
T4	0.0210
T5	0.0171
T6	0.0209
T7	-
T8	0.0230
T9	0.0220
T3	0.0218
D5	0.0300
D6	0.0330

### BRACE ②

$$\frac{\delta_c}{P} = \frac{(0.0225 + 0.0210)}{2} \sin 60 \quad (T2, T4)$$

$$= 0.0188 \text{ mm/kN}$$

$$\frac{\delta_e}{P} = 0.0003 \text{ mm/kN}$$

$$\frac{\delta_T}{P} = \frac{(0.0220 + 0.0330)}{2} \quad (D6, T9)$$

$$= 0.0275 \text{ mm/kN}$$

$$\frac{\delta_F}{P} = 0.0275 - 0.0003 - 0.0188$$

$$= 0.0084 \text{ mm/kN}$$



# WIMPEY OFFSHORE LIMITED

## CALCULATIONS

Date May 83

Sheet 5 of 11

Made by SMR

Checked by

Client Amoco

Contract k joint tests

Account No.

Location AMK 14

Item

BRACE (1)

$$\frac{\delta_c}{P} = \frac{(0.0210 + 0.0218)}{2} \sin 60$$

$$= 0.0185 \text{ mm/kN} \quad (\text{gauges T1 \& T3})$$

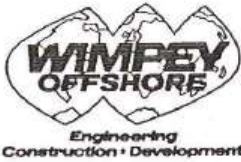
$$\frac{\delta_e}{P} = 0.0003 \text{ mm/kN}$$

$$\frac{\delta_T}{P} = \frac{(0.0209 + 0.0300)}{2} \quad (\text{T6, D5})$$

$$= 0.0255 \text{ mm/kN}$$

$$\frac{\delta E}{P} = 0.0255 - 0.0003 - 0.0185$$

$$= \underline{0.0067 \text{ mm/kN}}$$



# WIMPEY OFFSHORE LIMITED

## CALCULATIONS

Date May 83 Sheet 10a of 11  
 Made by SMR Checked by

Client Amoco

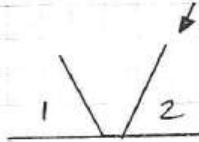
Contract k joint tests

Account No.

Location AMK 15

Item

LOAD CASE NO. 5



GAUGE	DISP/UNIT LOAD mm/kN
T2	0.0101
T1	0.0107
T4	0.0113
T5	0.0081
T6	0.0091
T7	
T8	0.0116
T9	0.0120
T3	0.0104
D5	0.0124
D6	0.0149

Brace (2)

$$\frac{\delta_c}{P} = \frac{(0.0101 + 0.0113)}{2} \sin 60 \quad (T2, T4)$$

$$= 0.0093$$

$$\frac{\delta_T}{P} = \frac{(0.0120 + 0.0149)}{2} \quad (T9, D6)$$

$$= 0.0135 \text{ mm/kN}$$

$$\frac{\delta_e}{P} = 0.0003 \text{ mm/kN}$$

$$\frac{\delta_F}{P} = 0.035 - 0.0093 - 0.0003$$

$$= 0.0254 \text{ mm/kN}$$



# WIMPEY OFFSHORE LIMITED

## CALCULATIONS

Date May 83 Sheet 11a of 11  
Made by SMR Checked by

Client Amoco

Contract K joint tests

Account No.

Location AMK 15

Item

BRACE ①

$$\frac{\delta_T}{P} = \frac{(0.0091 + 0.0124)}{2} \quad (T6, D5)$$

$$= 0.0107 \text{ mm/kN}$$

$$\frac{\delta_C}{P} = \frac{(0.0107 + 0.0104)}{2} \sin 60 \quad (T1, T3)$$

$$= 0.0091 \text{ mm/kN}$$

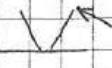
$$\delta_f = 0.0107 - 0.0091$$

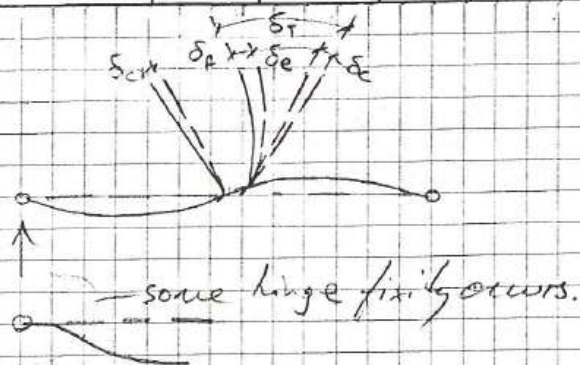
$$= \underline{\underline{0.0016 \text{ mm/kN}}}$$

CALCULATION SHEET	JOB AMCO K JOINT TESTS.	Lab. Ref. No.	Calculated by D. Garrett.
	SPECIMEN N°1	Sheet No. D1b	
	LOCAL JOINT FLEXIBILITIES	Date 16.5.83	

**(B) IN-PLANE BENDING**

Notation:

eg. Load. 



$$\delta_F = \delta_T + \delta_e + \delta_c$$

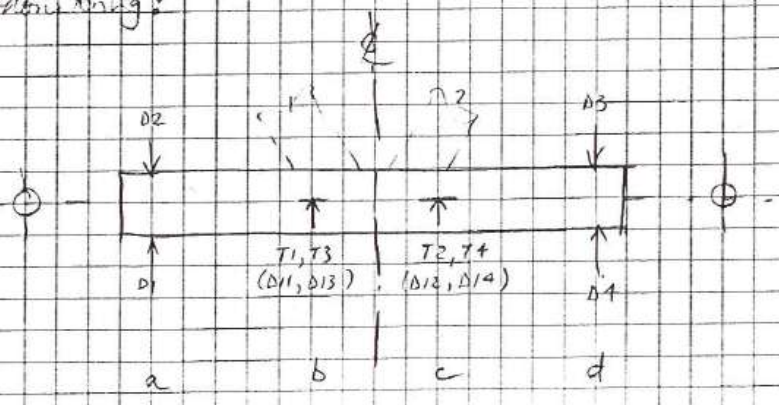
$$\phi_F = \tan^{-1} \frac{\delta_F}{L} = \frac{\delta_F}{L} \text{ for these small angles.}$$

Where,

- $\delta_F$  = displacement at brace end due to local joint flexibility
- $\delta_c$  = — " — due to chord bending
- $\delta_e$  = — " — due to elastic bending of brace.

The Local Joint Flexibility =  $\frac{\phi_F}{M}$  Rads/kNm.

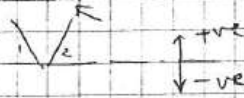
Chord Bending:



WIMPEY LABORATORIES LIMITED

CALCULATION SHEET	JOB <u>ALCO K JOINT TESTS</u>	Lab. Ref. No.	Calculated by <u>D. Garnett</u>
	<u>SPECIMEN N°1</u>	Sheet No. <u>D2B</u>	
	<u>LOCAL JOINT FLEXIBILITIES</u>	Date <u>16.5.93</u>	Checked by

LOAD CASE N°7



① CHORD DEFLECTIONS

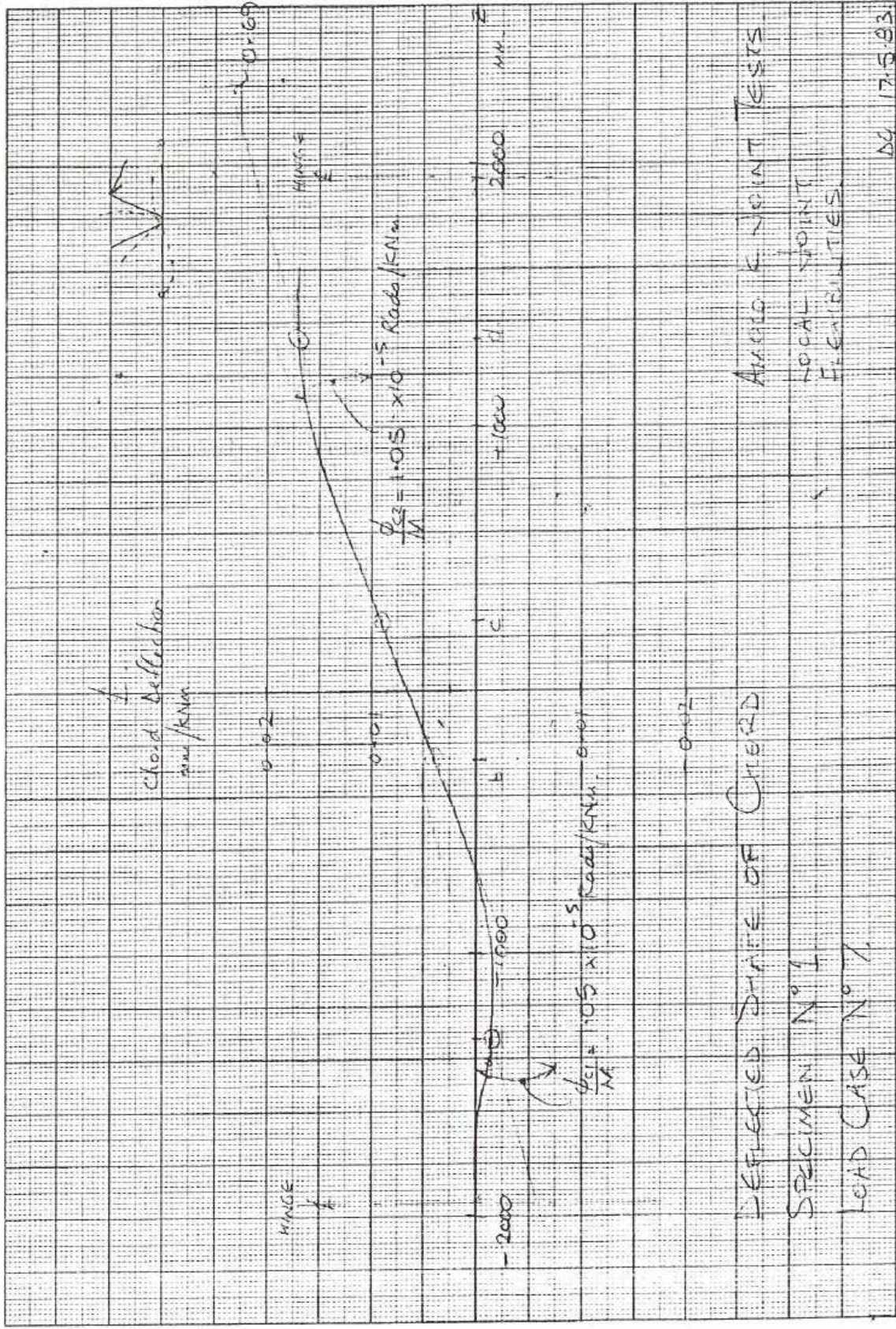
BRACE MOMENT (kNm)	DEFLECTIONS (mm)*					
	D1	D2	AVE. D1, D2	D3	D4	AVE. D3, D4
0	0	0	0	0	0	0
4.64	+0.01	0.00	+0.01	+0.01	+0.01	+0.01
8.45	+0.01	+0.01	+0.01	+0.03	+0.02	+0.03
12.77	+0.02	0.00	+0.01	+0.06	+0.04	+0.05
16.17	+0.02	+0.01	+0.02	+0.09	+0.06	+0.08
19.67	+0.02	0.00	+0.01	+0.12	+0.09	+0.11
23.07	+0.01	0.00	+0.01	+0.15	+0.12	+0.14
26.57	0.00	0.00	0.00	+0.20	+0.16	+0.18
30.08	0.00	-0.01	-0.01	+0.26	+0.22	+0.24
33.48	-0.02	-0.01	-0.02	+0.29	+0.34	+0.32
36.98	-0.04	-0.01	-0.03	+0.48	+0.54	+0.51
38.73	-0.05	-0.02	-0.04	+0.62	+0.68	+0.65
40.89	-0.05	-0.02	-0.04	+0.80	+0.86	+0.83

BRACE MOMENT (kNm)	DEFLECTIONS (mm)					
	T1 ch. 182	T3 ch. 189	AVE. T1, T3	T2 ch. 181	T4 ch. 183	AVE. T2, T4
0	0	0	0	0	0	0
4.64	+0.01	+0.01	+0.01	-0.01	+0.02	+0.01
8.45	+0.01	0.00	+0.01	+0.01	+0.02	+0.01
12.77	0.00	+0.01	+0.01	+0.01	+0.04	+0.03
16.17	+0.01	+0.02	+0.02	+0.04	+0.07	+0.06
19.67	+0.02	+0.05	+0.04	+0.07	+0.13	+0.10
23.07	+0.04	+0.06	+0.05	+0.07	+0.12	+0.10
26.57	+0.03	+0.06	+0.05	+0.09	+0.14	+0.12
30.08	+0.02	+0.09	+0.06	+0.11	+0.19	+0.15
33.48	+0.03	+0.11	+0.07	+0.13	+0.22	+0.18
36.98	+0.06	+0.17	+0.12	+0.25	+0.32	+0.29
38.73	+0.08	+0.21	+0.15	+0.30	+0.39	+0.35
40.89	+0.14	+0.25	+0.20	+0.36	+0.47	+0.44

Regressed Slopes: Intercepts on y axis in mm in brackets

$D1, D2 = -0.00124$  mm/kNm;  $D3, D4 = +0.01735$  mm/kNm  
 (0.022) (0.147)

$T1, T3 = +0.00401$  mm/kNm;  $T2, T4 = +0.00944$  mm/kNm  
 (0.029) (-0.0701)



DEFLECTED SHAPE OF CHORD  
 SPECIMEN N° 1  
 LOAD CASE N° 1.

ANGULO E JUNTAS TESTS  
 LOCAL JOINT  
 FLEXIBILITIES

Dg 17.5.83

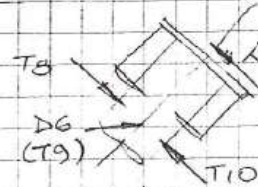
WIMPEY LABORATORIES LIMITED

CALCULATION SHEET	JOB AMOCO K JOINT TESTS.	Lab. Ref. No.	D36	Calculated by	D. Gamett.
	SPECIMEN N° 1	Sheet No.		Checked by	
	LOCAL JOINT FLEXIBILITIES.	Date	16.5.83		

② BRACE DEFLECTIONS.

→ve in direction of load.

i) Brace N° 2.



BRACE MOMENT (KNM)	DEFLECTIONS (MM.)			(mm)	
	T8 ch 187	T10 ch 190	AVE.	D6*	T9*
0	0			0	0
4.64	0.08			-0.01	0.00
8.45	0.15			-0.01	0.01
12.77	0.26			-0.02	0.02
16.17	0.33			-0.01	0.03
19.67	0.42			-0.01	0.05
23.07	0.50			-0.02	0.05
26.57	0.59			-0.02	0.06
30.08	0.72		As T8	+0.01	0.05
33.48	0.86			0.09	0.05
36.98	1.09			0.12	0.06
38.73	1.23			0.12	0.06
40.89	1.40			0.14	0.09

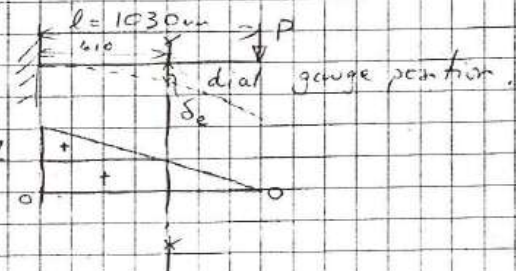
No output obtained

\* Not used in calculation of L.J.F. but indicate extent of out-of-plane bending.

Slope of regressed line through T8 v Brace Moment =

$$\frac{\delta_{T2}}{M} = 0.03238 \text{ mm/kNm. (Intercept} = -0.139 \text{ mm)}$$

Elastic Bending of brace:



Using Area Moment principle N° 2:

$$M = PL$$

$$\delta_e = \frac{1}{M EI} \left[ \frac{610^3}{3} + \left(1 - \frac{610}{1030}\right) \frac{610^2}{2} \right]$$

$$= \frac{149322 \text{ m}^3}{EI}$$

Assuming  $E = 210 \times 10^6 \text{ kN/m}^2$

$$I = \frac{\pi (D_1^4 - D_2^4)}{64} = \frac{\pi (406^4 - (406-19)^4)}{64} \text{ mm}^4 = 2.327 \times 10^8 \text{ mm}^4$$

$$\therefore \frac{\delta_e}{M} = \frac{149322 \times 10^{-6}}{210 \times 10^6 \times 2.327 \times 10^{-4}} \text{ m/kNm}$$

WIMPEY LABORATORIES LIMITED

CALCULATION SHEET	JOB	ANGLO K JOINT TESTS	Lab. Ref. No.		Calculated by	D. Garnett
		SPECIMEN N° 1	Sheet No.	D4B	Checked by	
		LOCAL JOINT FLEXIBILITIES	Date	6.5.83		

$$\Rightarrow \frac{\delta_{e2}}{M} = 0.00306 \text{ mm / KN.M.}$$

$$\phi_f = \frac{\delta_f}{L} \text{ for small angles such as these}$$

$$\therefore \frac{\phi_f}{M} = \frac{\delta_f}{ML} = \frac{\delta_T - \delta_e - \delta_c}{ML}$$

$$= \frac{1}{L} \left( \frac{\delta_T}{M} - \frac{\delta_e}{M} \right) - \frac{\phi_c}{M}$$

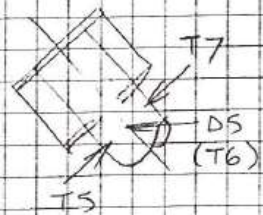
In this load case then,

$$F_{IPB2} = \frac{1}{610} (0.03238 - 0.00306) - 1.05 \times 10^{-5} \text{ Rads / KNm}$$

$$= \underline{3.76 \times 10^{-5} \text{ Rads / KNm.}}$$

i) Brace N° 1 (unloaded.)

BRACE MOMENT (KNm)	DEFLECTIONS (µm)			(mm)	
	T5 c.l. 184	T7 c.l. 186	AVE.	D5	T6 c.l. 185
0	0	0	0	0	0
4.64	0.02	0.05	0.04	0.00	0.01
8.45	0.02	0.05	0.04	0.00	0.01
12.77	0.03	0.07	0.05	0.01	-0.01
16.17	0.04	0.11	0.08	0.02	+0.01
19.67	0.08	0.16	0.12	0.05	0.04
23.07	0.10	0.18	0.13	0.06	0.05
26.57	0.11	0.18	0.15	0.06	0.04
30.08	0.17	0.19	0.18	0.08	0.06
33.48	0.22	0.27	0.25	0.10	0.07
36.98	0.35	0.36	0.36	0.11	0.10
38.73	0.42	0.44	0.43	0.13	0.12
40.89	0.48	0.51	0.50	0.14	0.12



WIMPEY LABORATORIES LIMITED

CALCULATION SHEET	JOB AMCO K JOINT TESTS	Lab. Ref. No.	D5b	Calculated by	D. Garnett.
	SPECIMEN N°1	Sheet No.		Checked by	
	LOCAL JOINT FLEXIBILITIES.	Date	16.5.83		

Slope of regressed best-fit straight line through plot of Average In plane deflection against IPM gives,

$$\frac{\delta_{T1}}{M} = 0.01102 \text{ mm/kNm (intercept } -0.0672 \text{ mm)}$$

$$\frac{\delta_{e1}}{M} = 0 \quad (\text{since no load is applied to this brace.})$$

$$\frac{\phi_{c1}}{M} = 1.05 \times 10^{-5} \text{ Rads/kNm}$$

$$F = \frac{1}{L} \left( \frac{\delta_T}{M} - \frac{\delta_e}{M} \right) - \frac{\phi_c}{M}$$

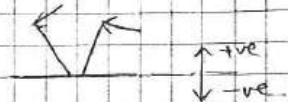
$$\therefore F_1 = \frac{1}{610} (0.01102 - 0) - 1.05 \times 10^{-5} \text{ Rads/kNm}$$

$$= 0.76 \times 10^{-5} \text{ Rads/kNm}$$

WIMPEY LABORATORIES LIMITED

CALCULATION SHEET	JOB	AMOCO K JOINT TESTS. SPECIMEN N°1 LOCAL JOINT FLEXIBILITIES.	Lab. Ref. No.		Calculated by	D. Garrett.
	Sheet No.	D61	Date	17.5.83	Checked by	

LOAD CASE N°8



CHORD DEFLECTIONS

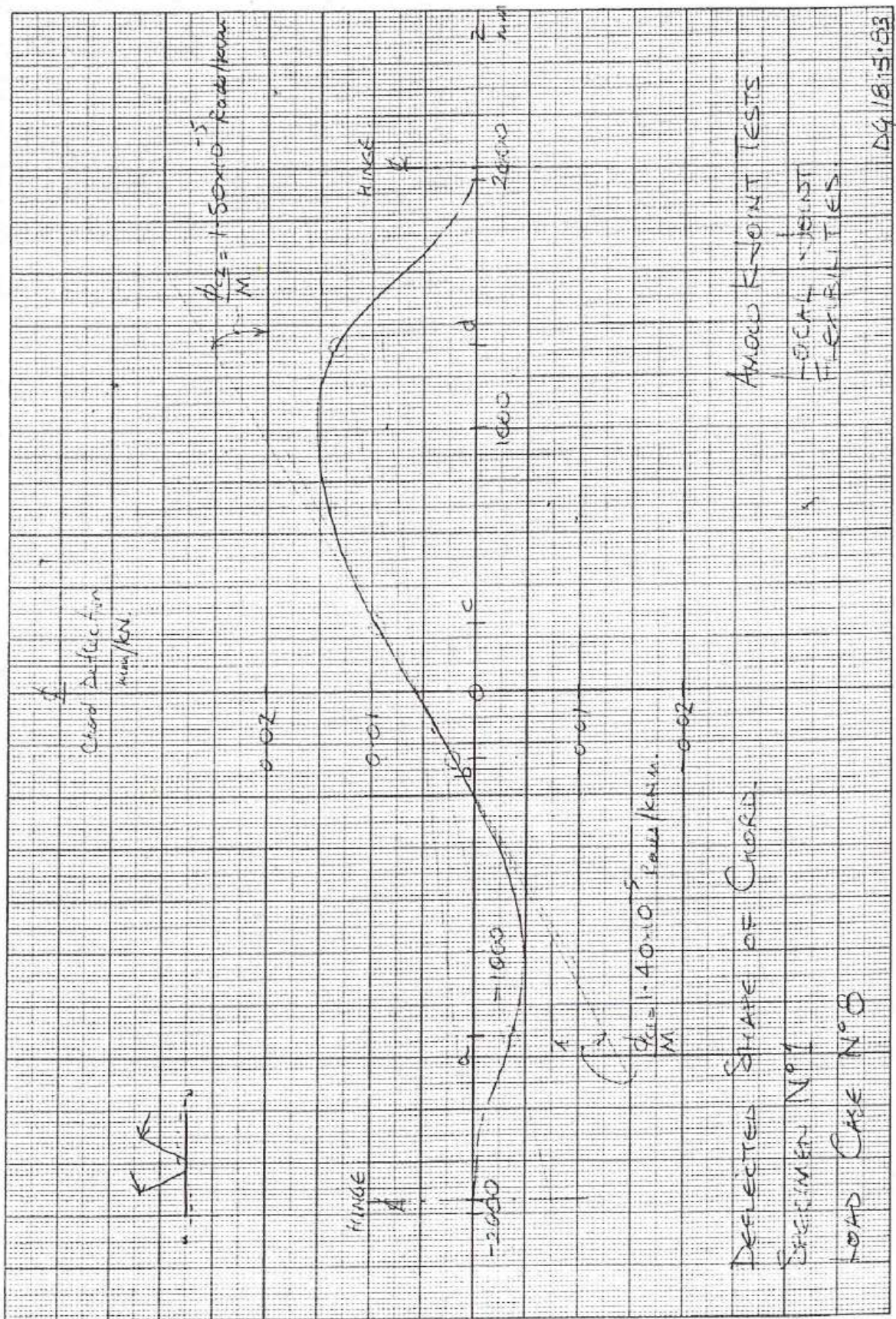
AVE. BRACE MOMENT (KNM)	DEFLECTIONS (mm)					
	D1	D2	AVE. D1, D2	D3	D4	AVE. D3, D4
0	0	0	0	0	0	0
2.88	-0.01	-0.02	-0.02	-0.01	+0.01	0.00
5.97	-0.02	-0.02	-0.02	+0.01	+0.02	0.02
9.17	+0.01	-0.01	0.00	-0.02	+0.02	0.00
12.36	0.00	-0.03	-0.02	0.00	+0.02	0.01
15.45	-0.01	-0.05	-0.03	+0.01	+0.03	0.02
18.54	-0.02	-0.07	-0.05	+0.04	+0.05	0.05
21.53	-0.03	-0.10	-0.07	+0.07	+0.07	0.07
24.62	-0.04	-0.13	-0.09	+0.09	+0.09	0.09
27.50	-0.06	-0.14	-0.10	+0.14	+0.10	0.12
30.49	-0.07	-0.14	-0.11	+0.20	-0.17	0.19
33.37	-0.06	-0.20	-0.13	+0.34	+0.30	0.32
36.26	-0.06	-0.20	-0.13	+0.44	+0.39	0.42
39.04	-0.05	-0.21	-0.13	+0.55	+0.50	0.53
40.58	-0.04	-0.20	-0.12	+0.61	+0.56	0.59

AVE. BRACE MOMENT (KNM)	DEFLECTIONS (mm)					
	T1	T3	AVE. T1, T3	T2	T4	AVE. T2, T4
0	0	0	0	0	0	0
2.88	-0.02	0.00	-0.01	-0.01	0.00	-0.01
5.97	-0.04	0.00	-0.02	-0.01	+0.02	+0.01
9.17	+0.06	+0.12	+0.09	+0.08	+0.12	+0.10
12.36	+0.03	+0.11	+0.07	+0.09	+0.13	+0.11
15.45	+0.02	+0.11	+0.07	+0.09	+0.14	+0.12
18.54	-0.01	+0.11	+0.05	+0.08	+0.17	+0.13
21.53	-0.02	+0.12	+0.05	+0.09	+0.18	+0.14
24.62	-0.03	+0.11	+0.04	+0.08	+0.21	+0.15
27.50	-0.04	+0.11	+0.04	+0.09	+0.24	+0.17
30.49	-0.06	+0.11	+0.03	+0.08	+0.29	+0.19
33.37	-0.07	+0.17	+0.05	+0.14	+0.38	+0.26
36.26	-0.07	+0.21	+0.07	+0.21	+0.46	+0.34
39.04	-0.07	+0.26	+0.10	+0.24	+0.56	+0.40
40.58	-0.07	+0.30	+0.12	+0.27	+0.59	+0.43

Regressed slopes, (intercepts with 'y' axis in mm in brackets):

a  $\Delta_1, \Delta_2 = -0.00363$  mm/kNm;  $d$   $\Delta_3, \Delta_4 = 0.01342$  mm/kNm  
 (0.0083) (-0.1222)

b  $T_1, T_3 = 0.00190$  mm/kNm;  $c$   $T_2, T_4 = 0.00366$  mm/kNm  
 (0.0029) (-0.0357)

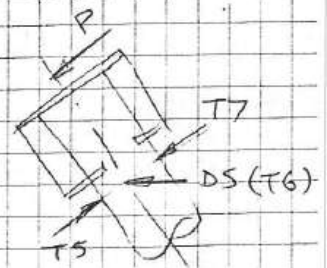


WIMPEY LABORATORIES LIMITED

CALCULATION SHEET	JOB AMOCO K JOINT TESTS, SPEIMEN N°1 LOCAL JOINT FLEXIBILITIES.	Lab. Ref. No.	Calculated by D. Gamett.
		Sheet No. 07b	Checked by
		Date 18.5.83	

② BRACE DEFLECTIONS

i) Brace N° 1.



AVE. BRACE MOMENT (KNM)	DEFLECTIONS (MM)				
	T5 ch 184	T7 ch 186	AVE T5, T7	D5	T6 ch 185
0	0	0	0	0	0
2.88	0.09	0.04	0.07	0.00	0.00
5.97	0.18	0.15	0.17	0.02	0.01
9.17	0.27	0.40	0.34	-0.10	0.01
12.36	0.36	0.48	0.42	-0.09	0.02
15.45	0.46	0.56	0.51	-0.04	0.01
18.54	0.56	0.62	0.59	0.00	0.04
21.53	0.67	0.74	0.71	0.04	0.09
24.62	0.78	0.86	0.82	0.07	0.13
27.50	0.91	0.86	0.89	0.12	0.17
30.49	1.05	1.01	1.03	0.17	0.24
33.37	1.19	1.09	1.14	0.24	0.34
36.26	1.32	1.38	1.35	0.30	0.41
39.04	1.43	1.42	1.43	0.36	0.47
40.58	1.50	1.51	1.51	0.39	0.50

Deflections recorded here as +ve in direction of load, P.

Slope of regressed best fit line through Ave of T5, T7

∴ Ave. brace moment plot =

$$\frac{\delta_{T1}}{M} = 0.03667 \text{ mm/KNm} \quad (\text{Intercept} = -0.0449 \text{ mm})$$

$$\frac{\delta_{e1}}{M} = 0.00306 \text{ mm/KNm} \quad \text{from page 4}$$

$$\frac{\phi_f}{M} = \frac{1}{L} \left( \frac{\delta_f}{M} - \frac{\delta_e}{M} \right) - \frac{\phi_c}{M}$$

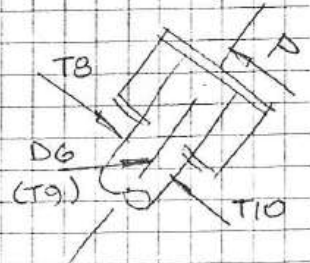
$$\begin{aligned} \therefore F_{IPB1} &= \frac{1}{610} (0.03667 - 0.00306) - 1.4 \times 10^{-5} \text{ Rads/KNm} \\ &= \underline{\underline{4.11 \times 10^{-5} \text{ Rads/KNm}}} \end{aligned}$$

WIMPEY LABORATORIES LIMITED

CALCULATION SHEET	JOB AMOCO K JOINT TESTS.	Lab. Ref. No.	Calculated by
	SPECIMEN N°1	Sheet No. D83	D. Garnett
	LOCAL JOINT FLEXIBILITIES.	Date 18.5.83	

ii) Brace N° 2.

AVG. BRACE MOMENT (KNM)	DEFLECTIONS. (MM)				
	T8 ch 187	T10 ch 190	Ave TB, T10	D6	T9 ch 188
0	0			0	0
2.38	0.10			0.00	0.01
3.97	0.19			0.00	0.03
9.17	0.30			-0.01	-0.01
12.36	0.41			0.01	0.01
15.45	0.52			0.03	0.02
18.54	0.62			0.06	0.05
21.53	0.72			0.08	0.07
24.62	0.84			0.10	0.09
27.50	0.97			0.14	0.13
30.49	1.12			0.19	0.19
33.37	1.32			0.25	0.25
36.26	1.49			0.28	0.30
39.04	1.64			0.30	0.37
40.58	1.73			0.30	0.40



Slope of regression best-fitting line through plot of TB v Ave brace moment, =

$$\frac{\delta_{T2}}{M} = 0.04203 \text{ mm/kNm} \quad (\text{Intercept} = -0.0923 \text{ mm})$$

$$\frac{\delta_{e2}}{M} = 0.00306 \text{ mm/kNm} \quad \text{from p4.}$$

$$\frac{\phi_{c2}}{M} = 1.50 \times 10^{-5} \text{ Rads/kNm} \quad \text{from graph.}$$

$$\frac{\phi_A}{M} = \frac{1}{L} \left( \frac{\delta_r}{M} - \frac{\delta_e}{M} \right) - \frac{\phi_c}{M}$$

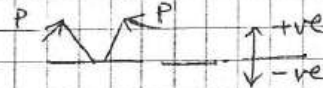
$$\Rightarrow F_{1PB2} = \frac{1}{610} (0.04203 - 0.00306) - 1.50 \times 10^{-5} \text{ Rads/kNm}$$

$$= \underline{\underline{4.89 \times 10^{-5} \text{ Rads/kNm}}}$$

WIMPEY LABORATORIES LIMITED

CALCULATION SHEET	JOB. AMOCO K-JOINT TESTS	Lab. Ref. No.	Calculated by D. Garnett	
	SPECIMEN N°1	Sheet No. D95		Checked by
	LOCAL JOINT FLEXIBILITIES	Date 18.5.83		

LOAD CASE N°6



CHORD DEFLECTIONS

AVE. BRACE MOMENT (kNm)	DEFLECTIONS (mm)					
	D1	D2	AVE. D1, D2	D3	D4	AVE. D3, D4
0	0	0	0	0	0	0
2.88	+0.01	0.00	+0.01	0.00	+0.02	+0.01
5.87	+0.02	+0.01	+0.02	+0.01	+0.03	+0.02
8.56	+0.04	+0.03	+0.04	+0.02	+0.05	+0.04
11.85	+0.07	+0.07	+0.07	+0.05	+0.07	+0.06
14.83	+0.10	+0.11	+0.11	+0.08	+0.10	+0.09
17.82	+0.14	+0.17	+0.16	+0.13	+0.13	+0.13
20.81	+0.19	+0.24	+0.22	+0.15	+0.16	+0.16
23.90	+0.24	+0.29	+0.27	+0.20	+0.20	+0.20
26.99	+1.31	+1.39	+1.35	+0.46	+0.47	+0.47
29.97	+3.41	+3.55	+3.48	+0.95	+0.97	+0.96
32.96	+3.99	+4.16	+4.09	+1.10	+1.12	+1.11
36.05	+4.07	+4.25	+4.16	+1.16	+1.17	+1.17
39.14	+4.12	+4.31	+4.22	+1.19	+1.21	+1.20
40.79	+4.14	+4.33	+4.24	+1.22	+1.23	+1.23

← Specimen is picked-up by jacks movement = 'play' in hinges.

AVE. BRACE MOMENT (kNm)	DEFLECTIONS (mm)					
	T1	T3	AVE. T1, T3	T2	T4	AVE. T2, T4
0	0	0	0	0	0	0
2.88	0.01	0.01	0.01	0.01	0.00	0.01
5.87	0.01	0.02	0.02	0.01	0.01	0.01
8.56	0.03	0.06	0.05	0.04	0.05	0.05
11.85	0.04	0.09	0.07	0.04	0.09	0.07
14.83	0.05	0.13	0.09	0.05	0.13	0.09
17.82	0.07	0.17	0.12	0.07	0.16	0.12
20.81	0.10	0.24	0.17	0.10	0.24	0.17
23.90	0.13	0.30	0.22	0.13	0.28	0.21
26.99	0.27	0.48	0.38	0.25	0.46	0.36
29.97	1.29	1.49	1.39	1.04	1.29	1.17
32.96	1.89	2.13	2.01	1.52	1.79	1.66
36.05	1.95	2.21	2.08	1.55	1.88	1.72
39.14	1.99	2.25	2.12	1.59	1.95	1.77
40.79	2.02	2.29	2.18	1.61	1.98	1.80

4

Regression slopes: Intercepts in mm in brackets. (1<sup>st</sup> 2 points only)

a  $D1, D2 = +0.01150$  mm/kNm ;  $D3, D4 = +0.00848$  mm/kNm  
 (-0.0361) ; (-0.0215)

b  $T1, T3 = 0.00392$  mm/kNm ;  $T2, T4 = 0.00381$  mm/kNm  
 (-0.0733) ; (-0.0232)

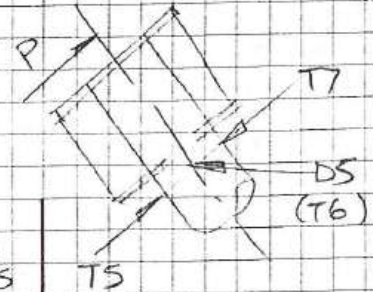


WIMPEY LABORATORIES LIMITED

CALCULATION SHEET	JOB AMGCO K JOINT TESTS	Lab. Ref. No.	Calculated by D. Gandy	
	SPECIMEN N°1	Sheet No. D106		Checked by
	LOCAL JOINT FLEXIBILITIES	Date 18.5.83		

(2) BRACE DEFLECTIONS.

i) Brace N°1



AVE. BRACE MOMENT (kNm)	DEFLECTIONS (mm)				
	T5 ch 184	T7 ch 186	AVE	D5	T6 ch 185
0	0	0	0	0	0
2.88	0.04	0.03	0.04	0.02	0.01
5.87	0.10	0.04	0.07	0.02	0.03
8.56	0.16	0.08	0.12	0.07	0.07
11.85	0.21	0.14	0.18	0.10	0.08
14.83	0.27	0.25	0.26	0.14	0.12
17.82	0.34	0.31	0.33	0.19	0.16
20.81	0.40	0.38	0.39	0.25	0.20
23.90	0.47	0.43	0.45	0.31	0.26
26.99	0.64	0.56	0.60	0.39	0.31
29.97	1.49	1.36	1.43	0.48	0.35
32.96	2.04	1.57	1.81	0.56	0.41
36.05	2.14	1.63	1.89	0.61	0.45
39.14	2.17	1.69	1.93	0.66	0.48
40.79	2.21	1.74	1.98	0.68	0.50

← Specimen 'pick-up'

Slope of regressed line through TS, T7 Ave. v Ave Brace =  
(11.9 points) Moment,

$$\frac{\delta_T}{M} = 0.01957 \text{ mm/kNm. (Intercept} = -0.0271 \text{ mm)}$$

$$\frac{\delta_{e1}}{M} = 0.00306 \text{ mm/kNm from p4.}$$

$$\frac{\phi_{c1}}{M} = 0 \text{ from graph,}$$

$$\frac{\phi_r}{M} = \frac{1}{L} \left( \frac{\delta_T}{M} - \frac{\delta_e}{M} \right) - \frac{\phi_c}{M}$$

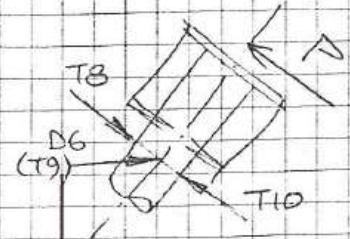
$$\therefore F_{IPB1} = \frac{1}{610} (0.01957 - 0.00306) - 0 \text{ Rads/kNm}$$

$$= 2.71 \times 10^{-5} \text{ Rads/kNm}$$

WIMPEY LABORATORIES LIMITED

CALCULATION SHEET	JOB	Amoco K JOINT TESTS. SPECIMEN N° 1. LOCAL JOINT FLEXIBILITIES.	Lab. Ref. No.		Calculated by	D. Garnett.
			Sheet No.	D11A	Checked by	
			Date	13.5.83		

ii) Brace N° 2



AVE. BRACE MOMENT (KNm)	DEFLECTIONS (MM)				
	T8 ch 187	T10 ch 190	AVE.	D6	T9 ch 188
0	0			0	0
2.88	0.04	No output available	As T8.	-0.01	0.00
5.87	0.10			-0.02	0.01
8.56	0.16			-0.04	0.05
11.95	0.21			-0.05	0.07
14.83	0.26			-0.07	0.11
17.92	0.31			-0.11	0.14
20.81	0.35			-0.15	0.18
23.90	0.41			-0.22	0.23
26.99	0.47			-0.29	0.26
29.97	0.52	-0.37	0.28		
32.96	0.58	-0.42	0.35		
36.05	0.64	-0.48	0.39		
39.14	0.71	-0.54	0.41		
40.79	0.74	-0.58	0.46		

Slope of regressed line through first 9 points =  
 $\frac{\delta_{T2}}{M} = 0.01720 \text{ mm/kNm}$  (Intercept = 0.0009 mm)

$$\frac{\delta_{e2}}{M} = 0.00306 \text{ mm/kNm}$$

$$\frac{\phi_{e2}}{M} = 0$$

$$\frac{\phi_f}{M} = \frac{1}{L} \left( \frac{\delta_f}{M} - \frac{\delta_e}{M} \right) - \frac{\phi_e}{M}$$

$$\therefore F_{1952} = \frac{1}{610} (0.01720 - 0.00306) - 0 \quad \text{Rads/kNm}$$

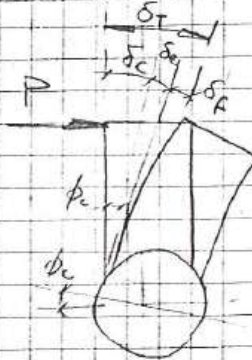
$$= \underline{\underline{2.32 \times 10^{-5} \text{ Rads/kNm}}}$$

CALCULATION SHEET	JOB <u>ANCO K JOINT TESTS</u>	Lab. Ref. No.	Calculated by
	<u>SPECIMEN N°1</u>	Sheet No. <u>D126</u>	Checked by
	<u>LOCAL JOINT FLEXIBILITIES</u>	Date <u>19.5.83</u>	

③ OUT-OF PLANE BENDING

Notation:

eg: Load 



If  $\delta_F$  = displacement at brace, and due to local joint flexibility

$\delta_e$  = ———— due to elastic bending of brace.

$\delta_c$  = ———— due to chord rotation.

and  $\delta_T$  = total measured displacement at brace end.

then,  $\delta_F = \delta_T - \delta_e - \delta_c$

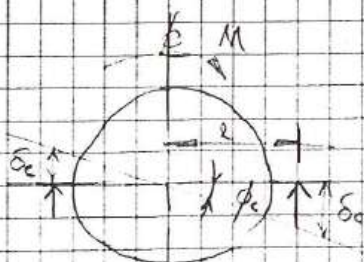
$\phi = \tan^{-1}(\frac{\delta}{L}) = \frac{\delta}{L}$  for these small angles.

Local Joint Flexibility =

$$\frac{\phi_F}{M} = \frac{\delta_F}{ML} = \frac{1}{L} \left( \frac{\delta_T}{M} - \frac{\delta_e}{M} - \frac{\delta_c}{M} \right)$$

$$= \frac{1}{L} \left( \frac{\delta_T}{M} - \frac{\delta_e}{M} \right) - \frac{\phi_c}{M} \quad \text{as before.}$$

Chord rotation is found thus:-



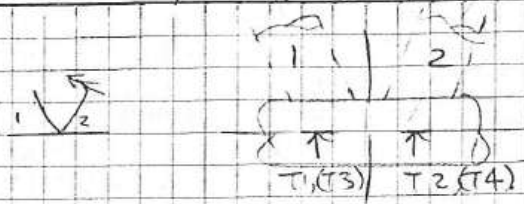
$$\phi_c = \frac{\delta_c}{l} \quad \neq \quad \frac{\phi_c}{M} = \frac{1}{l} \left( \frac{\delta_c}{M} \right)$$

$$l = \frac{457}{2} + 20 = 249 \text{ mm.}$$

WIMPEY LABORATORIES LIMITED

CALCULATION SHEET	JOB. <u>AMOCO K JOINT TESTS.</u>	Lab. Ref. No.	Calculated by	<u>D. Garrett</u>
	<u>SPECIMEN N°1</u>	Sheet No.	Checked by	
	<u>LOCAL JOINT FLEXIBILITIES.</u>	Date		

LOAD CASE N°10



① CHORD ROTATION.

AVE. BRACE MOMENT (KNm.) M	DEFLECTIONS. (mm)						Deflections looked as +ve if in direction of applied moment.
	T1 ch182	T3 ch189	AVE	T2 ch181	T4 ch183	AVE.	
0	0	0	0	0	0	0	
1.55	+0.01	+0.03	0.02	0.01	0.04	0.03	
3.40	+0.03	+0.06	0.05	0.03	0.06	0.05	
5.36	+0.05	+0.10	0.08	0.06	0.09	0.07	
7.21	+0.09	+0.15	0.12	0.11	0.15	0.13	
8.96	+0.15	+0.16	0.16	0.16	0.18	0.17	
10.71	+0.20	+0.22	0.21	0.23	0.26	0.25	
12.57	+0.26	+0.31	0.29	0.29	0.36	0.32	
14.32	+0.33	+0.41	0.37	0.32	0.43	0.38	
16.07	+0.36	+0.40	0.38	0.37	0.47	0.42	
17.82	+0.41	+0.47	0.44	0.43	0.56	0.50	

Slopes of regressed lines through T1, T3 v M & T2, T4 v M give

$$\frac{\delta_{c1}}{M} = 0.02581 \text{ mm/KNm (Intercept} = -0.0037 \text{ mm)}$$

$$\frac{\delta_{c2}}{M} = 0.02863 \text{ mm/KNm (Intercept} = -0.0441 \text{ mm)}$$

$$\therefore \frac{\phi_{c1}}{M} = \frac{0.02581}{249} = 1.04 \times 10^{-4} \text{ rads/KNm}$$

$$\neq \frac{\phi_{c2}}{M} = \frac{0.02863}{249} = 1.15 \times 10^{-4} \text{ rads/KNm}$$

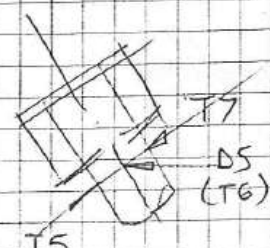
WIMPEY LABORATORIES LIMITED

CALCULATION SHEET	JOB AMOCO K JOINT TESTS	Lab. Ref. No.	Calculated by D. Garrett
	SPECIMEN No. 1	Sheet No. D14b	
	LOCAL JOINT FLEXIBILITIES.	Date 19.5.83	

(2) BRACE DEFLECTIONS.

i) Brace N°1

AVE. BRACE MOMENT (KNM)	DEFLECTIONS. (mm)				
	DS	T6 ch 185	AVE	T5 ch 184	T7 ch 186
0	0	0	0	0	0
1.55	0.12	0.13	0.13	0.00	0.00
3.40	0.26	0.24	0.25	0.00	-0.01
5.36	0.45	0.45	0.45	0.01	+0.01
7.21	0.70	0.71	0.71	0.03	-0.01
8.96	0.97	0.94	0.96	0.04	-0.01
10.71	1.24	1.27	1.26	0.04	-0.01
12.57	1.58	1.55	1.57	0.03	-0.02
14.32	1.92	1.92	1.92	0.04	-0.01
16.07	1.99	2.00	2.00	0.05	-0.01
17.92	2.22	2.24	2.23	0.07	-0.02



Slope of regression line through AVE DS, T6 vs M gives,

$$\frac{\delta_{T1}}{M} = 0.13203 \text{ mm/kNm (Intercept} = -0.1414 \text{ mm)}$$

$$\frac{\delta_{e1}}{M} = 0 \text{ (brace is unloaded)}$$

$$\frac{\phi_f}{M} = \frac{1}{L} \left( \frac{\delta_f}{M} - \frac{\delta_e}{M} \right) - \frac{\phi_c}{M}$$

$$\Rightarrow F_{OPB1} = \frac{1}{610} (0.13203 - 0) - 1.04 \times 10^{-4} \text{ Rads/kNm.}$$

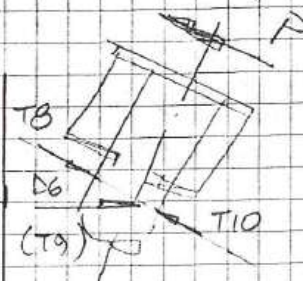
$$= \underline{\underline{1.12 \times 10^{-4} \text{ Rads/kNm.}}}$$

WIMPEY LABORATORIES LIMITED

CALCULATION SHEET	JOB AMOCO K JOINT TESTS	Lab. Ref. No.	Calculated by D. Garrett	
	SPECIMEN N° 1	Sheet No. D15b		Checked by
	LOCAL JOINT FLEXIBILITIES	Date 19.5.83		

ii) Brace N° 2.

AVE BRACE MOMENT (kNm) M	DEFLECTIONS (mm)				
	D6	T9 cl 188	AVE.	TB cl 187	T10 cl 190
0	0	0	0	0	No out put available.
1.55	0.05	0.16	0.11	0.00	
3.40	0.34	0.32	0.33	0.02	
5.36	0.57	0.56	0.57	0.02	
7.21	0.84	0.86	0.85	0.01	
8.96	1.15	1.10	1.13	0.00	
10.71	1.46	1.45	1.46	-0.01	
12.57	1.78	1.75	1.77	-0.04	
14.32	2.04	2.04	2.04	-0.03	
16.07	2.25	2.25	2.25	0.00	
17.92	2.49	2.47	2.48	-0.02	



Slope of regressed line through AVE. D6, T9 v. M plot gives,

$$\frac{\delta_{Tz}}{M} = 0.14708 \text{ mm/kNm (intercept} = -0.1291 \text{ mm)}$$

$$\frac{\delta_{e2}}{M} = 0.00306 \text{ mm/kNm from p 4.}$$

$$\frac{\phi_f}{M} = \frac{1}{L} \left( \frac{\delta_f}{M} - \frac{\delta_e}{M} \right) - \frac{\phi_c}{M}$$

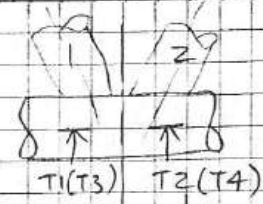
$$\Rightarrow F_{OPBz} = \frac{1}{610} (0.14708 - 0.00306) - 1.15 \times 10^{-4} \text{ Rads/kNm}$$

$$= \underline{\underline{1.21 \times 10^{-4} \text{ Rads/kNm}}}$$

WIMPEY LABORATORIES LIMITED

CALCULATION SHEET	JOB AMOCO K JOINT TESTS	Lab. Ref. No.	Calculated by D. Gamett	
	SPECIMEN N° 1.	Sheet No. D166		Checked by
	LOCAL JOINT FLEXIBILITIES.	Date 19.5.83		

LOAD CASE N° 9



Ø CHORD ROTATION.

AVE. M BRACE MOMENT (KNM)	DEFLECTIONS (mm)					
	T1 ch182	T3 ch189	AVE	T2 ch181	T4 ch183	AVE
0	0	0	0	0	0	0
0.72	-0.01	0.05	0.02	0.00	0.03	0.02
1.85	0.00	0.09	0.05	0.02	0.07	0.05
2.88	0.02	0.14	0.08	0.07	0.13	0.10
4.02	0.11	0.20	0.16	0.15	0.20	0.18
5.15	0.21	0.31	0.26	0.24	0.32	0.28
6.18	0.29	0.40	0.35	0.33	0.42	0.38
7.11	0.36	0.46	0.41	0.38	0.49	0.44
8.34	0.45	0.51	0.48	0.46	0.59	0.53
9.48	0.52	0.59	0.56	0.55	0.69	0.62
10.61	0.59	0.68	0.64	0.61	0.76	0.69

Slopes of regression lines through T1, T3 v M & T2, T4 v M give,

$$\frac{\delta_{c1}}{M} = 0.06360 \text{ mm/kNm (Intercept} = -0.0521 \text{ mm)}$$

$$\frac{\delta_{c2}}{M} = 0.06928 \text{ mm/kNm (Intercept} = -0.0557 \text{ mm)}$$

$$\therefore \frac{\phi_{c1}}{M} = \frac{0.06360}{249} = 2.55 \times 10^{-4} \text{ Rads/kNm}$$

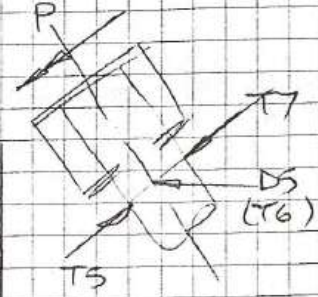
$$\neq \frac{\phi_{c2}}{M} = \frac{0.06928}{249} = 2.78 \times 10^{-4} \text{ Rads/kNm}$$

WIMPEY LABORATORIES LIMITED

CALCULATION SHEET	108 ANGLO K JOINT TESTS	Lab. Ref. No.	Calculated by D. Gamell.	
	SPECIMEN N° 1	Sheet No. D176		Checked by
	LOCAL JOINT FLEXIBILITIES	Date 19.5.83		

② BRACE DEFLECTIONS

1) Brace N° 1



AVG. BRACE MOMENT (KNm)	DEFLECTIONS (mm)				
	DS	TG cL 135	AVG.	TS cL 184	T7 cL 186
0	-	0		0	-
0.72	-	0.08		-0.01	-
1.85	-	0.25		0.00	-
2.88	-	0.45		0.00	-
4.02	⊙	0.84		0.01	-
5.15	0.35	0.91		0.00	0
6.18	0.73	1.32	AS TG	0.01	0.01
7.11	1.03	1.66		0.04	0.09
8.34	1.43	2.05		0.05	0.08
9.48	1.76	2.42		0.05	0.08
10.61	2.07	2.72		0.07	0.08

Slope of regressed line through TG v M gives

$$\frac{\delta_{TG}}{M} = 0.26507 \text{ mm / KNm (Intercept = -0.2031 mm)}$$

$$\frac{\delta_{e1}}{M} = 0.00306 \text{ mm / KNm from p4.}$$

$$\frac{d_f}{M} = \frac{1}{L} \left( \frac{\delta_f}{M} - \frac{\delta_e}{M} \right) - \frac{d_c}{M}$$

$$\Rightarrow F_{OPB1} = \frac{1}{610} (0.26507 - 0.00306) - 2.55 \times 10^{-4} \text{ rads / KNm}$$

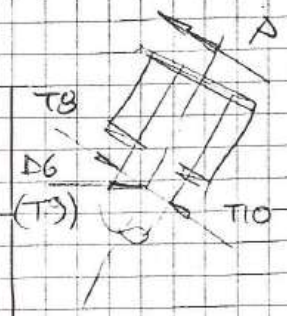
$$= 1.74 \times 10^{-4} \text{ Rads / KNm}$$

WIMPEY LABORATORIES LIMITED

CALCULATION SHEET	JOB. AMCO K JOINT TESTS	Lab. Ref. No.	Calculated by D. Canett.	
	SPECIMEN N° 1	Sheet No. D186		Checked by
	LOCAL JOINT FLEXIBILITIES	Date 19.5.93		

ii) Brace N° 2.

AVG. BRACE MOMENT (kNm) M	DEFLECTIONS (mm)				
	D6	T9 ch.188	AVG.	T8 ch.187	T10 ch.190
0	0	0	0	0	No output available.
0.72	0.11	0.11	0.11	0.03	
1.85	0.29	0.31	0.30	0.04	
2.88	0.54	0.56	0.55	0.04	
4.02	0.92	0.91	0.92	0.03	
5.15	1.25	1.05	1.15	0.11	
6.18	1.61	1.42	1.52	0.09	
7.11	1.91	1.70	1.81	0.10	
8.34	2.27	2.06	2.17	0.16	
9.48	2.59	2.39	2.49	0.18	
10.61	2.99	2.66	2.78	0.22	



Slope of regressed line through Ave D6, T9 v M given

$$\frac{\delta_{T9}}{M} = 0.27239 \text{ mm/kNm (Intercept} = -0.1406 \text{ mm)}$$

$$\frac{\delta_{e2}}{M} = 0.00306 \text{ mm/kNm from p4.}$$

$$\frac{\phi_f}{M} = \frac{1}{L} \left( \frac{\delta_T}{M} - \frac{\delta_e}{M} \right) - \frac{\phi_c}{M}$$

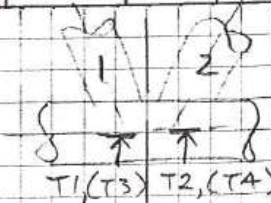
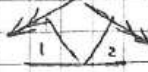
$$\Rightarrow F_{OPB2} = \frac{1}{610} (0.27239 - 0.00306) - 2.78 \times 10^{-4} \text{ Rads/kNm}$$

$$= \underline{\underline{1.63 \times 10^{-4} \text{ Rads/kNm}}}$$

WIMPEY LABORATORIES LIMITED

CALCULATION SHEET	JOB. AMOCO K JOINT TESTS	Lab. Ref. No.	Calculated by
	SPECIMEN N° 1	Sheet No. D196	D. Garnett.
	LOCAL JOINT FLEXIBILITIES	Date 19.5.83	

LOAD CASE N° 11



○ CHORD ROTATION.

AVE. BRACE MOMENT (kNm) M	DEFLECTIONS (mm)					
	T1 ch 182	T3 ch 189	AVE.	T2 ch 181	T4 ch 183	AVE
0	0	0	0	0	0	0
1.96	0.01	0.01	0.01	-0.01	0.01	0.00
4.12	0.01	0.02	0.02	0.00	0.00	0.00
6.28	0.02	0.01	0.02	0.00	0.00	0.00
8.45	0.01	0.01	0.01	0.00	0.00	0.00
11.54	0.03	0.02	0.03	-0.01	0.00	-0.01
13.80	0.04	0.01	0.03	-0.01	0.01	0.00
15.97	0.06	0.01	0.04	+0.02	0.02	0.02
18.23	0.06	0.02	0.04	-0.01	0.02	0.01
20.39	0.07	0.01	0.04	0.00	0.04	0.02
21.73	0.07	0.02	0.05	-0.01	0.04	0.02

Slopes of regressed lines through T1, T3 vs M & T2, T4 vs M give,

$$\frac{\delta c_1}{M} = 0.00196 \text{ mm/kNm (Intercept} = 0.0045 \text{ mm)}$$

$$\neq \frac{\delta c_2}{M} = 0.00099 \text{ mm/kNm (Intercept} = -0.0056 \text{ mm)}$$

$$\therefore \frac{\phi_{c1}}{M} = \frac{0.00196}{249} = 0.08 \times 10^{-4} \text{ Rads/kNm}$$

$$\neq \frac{\phi_{c2}}{M} = \frac{0.00099}{249} = 0.04 \times 10^{-4} \text{ Rads/kNm}$$

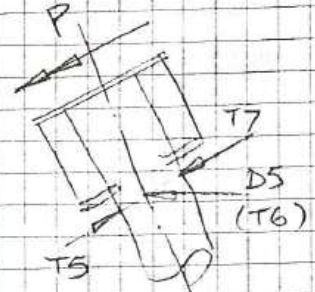
WIMPEY LABORATORIES LIMITED

CALCULATION SHEET	JOB	ALUO K JOINT TESTS	Lab. Ref. No.		Calculated by	D. Garnett
		SPECIMEN N° 1	Sheet No.	206	Checked by	
		LOCAL JOINT FLEXIBILITIES.	Date	19.5.83		

② BRACE DEFLECTIONS

i) Brace N° 1.

AVE. BRACE MOMENT (KN.m) M	DEFLECTIONS (mm)				
	D5	T6 ch 185	AVE	T5 ch 184	T7 ch 186
0	0	0	0	0	0
1.96	0.04	0.05	0.05	0.00	+0.01
4.12	0.08	0.08	0.08	0.01	+0.01
6.28	0.13	0.15	0.14	0.00	+0.01
8.45	0.18	0.20	0.19	0.01	+0.01
11.54	0.26	0.27	0.27	0.02	+0.01
13.80	0.30	0.32	0.31	0.01	+0.01
15.97	0.35	0.36	0.36	0.01	+0.01
18.23	0.41	0.43	0.42	0.01	+0.01
20.39	0.46	0.49	0.48	0.00	+0.02
21.73	0.50	0.55	0.53	0.01	+0.01



Slope of regression best-fitting line through

AVE. D5, T6 v. M gives,

$$\frac{\delta_{T1}}{M} = 0.02382 \text{ mm/kNm (Intercept} = -0.0079 \text{ mm)}$$

$$\frac{\delta_{e1}}{M} = 0.00306 \text{ mm/kNm from page 4.}$$

$$\frac{\phi_f}{M} = \frac{1}{L} \left( \frac{\delta_f}{M} - \frac{\delta_e}{M} \right) - \frac{\phi_e}{M}$$

$$\Rightarrow F_{OPB1} = \frac{1}{610} (0.02382 - 0.00306) - 0.08 \times 10^{-4} \text{ Rads/kNm}$$

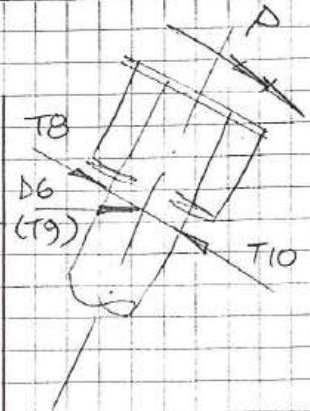
$$= 0.26 \times 10^{-4} \text{ Rads/kNm.}$$

WIMPEY LABORATORIES LIMITED

CALCULATION SHEET	JOB AMOCO K JOINT TESTS.	Lab. Ref. No.	Calculated by	D. Garnett.
	SPECIMEN N°1.	Sheet No.	DZ16	Checked by
	LOCAL JOINT FLEXIBILITIES.	Date	19.5.83	

ii) Brace N°2.

AVG. BRACE MOMENT (KNM) M	DEFLECTIONS (MM)				
	D6	T9 cl 188	AVE.	T8 cl 187	T10 cl 190
0	0	0	0	0	
1.96	0.07	0.06	0.07	0.01	
4.12	0.13	0.12	0.13	0.02	
6.28	0.19	0.16	0.18	0.02	
8.45	0.25	0.21	0.23	0.02	
11.54	0.33	0.29	0.31	0.03	
13.80	0.39	0.33	0.36	0.03	
15.97	0.44	0.38	0.41	0.03	
18.23	0.48	0.43	0.46	-0.01	
20.39	0.53	0.47	0.50	-0.01	
21.75	0.58	0.50	0.54	-0.01	



No out put available.

Slope of regressed best-fitting line through

AVE. D6, T9 v. M gives,

$$\frac{\delta_{T2}}{M} = 0.02405 \text{ mm/kNm (Intercept = 0.0222 mm)}$$

$$\frac{\delta_{e2}}{M} = 0.00306 \text{ mm/kNm from page 4.}$$

$$\frac{\phi_c}{M} = \frac{1}{L} \left( \frac{\delta_T}{M} - \frac{\delta_e}{M} \right) - \frac{\phi_c}{M}$$

$$\Rightarrow F_{OPB2} = \frac{1}{610} (0.02405 - 0.00306) - 0.04 \times 10^{-4} \text{ Rods/kNm}$$

$$= \underline{\underline{0.30 \times 10^{-4} \text{ Rods/kNm.}}}$$

## **APPENDIX 4 - LJF Calculations for Benchmarking Model**

**(RK-FEA)**

LOAD CASE NO 01														
1	Young's Modulus	2.10E+02	kN/mm^2			Geometric Properties								
2	Brace OD (d)	16	(in) = 406.4	(mm)		d/D = 0.89								
3	Brace WT (t)	3/8	(in) = 9.5	(mm)		g/D = 0.12								
4	Chord OD (D)	18	(in) = 457.2	(mm)		t/T = 1.00								
5	Chord WT (T)	3/8	(in) = 9.5	(mm)		D/2T = 24.00								
6	Brace-Chord Angle	60	deg	1.047	(Rad)									
7	Gap (g)	2 1/6	(in) = 55.0	(mm)		Theoretical Calculations								
8	Brace Length ( $l_b$ )		777	(mm, clamp to crown, long)		117.32	777.4							
			543	(mm, clamp to crown, short)		117.32	542.7							
			803	(mm, clamp to saddle)		104.73	803.1							
			660	(mm, average clamp to crown)										
9	Brace Area ( $A_b$ )	18.41	(in^2) = 11,876.0	(mm^2)										
10	Brace M.O.I. ( $I_b$ )	562.08	(in^4) = 233,957,073	(mm^4)										
11	Chord Length ( $l_c$ )		3,056.0	(mm)	1658	(mm, loading point)								
12	Chord Area ( $A_c$ )	20.76	(in^2) = 13,396.1	(mm^2)										
13	Chord M.O.I. ( $I_c$ )	806.63	(in^4) = 335,745,310	(mm^4)										
14	Applied Load (P)		300	(kN)										
<p><math>\delta_r</math> = overall displacement</p> <p><math>\delta_f</math> = displacement due to local joint flexibility</p> <p><math>\delta_c</math> = elastic displacement of chord (use component in the direction of brace)</p> <p><math>\delta_e</math> = elastic displacement of brace</p>														
<table border="1"> <thead> <tr> <th colspan="2">Beam theory</th> </tr> </thead> <tbody> <tr> <td>Chord lateral displacement</td> <td>2.159</td> </tr> <tr> <td>Chord displacement in brace direction</td> <td>1.870</td> </tr> <tr> <td>Elastic displacement of brace</td> <td>0.079</td> </tr> </tbody> </table>							Beam theory		Chord lateral displacement	2.159	Chord displacement in brace direction	1.870	Elastic displacement of brace	0.079
Beam theory														
Chord lateral displacement	2.159													
Chord displacement in brace direction	1.870													
Elastic displacement of brace	0.079													
Load Case	Description	$\delta_r / P$ (mm/kN)	$\delta_c / P$ (mm/kN)	$\delta_e / P$ (mm/kN)	$\delta_f / P$ (mm/kN)									
1	Tension in one brace	0.0097	0.0062	0.0003	0.0032	FE Analysis								
		0.0145	0.0104	0.0003	0.0038	Test Data								



LOAD CASE NO 03																										
1	Young's Modulus	2.10E+02	kN/mm <sup>2</sup>			<table border="1"> <tr> <th colspan="2">Geometric Properties</th> </tr> <tr> <td>d/D =</td> <td>0.89</td> </tr> <tr> <td>g/D =</td> <td>0.12</td> </tr> <tr> <td>t/T =</td> <td>1.00</td> </tr> <tr> <td>D/2T =</td> <td>24.00</td> </tr> <tr> <th colspan="2">Theoretical calculations</th> </tr> <tr> <td>117.32</td> <td>777.4</td> </tr> <tr> <td>117.32</td> <td>542.7</td> </tr> <tr> <td>104.73</td> <td>803.1</td> </tr> <tr> <td colspan="2">1658 (mm, loading point)</td> </tr> </table>	Geometric Properties		d/D =	0.89	g/D =	0.12	t/T =	1.00	D/2T =	24.00	Theoretical calculations		117.32	777.4	117.32	542.7	104.73	803.1	1658 (mm, loading point)	
Geometric Properties																										
d/D =	0.89																									
g/D =	0.12																									
t/T =	1.00																									
D/2T =	24.00																									
Theoretical calculations																										
117.32	777.4																									
117.32	542.7																									
104.73	803.1																									
1658 (mm, loading point)																										
2	Brace OD (d)	16	(in) =	406.4	(mm)																					
3	Brace WT (t)	3/8	(in) =	9.5	(mm)																					
4	Chord OD (D)	18	(in) =	457.2	(mm)																					
5	Chord WT (T)	3/8	(in) =	9.5	(mm)																					
6	Brace-Chord Angle	60	deg	1.047	(Rad)																					
7	Gap (g)	2 1/6	(in) =	55.0	(mm)																					
8	Brace Length ( <i>l<sub>b</sub></i> )			777	(mm, clamp to crown, long)																					
				543	(mm, clamp to crown, short)																					
				803	(mm, clamp to saddle)																					
				660	(mm, average clamp to crown)																					
9	Brace Area ( <i>A<sub>b</sub></i> )	18.41	(in <sup>2</sup> ) =	11,876.0	(mm <sup>2</sup> )																					
10	Brace M.O.I. ( <i>I<sub>b</sub></i> )	562.08	(in <sup>4</sup> ) =	233,957,073	(mm <sup>4</sup> )																					
11	Chord Length ( <i>l<sub>c</sub></i> )			3,056.0	(mm)																					
12	Chord Area ( <i>A<sub>c</sub></i> )	20.76	(in <sup>2</sup> ) =	13,396.1	(mm <sup>2</sup> )																					
13	Chord M.O.I. ( <i>I<sub>c</sub></i> )	806.63	(in <sup>4</sup> ) =	335,745,310	(mm <sup>4</sup> )																					
14	Applied Load (P)			300	(kN)																					
<p><math>\delta_r</math> = overall displacement</p> <p><math>\delta_f</math> = displacement due to local joint flexibility</p> <p><math>\delta_c</math> = elastic displacement of chord (use component in the direction of brace)</p> <p><math>\delta_e</math> = elastic displacement of brace</p>						<table border="1"> <tr> <td>Beam theory</td> <td>mm</td> </tr> <tr> <td>Chord lateral displacement</td> <td>2.159</td> </tr> <tr> <td>Chord displacement in brace direction</td> <td>1.870</td> </tr> <tr> <td>Elastic displacement of brace</td> <td>0.079</td> </tr> </table>	Beam theory	mm	Chord lateral displacement	2.159	Chord displacement in brace direction	1.870	Elastic displacement of brace	0.079												
Beam theory	mm																									
Chord lateral displacement	2.159																									
Chord displacement in brace direction	1.870																									
Elastic displacement of brace	0.079																									
Load Case	Description	$\delta_r / P$ (mm/kN)	$\delta_c / P$ (mm/kN)	$\delta_e / P$ (mm/kN)	$\delta_f / P$ (mm/kN)																					
3	Compression in one	0.0097	0.0062	0.0003	0.0032	FE Analysis																				
	brace (symmetric)	0.0130	0.0101	0.0003	0.0026	Test Data																				

LOAD CASE NO 04						
1	Young's Modulus	2.10E+02	kN/mm <sup>2</sup>			Geometric Properties
2	Brace OD (d)	16	(in) =	406.4	(mm)	d/D = 0.89
3	Brace WT (t)	3/8	(in) =	9.5	(mm)	g/D = 0.12
4	Chord OD (D)	18	(in) =	457.2	(mm)	t/T = 1
5	Chord WT (T)	3/8	(in) =	9.5	(mm)	D/2T = 24.00
6	Brace-Chord Angle	60	deg	1.047	(Rad)	
7	Gap (g)	2 1/6	(in) =	55.0	(mm)	Theoretical calculations
8	Brace Length ( <i>l<sub>b</sub></i> )			777	(mm, clamp to crown, long)	117.32 <b>777.4</b>
				543	(mm, clamp to crown, short)	117.32 <b>542.7</b>
				803	(mm, clamp to saddle)	104.73 <b>803.1</b>
				660	(mm, average clamp to crown)	
9	Brace Area ( <i>A<sub>b</sub></i> )	18.41	(in <sup>2</sup> ) =	11,876.0	(mm <sup>2</sup> )	
10	Brace M.O.I. ( <i>I<sub>b</sub></i> )	562.08	(in <sup>4</sup> ) =	233,957,073	(mm <sup>4</sup> )	For B1 Load For B2 Load
11	Chord Length ( <i>l<sub>c</sub></i> )			3,056.0	(mm)	A 1398 1658
12	Chord Area ( <i>A<sub>c</sub></i> )	20.76	(in <sup>2</sup> ) =	13,396.1	(mm <sup>2</sup> )	B 1658 1398
13	Chord M.O.I. ( <i>I<sub>c</sub></i> )	806.63	(in <sup>4</sup> ) =	335,745,310	(mm <sup>4</sup> )	
14	Applied Load (P)			300	(kN)	
$\delta_r$ = overall displacement $\delta_f$ = displacement due to local joint flexibility $\delta_c$ = elastic displacement of chord (use component in the direction of brace) $\delta_e$ = elastic displacement of brace					Beam theory	B1 Load B2 Load B1 & B2 Load
					Chord lateral displacement -B1 (mm), x=	1398 -2.159 -2.133 -4.292
					Chord lateral displacement -B2 (mm), x=	1658 -2.133 -2.159 -4.292
					Chord displacement in brace direction at Brace 1 (B1) (mm)	-3.717
					Chord displacement in brace direction at Brace 2 (B2) (mm)	-3.717
					Elastic displacement of brace (mm)	0.079
4	Unbalanced Axial Load	<b>-0.0174</b>	<b>-0.0124</b>	<b>-0.0003</b>	<b>-0.0048</b>	FE Analysis
	(Compression Brace 1)	<b>0.0255</b>	<b>0.0185</b>	<b>0.0003</b>	<b>0.0067</b>	Test Data
	Balanced Axial Load	<b>-0.0174</b>	<b>-0.0124</b>	<b>-0.0003</b>	<b>-0.0048</b>	FE Analysis
	(Compression Brace 2)	<b>0.0275</b>	<b>0.0188</b>	<b>0.0003</b>	<b>0.0084</b>	Test Data

**LOAD CASE NO 05**

1	Young's Modulus	2.10E+02	kN/mm <sup>2</sup>		
2	Brace OD (d)	16	(in) =	406.4	(mm)
3	Brace WT (t)	3/8	(in) =	9.5	(mm)
4	Chord OD (D)	18	(in) =	457.2	(mm)
5	Chord WT (T)	3/8	(in) =	9.5	(mm)
6	Brace-Chord Angle	60	deg	1.047	(Rad)
7	Gap (g)	2 1/6	(in) =	55.0	(mm)
8	Brace Length ( <i>l<sub>b</sub></i> )			777	(mm, clamp to crown, long)
				543	(mm, clamp to crown, short)
				803	(mm, clamp to saddle)
				660	(mm, average clamp to crown)
9	Brace Area ( <i>A<sub>b</sub></i> )	18.41	(in <sup>2</sup> ) =	11,876.0	(mm <sup>2</sup> )
10	Brace M.O.I. ( <i>I<sub>b</sub></i> )	562.08	(in <sup>4</sup> ) =	233,957,073	(mm <sup>4</sup> )
11	Chord Length ( <i>l<sub>c</sub></i> )			3,056.0	(mm)
12	Chord Area ( <i>A<sub>c</sub></i> )	20.76	(in <sup>2</sup> ) =	13,396.1	(mm <sup>2</sup> )
13	Chord M.O.I. ( <i>I<sub>c</sub></i> )	806.63	(in <sup>4</sup> ) =	335,745,310	(mm <sup>4</sup> )
14	Applied Load (P)			300	(kN)

Geometric Properties	
$\beta = d/D =$	0.89
$\xi = g/D =$	0.12
$\tau = t/T =$	1.00
$\gamma = D/2T =$	24.00

Theoretical calculations	
117.32	777.4
117.32	542.7
104.73	803.1

$\delta_r =$ overall displacement	Beam theory	
$\delta_f =$ displacement due to local joint flexibility	Chord lateral displacement	2.159 (mm)
$\delta_c =$ elastic displacement of chord (use component in the direction of brace)	Chord displacement in brace direction	1.870 (mm)
$\delta_e =$ elastic displacement of brace	Elastic displacement of brace	0.079 (mm)

Load Case	Description	$\delta_r / P$ (mm/kN)	$\delta_c / P$ (mm/kN)	$\delta_e / P$ (mm/kN)	$\delta_f / P$ (mm/kN)	
5	Compression in one	-0.0097	-0.0062	-0.0003	-0.0032	FE Analysis
	Brace	0.0135	0.0093	0.0003	0.0039	Test Data

LOAD CASE NO 06									
1	Young's Modulus	2.10E+02	kN/mm <sup>2</sup>			Geometric Properties			
2	Brace OD (d)	16	(in) =	406.4	(mm)	$\beta = d/D =$ 0.89			
3	Brace WT (t)	3/8	(in) =	9.5	(mm)	$\xi = g/D =$ 0.12			
4	Chord OD (D)	18	(in) =	457.2	(mm)	$\tau = t/T =$ 1			
5	Chord WT (T)	3/8	(in) =	9.5	(mm)	$\gamma = D/2T =$ 24.00			
6	Brace-Chord Angle	60	deg	1.047	(Rad)				
7	Gap (g)	2 1/6	(in) =	55.0	(mm)	Theoretical calculations			
8	Brace Length ( <i>l<sub>b</sub></i> )			777	(mm, clamp to crown, long)	117.32	777.4		
				543	(mm, clamp to crown, short)	117.32	542.7		
				803	(mm, clamp to saddle)	104.73	803.1		
				660	(mm, average clamp to crown)				
9	Brace Area ( <i>A<sub>b</sub></i> )	18.41	(in <sup>2</sup> ) =	11,876.0	(mm <sup>2</sup> )				
10	Brace M.O.I. ( <i>I<sub>b</sub></i> )	562.08	(in <sup>4</sup> ) =	233,957,073	(mm <sup>4</sup> )	For B1 Load	For B2 Load		
11	Chord Length ( <i>l<sub>c</sub></i> )			3,056.0	(mm)	a	1398	1658	
12	Chord Area ( <i>A<sub>c</sub></i> )	20.76	(in <sup>2</sup> ) =	13,396.1	(mm <sup>2</sup> )	b	1658	1398	
13	Chord M.O.I. ( <i>I<sub>c</sub></i> )	806.63	(in <sup>4</sup> ) =	335,745,310	(mm <sup>4</sup> )				
14	Applied Load (P)			300	(kN)				
15	Applied Moment (M)			277.2	(kN*m)				
$\phi_r =$ overall rotation = $\delta_r / l$			Beam theory			B1 Load	B2 Load	B1 & B2 Load	
$\phi_f =$ rotation due to local joint flexibility			Chord rotation at B1 (rad), where x=			1398	1.02298E-06	-5.11875E-07	5.11102E-07
$\phi_c =$ elastic rotation of chord			Chord rotation at B2 (rad), where x=			1658	5.11875E-07	-1.02298E-06	-5.11102E-07
$\phi_e =$ elastic rotation of brace = $\delta_e / l$			Elastic end displacement of brace (mm)				0.797		
Load Case	Description	$\phi_r / M$ (rad/kN-m)	$\phi_c / M$ (rad/kN-m)	$\delta_e / P$ (mm/kN)	$\delta_f / P$ (mm/kN)				
6	Balanced IPB	3.164E-05	1.844E-09	3.930E-06	2.771E-05	FE Analysis			
	Brace 1 (B1)	3.21E-05	0.00E+00	5.02E-06	2.71E-05	Test Data			
	Balanced IPB	3.164E-05	1.844E-09	3.930E-06	2.771E-05	FE Analysis			
	Brace 2 (B2)	2.82E-05	0.00E+00	5.02E-06	2.32E-05	Test Data			

LOAD CASE NO 07							
1	Young's Modulus	2.10E+02	kN/mm <sup>2</sup>			Geometric Properties	
2	Brace OD (d)	16	(in) =	406.4	(mm)		$\beta = d/D =$ 0.89
3	Brace WT (t)	3/8	(in) =	9.5	(mm)	$\xi = g/D =$ 0.12	
4	Chord OD (D)	18	(in) =	457.2	(mm)	$\tau = t/T =$ 1.00	
5	Chord WT (T)	3/8	(in) =	9.5	(mm)	$\gamma = D/2T =$ 24.00	
6	Brace-Chord Angle ( $\alpha$ )	60	deg	1.047	(Rad)		
7	Gap (g)	2 1/6	(in) =	55.0	(mm)	Theoretical calculations	
8	Brace Length ( $l_b$ )			777	(mm, clamp to crown, long)	117.32	777.4
				543	(mm, clamp to crown, short)	117.32	542.7
				803	(mm, clamp to saddle)	104.73	803.1
				660	(mm, average clamp to crown)		
9	Brace Area ( $A_b$ )	18.41	(in <sup>2</sup> ) =	11,876.0	(mm <sup>2</sup> )		
10	Brace M.O.I. ( $I_b$ )	562.08	(in <sup>4</sup> ) =	233,957,073	(mm <sup>4</sup> )	For B1 Load	
11	Chord Length ( $l_c$ )			3,056.0	(mm)	a 1398	
12	Chord Area ( $A_c$ )	20.76	(in <sup>2</sup> ) =	13,396.1	(mm <sup>2</sup> )	b 1658	
13	Chord M.O.I. ( $I_c$ )	806.63	(in <sup>4</sup> ) =	335,745,310	(mm <sup>4</sup> )	For B2 Load	
14	Applied Load (P)			300	(kN)	1658	
15	Applied Moment (M)			277.2	(kN*m)	1398	
$\phi_r$ = overall rotation = $\delta_r / l$ $\phi_f$ = rotation due to local joint flexibility $\phi_c$ = elastic rotation of chord $\phi_e$ = elastic rotation of brace = $\delta_e / l$				Beam theory			B2 Load
				Chord rotation at B1 (rad), where x=			1398
				Chord rotation at B2 (rad), where x=			1658
				Elastic end displacement of brace (mm)			0.797
Load Case	Description	$\phi_r / M$ (rad/kN-m)	$\phi_c / M$ (rad/kN-m)	$\delta_e / P$ (mm/kN)	$\delta_f / P$ (mm/kN)		
7	IPB in one brace	3.467E-06	-1.847E-09	0.000E+00	3.469E-06	FE Analysis	
	Brace 1 (B1)	1.81E-05	1.05E-05	0.00E+00	7.57E-06	Test Data	
	IPB in one brace	3.405E-05	3.690E-09	3.930E-06	3.012E-05	FE Analysis	
	Brace 2 (B2)	5.31E-05	1.05E-05	5.02E-06	3.76E-05	Test Data	

LOAD CASE NO 08																								
1	Young's Modulus	2.10E+02	kN/mm <sup>2</sup>			<table border="1"> <tr> <th colspan="2">Geometric Properties</th> </tr> <tr> <td><math>\beta = d/D =</math></td> <td>0.89</td> </tr> <tr> <td><math>\xi = g/D =</math></td> <td>0.12</td> </tr> <tr> <td><math>\tau = t/T =</math></td> <td>1.00</td> </tr> <tr> <td><math>\gamma = D/2T =</math></td> <td>24.00</td> </tr> <tr> <th colspan="2">Theoretical calculations</th> </tr> <tr> <td>117.32</td> <td>777.4</td> </tr> <tr> <td>117.32</td> <td>542.7</td> </tr> <tr> <td>104.73</td> <td>803.1</td> </tr> </table>	Geometric Properties		$\beta = d/D =$	0.89	$\xi = g/D =$	0.12	$\tau = t/T =$	1.00	$\gamma = D/2T =$	24.00	Theoretical calculations		117.32	777.4	117.32	542.7	104.73	803.1
Geometric Properties																								
$\beta = d/D =$	0.89																							
$\xi = g/D =$	0.12																							
$\tau = t/T =$	1.00																							
$\gamma = D/2T =$	24.00																							
Theoretical calculations																								
117.32	777.4																							
117.32	542.7																							
104.73	803.1																							
2	Brace OD (d)	16	(in) =	406.4	(mm)																			
3	Brace WT (t)	3/8	(in) =	9.5	(mm)																			
4	Chord OD (D)	18	(in) =	457.2	(mm)																			
5	Chord WT (T)	3/8	(in) =	9.5	(mm)																			
6	Brace-Chord Angle	60	deg	1.047	(Rad)																			
7	Gap (g)	2 1/6	(in) =	55.0	(mm)																			
8	Brace Length ( $l_b$ )			777	(mm, clamp to crown, long)																			
				543	(mm, clamp to crown, short)																			
				803	(mm, clamp to saddle)																			
				660	(mm, average clamp to crown)																			
9	Brace Area ( $A_b$ )	18.41	(in <sup>2</sup> ) =	11,876.0	(mm <sup>2</sup> )	<table border="1"> <tr> <td></td> <td>For B1 Load</td> <td>For B2 Load</td> </tr> <tr> <td>a</td> <td>1398</td> <td>1658</td> </tr> <tr> <td>b</td> <td>1658</td> <td>1398</td> </tr> </table>		For B1 Load	For B2 Load	a	1398	1658	b	1658	1398									
	For B1 Load	For B2 Load																						
a	1398	1658																						
b	1658	1398																						
10	Brace M.O.I. ( $I_b$ )	562.08	(in <sup>4</sup> ) =	233,957,073	(mm <sup>4</sup> )																			
11	Chord Length ( $l_c$ )			3,056.0	(mm)																			
12	Chord Area ( $A_c$ )	20.76	(in <sup>2</sup> ) =	13,396.1	(mm <sup>2</sup> )																			
13	Chord M.O.I. ( $I_c$ )	806.63	(in <sup>4</sup> ) =	335,745,310	(mm <sup>4</sup> )																			
14	Applied Load (P)			300	(kN)																			
15	Applied Moment (M)			277.2	(kN*m)																			
$\phi_r = \text{overall rotation} = \delta_r / l$ $\phi_f = \text{rotation due to local joint flexibility}$ $\phi_c = \text{elastic rotation of chord}$ $\phi_e = \text{elastic rotation of brace} = \delta_e / l$			Beam theory Chord rotation at B1 (rad), where x= 1398 Chord rotation at B2 (rad), where x= 1658 Elastic end displacement of brace (mm)			<table border="1"> <tr> <td>B1 Load</td> <td>B2 Load</td> <td>B1 &amp; B2 Load</td> </tr> <tr> <td>1.02298E-06</td> <td>5.11875E-07</td> <td>1.53485E-06</td> </tr> <tr> <td>5.11875E-07</td> <td>1.02298E-06</td> <td>1.53485E-06</td> </tr> <tr> <td colspan="3">0.797</td> </tr> </table>	B1 Load	B2 Load	B1 & B2 Load	1.02298E-06	5.11875E-07	1.53485E-06	5.11875E-07	1.02298E-06	1.53485E-06	0.797								
B1 Load	B2 Load	B1 & B2 Load																						
1.02298E-06	5.11875E-07	1.53485E-06																						
5.11875E-07	1.02298E-06	1.53485E-06																						
0.797																								
Load Case	Description	$\phi_r / M$ (rad/kN-m)	$\phi_c / M$ (rad/kN-m)	$\delta_e / P$ (mm/kN)	$\delta_f / P$ (mm/kN)																			
8	Unbalanced IPB	3.666E-05	5.537E-09	3.930E-06	3.272E-05	FE Analysis																		
	Brace 1 (B1)	6.01E-05	1.40E-05	5.02E-06	4.11E-05	Test Data																		
	Unbalanced IPB	3.666E-05	5.537E-09	3.930E-06	3.272E-05	FE Analysis																		
	Brace 2 (B2)	6.89E-05	1.50E-05	5.02E-06	4.89E-05	Test Data																		

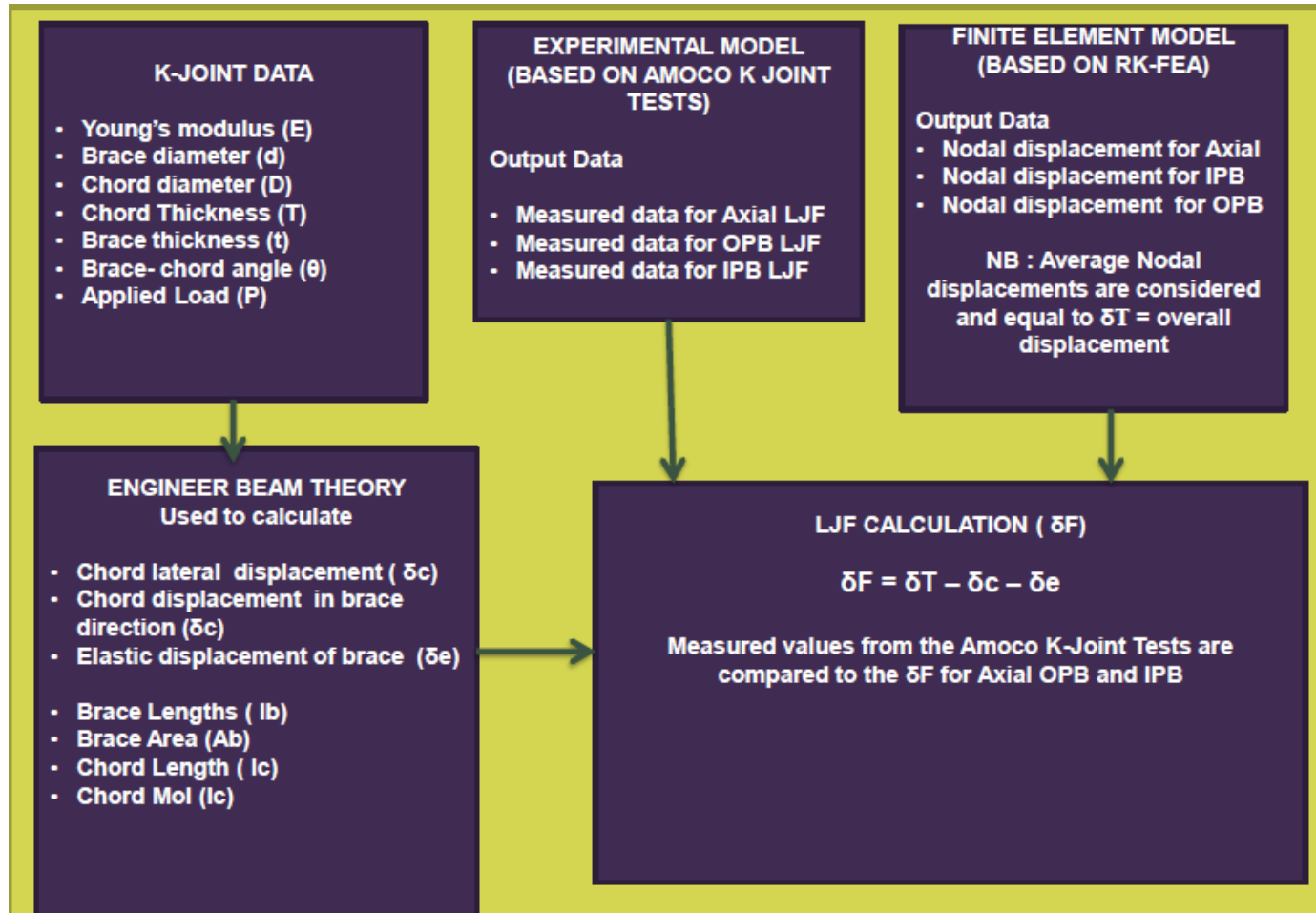
LOAD CASE NO 09								
1	Young's Modulus	2.10E+02	kN/mm <sup>2</sup>			Geometric Properties		
2	Brace OD (d)	16	(in) =	406.4	(mm)	b = d/D =	0.89	
3	Brace WT (t)	3/8	(in) =	9.5	(mm)	x = g/D =	0.12	
4	Chord OD (D)	18	(in) =	457.2	(mm)	t = t/T =	1.00	
5	Chord WT (T)	3/8	(in) =	9.5	(mm)	g= D/2T =	24.00	
6	Brace-Chord Angle	60	Deg	1.047	(Rad)			
7	Gap (g)	2 1/6	(in) =	55.0	(mm)	Theoretical calculations		
8	Brace Length ( <i>l<sub>b</sub></i> )			777	(mm, clamp to crown, long)	117.32	777.4	
				543	(mm, clamp to crown, short)	117.32	542.7	
				803	(mm, clamp to saddle)	104.73	803.1	
				660	(mm, average clamp to crown)			
9	Brace Area ( <i>A<sub>b</sub></i> )	18.41	(in <sup>2</sup> ) =	11,876.0	(mm <sup>2</sup> )			
10	Brace M.O.I. ( <i>I<sub>b</sub></i> )	562.08	(in <sup>4</sup> ) =	233,957,073	(mm <sup>4</sup> )		For B1 Load For B2 Load	
11	Chord Length ( <i>l<sub>c</sub></i> )			3,056.0	(mm)	a	1398 1658	
12	Chord Area ( <i>A<sub>c</sub></i> )	20.76	(in <sup>2</sup> ) =	13,396.1	(mm <sup>2</sup> )	b	1658 1398	
13	Chord M.O.I. ( <i>I<sub>c</sub></i> )	806.63	(in <sup>4</sup> ) =	335,745,310	(mm <sup>4</sup> )			
14	Applied Load (P)			60	(kN)			
15	Applied Moment (M)			39.6	(kN*m)			
$\phi_T = \text{overall rotation} = \delta_T / l$						B1 Load	B2 Load	B1 & B2 Load
$\phi_F = \text{rotation due to local joint flexibility}$		Chord rotation at B1 (rad), where x=				1398	4.26358E-03	3.40658E-03 7.67016E-03
$\phi_c = \text{elastic rotation of chord}$		Chord rotation at B2 (rad), where x=				1658	3.40658E-03	4.26358E-03 7.67016E-03
$\phi_e = \text{elastic rotation of brace} = \delta_e / l$		Elastic end displacement of brace (mm)				0.159		
Load Case	Description	$\phi_T / M$ (rad/kN-m)	$\phi_c / M$ (rad/kN-m)	$\delta_c / P$ (mm/kN)	$\delta_F / P$ (mm/kN)			
9	Unbalanced OPB	2.210E-04	2.557E-05	5.501E-06	1.899E-04	FE Analysis		
	Brace 1 (B1)	4.35E-04	2.55E-04	5.02E-06	1.75E-04	Test Data		
	Unbalanced OPB	2.210E-04	2.557E-05	5.501E-06	1.899E-04	FE Analysis		
	Brace 2 (B2)	4.47E-04	2.78E-04	5.02E-06	1.64E-04	Test Data		

LOAD CASE NO 10																								
1	Young's Modulus	2.10E+02	kN/mm <sup>2</sup>			<table border="1"> <thead> <tr> <th colspan="2">Geometric Properties</th> </tr> </thead> <tbody> <tr> <td><math>\beta = d/D =</math></td> <td>0.89</td> </tr> <tr> <td><math>\xi = g/D =</math></td> <td>0.12</td> </tr> <tr> <td><math>\tau = t/T =</math></td> <td>1</td> </tr> <tr> <td><math>\gamma = D/2T =</math></td> <td>24.00</td> </tr> <tr> <th colspan="2">Theoretical calculations</th> </tr> <tr> <td></td> <td>117.32</td> </tr> <tr> <td></td> <td>117.32</td> </tr> <tr> <td></td> <td>104.73</td> </tr> </tbody> </table>	Geometric Properties		$\beta = d/D =$	0.89	$\xi = g/D =$	0.12	$\tau = t/T =$	1	$\gamma = D/2T =$	24.00	Theoretical calculations			117.32		117.32		104.73
Geometric Properties																								
$\beta = d/D =$	0.89																							
$\xi = g/D =$	0.12																							
$\tau = t/T =$	1																							
$\gamma = D/2T =$	24.00																							
Theoretical calculations																								
	117.32																							
	117.32																							
	104.73																							
2	Brace OD (d)	16	(in) =	406.4	(mm)																			
3	Brace WT (t)	3/8	(in) =	9.5	(mm)																			
4	Chord OD (D)	18	(in) =	457.2	(mm)																			
5	Chord WT (T)	3/8	(in) =	9.5	(mm)																			
6	Brace-Chord Angle	60	Deg	1.047	(Rad)																			
7	Gap (g)	2 1/6	(in) =	55.0	(mm)																			
8	Brace Length ( $l_b$ )			777	(mm, clamp to crown, long)																			
				543	(mm, clamp to crown, short)																			
				803	(mm, clamp to saddle)																			
				660	(mm, average clamp to crown)																			
9	Brace Area ( $A_b$ )	18.41	(in <sup>2</sup> ) =	11,876.0	(mm <sup>2</sup> )	<table border="1"> <thead> <tr> <th></th> <th>For B1 Load</th> <th>For B2 Load</th> </tr> </thead> <tbody> <tr> <td>a</td> <td>1398</td> <td>1658</td> </tr> <tr> <td>b</td> <td>1658</td> <td>1398</td> </tr> </tbody> </table>		For B1 Load	For B2 Load	a	1398	1658	b	1658	1398									
	For B1 Load	For B2 Load																						
a	1398	1658																						
b	1658	1398																						
10	Brace M.O.I. ( $I_b$ )	562.08	(in <sup>4</sup> ) =	233,957,073	(mm <sup>4</sup> )																			
11	Chord Length ( $l_c$ )			3,056.0	(mm)																			
12	Chord Area ( $A_c$ )	20.76	(in <sup>2</sup> ) =	13,396.1	(mm <sup>2</sup> )																			
13	Chord M.O.I. ( $I_c$ )	806.63	(in <sup>4</sup> ) =	335,745,310	(mm <sup>4</sup> )																			
14	Applied Load (P)			60	(kN)																			
15	Applied Moment (M)			39.6	(kN*m)																			
$\phi_r = \text{overall rotation} = \delta_r / l$ $\phi_f = \text{rotation due to local joint flexibility}$ $\phi_c = \text{elastic rotation of chord}$ $\phi_e = \text{elastic rotation of brace} = \delta_e / l$				Chord rotation at B1 (rad), where x= Chord rotation at B2 (rad), where x= Elastic end displacement of brace (mm)		<table border="1"> <thead> <tr> <th></th> <th>B1 Load</th> <th>B2 Load</th> </tr> </thead> <tbody> <tr> <td></td> <td>1398</td> <td>3.40658E-03</td> </tr> <tr> <td></td> <td>1658</td> <td>4.26358E-03</td> </tr> <tr> <td></td> <td></td> <td>0.159</td> </tr> </tbody> </table>		B1 Load	B2 Load		1398	3.40658E-03		1658	4.26358E-03			0.159						
	B1 Load	B2 Load																						
	1398	3.40658E-03																						
	1658	4.26358E-03																						
		0.159																						
Load Case	Description	$\phi_r / M$ (rad/kN-m)	$\phi_c / M$ (rad/kN-m)	$\delta_e / P$ (mm/kN)	$\delta_f / P$ (mm/kN)																			
10	OPB in one brace	<b>9.092E-05</b>	<b>1.136E-05</b>	<b>5.501E-06</b>	<b>7.406E-05</b>	FE Analysis																		
	Brace 1 (B1)	<b>2.16E-04</b>	<b>1.04E-04</b>	<b>0.00E+00</b>	<b>1.12E-04</b>	Test Data																		
	OPB in one brace	<b>1.301E-04</b>	<b>1.421E-05</b>	<b>5.501E-06</b>	<b>1.104E-04</b>	FE Analysis																		
	Brace 2 (B2)	<b>2.41E-04</b>	<b>1.15E-04</b>	<b>5.02E-06</b>	<b>1.21E-04</b>	Test Data																		



## APPENDIX 5 - Sample Calculations for LJF for AXIAL, IPB, OPB

(for  $\beta = 0.5$  and  $\theta = 30$ ,  $\gamma = 8-30$  Case)



Appendix 4 Figure 1 LJF Calculation Methodology

$\beta$	$\theta$		$\gamma$						
0.5	30		8	10	15	20	25	30	
	All LJF values extracted from the FEA analysis  $\delta_T/P$	Axial	-5.3524E-04	-6.0584E-04	-8.0488E-04	-1.0282E-03	-1.2726E-03	-1.5384E-03	
			5.3524E-04	6.0585E-04	8.0490E-04	1.0283E-03	1.2726E-03	1.5384E-03	
		IPB	-1.2795E-03	-1.8635E-03	-3.6940E-03	-5.7723E-03	-7.9806E-03	-1.0329E-02	
				-1.8302E-02	-2.1506E-02	-3.0842E-02	-4.1502E-02	-5.3291E-02	-6.6237E-02
		OPB	-2.2355E-03	-4.2806E-03	-1.2912E-02	-2.6631E-02	-4.5385E-02	-6.9304E-02	
				-1.8619E-02	-2.3307E-02	-4.0249E-02	-6.4019E-02	-9.4163E-02	-1.3084E-01
Brace OD	228.5			g	55				
lmin & lmax	259.113195	654.886804		a	1856				
1	457			b	1344				
				x1	1344	x2	1856		

### 1. Axial

Total tension		Balanced					
$\gamma$		8	10	15	20	25	30
Brace 1	$\delta_T/P$	-5.3524E-04	-6.0584E-04	-8.0488E-04	-1.0282E-03	-1.2726E-03	-1.5384E-03
Brace 2	$\delta_T/P$	5.3524E-04	6.0585E-04	8.0490E-04	1.0283E-03	1.2726E-03	1.5384E-03

<b>Chord elastic rotation</b>	<b>Balanced</b>					
<b>Beam theory</b>						
$\gamma$	<b>8</b>	<b>10</b>	<b>15</b>	<b>20</b>	<b>25</b>	<b>30</b>
Chord OD(mm)	457	457	457	457	457	457
Thickness (mm)	28.5625	22.85	15.23333333	11.425	9.14	7.616666667
$\theta$	30	30	30	30	30	30
E(KN/mm <sup>2</sup> )	210	210	210	210	210	210
I(mm <sup>4</sup> )	886021893.9	736320471	516356628.6	397158608.2	322562407.4	271519148.4
P <sub>y</sub> (KN) at x2	-0.5	-0.5	-0.5	-0.5	-0.5	-0.5
a(mm)	1856	1856	1856	1856	1856	1856
b(mm)	1344	1344	1344	1344	1344	1344
L(mm)	3200	3200	3200	3200	3200	3200
x1(mm)	1344	1344	1344	1344	1344	1344
x2(mm)	1856	1856	1856	1856	1856	1856
unbalanced displ1(mm)	0.001675491	0.002016135	0.002874993	0.003737855	0.004602277	0.005467465
unbalanced displ2(mm)	0.001741765	0.002095883	0.002988713	0.003885706	0.00478432	0.005683731
Chord 1 (mm) $\delta_c$	-3.3137E-05	-3.98741E-05	-5.68602E-05	-7.39254E-05	-9.10215E-05	-0.000108133
Chord 2 (mm) $\delta_c$	3.3137E-05	3.98741E-05	5.68602E-05	7.39254E-05	9.10215E-05	0.000108133

Brace elastic tension		Balanced					
$\gamma$		8	10	15	20	25	30
Brace OD(mm)		228.5	228.5	228.5	228.5	228.5	228.5
Thickness (mm)		9.5	9.5	9.5	9.5	9.5	9.5
$\theta$		30	30	30	30	30	30
E(KN/mm <sup>2</sup> )		210	210	210	210	210	210
A(mm <sup>2</sup> )		6536.083516	6536.083516	6536.083516	6536.083516	6536.083516	6536.083516
I(mm)		456.9999995	456.9999995	456.9999995	456.9999995	456.9999995	456.9999995
F(KN)		1	1	1	1	1	1
Chord 1	$\delta_e/P$	-0.00033295	-0.00033295	-0.00033295	-0.00033295	-0.00033295	-0.00033295
Chord 2	$\delta_e/P$	0.00033295	0.00033295	0.00033295	0.00033295	0.00033295	0.00033295

Axial LJF	Balanced				LJF
$\gamma$		$\delta_T/P$	$\delta_c/P$	$\delta_e/P$	$\delta_F/P$
8	brace1	-0.000535235	-3.3137E-05	-0.00033295	-0.000169148
	brace2	0.000535239	3.3137E-05	0.00033295	0.000169152
10	brace1	-0.000605842	-3.9874E-05	-0.00033295	-0.000233017
	brace2	0.000605849	3.9874E-05	0.00033295	0.000233025
15	brace1	-0.000804881	-5.68602E-05	-0.00033295	-0.00041507
	brace2	0.000804896	5.68602E-05	0.00033295	0.000415086
20	brace1	-0.001028231	-7.39254E-05	-0.00033295	-0.000621355
	brace2	0.001028259	7.39254E-05	0.00033295	0.000621383
25	brace1	-0.001272556	-9.10215E-05	-0.00033295	-0.000848584
	brace2	0.001272596	9.10215E-05	0.00033295	0.000848624
30	brace1	-0.001538358	-0.000108133	-0.00033295	-0.001097275
	brace2	0.001538416	0.000108133	0.00033295	0.001097333

## 2. IPB Unbalanced

IPB unbalanced							
Total rotation		Moment on brace 2					
$\gamma$		8	10	15	20	25	30
l (mm)		456.9999995	456.9999995	456.9999995	456.9999995	456.9999995	456.9999995
M (KN·m)		1	1	1	1	1	1
Brace2 (rad) $\delta_T$		-1.2795E-03	-1.8635E-03	-3.6940E-03	-5.7723E-03	-7.9806E-03	-1.0329E-02
Brace2 (rad) $\delta_T$		-1.8302E-02	-2.1506E-02	-3.0842E-02	-4.1502E-02	-5.3291E-02	-6.6237E-02
Brace1 (rad/KN-m) $\delta_T/IM$		2.79987E-06	4.07775E-06	8.0831E-06	1.26308E-05	1.7463E-05	2.26007E-05
Brace2 (rad/KN-m) $\delta_T/IM$		4.00477E-05	4.70598E-05	6.74886E-05	9.08138E-05	0.000116611	0.000144939

Chord elastic rotation	Moment on brace 2					
Beam theory						
$\gamma$	8	10	15	20	25	30
Chord OD(mm)	457	457	457	457	457	457
Thickness(mm)	28.5625	22.85	15.23333333	11.425	9.14	7.616666667
$\theta(^{\circ})$	30	30	30	30	30	30
E(KN/mm <sup>2</sup> )	210	210	210	210	210	210
I(mm <sup>4</sup> )	886021893.9	736320471	516356628.6	397158608.2	322562407.4	271519148.4
M <sub>z</sub> (KN-mm)	1000	1000	1000	1000	1000	1000
a(mm)	1856	1856	1856	1856	1856	1856
b(mm)	1344	1344	1344	1344	1344	1344
L(mm)	3200	3200	3200	3200	3200	3200
x1(mm)	1344	1344	1344	1344	1344	1344
x2(mm)	1856	1856	1856	1856	1856	1856

$\phi_c$ Chord 1 (rad)	1.67397E-07	2.01431E-07	2.87238E-07	3.73446E-07	4.5981E-07	5.4625E-07
$\phi_c$ Chord 2 (rad)	1.54326E-06	1.85702E-06	2.6481E-06	3.44287E-06	4.23907E-06	5.03598E-06
$\phi_c/M$ Chord1 (rad/KN-m)	1.67397E-07	2.01431E-07	2.87238E-07	3.73446E-07	4.5981E-07	5.4625E-07
$\phi_c/M$ Chord2 (rad/KN-m)	1.54326E-06	1.85702E-06	2.6481E-06	3.44287E-06	4.23907E-06	5.03598E-06

Brace elastic rotation	Moment on brace 2						
	$\gamma$	8	10	15	20	25	30
Brace OD(mm)		228.5	228.5	228.5	228.5	228.5	228.5
Thickness (mm)		9.5	9.5	9.5	9.5	9.5	9.5
$\theta(^{\circ})$		30	30	30	30	30	30
E(KN/mm <sup>2</sup> )		210	210	210	210	210	210
I(mm <sup>4</sup> )		39258372.88	39258372.88	39258372.88	39258372.88	39258372.88	39258372.88
M <sub>z</sub> (KN-mm)		-1000	-1000	-1000	-1000	-1000	-1000
x(mm)		456.9999995	456.9999995	456.9999995	456.9999995	456.9999995	456.9999995
$\delta_e$ Brace 1 (rad)		0	0	0	0	0	0
$\delta_e$ Brace 2 (rad)		0.01266633	0.01266633	0.01266633	0.01266633	0.01266633	0.01266633
$\delta_e/IM$ Brace 1 (rad/KN-m)		0.0000E+00	0.0000E+00	0.0000E+00	0.0000E+00	0.0000E+00	0.0000E+00
$\delta_e/IM$ Brace 2 (rad/KN-m)		2.7716E-05	2.7716E-05	2.7716E-05	2.7716E-05	2.7716E-05	2.7716E-05

<b>In-plane LJF</b>	<b>Moment on brace 2</b>				
$\gamma$		$\delta_T/IM$	$\phi_c/M$	$\delta_e/IM$	$\delta_F/IM$
		<b>FEA</b>	<b>Beam Theory</b>	<b>Beam Theory</b>	<b>LJF</b>
8	brace1	2.79987E-06	1.67397E-07	0	2.63248E-06
	brace2	4.00477E-05	1.54326E-06	2.77163E-05	1.07882E-05
10	brace1	4.07775E-06	2.0143E-07	0	3.87632E-06
	brace2	4.70598E-05	1.8570E-06	2.77163E-05	1.74865E-05
15	brace1	8.0831E-06	2.87238E-07	0	7.79586E-06
	brace2	6.74886E-05	2.6481E-06	2.77163E-05	3.71242E-05
20	brace1	1.26308E-05	3.73446E-07	0	1.22574E-05
	brace2	9.08138E-05	3.44287E-06	2.77163E-05	5.96547E-05
25	brace1	1.7463E-05	4.5981E-07	0	1.70032E-05
	brace2	0.000116611	4.23907E-06	2.77163E-05	8.46562E-05
30	brace1	2.26007E-05	5.4625E-07	0	2.20544E-05
	brace2	0.000144939	5.03598E-06	2.77163E-05	0.000112186

### 3. OPB Unbalanced

Total torsion	Moment on brace 2						
	$\gamma$	8	10	15	20	25	30
l (mm)		228.5	228.5	228.5	228.5	228.5	228.5
M (KN·m)		1	1	1	1	1	1
$\delta_T$ Brace 1 (rad)		-2.2355E-03	-4.2806E-03	-1.2912E-02	-2.6631E-02	-4.5385E-02	-6.9304E-02
$\delta_T$ Brace 2(rad)		-1.8619E-02	-2.3307E-02	-4.0249E-02	-6.4019E-02	-9.4163E-02	-1.3084E-01
$\delta_T/IM$ Brace 1 (rad/KN-m)		9.78345E-06	1.87334E-05	5.65059E-05	0.000116547	0.000198621	0.0003033
$\delta_T/IM$ Brace2 (rad/KN-m)		8.14844E-05	0.000102	0.000176144	0.000280169	0.000412094	0.000572595

Chord elastic torsion	Moment on brace 2							
	Torsion theory	$\gamma$	8	10	15	20	25	30
Chord OD(mm)			457	457	457	457	457	457
Thickness (mm)			28.5625	22.85	15.23333333	11.425	9.14	7.616666667
$\theta(^{\circ})$			30	30	30	30	30	30
E(KN/mm <sup>2</sup> )			210	210	210	210	210	210
$\mu$			0.3	0.3	0.3	0.3	0.3	0.3
G(KN/mm <sup>2</sup> )			80.76923077	80.76923077	80.76923077	80.76923077	80.76923077	80.76923077
$I_p(\text{mm}^4)$			1772043788	1472640942	1032713257	794317216.5	645124814.8	543038296.8
$T_x(\text{KN-mm})$			500	500	500	500	500	500
a(mm)			1856	1856	1856	1856	1856	1856

b(mm)	1344	1344	1344	1344	1344	1344
L(mm)	3200	3200	3200	3200	3200	3200
T <sub>a</sub>	-210	-210	-210	-210	-210	-210
T <sub>b</sub>	-290	-290	-290	-290	-290	-290
x1(mm)	1344	1344	1344	1344	1344	1344
x2(mm)	1856	1856	1856	1856	1856	1856
$\phi_c$ Chord 1 (rad)	1.97196E-06	2.37288E-06	3.38371E-06	4.39925E-06	5.41663E-06	6.43491E-06
$\phi_c$ Chord 2 (rad)	2.72318E-06	3.27683E-06	4.67274E-06	6.07515E-06	7.4801E-06	8.8863E-06
$\phi_c/M$ Chord 1 (rad/KN-m)	1.97196E-06	2.37288E-06	3.38371E-06	4.39925E-06	5.41663E-06	6.43491E-06
$\phi_c/M$ Chord 2 (rad/KN-m)	2.72318E-06	3.27683E-06	4.67274E-06	6.07515E-06	7.4801E-06	8.8863E-06

Brace elastic rotation	Moment on brace 2					
	8	10	15	20	25	30
$\gamma$						
Brace OD(mm)	228.5	228.5	228.5	228.5	228.5	228.5
Thickness (mm)	9.5	9.5	9.5	9.5	9.5	9.5
$\theta$ (°)	30	30	30	30	30	30
E(KN/mm <sup>2</sup> )	210	210	210	210	210	210
I (mm <sup>4</sup> )	39258372.88	39258372.88	39258372.88	39258372.88	39258372.88	39258372.88
M <sub>x</sub> (KN-mm)	-1000	-1000	-1000	-1000	-1000	-1000
X (mm)	456.9999995	456.9999995	456.9999995	456.9999995	456.9999995	456.9999995

$\delta_e$ Brace 1 (rad)	0	0	0	0	0	0
$\delta_e$ Brace 2 (rad)	0.01266633	0.01266633	0.01266633	0.01266633	0.01266633	0.01266633
$\delta_e/IM$ Brace1 (rad/KN-m)	0.0000E+00	0.0000E+00	0.0000E+00	0.0000E+00	0.0000E+00	0.0000E+00
$\delta_e/IM$ Brace 2 (rad/KN-m)	5.5433E-05	5.5433E-05	5.5433E-05	5.5433E-05	5.5433E-05	5.5433E-05

$\gamma$	Out-of-Plane LJF	Moment on brace2		$\delta_e/IM$ Beam Theory	$\delta_F/IM$ LJF
		$\delta_T/IM$ FEA	$\phi_c/M$ Beam Theory		
8	brace1	9.78345E-06	1.97196E-06	0	7.81149E-06
	brace2	8.14844E-05	2.72318E-06	5.54325E-05	2.33287E-05
10	brace1	1.87334E-05	2.3729E-06	0	1.63605E-05
	brace2	0.000102	3.2768E-06	5.54325E-05	4.32906E-05
15	brace1	5.65059E-05	3.38371E-06	0	5.31222E-05
	brace2	0.000176144	4.67274E-06	5.54325E-05	0.000116039
20	brace1	0.000116547	4.39925E-06	0	0.000112148
	brace2	0.000280169	6.07515E-06	5.54325E-05	0.000218661
25	brace1	0.000198621	5.41663E-06	0	0.000193205
	brace2	0.000412094	7.4801E-06	5.54325E-05	0.000349181
30	brace1	0.0003033	6.43491E-06	0	0.000296865
	brace2	0.000572595	8.8863E-06	5.54325E-05	0.000508276

**4. Summary LJF Results for Axial, IPB and OPB for  $\beta = 0.5$  and  $\theta = 30$ ,  $\gamma = 8 - 30$**

$\gamma$		<b>Axial Balanced</b>	<b>IPB brace2</b>	<b>OPB brace2</b>
8	brace1	-1.6915E-04	2.6325E-06	7.8115E-06
	brace2	1.6915E-04	1.0788E-05	2.3329E-05
10	brace1	-2.3302E-04	3.8763E-06	1.6360E-05
	brace2	2.3302E-04	1.7486E-05	4.3291E-05
15	brace1	-4.1507E-04	7.7959E-06	5.3122E-05
	brace2	4.1509E-04	3.7124E-05	1.1604E-04
20	brace1	-6.2136E-04	1.2257E-05	1.1215E-04
	brace2	6.2138E-04	5.9655E-05	2.1866E-04
25	brace1	-8.4858E-04	1.7003E-05	1.9320E-04
	brace2	8.4862E-04	8.4656E-05	3.4918E-04
30	brace1	-1.0973E-03	2.2054E-05	2.9686E-04
	brace2	1.0973E-03	1.1219E-04	5.0828E-04

# APPENDIX 6 - USFOS Files for the Development of the K-Frame Analysis

## Validation of RK-LJF in BOMEL Frame VII Tests

```
*****
**** NODE COORDINATES ****
*****
NODE  1010    0.000    0.000    0.000 1 1 1
NODE  1020    5.944    0.000    0.000 1 1 1
NODE  1030    2.400    0.000    0.000
NODE  1040    3.544    0.000    0.000
NODE  2010    0.000    0.000    1.524
NODE  2011    1.599    0.000    1.524
NODE  2012    1.939    0.000    1.524
NODE  2020    5.944    0.000    1.524
NODE  2030    2.972    0.000    1.524
NODE  2031    2.619    0.000    2.047
NODE  2032    3.324    0.000    2.047
NODE  2110    2.057    0.000    3.039
NODE  2120    1.890    0.000    3.334
NODE  2210    5.147    0.000    5.291
NODE  2220    4.977    0.000    4.996
NODE  3010    0.000    0.000    6.672
NODE  3020    5.944    0.000    6.672
NODE  4010    0.000    0.000    8.196 0 1 0
NODE  4020    5.944    0.000    8.196 0 1 0
NODE  4030    2.400    0.000    8.196 0 1 0
NODE  4040    3.544    0.000    8.196 0 1 0
*****
**** BEAM ELEMENTS ****
*****
BEAM   1 2010 1030 1001 1001  0 20001 30001
ECCENT 20001 0.179000E+00 0.000000E+00 -0.231200E+00
ECCENT 30001 0.000000E+00 0.000000E+00 0.000000E+00
BEAM   2 2020 1040 1001 1001  0 20002 30002
ECCENT 20002 -0.179000E+00 0.000000E+00 -0.231200E+00
ECCENT 30002 0.000000E+00 0.000000E+00 0.000000E+00
BEAM   3 3010 4030 1001 1001  0 20003 30003
ECCENT 20003 0.179000E+00 0.000000E+00 0.231190E+00
ECCENT 30003 0.000000E+00 0.000000E+00 0.000000E+00
BEAM   4 3020 4040 1001 1001  0 20004 30004
ECCENT 20004 -0.179000E+00 0.000000E+00 0.231190E+00
ECCENT 30004 0.000000E+00 0.000000E+00 0.000000E+00
BEAM   5 4010 4030 1002 1002  0 0 0
BEAM   6 4030 4040 1002 1002  0 0 0
BEAM   7 4040 4020 1002 1002  0 0 0
BEAM   8 1010 1030 1003 1003  0 0 0
BEAM   9 1030 1040 1003 1003  0 0 0
BEAM  10 1040 1020 1003 1003  0 0 0
BEAM  11 2110 2031 1004 1004  0 0 0
BEAM  12 2220 2032 1004 1004  0 20012 30012
ECCENT 20012 0.342000E-02 0.000000E+00 -0.195000E-02
```

```

ECCENT 30012 0.000000E+00 0.000000E+00 0.000000E+00
BEAM 13 3010 2120 1004 1004 0 20013 30013
ECCENT 20013 0.179000E+00 0.000000E+00 -0.316200E+00
ECCENT 30013 0.000000E+00 0.000000E+00 0.000000E+00
BEAM 14 3020 2210 1004 1004 0 20014 30014
ECCENT 20014 -0.179000E+00 0.000000E+00 -0.316200E+00
ECCENT 30014 0.000000E+00 0.000000E+00 0.000000E+00
BEAM 15 2010 2011 1005 1005 0 20015 30015
ECCENT 20015 0.179000E+00 0.000000E+00 0.000000E+00
ECCENT 30015 0.000000E+00 0.000000E+00 0.000000E+00
BEAM 16 2012 2030 1005 1005 0 0 0
BEAM 17 2030 2020 1005 1005 0 20017 30017
ECCENT 20017 0.000000E+00 0.000000E+00 0.000000E+00
ECCENT 30017 -0.179000E+00 0.000000E+00 0.000000E+00
BEAM 18 3010 3020 1006 1006 0 20018 30018
ECCENT 20018 0.179000E+00 0.000000E+00 0.000000E+00
ECCENT 30018 -0.179000E+00 0.000000E+00 0.000000E+00
BEAM 19 2011 2012 1007 1007 0 0 0
BEAM 20 2120 2110 1007 1007 0 0 0
BEAM 21 2210 2220 1007 1007 0 20021 30021
ECCENT 20021 0.000000E+00 0.000000E+00 0.000000E+00
ECCENT 30021 0.342000E-02 0.000000E+00 -0.195000E-02
BEAM 22 1010 2010 1008 1008 0 0 0
BEAM 23 1020 2020 1008 1008 0 0 0
BEAM 24 2010 3010 1008 1008 0 0 0
BEAM 25 2020 3020 1008 1008 0 0 0
BEAM 26 3010 4010 1008 1008 0 0 0
BEAM 27 3020 4020 1008 1008 0 0 0
BEAM 28 2031 2030 1009 1009 0 20028 30028
ECCENT 20028 0.000000E+00 0.000000E+00 0.000000E+00
ECCENT 30028 -0.104900E+00 0.000000E+00 0.840000E-01
BEAM 29 2032 2030 1009 1009 0 20029 30029
ECCENT 20029 0.000000E+00 0.000000E+00 0.000000E+00
ECCENT 30029 0.104930E+00 0.000000E+00 0.840000E-01
*****
**** BEAM GEOMETRY ****
*****
PIPE 1001 0.168000E+00 0.710000E-02 !B01 168X7.1
IHPROFIL 1002 0.400000E+00 0.135000E-01 0.300000E+00 0.240000E-01 0.300000E+00 0.240000E-01
!C01 IH
IHPROFIL 1003 0.400000E+00 0.135000E-01 0.300000E+00 0.240000E-01 0.300000E+00 0.240000E-01
!C02 IH
PIPE 1004 0.168000E+00 0.450000E-02 !KB1 168X4.5
PIPE 1005 0.168000E+00 0.450000E-02 !KC1 168X4.5
PIPE 1006 0.168000E+00 0.450000E-02 !KC2 168X4.5
PIPE 1007 0.168000E+00 0.500000E-02 !KT1 168X5
PIPE 1008 0.358000E+00 0.127000E-01 !L01 358X12.
'PIPE 1009 0.168000E+00 0.450000E-02 !LJF 168X4.5
GENBEAM 1009 1.168656 7.73516E-06 4.95951E-06 2.77565E-06 9.21E-05 5.9E-05 3.3E-05 1.68656
1.168656 !LJF
*****
**** BEAM MATERIAL ****
*****

```

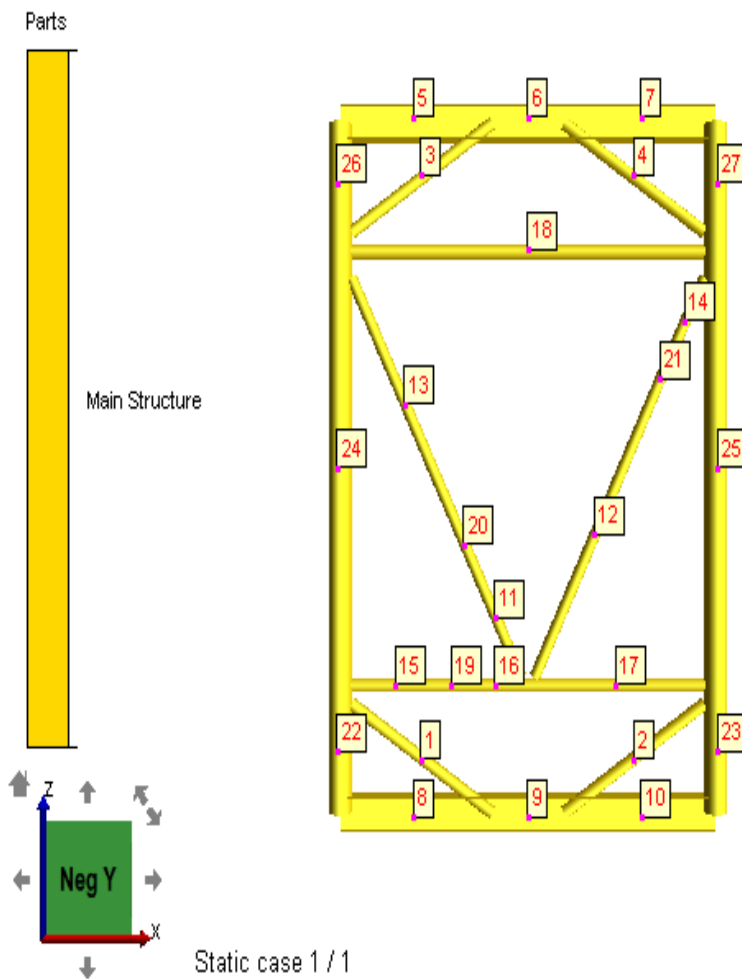
MISOIEP	1001	0.200000E+12	0.3	0.390700E+09	0.784900E+04	!B01
MISOIEP	1002	0.200000E+12	0.3	0.390700E+09	0.784900E+04	!C01
MISOIEP	1003	0.200000E+12	0.3	0.390700E+09	0.784900E+04	!C02
MISOIEP	1004	0.200000E+12	0.3	0.292000E+09	0.784900E+04	!KB1
MISOIEP	1005	0.200000E+12	0.3	0.292000E+09	0.784900E+04	!KC1
MISOIEP	1006	0.200000E+12	0.3	0.292000E+09	0.784900E+04	!KC2
MISOIEP	1007	0.200000E+12	0.3	0.355000E+09	0.784900E+04	!KT1
MISOIEP	1008	0.200000E+12	0.3	0.390700E+09	0.784900E+04	!L01
MISOIEP	1009	0.200000E+12	0.3	0.292000E+09	0.784900E+04	!LJF

\*\*\*\*\*

\*\*\*\* GROUP DEFINITION \*\*\*\*

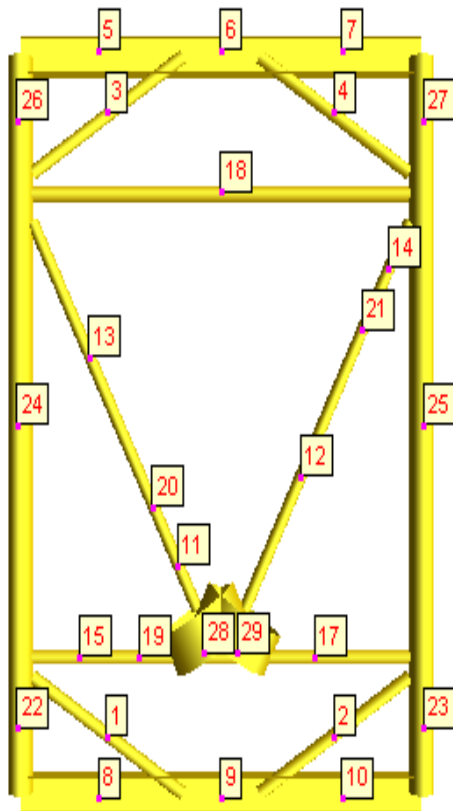
\*\*\*\*\*

GROUPDEF 1001 MAT 1001  
 GROUPDEF 1002 MAT 1002  
 GROUPDEF 1003 MAT 1003  
 GROUPDEF 1004 MAT 1004  
 GROUPDEF 1005 MAT 1005  
 GROUPDEF 1006 MAT 1006  
 GROUPDEF 1007 MAT 1007  
 GROUPDEF 1008 MAT 1008  
 GROUPDEF 1009 MAT 1009



USFOS GUI 2.6-02 2016-04-21  
18:17

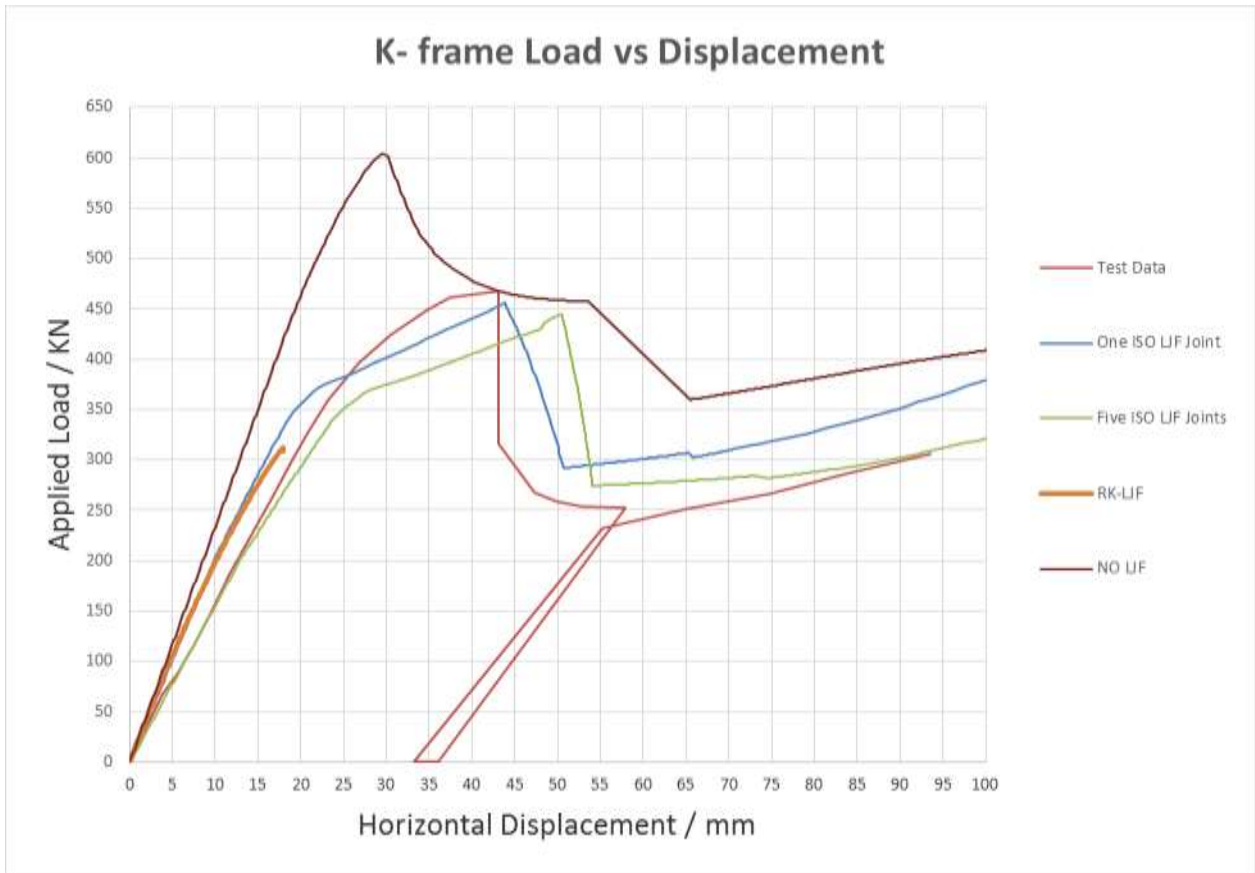
Appendix 5 Figure 1 BOMEL Frame VII – No LJF included



Static case 1 / 1

USFOS GUI 2.6-02 2016-04-21  
18:28

**Appendix 5 Figure 2 BOMEL Frame VII – L.J.F included**



**Appendix 5 Figure 3 Load vs Displacement Curve (RK-LJF included)**